A NEW MODEL FOR DEFLECTIONS OF FRP-REINFORCED CONCRETE BEAMS

by

QUINN JACOBS

B.S., Washburn University, 2009

A THESIS

submitted in partial fulfillment of the requirements for the degree

MASTER OF SCIENCE

Department of Civil Engineering
College of Engineering

KANSAS STATE UNIVERSITY
Manhattan, Kansas

2012

Approved by:

Major Professor
Hayder A. Rasheed

Abstract

Fiber reinforced polymer has recently become a popular replacement for steel rebar, used to reinforce concrete. Therefore much research is taking place to help develop and propose methods for best approximating the response of FRP reinforced members, to make them comparable to steel reinforced members. With this popularity comes multiple approaches to FRP deflection calculations. However, this study is significant, because it investigates the cracking moment equation adopted by ACI 318, in conjunction with state of the art deflection calculation methods. Specifically this research compares four deflection calculation methods. The first approach is proposed by Bischoff and implemented by ACI 440 in its latest revision. The second deflection calculation method is proposed by Rasheed et al. The third calculation is also suggested by Bischoff, as it is specific to four point bending. The fourth calculation method is proposed by this specific research and seeks to find a median between both the Bischoff and Rasheed equations.

This fourth technique will be referred to as the Rasheed-Jacobs method, proposed to create a more conservative and relevant method for investigating the effect of cracking moment on the deflection calculations. This research was done with the help of Dr. Shawn Gross, and the database he had previously built through his investigation on FRP reinforced beams. Gross's database shows results for 106 samples tested using the actual experimental cracking moment as well as the ultimate moment capacity values. Of these 106 samples, 56 independent samples were used to investigate three different moment levels of 0.333Mn, 0.400Mn, and 0.467Mn.

From this research, Gross's database was used to calculate the cracking moment of FRP reinforced beams based on ACI 318-08. A program was developed that uses the Gross database samples to calculate the cracking moment and deflection with the Rasheed, Bischoff, and Bischoff2 models as well as the new Rasheed-Jacobs model. This program calculates the Rasheed-Jacobs results, and then graphs the findings against the deflection values from the Rasheed, Bischoff, Bischoff2 models. These graphs showed very similar patterns amongst all four models, with the Rasheed-Jacobs results mainly falling on the more conservative side. However, when looking at the predicted deflection verse the Gross experimental deflection, the best results came from the $0.467M_n$ moment level, which shows consistent correlation while the

lower moment levels are being less predictable using the cracking moment based on the ACI equation. It can reasonably be said that the 0.467Mn shows the best correlation between the four methods and the experimental results, because it is farther away from the actual nominal cracking moment of the FRP reinforced concrete beams.

Table of Contents

List of Figures

List of Tables

Acknowledgements

To my Lord and Savior, Jesus Christ: I am very grateful for the opportunity to be able to pursue my master's degree in civil engineering for His glory. I am also thankful for His continued guidance through the frustrating and difficult times along the way, for the confidence and patience He provides, and the many second chances allowed merely through God alone. It is only through God's strength and power that I am at such a blessed time in my life capable of succeeding.

To my husband, Christopher Jacobs: I am so thankful to have such a wonderful man in my life to lead our marriage and guide our future. I am very appreciative of all the support and encouragement I received from him along this journey, and the many hours he sacrificed either to listen to me talk about this research or to allow me to focus my effort on this research alone.

To Dr. Shawn P. Gross: I would like to express a sincere appreciation for sharing with us his database for FRP-reinforced concrete beams that he used to validate the analysis carried out by Bischoff and Gross (2011a and b).

To my Major Professor Dr. Hayder Rasheed: I sincerely appreciate the advice, guidance, many long hours of editing, multiple dedicated discussions about the research, and for always challenging me to move forward. Thank you for working alongside me to produce such in depth research and individual growth.

Copyright approvals granted:

With permission from ASCE.

With permission from ACI.

With permission from SAGE Journals.

Dedication

To my Grandpa, Henry Stenzel, for showing me what is truly important in life.

Chapter 1 - Introduction

1.1 Background

Fiber reinforced polymer reinforcement is swiftly growing popular throughout the engineering world. This FRP is much more durable than steel, and can withstand the weather changes and aging of beams more effectively than the steel currently being used. Among the benefits to using steel is that we have specifications and codes such as ACI 318 that provide equations for strength and serviceability design prior to actual use for building purposes. These design procedures guide the engineer in how to utilize the steel reinforcement to produce safe and economical designs. With FRP being more recently introduced, well established equations may not be readily available to provide predicted values for the use of FRP prior to actual use especially in serviceability requirements. However, much research is taking place to help develop and propose methods for best capturing the response of FRP reinforced members, to make them comparable to steel reinforced members. Various research has been done comparing the actual experimental values for FRP reinforced beams to the values obtained by using the ACI 318 code. Although these values sparingly run similar, there is a big enough difference in the results of experiment FRP reinforced values and the predicted values using the ACI 318 code. Therefore, new equations must be developed to provide minimum acceptable limits for the use of FRP reinforced members. Knowing that the ACI 318 code does not work to predict FRP response, the development of FRP deflection equations along with other design equations has attracted more and more attention over the years.

1.2 Objectives

The purpose of this research is to compare four different deflection calculation methods. One of the four methods is a newly proposed deflection equation expected to be more compatible with the ACI 318 equation for cracking moment more so than any of the other three equations. The four equations being compared are the Bischoff, Rasheed, Bischoff2, and the newly developed Rasheed-Jacobs equation. More specifically, this study investigated the effect of cracking moment on the deflection calculation. With the use of experimental values from the Gross database for all 56 independent samples tested, the predicted response using ACI 318 cracking moment is possible to be compared to the experimental behavior, Figure 1.1. The M_{cr}

being used from the ACI 318 code is $M_{cr} = \frac{f_r I_g}{y_{bot}}$ where, $f_r = 0.62\sqrt{f'_c}$ in MPa and $f_r = 7.5\sqrt{f'_c}$ in psi.

Another objective of this research was to use the program to develop load-deflection graphs for each current sample or future sample that might be tested. These graphs provide data for the Bischoff, Rasheed, Bischoff2 and Rasheed-Jacobs deflection equations and the impact of the cracking moment on them. All of this research was used to determine which deflection calculation method provides the best practical design for the real world utilization.

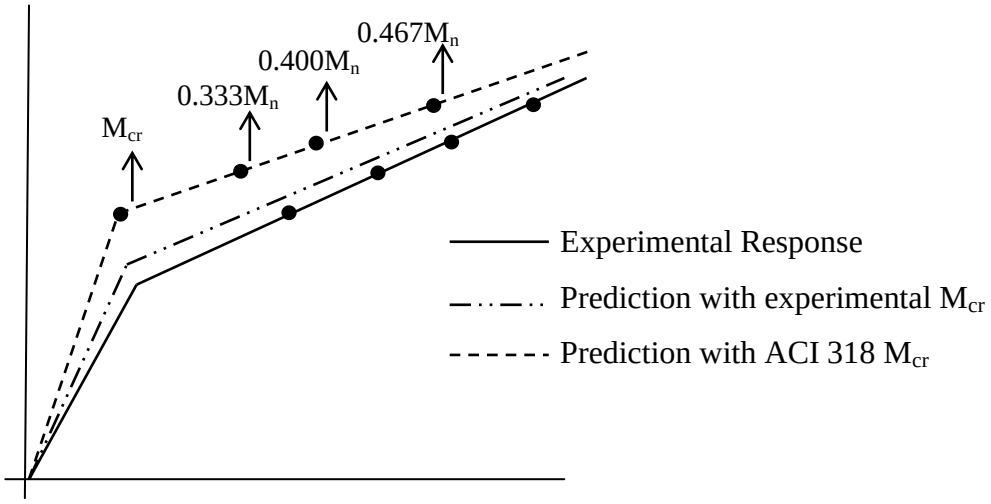

Figure 1.1: Expected overall comparison of experimental response vs. predicted values.

1.3 Scope

The product of all of this FRP reinforced beams research and deflection design methods is discussed throughout five chapters. The first chapter is an introduction and background to FRP. Chapter two is a compilation of literature reviews from all of the papers used for the 56 independent samples or information throughout the research process. Most of the resources for this research came from the Gross database. In chapter three, the advancement of the research and where the research began is introduced beginning with the development of the Rasheed-Jacobs model. Chapter four presents the results and discussions and chapter five addresses the conclusions and recommendations for future work.

1.4 Gross Database

The Gross Database is a compilation of 106 samples with deflection results at three moment levels. The first moment level is 0.333Mn followed by 0.400Mn and 0.467Mn. Gross used eleven different papers for the collection of all 106 samples. The choice to use the Gross database was made, because values were already readily available, and time consuming collection of data could be avoided to further the knowledge that is already available rather than duplicating what was already known. From the Gross database, 64 independent samples were used as shown in Table 1.1. Only 56 of the 106 samples were chosen, because some of the samples had exactly the same material and geometric parameters, while the only value that differed, was the experimental deflection. Therefore we selected the first sample out of all the duplicated samples and eliminated the rest of the duplication.

Table 1.1 The list of independent beam specimens from the Gross database with the number of dependent deflections used for comparison.

Author	Dependent samples excluded	Independent sample names used for the 64 count
Yost (16)	27	1a-NL, 2a-NL, 3a-NL, 4a-NL, 1a-NS, 2a-NS, 3a-NS, 4a-NS, 1a-HS, 2a-HS, 3a-HS, 4a-HS, 1a-HL, 2a-HL, 3a-HL, 4a-HL
Toutanji (2)	0	GB2, GB3
Benmokrane (2)	1	ISO1, ISO2
Masmoudi (4)	3	CB2B-1, CB3B-2, CB4B-1, CB6B-1
Theriault (6)	2	BC2NA, BC2HA, BC2VA, BC4NA, BC4HA, BC4VA
Al-Sunna (11)	7	BG2a, BG3a, SG2a, SG3a, BC1a, BC2a, BC3a, SC2a, SC2b, SC3a, SC3b
Faza (3)	2	ED, EE, EVH1
Theisz (4)	8	8-2-1, 8-3-1, 11-2-1, 11-3-1,
Kakizawa (1)	0	2
Kassem (6)	0	IS-4, IS-6, IS-8, CB-4, CB-6, CB-8
Nakano (1)	0	RC-C1

However, with 56 independent samples selected, the differing experimental deflection values were taken into consideration when the comparison of deflection values came into play. The extra 50 beams although repeated tested specimens of the independent 56 samples, were considered using only their representative experimental deflection value. Since the newly developed program calculates the deflection for each of the four models that are being investigated, a comparison was done using all 106 experimental deflection values from the Goss database. These deflection values from the Gross database were used to compare all four

equations including the Rasheed, Bischoff, Bischoff2 and Rasheed-Jacobs deflection values obtained from the developed program. This provides a comparison of how close the deflection values are between the four suggested equations. The Gross database came in very handy to make comparisons throughout this investigation of deflection calculation models.

Chapter 2 - Literature Reviews

2.1 Overview

FRP research has grown especially popular in the structural engineering field as a replacement for steel reinforcement in applications where corrosion is of primary concern. This study continues this research and presents a new model for deflection of FRP reinforced beams. This research was conducted with the help of a database built by Shawn P. Gross. Gross collected samples and each sample's test results were used in this research to analyze and help develop a new model for deflection in FRP reinforced beams. Although Gross's original database included 106 samples pulled from 11 different references, only 56 samples were found to be completely independent and were actually reanalyzed using the new verified program as referenced in section 4.1. Using only part of the original database was decided upon due to the repeated samples and data as explained in section 1.4. As the following literature review will show, Gross did not use all of the available samples from all of his collected work, but chose wisely which to use and not to use. Since the 106 samples were composed of 56 independent samples with a different M_{cr} selected from experimental data and since this study focuses on deflection results using ACI 318 M_{cr} calculation, only 56 samples are analyzed here. The following are reviews of each of references used in Gross's research. The literature was used to verify values and data to make sure accurate numbers were being used.

2.2 Chronological Order of Literature Reviews

Faza (1991) investigated the durability of FRP rebar when used in bridge decks and concrete beams as a replacement to the classical use of steel rebar. He used mechanical characteristics of FRP bar provided by Wu (1990) to study the pre- and post-cracking behaviors, the bending and bond resistance, and the deflection limits of concrete beams reinforced with FRP bars. Amongst all of these studies, Faza was able to work towards developing design equations for FRP reinforced concrete members. Throughout Faza's research, he examined the bending and bond behaviors, as well as analyzed static loading tests on 51 different samples altering the involved variables such as rebar size, concrete compressive strength, and embedment length along with other variables. This helped create correlation amongst all the samples and results. Faza came to the conclusion that a 90% increase in ultimate moment capacity was obtained over

steel reinforced concrete for the same rebar area and concrete strength. Faza also determined through all of the correlations that current ACI methods for steel rebar used for reinforcement cannot be used to determine values for FRP reinforcement. He found that the actual values compared to the results provided from the steel rebar equations do not match up. In determining this outcome, Faza developed an ultimate strength design method and a working stress design method. These two methods helped determine benchmark numbers prior to the use of FRP that produce very comparable results to the actual values. Out of the 51 samples used in Faza's research, three of these samples are independent and used throughout this current research on FRP deflection modeling.

Nakano et al. (1993) studied and evaluated the flexural performance of concrete beams reinforced with Fiber Reinforced Polymer bars. Nakano performed two series of flexural tests on eighteen samples for his research. All eighteen samples were investigated for bending stiffness, bending strength and failure mode, but eight of these samples were also investigated for the width of bending cracks. Prestressing tendons were also used in these eight samples so that the prestressing force was present during testing and investigation. All of this research was used to determine the factors present in controlling the ductility capacity of the samples. Nakano's investigation resulted in knowing that the ductility capacity can be controlled by crushing the concrete under certain conditions and also that the initial cracking load and width of cracks can be controlled using prestressing force in the samples. From Nakano's eighteen samples, one independent sample without the prestressing tendons was used in the current research to help correlate a model for FRP deflection.

Kakizawa et al. (1993) investigated concrete beams reinforced with FRP bars with specific focus on serviceability and the ultimate limit states. In Kakizawa's research, sixteen samples reinforced with FRP bars and cables were put through loading tests. From these loading tests, load-deflection curves were developed and analyzed to further the knowledge of the ultimate limit states. The main focus of the load-deflection curves was the energy absorption, which was defined to be the area enclosed by this curve for each given sample. This energy absorption was then used to calculate the ductility which then led to the deformation capacity. Through all of these calculations and tests, Kakizawa was able to state that reasonable serviceability is obtainable by controlling the deformation and cracking behavior. Along with these results, it was determined that failure mode and deformation behavior changed according to

the reinforcement system and variables. Out of these sixteen samples that were tested, one independent sample along with its provided data was used in this research.

Benmokrane et al. (1996) performed experimental and theoretical comparisons on flexural behavior of FRP reinforced concrete beams. These comparisons were made using seven different sets of collected data on eight different samples. These sets of data included: flexural rigidity, mode of failure, load-deflection curves, strain distribution, stress-strain comparisons, load carrying capacities, and cracking patterns. With much assessment of the strain distribution, Benmokrane was able to state that perfect bond exists between the FRP bars and the concrete being reinforced. Also, Benmokrane was able to conclude that with a service load applied, the number of cracks increases as well as the width of the cracks compared to the classic use of steel. Another outcome of Benmokrane's research was that the use of ACI steel equations are appropriate when specific modifications are made. From Benmokrane's research, two independent samples of the eight were used in this research.

Theriault et al. (1998) investigated the reinforcement ratio and concrete strength in FRP reinforced concrete beams. Theriault tested twelve samples under static loading conditions until complete failure. With the results from all of the samples Theriault was able to propose theoretical models as well as make three influential conclusions. The first conclusion was that the ultimate moment capacity increases as the reinforcement ratio and concrete strength increase. Secondly, a good bond exists between the FRP and concrete as reflected by the strain distribution, the steady stiffness, the crack correlations, and the flexibility of deflection. Lastly, Theriault was able to conclude that the concrete compressive failure strain restricts the increase of the ultimate moment capacity. Theriault contributed six independent samples to the current research.

Masmoudi et al. (1998) performed extensive research studying the flexural behavior of FRP reinforced concrete. Masmoudi's researched was a continued study from Theriault's (1998) study. However, Masmoudi, although basing his research off of Theriault's (1998), tested ten new samples for verification of his investigation. Masmoudi proposed that the average crack spacing in FRP reinforced concrete was very similar to the classic steel reinforced concrete. Next, Masmoudi proposed that the reinforcement ratio was negligible in realm of spacing, and that the crack width in FRP samples were three to five times that of steel reinforced samples. Masmoudi also developed a prediction model for maximum deflection and also included an

already developed prediction for deflection model to verify that his is in the realm of functional for the purposes of FRP reinforced concrete. Masmoudi contributed four independent samples to this new FRP model for deflection research.

Toutanji et al. (2000) focused directly on presenting new design equations used for predictions about FRP data similar to the equations used for steel reinforcement in the ACI code. Toutanji also focused on providing understanding to readers about the performance of Glass-FRP reinforced concrete. Six samples were used to test for results throughout the research. After analysis, Toutanji proposed the prediction of deflection thru the use of the flexural stiffness. Also proposed was the prediction of effective moment of inertia thru the effect of the reinforcement ratio and elastic modulus. These predictions were proved to provide acceptable estimates to the actual experimental values thru Toutanji's research. Two independent samples of the six were used for furthering the FRP deflection model in this investigation.

Kassem et al. (2003) researched the deflection behavior of the newly developed Carbon-FRP. This was the first test to be carried out on CFRP in terms of size and number of beams. Kassem tested fourteen sample concrete beams to concrete crushing failure in four point bending. Demanding concrete crushing failure required a reinforced ratio of 1.2ρb or greater. Due to the forced compression failure, the ultimate concrete strain governs the beam carrying capacity. From the results and by comparisons made to previously presented models, Kassem was able conclude considerably new information on CFRP. Kassem concluded that increasing the reinforcement ratio would decrease both the deflection and maximum crack width at the service load limit. Also, Kassem concluded that the ACI steel equation underestimates the CFRP experimental deflection values. An average deformability factor was also discovered to be 7.0, which was obtained from the correlation of all the samples failing in compression. Six independent samples of the fourteen samples from Kassem's research were used in this study.

Yost et al. (2003) investigated more into the deflection behavior of GFRP. Enable to better study the influential parameters; he altered the concrete strength, reinforcement density, and the shear span-depth ration throughout his testing. Yost ran tests on 48 simply supported beam samples, and recorded the load-deflection response. With the load-deflection response, Yost studied the effective moment of inertia more in depth. After doing comparisons, Yost found that the ACI equation overestimated the effective moment of inertia in turn underestimating the service deflection. Yost then presented a modified version of the ACI

calculation for GFRP rather than steel. Yost also stated that the loss of stiffness in GFRP was much greater than the classically used steel, mainly due to the gross-to-cracked section properties. Yost contributed the most independent samples of all the authors to this current research at a sixteen samples.

Theisz et al. (2004) focused his research on comparing experimental results to theoretical values. Mainly theoretical values provided by the current ACI code and the Canadian Standards Association (CSA). Theisz tested twelve CFRP samples in high strength concrete which increases the flexural capacity. In turn this high strength concrete reinforced with CFRP will create a more structurally efficient section for use in building. Theisz evaluated each of his test samples for shear strength, service load crack width, and service load deflection. Although there are other parameters that occur in the use of CFRP, Theisz focused on these three variables specifically. In terms of comparison, Theisz concluded three statements: (1) the shear strength was underpredicted by both the ACI and CSA codes compared to the experimental values, although the CSA was a much closer prediction that ACI. (2) The service crack width was overpredicted in both cases, placing the experimental crack width in the theoretical maximum crack width range for both ACI and CSA. (3) The service load deflection was determined to be underestimated in comparison to the ACI code, but overpredicted in comparison to the CSA. From Theisz' research, all four independent samples were used in this current research on a new FRP model for deflection.

Al-Sunna (2006) investigated the short term deflection comparisons using both ACI code and Eurocode 2. Although many parameters are available, Al-Sunna focused his investigation on rebar strain, bond between flexural cracks, and tension stiffening. Al-Sunna's research included 28 samples of beams and slabs with the use of GFRP, CFRP, and steel for comparison, which underwent four-point loading. He was able to reasonably state that the ACI code was not appropriate for use with FRP without major modifications. However, Al-Sunna's main conclusion was that the deflection of FRP is principally due to the flexural curvature, and can be soundly evaluated by the tension stiffening model of the Eurocode 2. Al-Sunna contributed eleven independent samples to the current research.

2.3 Concluding Remarks

Of these eleven investigations and literature reviews, a total of 56 samples were used in the current research to help develop a new model for FRP deflection. Gross was a very important factor in the collection of data, as he provided a data base for this research. However, each of these literatures used in Gross' research were used to check the values and do comparisons enable to ensure accurate work and development of FRP information.

Chapter 3 - Deflection Formulation

3.1 The Deflection Problem at hand

With so many models being developed and critiqued on this topic of deflections of FRP reinforced beams, it is now known that estimating the cracking moment of FRP reinforced beams is a very sensitive undertaking. The ACI 318 overestimates the cracking moment therefore after cracking it will then underestimate the deflection. Thus, a more sensitive model is necessary to help alleviate this problem, and to provide a better estimate for deflection after the cracking has taken place. A projected load-deflection response of current models as well as the presented Rasheed-Jacobs model can be seen in Figure 3.1.

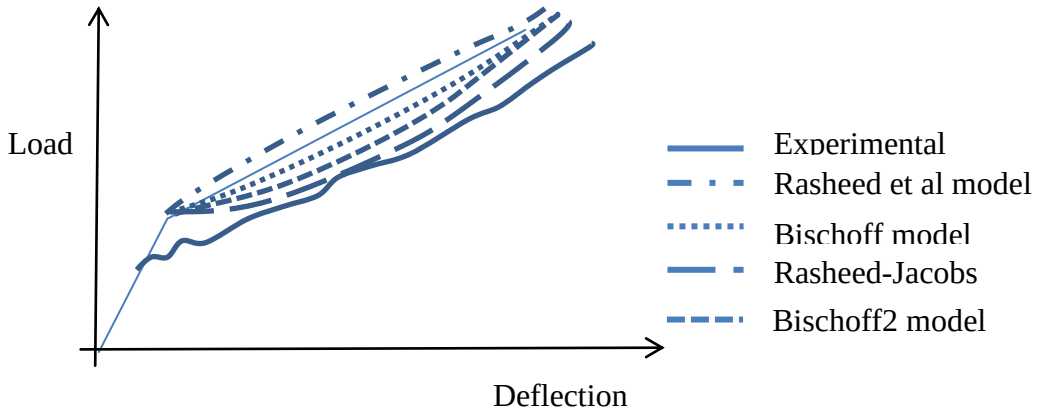

Figure 3.1 Load-deflection response of various models.

From Figure 3.1, it can be seen that although all four models under predict the deflection, the Rasheed-Jacobs model is known to be the most concave and is anticipated to be more closely in line with the projected experimental response. Therefore, the Rasheed-Jacobs model is expected to over predict the deflection by the least and hence provides a better estimate for the deflection analysis.

3.2 Section Analysis

The computation of cracking moment is very straight forward.

$$f_r = \frac{M_{cr} y_{bot}}{I_{gt}} \tag{1}$$

Where y_{bot} is the distance from the elastic centroid to the extreme tension fiber, I_{gt} is the elastic gross transformed moment of inertia of the beam section, and f_r is the rupture modulus of concrete:

$$f_r = 7.5\sqrt{f'c} \qquad f'c \text{ in psi} \tag{2}$$

$$f_r = 0.62\sqrt{f'c} \qquad f'c \text{ in MPA} \tag{3}$$

Thus,

$$M_{cr} = \frac{f_r I_{gt}}{y_{bot}} \tag{4}$$

$$\emptyset_{cr} = \frac{M_{cr}}{E_c I_{gt}} \tag{5}$$

Where

$$E_c = 57000\sqrt{f'c} \qquad f'c \text{ in psi} \tag{6}$$

$$E_c = 4723\sqrt{f'c} \qquad f'c \text{ in MPa} \tag{7}$$

There are pre-cracking and post cracking stages and the moment-curvature is considered a bilinear response for the FRP reinforced beam (Rasheed et al. 2004) as shown in Figure 3.4. Using the comparison of tension FRP and the balanced FRP ratio respectively, which determines the mode of failure, the ultimate-moment capacity is determined. In the process of calculating the ultimate moment, two modes of failure are possible. The first mode of failure is rupture which takes place when the FRP breaks prior to the concrete crushing. The second mode of failure is crushing which takes place when the FRP does not rupture before the concrete crushing. As previously stated, the comparison of the tension FRP reinforcement ratio of $\rho_f = \frac{A_f}{bd}$ with the doubly reinforced balanced FRP reinforcement ratio of $\bar{\rho}_{fb} = \rho_{fb} + \rho'_f \frac{f'_{fb}}{f_{fu}}$ determines the failure mode prior to the ultimate moment. Where the balanced reinforcement ratio of a singly reinforced section, compression FRP reinforcement ratio and the compressive stress in top of the FRP reinforcement are given as:

$$\rho_{fb} = 0.85\beta_1 \frac{f'_c}{f_{fu}} \frac{E_f \varepsilon_{cu}}{E_f \varepsilon_{cu} + f_{fu}} \quad (8)$$

$$\rho'_f = \frac{A'_f}{bd} \quad (9)$$

$$f'_f = E'_f \varepsilon'_f \quad (10)$$

To further explain these equations, we have:

$$\beta_1 = 1.05 - \frac{0.05 f'_c}{1000} \qquad 4000\ psi < f'c < 8000\ psi \quad (11)$$

$$\beta_1 = 1.09 - 0.008 f'c \qquad 30\ MPa < f'c < 55 MPa \quad (12)$$

Where, f'_c is the input compressive strength of concrete, E_f is the modulus of FRP reinforcement in tension, f_{fu} is the ultimate strength in the FRP reinforcement in tension, ε_{cu} is the maximum strain when the concrete crushes which is given as 0.003. Also, A'_f is the input area of compression reinforcement, b is the width of the beam, and d is the effective depth of the beam section up to the centroid of FRP tension reinforcement, d' is the depth of the centroid of compression reinforcement.

Now the stress of FRP in compression is calculated from the modulus of FRP reinforcement in compression and the ultimate strain of concrete in compression (ϵ_{cu}) given as:

$$\varepsilon'_f = \varepsilon_{cu}\left(\frac{c_b - d'}{c_b}\right) \quad (13)$$

Where ,

$$c_b = \frac{\varepsilon_{cu}}{\varepsilon_{cu} + \varepsilon_{fu}} d \quad (14)$$

$$\varepsilon_{fu} = \frac{f_{fu}}{E_f} \quad (15)$$

These calculations and the comparison of the reinforcement ratio to the balanced ratio then provide a mode of failure.

3.2.1 Rupture Failure Mode

If $\rho_f < \bar{\rho}_{fb}$, then the section fails by rupture of FRP reinforcement. Therefore, the FRP reaches the rupture strain prior to the concrete reaching crushing as seen in the strain compatibility diagram in Figure 3.2.

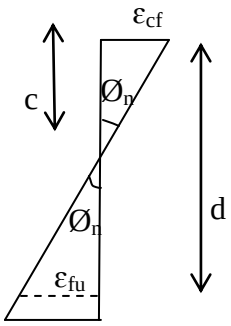

Figure 3.2 Strain compatibility at FRP rupture failure.

In this instance, the depth of the neutral axis, c, is acquired by setting the equilibrium equation equal to zero, therefore:

$$\alpha f'_c bc + A'_f f'_f - A_f f_{fu} = 0 \tag{16}$$

Where

$$\alpha = \frac{\varepsilon_{cf}}{\varepsilon'_c} - \frac{\varepsilon_{cf}^2}{3\varepsilon'^2_c} \tag{17}$$

$$\varepsilon_{cf} = c\frac{\varepsilon_{fu}}{d-c} \tag{18}$$

$$\varepsilon'_c = \frac{f'_c}{E_c}\left(\frac{\beta}{\beta-1}\right) \tag{19}$$

And,

$$f'_f = E'_f \frac{\varepsilon_{fu}}{d-c}(c-d') \tag{20}$$

$$\beta = \left(\frac{f'_c}{32.4}\right)^3 + 1.55 \qquad \text{where } f'c \text{ is in MPa} \tag{21}$$

Once the c-value is obtained by solving the nonlinear equation 16 for the lowest positive root, the ultimate nominal moment and curvature is then obtained using the following equations:

$$M_n = A_f f_{fu}(d - \gamma c) + A'_f f'_f(\gamma c - d') \tag{22}$$

Where

$$\gamma = \frac{\frac{1}{3} - \frac{\varepsilon_{cf}}{12\varepsilon'_c}}{1 - \frac{\varepsilon_{cf}}{3\varepsilon'_c}} \tag{23}$$

And,

$$\emptyset_n = \frac{\varepsilon_{fu}}{d-c} \tag{24}$$

These nominal moment and curvature values are then used for the moment curvature graphs using Rasheed et al. 2004 bilinear relationship.

3.2.2 Crushing Failure Mode

On the other hand, if $\rho_f > \bar{\rho}_{fb}$, then the section failure mode is crushing. Therefore, the FRP reinforcement does not reach the rupture strain prior to concrete crushing. This can be seen in the strain compatibility diagram in Figure 3.3.

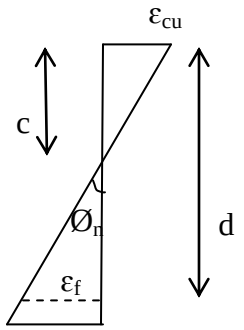

Figure 3.3 Strain compatibility for the crushing failure mode.

Just like in the rupture failure mode, the depth of the neutral axis, c, is acquired by setting the force equilibrium equation equal to zero, therefore:

$$0.85f'_c b\beta_1 c + A'_f f'_f - A_f f_f = 0 \tag{25}$$

Where

$$f_f = E_f \frac{\varepsilon_{cu}}{c}(d - c) \tag{26}$$

And

$$f'_f = E'_f \frac{\varepsilon_{cu}}{c}(c - d') \tag{27}$$

After solving the nonlinear equilibrium equation 25 for c, the ultimate nominal moment and curvature are then obtained for crushing failure mode using the following equations:

$$M_n = A_f f_f \left(d - \frac{\beta_1 c}{2}\right) + A'_f f'_f \left(\frac{\beta_1 c}{2} - d'\right) \tag{28}$$

And,

$$\emptyset_n = \frac{\varepsilon_{cu}}{c} \tag{29}$$

These nominal moment and curvature values are then used for the moment curvature graphs similar to the rupture failure mode.

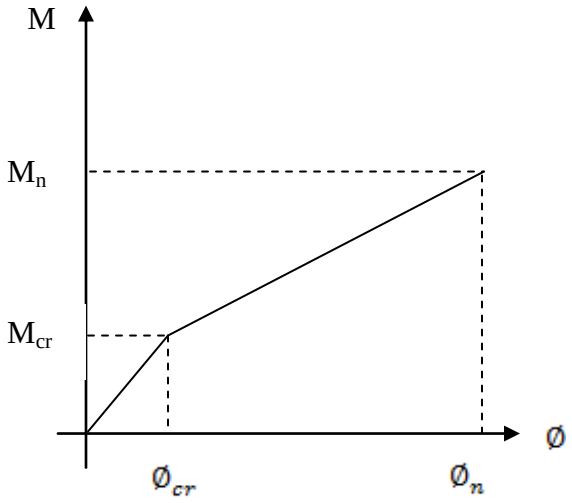

Figure 3.4 Bilinear moment curvature relationship.

3.3 Review of Models

Four models were used throughout this research to compare results from the 106 Gross samples. The first model is the Rasheed et al. (2004) model, which is based off of the integration of bilinear moment curvature distribution. This model yields the following mid-span deflection equation:

$$\Delta_R = \frac{\phi_{aR}}{24}(3L^2 - 4a^2) + \frac{L_g + a}{6}(\phi_{cr}a - \phi_{aR}L_g) \quad (30)$$

Where, the post cracking values from equation 25 above are:

$$\emptyset_{aR} = \emptyset_{cr} + \frac{\emptyset_n - \emptyset_{cr}}{M_n - M_{cr}}(M_a - M_{cr}) \quad (31)$$

$$M_a = \frac{P_a}{2}a \quad (32)$$

$$L_g = \frac{2M_{cr}}{P_a} \quad (33)$$

The second model is the Bischoff (2011) model, which is based off of the loading factor, γ, being kept constant throughout the model. This model is proposed for uniform loading distribution on beams. This model was adopted by ACI 440.1R, because most beams being used in practice will be of uniform load distribution. The integration of this model is then performed and presented as:

$$I_{eff} = \frac{I_{cr}}{1 - (\gamma\eta\left(\frac{M_{cr}}{M_a}\right)^2)} \quad (34)$$

Where

$$\eta = 1 - \frac{I_{cr}}{I_g} \quad (35)$$

$$\gamma = 1.72 - 0.72\frac{M_{cr}}{M_a} \quad (36)$$

$$\Delta_B = \frac{\phi_{aB}}{24}(3L^2 - 4a^2) \quad (37)$$

$$\emptyset_{aB} = \frac{P_a a}{2E_c I_{eff}} \quad (38)$$

The above equation of deflection is specialized to four point bending since the database has that loading condition even though the I_{eff} is determined for uniform loading to allow for equation evaluation against existing results.

The third model presented is the Bischoff2 (2011) model based on four-point bending as shown in Figure 3.5 rather than uniform loading. The Bischoff2 model equations are as follows:

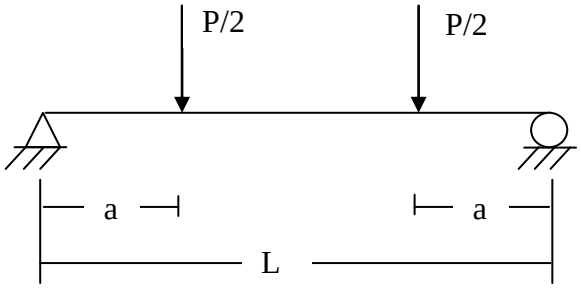

Figure 3.5 Four-point bending model for Bischoff2.

$$I_{eff2} = \frac{I_{cr}}{1-(\gamma_2 \eta \left(\frac{M_{cr}}{M_a}\right)^2)} \tag{39}$$

Where

$$\eta = 1 - \frac{I_{cr}}{I_g} \tag{40}$$

$$\gamma_2 = \frac{3\frac{a}{L} - 4\xi(\frac{a}{L})^3}{3\frac{a}{L} - 4(\frac{a}{L})^3} \tag{41}$$

$$\xi = 4\frac{M_{cr}}{M_a} - 3 \tag{42}$$

$$\Delta_{B2} = \frac{\phi_{aB2}}{24}(3L^2 - 4a^2) \tag{43}$$

$$\emptyset_{aB2} = \frac{P_a a}{2E_c I_{eff2}} \tag{44}$$

These last three models were used alongside the Gross database samples to examine the validity of the newly presented Rasheed-Jacobs equation. This research was specifically performed to propose and compare the new Rasheed-Jacobs model among the already presented models and

the ACI 318 cracking moment. The Rasheed-Jacobs equation was developed from the original Branson equation which is

$$I_e = \left(\frac{M_{cr}}{M_a}\right)^3 I_g + \left[1 - \left(\frac{M_{cr}}{M_a}\right)^3\right] I_{cr} \quad (45)$$

This Branson equation is based on a weighted average of stiffness, or moment of inertia. This is a cubic approximation function. Therefore, we are introducing the Rasheed-Jacobs equation as a weighted average of flexibilities or inverse moments of inertia. A weighted average of flexibilities creates a higher order function approximation meaning the variation is of the order $\frac{1}{x^3}$. The proposed Rasheed-Jacobs equation is based on the following:

$$\frac{1}{I_e} = \left(\frac{M_{cr}}{M_a}\right)^3 \frac{1}{I_g} + \left[1 - \left(\frac{M_{cr}}{M_a}\right)^3\right] \frac{1}{I_{cr}} \quad (46)$$

Introducing the, $\frac{1}{x^3}$ approximation, Rasheed-Jacobs equation is assumed to be a better fit for FRP beams, because earlier research by Rasheed and Dinno (1994) shows that parabolic flexibility variation, $\frac{1}{x^2}$,surpasses parabolic stiffness variation, x^2, by much. The Rasheed-Jacobs model can then be summarized as follows:

$$\frac{1}{I_e} = \left(\frac{M_{cr}}{M_a}\right)^3 \frac{1}{I_g} + \left[1 - \left(\frac{M_{cr}}{M_a}\right)^3\right] \frac{1}{I_{en}} \quad (47)$$

Where I_{en} is the effective or secant moment of inertia at the ultimate moment calibrated by Rasheed et al. (2004) to correlate to I_{cr} as follows:

$$\frac{I_{en}}{I_g} = 0.8365 \frac{I_{cr}}{I_g} + 0.0135 \quad (48)$$

And

$$\Delta_{RJ} = \frac{\emptyset_a}{24}(3L^2 - 4a^2) \quad (49)$$

$$\emptyset_a = \frac{Pa}{2E_c I_e} \quad (50)$$

3.4 Program Structure

A new Rasheed-Jacobs program was built to enable furthering the research on FRP reinforced beams and slabs. Each of the 56 independent samples from the Gross database was

used in this program. For this program to run smoothly from beginning to end, 15 input values are needed for each sample to be tested. These 15 parameters consist of: height (h), width (b), compressive strength (f'_c), Young's modulus of steel (E_s), area of compression reinforcement (A'_f), area of tension of FRP (A_f), effective depth of the section (d), depth from the top of the section to the centroid of the compressive reinforcement (d'), ultimate strength in the FRP bars in tension (f_{fu}), Young's modulus of FRP reinforcement in tension (E_f), Young's modulus of FRP reinforcement in compression (E'_f), ultimate strength of the FRP bars in compression (f'_{fu}), beam span (L), beam shear span (a), and the strain of the extreme concrete fiber in compression (ε_{cu}). This program was built with the advantage that all of the calculations can be found in both Metric and English units for a more beneficial and global use.

With all of the initial values established, the database then proceeds to determine necessary values for the use in the developed moment and deflection equations. Once the parameters are input, the program converts them to the necessary units, and then delivers the calculations thru 30 steps of strain compatibility and other equations to obtain values necessary for the force equilibrium equation. However, the results provided at this point in the program may or may not be applicable depending on the failure mode of the given FRP reinforced beam. As discussed in section 3.2, there are two types of failure modes. The program is designed to discern whether the beam fails in crushing mode or rupture mode, enable to calculate the correct results for each sample using the correct force equilibrium equation as shown in Figure 3.6. By comparing ρ_f and $\bar{\rho}_{fb}$, the program determines the failure mode of rupture or crushing as described in section 3.2. If the ρ_f value is greater than the $\bar{\rho}_{fb}$ value, then the program will guide you to use the crushing sheet as shown in Table 3.1. Otherwise the program will guide you to use the rupture sheet as shown in Table 3.2. Knowing the actual failure mode and using the correct program sheet for each sample is essential, because the equations used and therefore the results differ between crushing and rupture. This difference is due to the different M_n computed, which affects the Rasheed et al. model results. This is also important, because the crushing and rupture modes follow different patterns of calculations as shown in Figure 3.7 for crushing mode and described in section 3.2.2 and Figure 3.8 for rupture failure and described in section 3.2.1.

Table 3.1 Example of output for crushing mode sample.

c_b=	19.79255	ρ_f=	0.011871
$\varepsilon'_{f=}$	-0.00049	$\rho_{fb(bar)}$=	0.004899
E'_f=	200000	ρ'_f=	0.002825
f'_f=	-97.2306	ρ_{fb}=	0.005254
Crushing use this sheet			

Table 3.2 Example of output for rupture mode sample.

c_b=	47.86812	ρ_f=	0.002855
$\varepsilon'_{f=}$	0.003	$\rho_{fb(bar)}$=	0.004545
E'_f=	199947.8	ρ'_f=	0
f'_f=	599.8435	ρ_{fb}=	0.004545
Use Metric Rupture Sheet			

Once the correct failure mode is determined, then the program can be led to finalize all values from the click of "Run Button" encoded into the program. This "Run Button" controls the force equilibrium equation for the determination of the c-value, which differs between failure modes. Solving this force equilibrium equation equal to zero gives the accurate c-value for the specified mode used to solve the rest of the equations in the program. The program then uses all of the resulting values alongside the incremental load values to determine the moment at that specific load, the length of uncracked zone along the beam, and the curvature using all four models, Rasheed, Rasheed-Jacobs, Bischoff, and Bischoff 2. The cracking moment is used to determine the effective moments of inertia. Rasheed's curvature is determined from the ultimate nominal moment calculated using the c-value determined from the force equilibrium equation as mentioned above in section 3.3. From here, the program develops moment-curvature graphs including all four models on each graph for the beam being analyzed. These curvature values are then used to calculate the deflections for each of the four methods which lead to the load-deflection graphs that were used for the main comparison among all four investigated models. The deflections calculated from the four models are used in comparison with the Gross database experimental values for validity and similitude. Assessing the comparison of the load-deflection

graphs alongside the direct deflection comparison was also used to study the validity and accuracy of each method, enable to determine the best practical model of the four.

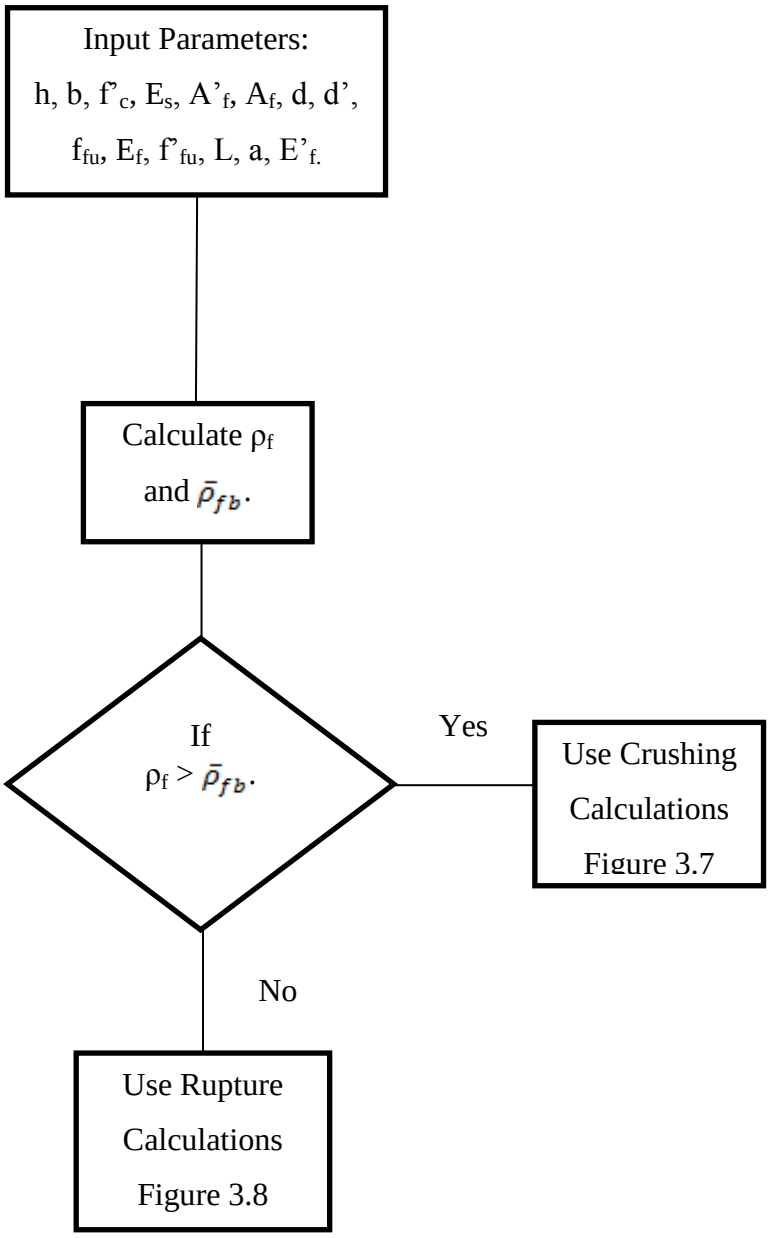

Figure 3.6 Basic procedure for the Rasheed-Jacobs program-structure.

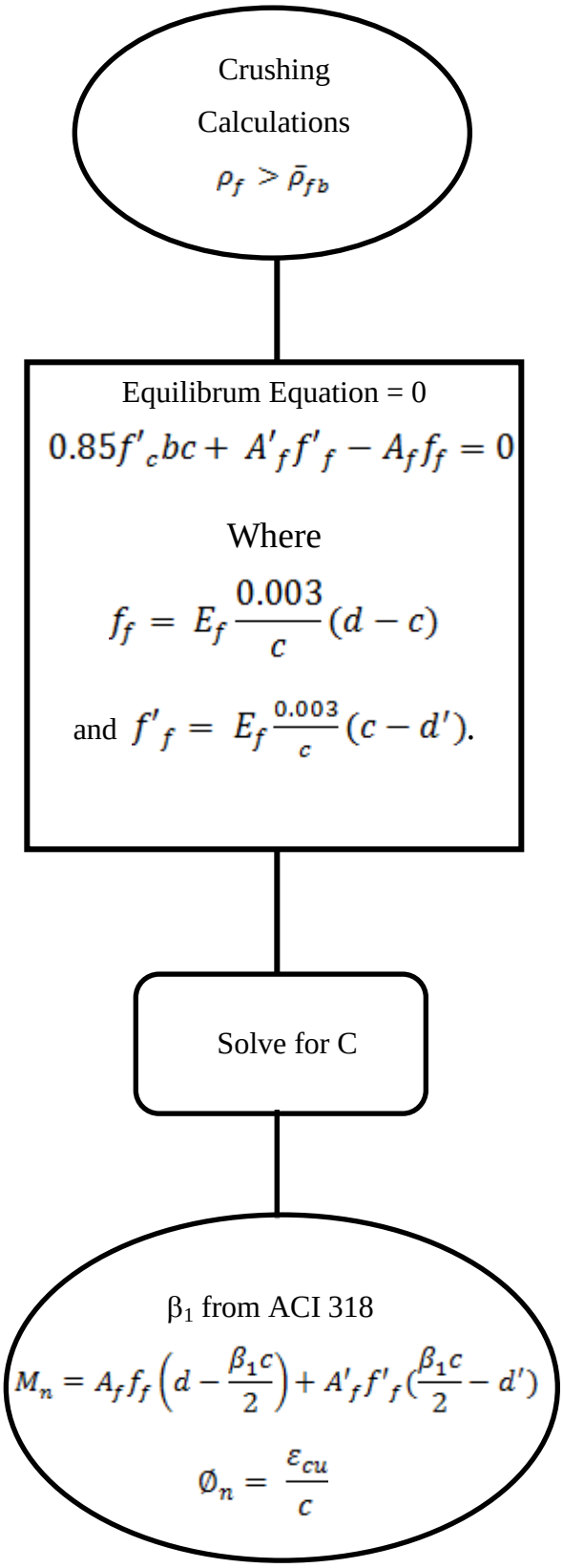

Figure 0.1 Crushing calculations for the Rasheed-Jacobs program.

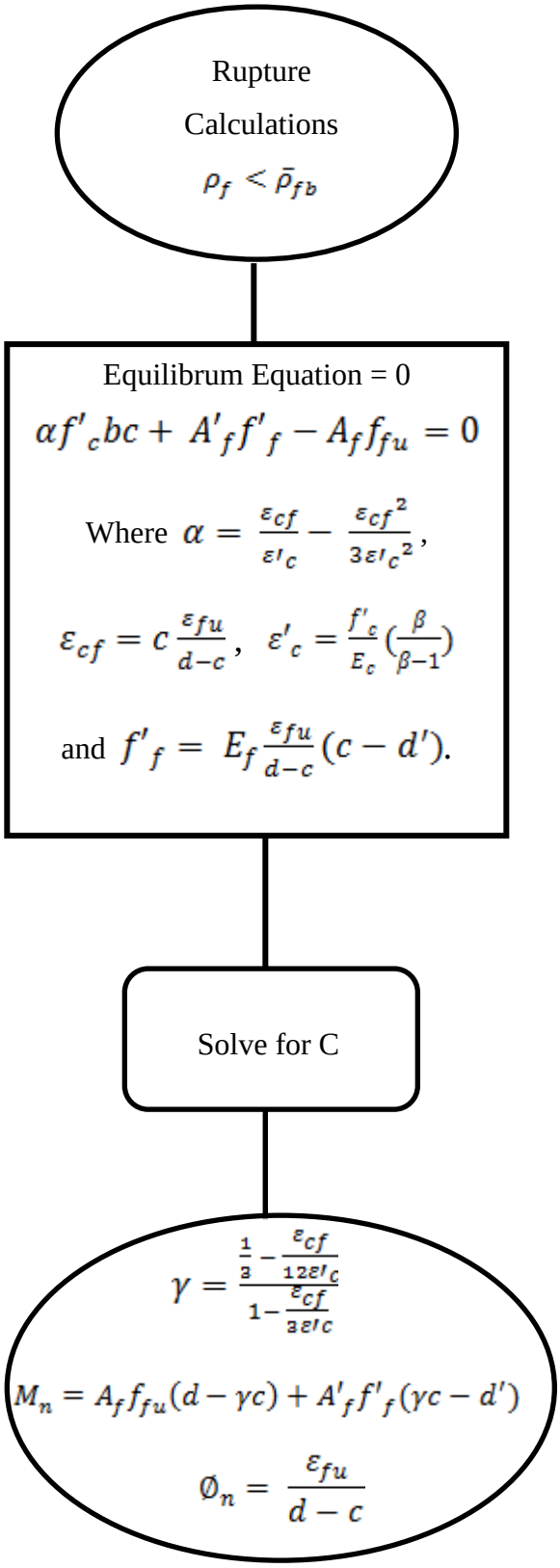

Figure 0.2 Rupture calculations for the Rasheed-Jacobs program.

Chapter 4 - Results

4.1 Qualifying Results

Before analyzing the 56 independent samples from the Gross database through the Rasheed-Jacobs Program, accuracy of this program had to be checked first. Therefore, three random crushing samples were chosen for comparison including: BC2HA (Theriault and Benmokrane, 1998), F1 (Pecce et al, 2000), and Group3 (Almusallam, 1997), which provide graphs of experimental data. A data digitizer was used then to allow for the digitization of all the experimental data being used to verify the accuracy of the program. The experimental data was compared against the program results to ensure an adequate response with closely comparable results. Three random rupture samples were also selected to check the accuracy of the FRP rupture as well, including: SC1 (Al-Sunna, 2006), ISO3 (Benmokrane et al., 1996), and BG1 (Al-Sunna, 2006).

4.2 Crushing Failure Mode Results

The first sample used for accuracy of the program is BC2HA (Theriault and Benmokrane, 1998), which has a crushing mode of failure. The initial parameters can be seen in Table 4.1 in both Metric and English units. This sample provided experimental values for the load-deflection response, and can be seen in Figure 4.1. The new Rasheed- Jacobs program results can be seen in Figure 4.2 with the experimental data included.

section properties		
h=	179.9999	mm
b=	130	mm
f'c	57.19998	MPA
E_c =	35720.36	MPA
E_s =	200000	MPA
A'f	56.54827	mm2
Af	237.6511	mm2
d=	153.9999	mm
d'=	22.99995	mm
d''=	25.99995	mm
f_{fu} =	773	MPA
E_f =	38000	MPA
f'_{fu} =	450	MPA
span properties:		
L=	1500	mm
a=	500	mm

section properties		
h=	7.08661	in
b=	5.11811	in
f'c	8.29616	ksi
E_c =	5191.746	ksi
E_s =	29007.56	ksi
A'f	0.08765	in^2
Af	0.36836	in^2
d=	6.06299	in
d'=	0.90551	in
d''=	1.02362	in
f_{fu} =	112.1142	ksi
E_f =	5511.437	ksi
f'_{fu} =	65.26702	ksi
span properties:		
L=	59.05512	in
a=	19.68504	in

Table 4.1 Initial parameters for Sample BC2HA in both Metric and English units.

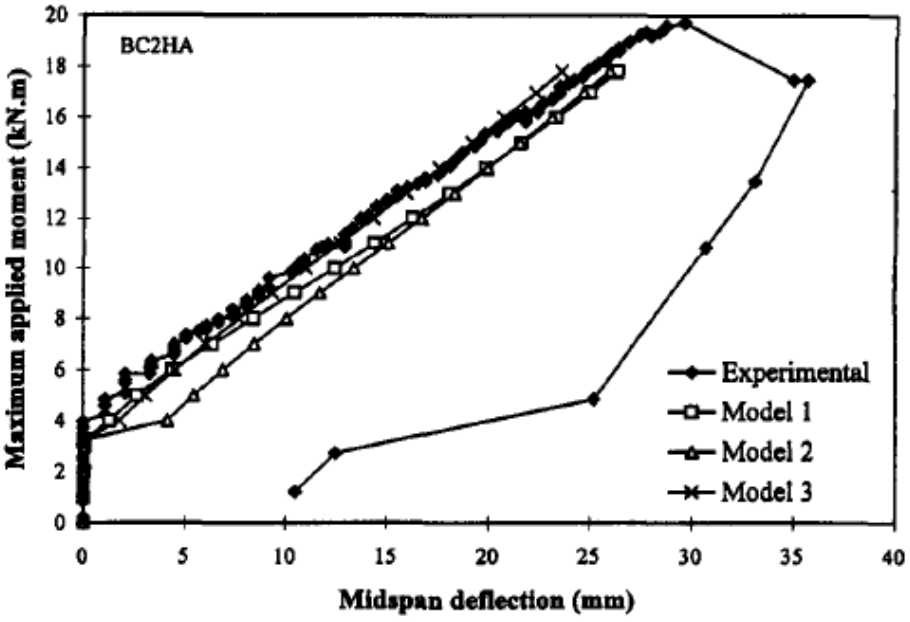

Figure 4.1 Experimental BC2HA deflection graph from Theriault and Benmokrane (1998).

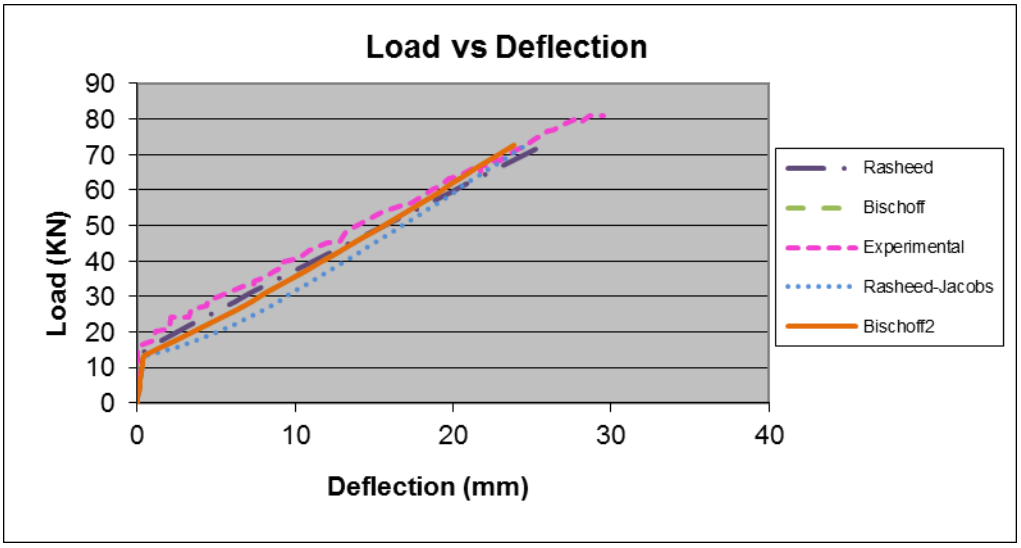

Figure 4.2 Experimental BC2HA load-deflection response in comparison with four models from the Rasheed-Jacobs Program.

Figure 4.2 shows that although load-deflection curves are not exactly the same, they are all within the same range, which is reassuring. We do not expect any model to match the experimental results perfectly, although that is the ultimate goal. Also, by comparing Figure 4.1 to 4.2, it can be shown that the experimental deflections were digitized from the Theriault and Benmokrane curve accurately. Therefore, BC2HA confirms that this program is accurate.

The second sample used for verification was F1 (Pecce et al, 2000), with a similar crushing mode of failure. Similar to the first sample, both the Metric and English parameters are given for F1, as well as the original experimental load-deflection graph and the new load-deflection comparison graph with the four models included. However, for this sample F1, an original experimental moment-curvature graph is also shown as well as the new moment-curvature comparison graph with the four models included. It can be shown that not only does the experimental load-deflection response correspond consistently to the numerical load-

deflections used for checking the accuracy of this program, but the moment-curvature response correctly corresponds to the Rasheed-Jacobs program results as well.

section properties		
h=	184.9999	mm
b=	500	mm
f'c	29.99997	MPA
E_c=	25868.92	MPA
E_s=	200000	MPA
A'f	253.3479	mm2
Af	886.7402	mm2
d=	145	mm
d'=	39.99992	mm
d''=	39.99992	mm
f_{fu}=	600	MPA
E_f=	42000	MPA
f'_{fu}=	600	MPA
span properties:		
L=	3400	mm
a=	1200	mm

section properties		
h=	7.28346	in
b=	19.68504	in
f'c	4.35113	ksi
E_c=	3759.896	ksi
E_s=	29007.56	ksi
A'f	0.39269	in^2
Af	1.37445	in^2
d=	5.70866	in
d'=	1.5748	in
d''=	1.5748	in
f_{fu}=	87.02269	ksi
E_f=	6091.589	ksi
f'_{fu}=	87.02269	ksi
span properties:		
L=	133.8583	in
a=	47.24409	in

Table 4.2 Initial parameters for Sample F1 in both Metric and English units.

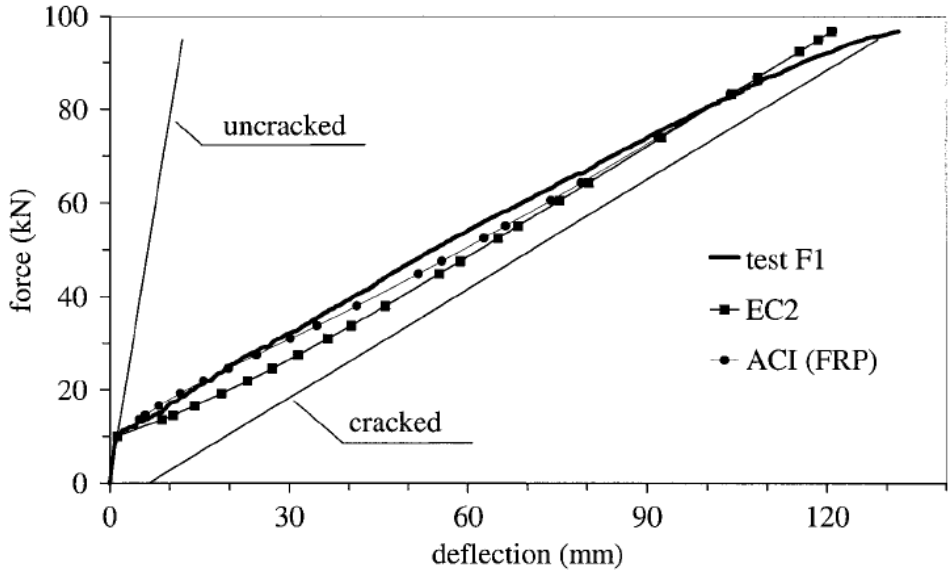

Figure 4.3 Experimental F1 load-deflection graph from Pecce et al (2000).

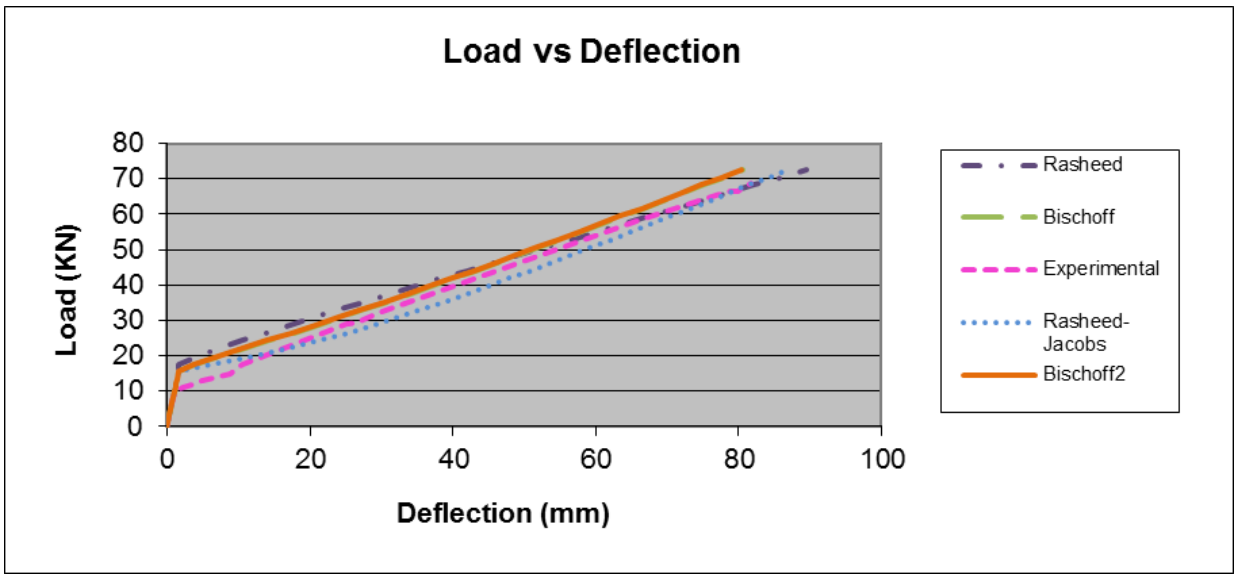

Figure 4.4 Experimental F1 load-deflection response in comparison to 4.3 with four models from the Rasheed-Jacobs Program.

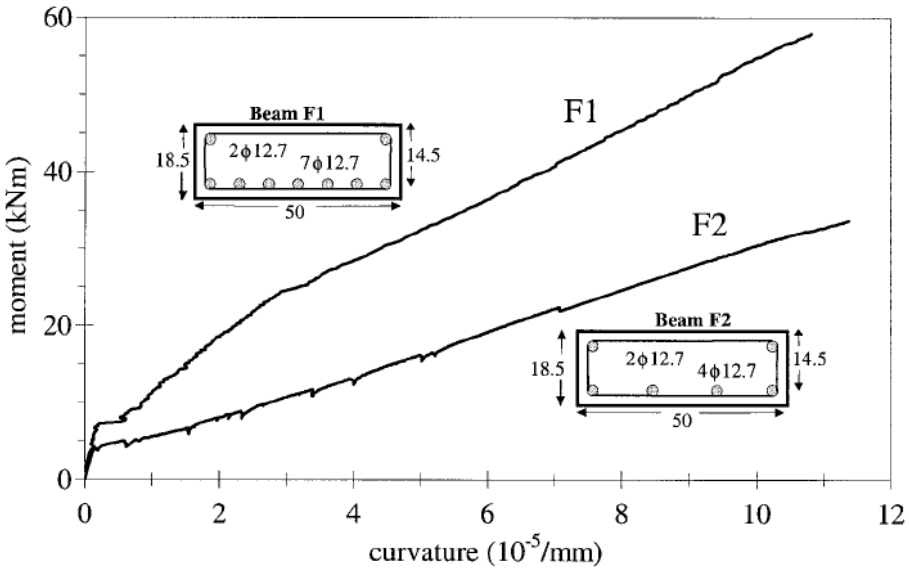

Figure 4.5 Experimental F1 moment-curvature graph from Pecce et al (2000).

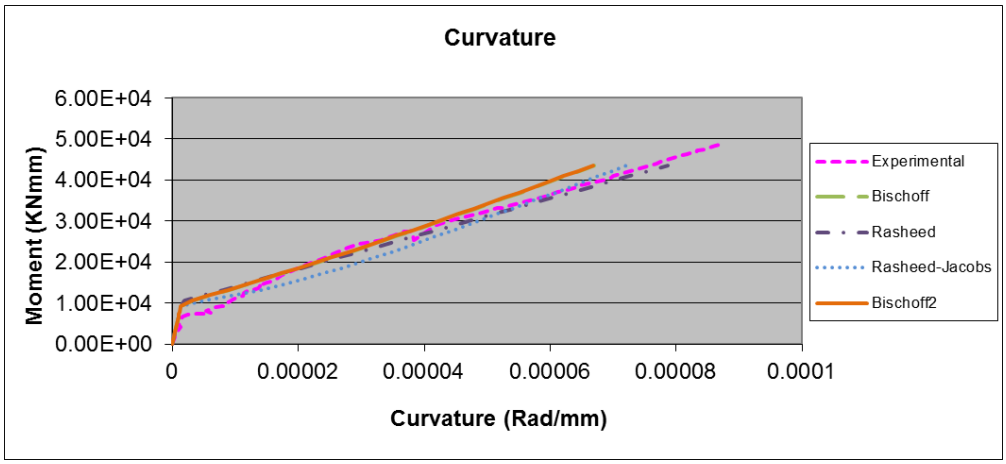

Figure 4.6 Experimental F1 moment-curvature response comparison to 4.5 with four models from the Rasheed-Jacobs Program.

The third sample used for verification was Group3 (Almusallam, 1997), with a similar mode of crushing failure. This sample has its Metric and English parameters tabulated in Table 4.3. The load-deflection comparisons are shown in Figures 4.7 and 4.8, and the moment-curvature comparisons are shown in Figures 4.9 and 4.10. The load-deflection and moment-curvature curves, similar to the previous examples, correlates accurately, Therefore, they validate the crushing program developed by Rasheed-Jacobs.

section properties		
h=	260	mm
b=	200.0001	mm
f'c	31.29997	MPA
E_c =	26423.47	MPA
E_s =	200000	MPA
A'f	30.67736	mm2
Af	506.7087	mm2
d=	218.0001	mm
d'=	37.99992	mm
d''=	41.99992	mm
f_{fu} =	886	MPA
E_f =	43370	MPA
f'_{fu} =	886	MPA
span properties:		
L=	2700	mm
a=	1250	mm

section properties		
h=	10.23622	in
b=	7.87402	in
f'c	4.53968	ksi
E_c =	3840.497	ksi
E_s =	29007.56	ksi
A'f	0.04755	in^2
Af	0.7854	in^2
d=	8.58268	in
d'=	1.49606	in
d''=	1.65354	in
f_{fu} =	128.5035	ksi
E_f =	6290.29	ksi
f'_{fu} =	128.5035	ksi
span properties:		
L=	106.2992	in
a=	49.2126	in

Table 4.3 Initial parameters for sample Group3 in both Metric and English units.

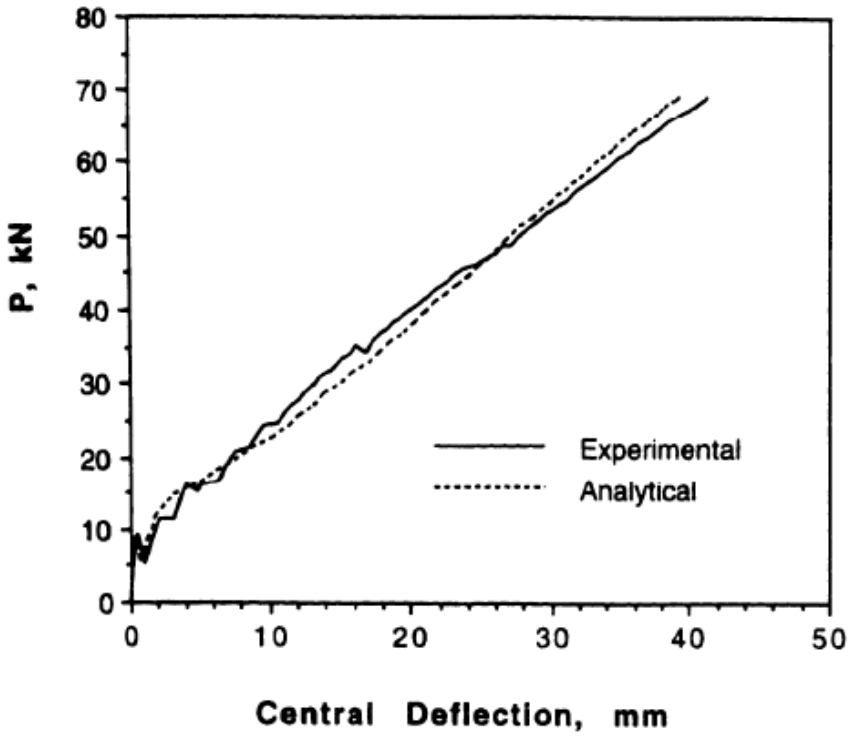

Figure 4.7 Experimental Group3 load-deflection graph from Almusallam (1997).

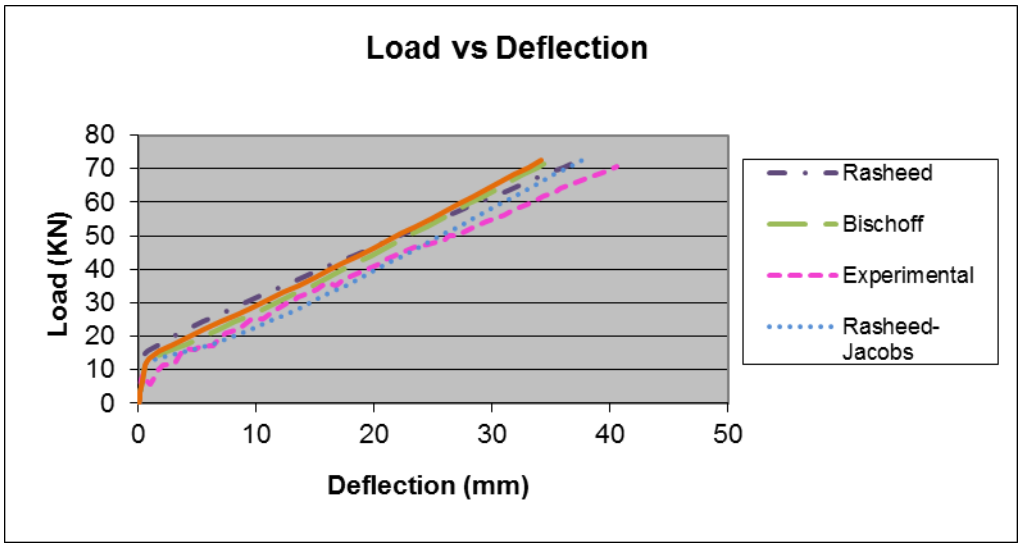

Figure 4.8 Experimental Group3 load-deflection response for Group3 in comparison to 4.7 with four models from the Rasheed-Jacobs Program.

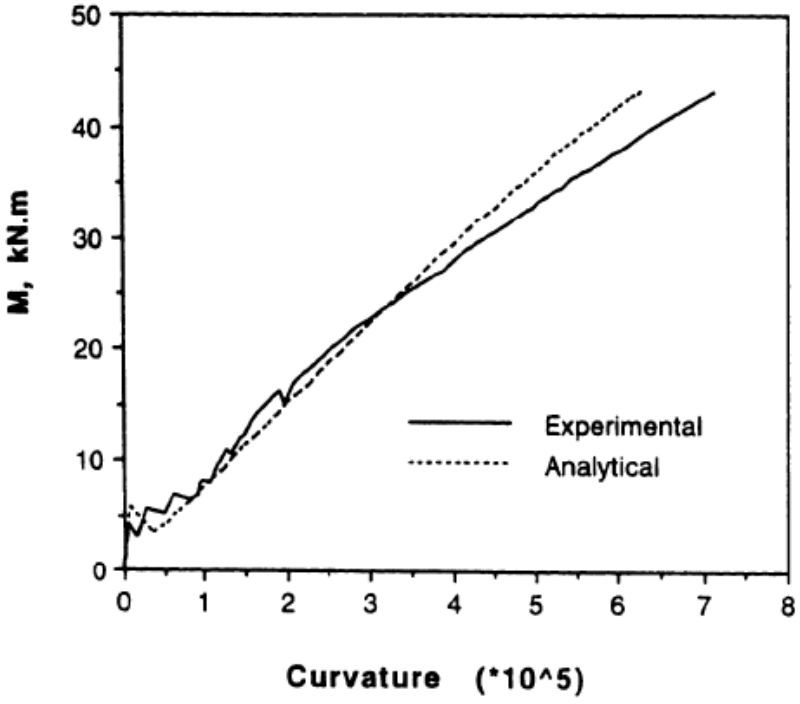

Figure 4.9 Experimental Group3 moment-curvature graph from Almusallam (1997).

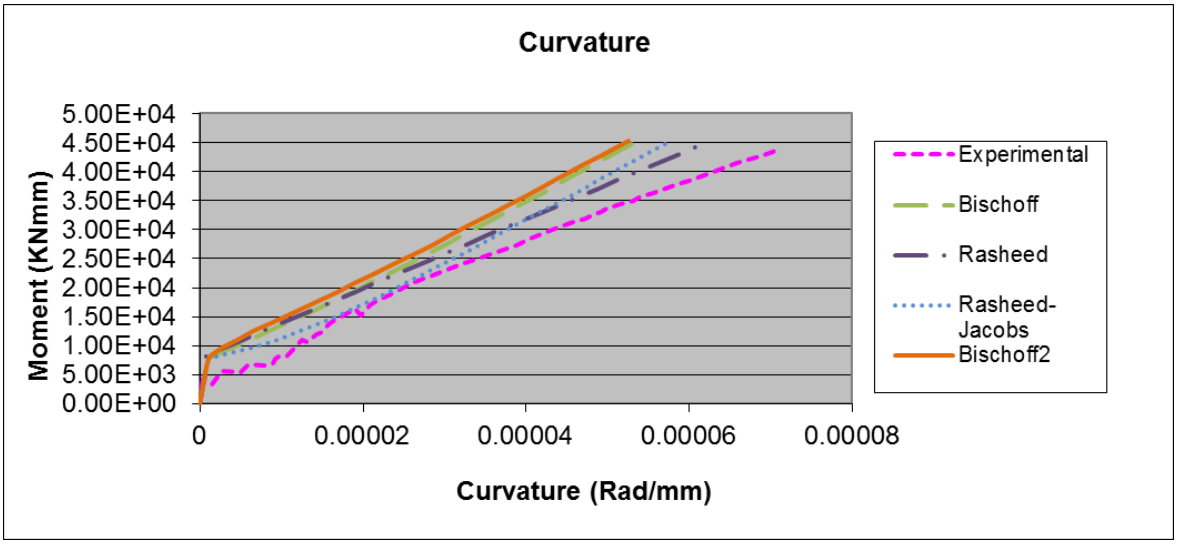

Figure 4.10 Experimental Group3 moment-curvature response in comparison to 4.9 with four models from the Rasheed-Jacobs Program.

4.3 Rupture Failure Mode Results

Three rupture samples were used to check the validity and accuracy of the rupture option in the Rasheed-Jacobs Program. The first sample was BC1 (Al-Sunna, 2006), which has a failure mode of FRP rupture. Similar routine used for the crushing failure samples is used for the rupture failure samples. Therefore, for sample BC1, the Metric and English parameters are given in Table 4.4. The original experimental load-deflection and moment-curvature graphs from Al-sunna (2006), as well as the new load-deflection and moment-curvature graphs with the four-model comparison are included in Figures 4.11, 4.12, 4.13, and 4.14.

section properties		
h=	250	mm
b=	150	mm
f'c	55.39802	MPA
E_c =	35153.22	MPA
E_s =	31498.87	MPA
A'f	0	mm^2
Af	95.00626	mm^2
d=	221.8251	mm
d'=	0	mm
d''=	28.17495	mm
f_{fu} =	1449.946	MPA
E_f =	132995	MPA
f'_{fu} =	413.6852	MPA
span properties:		
L=	2300	mm
a=	766.9999	mm

section properties		
h=	9.84252	in
b=	5.90551	in
f'c	8.034808	ksi
E_c =	5109.314	ksi
E_s =	4568.528	ksi
A'f	0	in^2
Af	0.14726	in^2
d=	8.73327	in
d'=	0	in
d''=	1.10925	in
f_{fu} =	210.297	ksi
E_f =	19289.3	ksi
f'_{fu} =	60	ksi
span properties:		
L=	90.55118	in
a=	30.19685	in

Table 4.4 Initial parameters for sample BC1 for both Metric and English units.

Figure 4.11 shows the original load-curvature graph from Al-Sunna, which was used to convert to the equivalent experimental moment and curvature values used for the comparison graph. When the digitized values are recorded and converted for sample BC1, it can be shown through Figure 4.12, that this Rasheed-Jacobs rupture program is accurate for the moment-curvature analysis. Also, using the digitized values from Figure 4.13, the positive deflections were determined and used for comparison in Figure 4.14, which shows that the rupture program is accurate for load-deflection analysis as well.

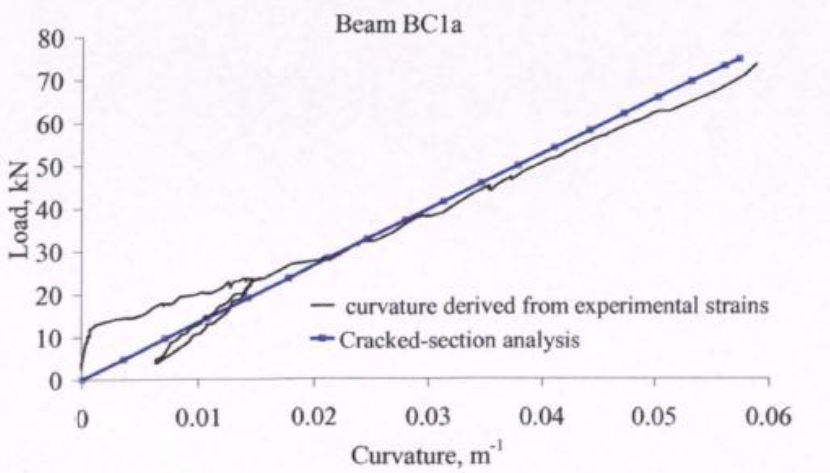

Figure 4.11 Experimental load-curvature graph for BC1 from Al-Sunna (2006).

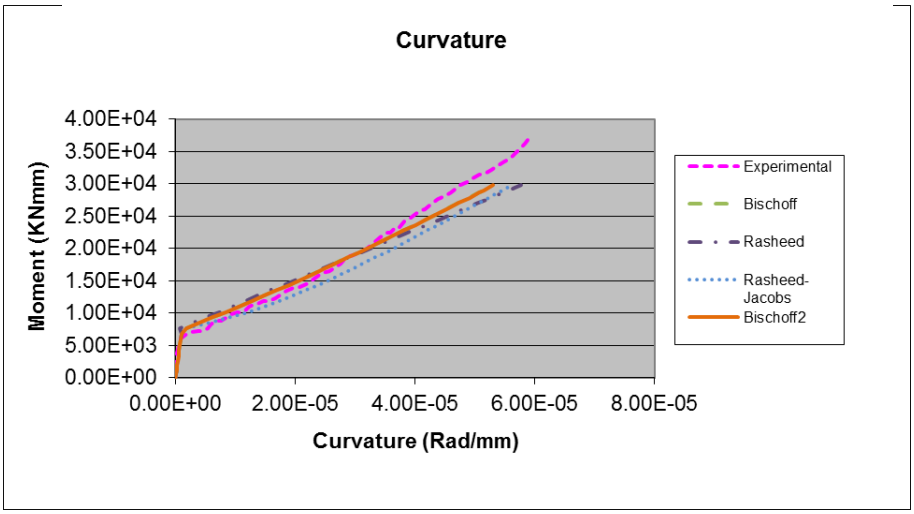

Figure 4.12 Experimental moment-curvature graph for BC1 in comparison to four models from the Rasheed-Jacobs Program.

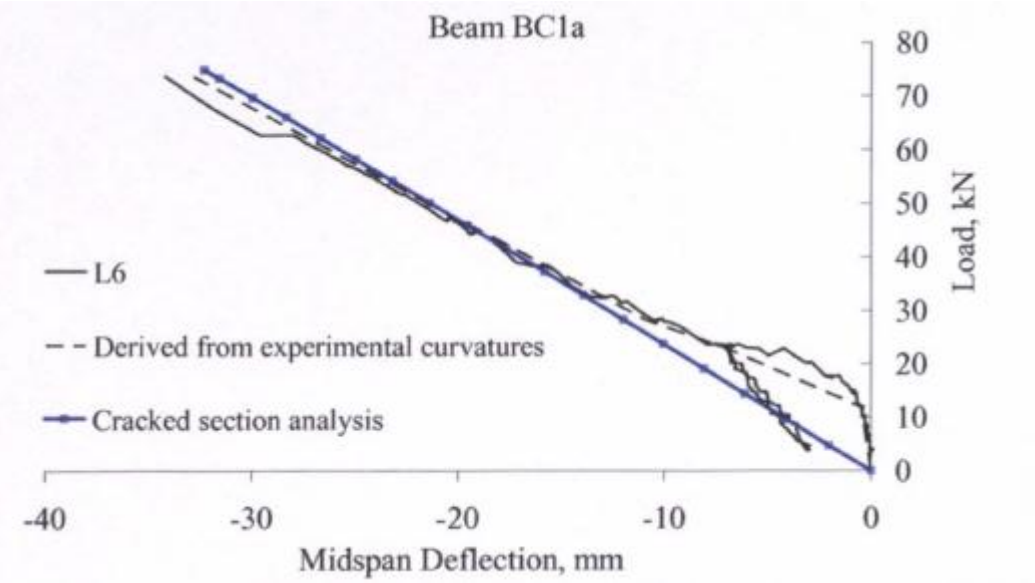

Figure 4.13 Experimental load-deflection graph for sample BC1 from Al-Sunna (2006).

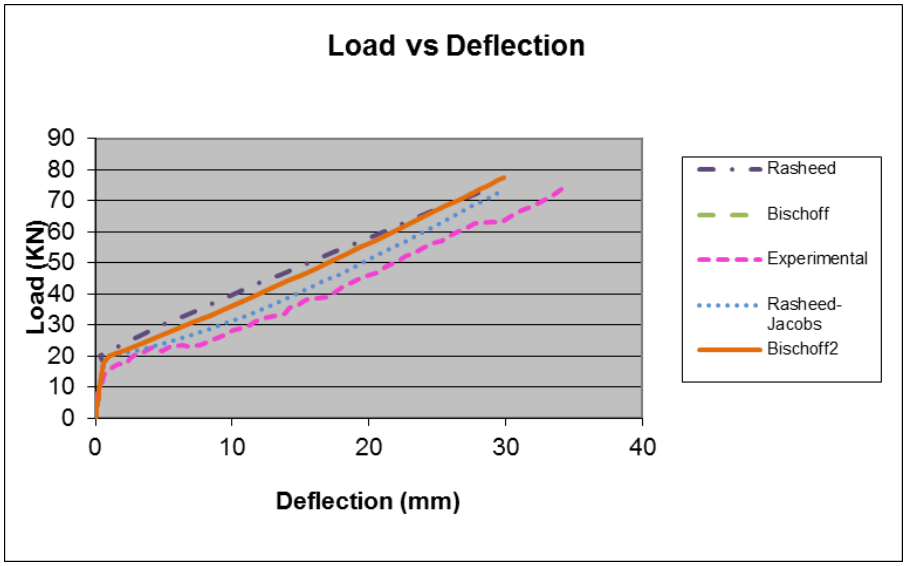

Figure 4.14 Experimental load-deflection graph for BC1 in comparison to four models from the Rasheed-Jacobs Program.

The second rupture sample is ISO3 (Benmokrane et al., 1996). For ISO3, the Metric and English parameters are given in Table 4.5, and the original experimental load-deflection graph from Benmokrane et al. (1996), as well as the new load-deflection comparison graph against the

four models is shown in Figure 4.15 and 16. This comparison provides added valid evidence that the rupture program is running correctly.

section properties		
h=	549.9999	mm
b=	200	mm
f'c	42.99846	MPA
E_c =	30970.23	MPA
E_s =	32998.82	MPA
A'f	112.903	mm^2
Af	573.0311	mm^2
d=	510	mm
d'=	33.00001	mm
d''=	39.99992	mm
f_{fu} =	689.9752	MPA
E_f =	41998.5	MPA
f'_{fu} =	299.9893	MPA
span properties:		
L=	3000	mm
a=	1000	mm

section properties		
h=	21.65354	in
b=	7.874016	in
f'c	6.236403	ksi
E_c =	4501.341	ksi
E_s =	4786.077	ksi
A'f	0.175	in^2
Af	0.8882	in^2
d=	20.07874	in
d'=	1.299213	in
d''=	1.5748	in
f_{fu} =	100.0725	ksi
E_f =	6091.371	ksi
f'_{fu} =	43.50979	ksi
span properties:		
L=	118.1102	in
a=	39.37008	in

Table 4.5 Initial parameters for sample ISO3 in both Metric and English units.

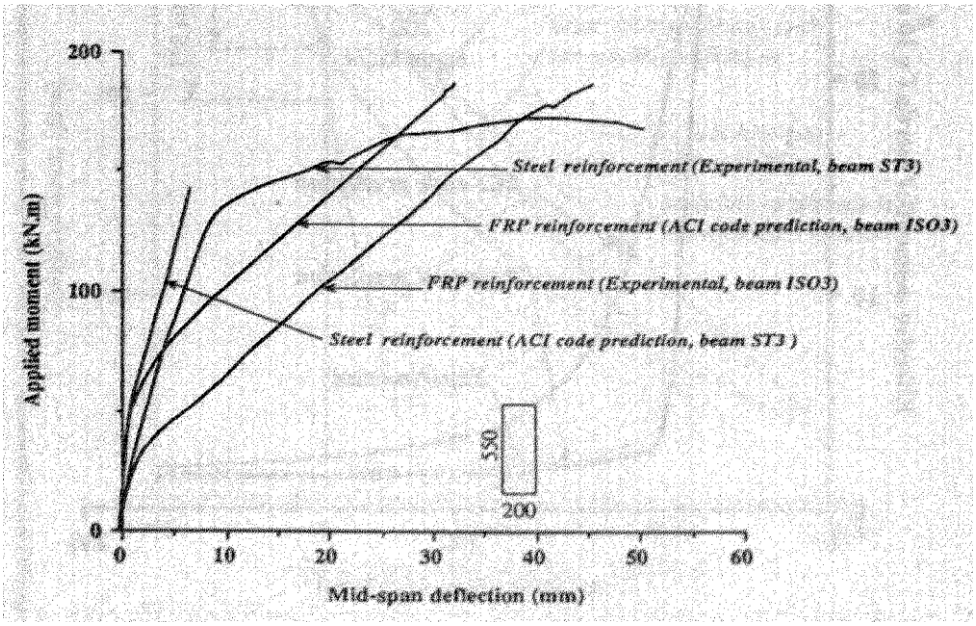

Figure 4.15 Experimental load-deflection graph for sample ISO3 from Benmokrane et al. (1996).

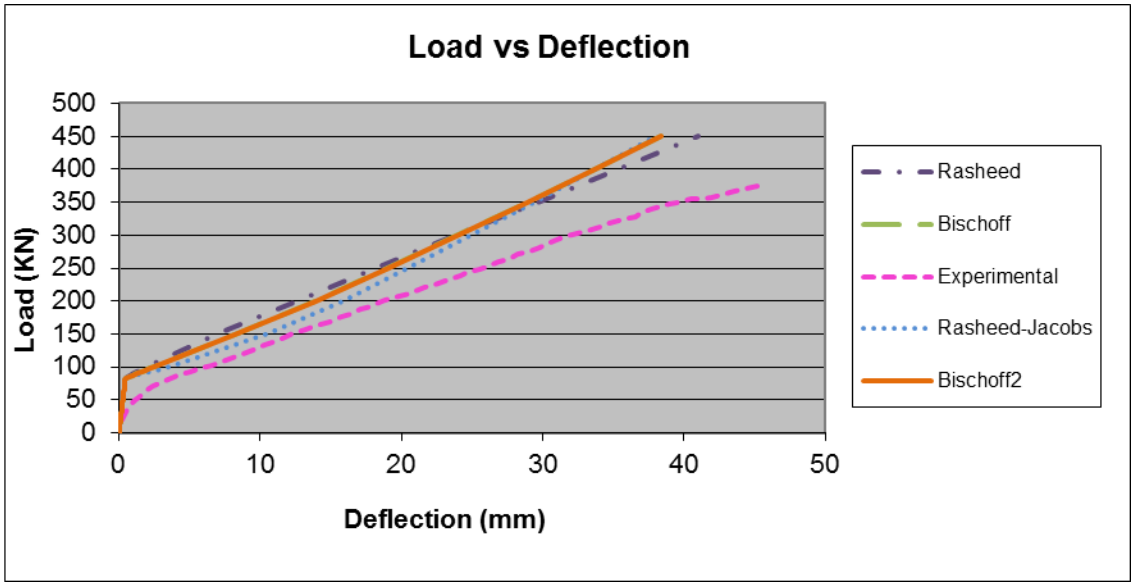

Figure 4.16 Experimental load-deflection curve for sample ISO3 in comparison to four models from the Rasheed-Jacobs Program.

Although the experimental load-deflection graph does not completely line-up with the four models in Figure 4.16, it can still be said that the rupture program is accurate. This statement can be made, because the experimental deflection still follows a similar pattern even though none of the four models accurately predicts this exact sample. In this specific sample, the four models uniformly under predict sample ISO3. However these four models can accurately predict other samples such as the first rupture sample BC1, and the next rupture sample BG1.

The third rupture sample used for accuracy and validity is BG1 (AlSunna, 2006). This sample, similar to BC1, provides validity with both the moment-curvature and the load-deflection graphs shown in Figures 4.17, 4.18, 4.19, and 4.20. Also, the initial parameters are given for BG1 in both Metric and English units in Table 4.6.

section properties		
h=	250	mm
b=	150	mm
f'c	47.6983	MPA
E_c =	32618.9	MPA
E_s =	31498.87	MPA
A'f	0	mm^2
Af	95.00626	mm^2
d=	221.8251	mm
d'=	0	mm
d''=	28.17495	mm
f_{fu} =	664.9762	MPA
E_f =	42748.5	MPA
f'_{fu} =	413.6852	MPA
span properties:		
L=	2300	mm
a=	766.9999	mm

section properties		
h=	9.84252	in
b=	5.90551	in
f'c	6.918057	ksi
E_c =	4740.967	ksi
E_s =	4568.528	ksi
A'f	0	in^2
Af	0.14726	in^2
d=	8.73327	in
d'=	0	in
d''=	1.10925	in
f_{fu} =	96.4467	ksi
E_f =	6200.15	ksi
f'_{fu} =	60	ksi
span properties:		
L=	90.55118	in
a=	30.19685	in

Table 4.6 Initial parameters for sample BG1 in both Metric and English units.

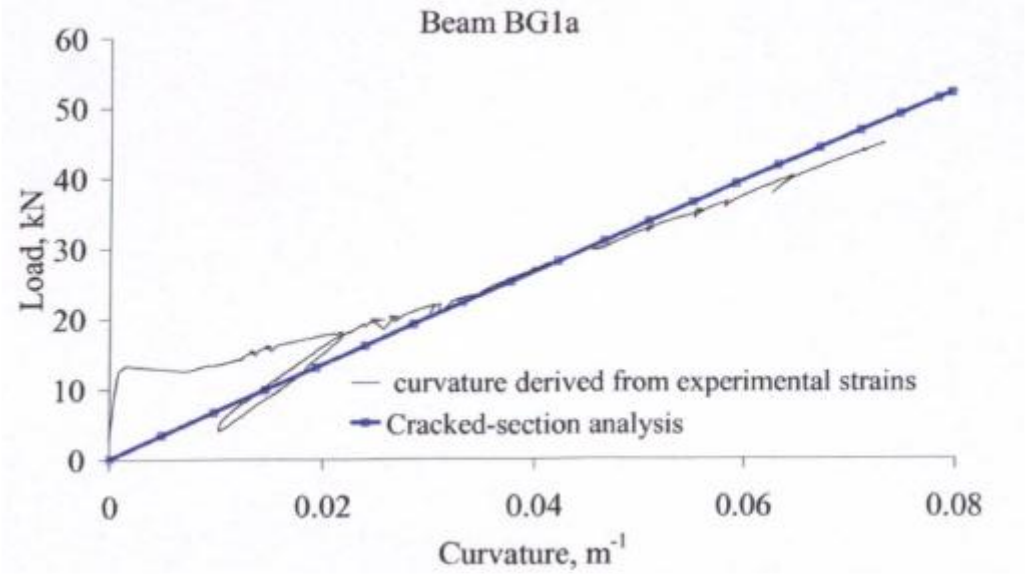

Figure 4.17 Experimental load-curvature graph for sample BG1 from Al-Sunna (2006).

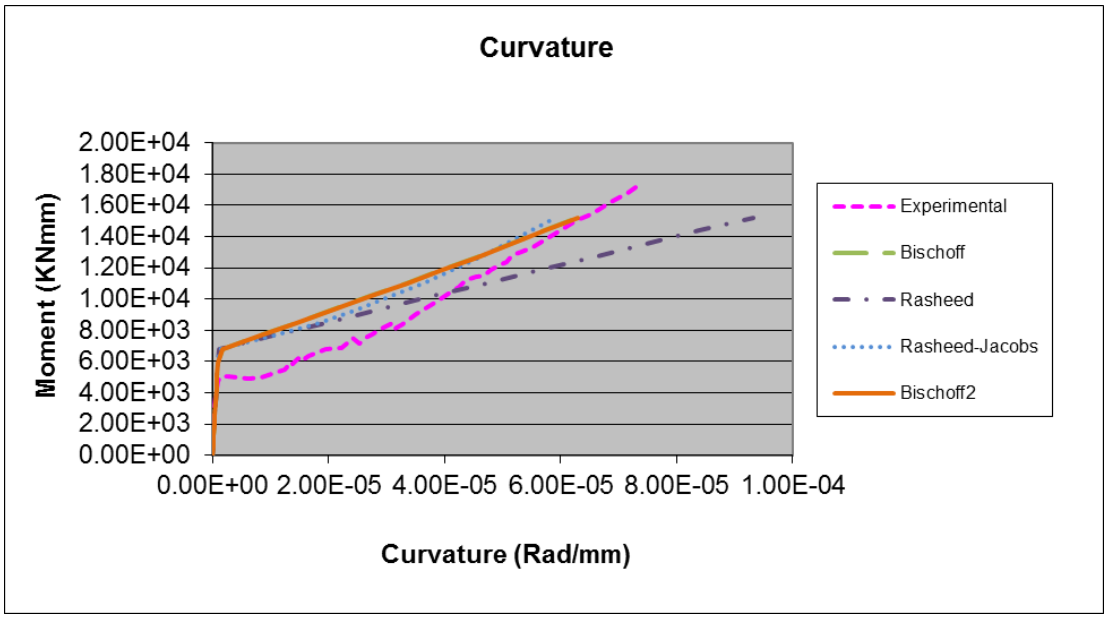

Figure 4.18 Experimental moment-curvature response for sample BG1 in comparison to four models from the Rasheed-Jacobs Program.

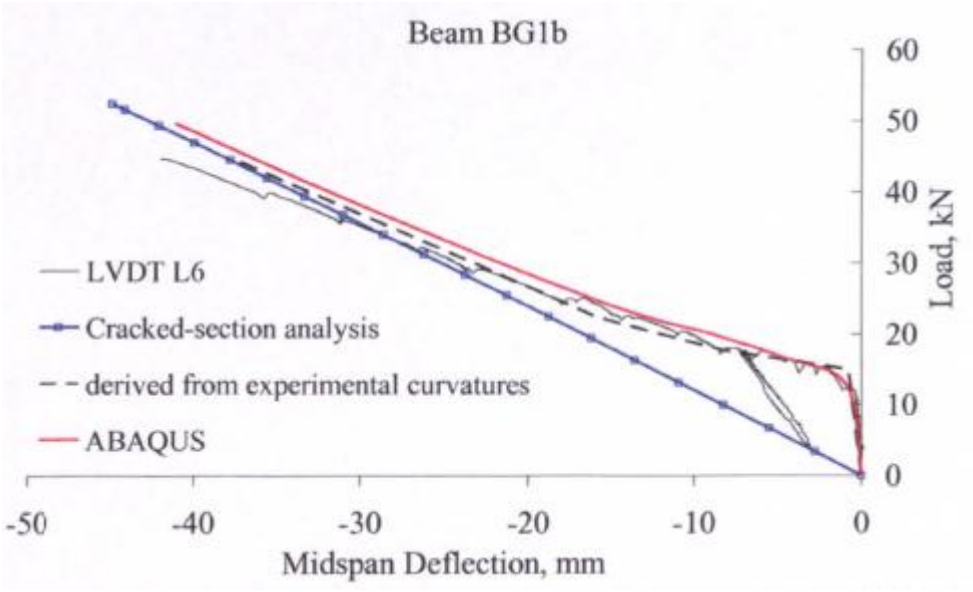

Figure 4.19 Experimental load-deflection graph for sample BG1 from Al-Sunna (2006).

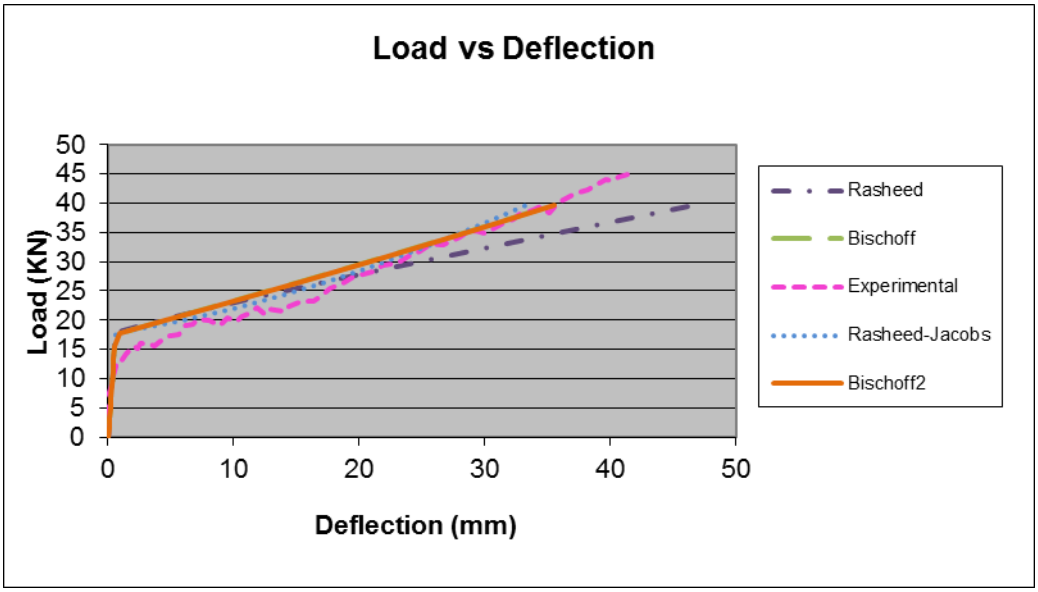

Figure 4.20 Experimental load-deflection response for sample BG1 in comparison to four models from the Rasheed-Jacobs Program.

It can be seen that the BG1 load-deflection graph in Figure 4.20 is the negative of the original experimental deflection values seen in Figure 4.19. This is an accurate representation of this comparison for BG1. With these three rupture samples shown, it can be said that the rupture option in the Rasheed-Jacobs program is accurate and is validated for further use in research and analyzing multiple samples for comparisons in the future.

Six samples, three failing in crushing and three failing in FRP rupture, were shown here to validate and check the Rasheed-Jacobs program for accuracy to ensure that further research done using this program will be adequate for multiple crushing or rupture samples in both Metric and English units.

4.4 Comparison of Database Samples

As previously stated, 56 independent samples from the Gross database were run through the Rasheed-Jacobs program. These 56 samples come from eleven different authors and will be sub-divided by their authors. Included for each of the 56 independent samples will be the table of initial parameters for both Metric and English, the numerical load-deflection graph for each sample, and a deflection bar chart. The bar chart consists of the ratio of the calculated deflection from each of the four models including Bischoff, Bischoff2, Rasheed, and Rasheed-Jacobs to the experimental deflection. These model ratios are then compared for unity to see how close each predicted deflection is to the actual. Therefore, the closer the bar for each specific model is to unity on the vertical axis, the better the deflection that the model predicts. Bars shorter than unity represents under predictions and bars exceeding unity represent over prediction, with unity being consistent with the value of 1 on the vertical axis.

4.4.1 Faza (1991)

Three independent Faza samples were used in this research including ED, EE, and EVH1. Also, two dependent samples were used, including EF and EVH2, which were investigated by merely comparing the already calculated deflection with the experimental deflection from Gross database. Where EF is dependent on ED and EVH2 is dependent on EVH1. The independent samples were best represented by the Rasheed-Jacobs model, which can be seen in the following bar charts. When the deflection from EF and EVH2 were compared to the experimental deflections from the Gross database, the Rahseed-Jacobs model was also the best qualified

model. Overall, the Rasheed-Jacobs model best represented the experimental results for the Faza dependent and independent samples in all three moment levels investigated.

4.4.1.1 – Sample ED

section properties		
h=	304.8	mm
b=	152.4	mm
f'c	51.71065	MPA
E_c =	33963.15	MPA
E_s =	28957.96	MPA
A'f	63.22568	mm^2
Af	380.6444	mm^2
d=	273.05	mm
d'=	28.575	mm
d''=	31.75	mm
f_{fu} =	737.7386	MPA
E_f =	49642.22	MPA
f'_{fu} =	413.6852	MPA
span properties:		
L=	2743.2	mm
a=	914.4	mm

section properties		
h=	12	in
b=	6	in
f'c	7.5	ksi
E_c =	4936.345	ksi
E_s =	4200	ksi
A'f	0.098	in^2
Af	0.59	in^2
d=	10.75	in
d'=	1.125	in
d''=	1.25	in
f_{fu} =	107	ksi
E_f =	7200	ksi
f'_{fu} =	60	ksi
span properties:		
L=	108	in
a=	36	in

Table 4.7 Initial parameters for Faza sample ED.

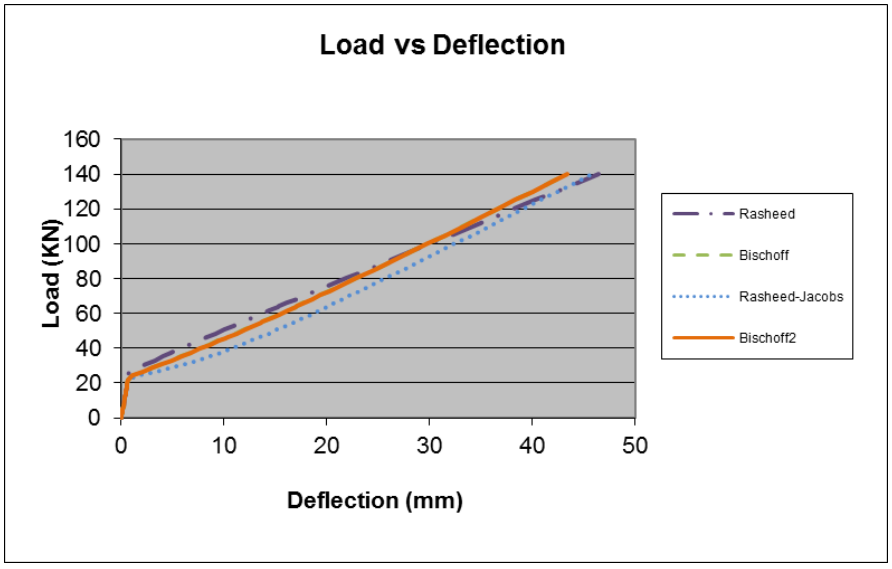

Figure 4.21 Load-deflection response for sample ED.

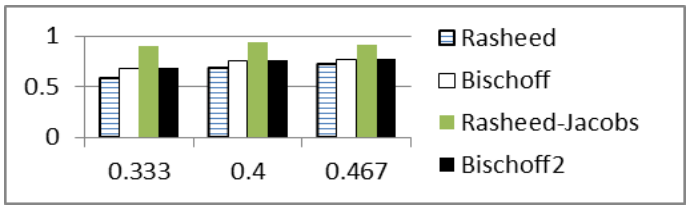

Table 4.8 Deflection comparison bar chart for sample ED.

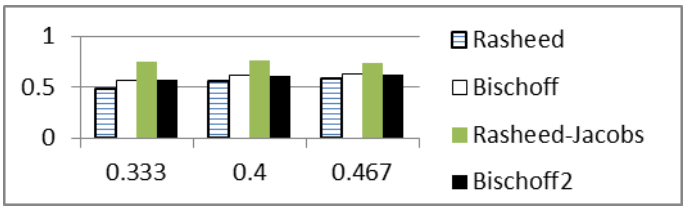

Table 4.9 Deflection comparison bar chart for dependent sample EF.

4.4.1.2 –Sample EE

section properties		
h=	304.8	mm
b=	152.4	mm
f'c	51.71065	MPA
E_c =	33963.15	MPA
E_s =	28957.96	MPA
A'f	63.22568	mm^2
Af	354.838	mm^2
d=	274.6375	mm
d'=	28.575	mm
d''=	30.1625	mm
f_{fu} =	896.3179	MPA
E_f =	49642.22	MPA
f'_{fu} =	413.6852	MPA
span properties:		
L=	2743.2	mm
a=	914.4	mm

section properties		
h=	12	in
b=	6	in
f'c	7.5	ksi
E_c =	4936.345	ksi
E_s =	4200	ksi
A'f	0.098	in^2
Af	0.55	in^2
d=	10.8125	in
d'=	1.125	in
d''=	1.1875	in
f_{fu} =	130	ksi
E_f =	7200	ksi
f'_{fu} =	60	ksi
span properties:		
L=	108	in
a=	36	in

Table 4.10 Initial parameters for Faza sample EE.

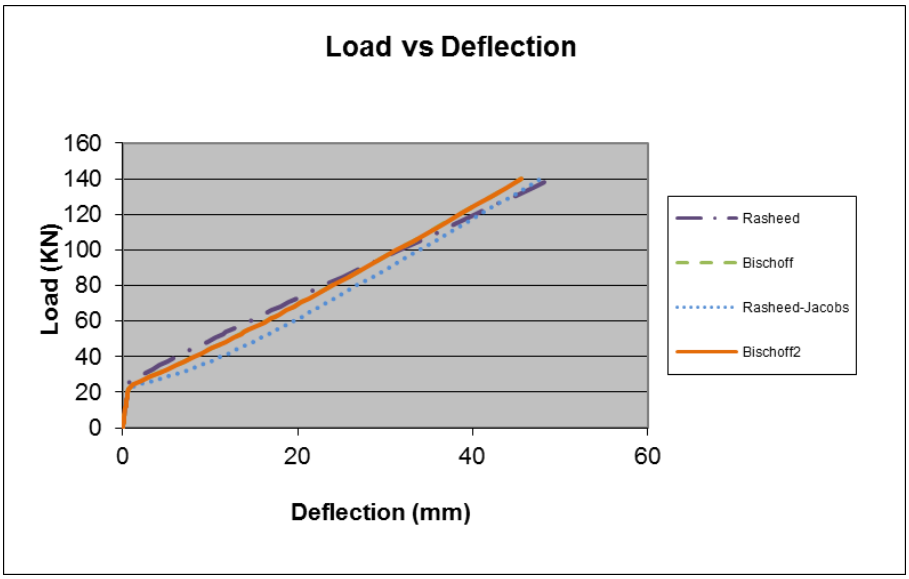

Figure 4.22 Load-deflection response for sample EE.

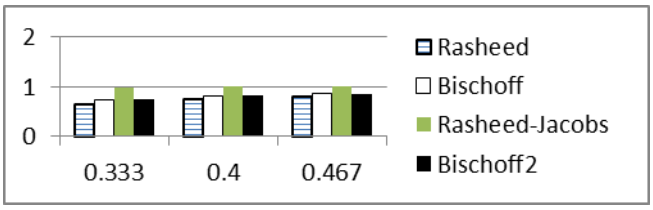

Table 4.11 Deflection comparison bar chart for sample EE.

4.4.1.3 – Sample EVH1

section properties		
h=	304.8	mm
b=	152.4	mm
f'c	68.94753	MPA
E_c =	39217.27	MPA
E_s =	31715.86	MPA
A'f	63.22568	mm^2
Af	380.6444	mm^2
d=	273.05	mm
d'=	28.575	mm
d''=	31.75	mm
f_{fu} =	737.7386	MPA
E_f =	49642.22	MPA
f'_{fu} =	413.6852	MPA
span properties:		
L=	2743.2	mm
a=	914.4	mm

section properties		
h=	12	in
b=	6	in
f'c	10	ksi
E_c =	5700	ksi
E_s =	4600	ksi
A'f	0.098	in^2
Af	0.59	in^2
d=	10.75	in
d'=	1.125	in
d''=	1.25	in
f_{fu} =	107	ksi
E_f =	7200	ksi
f'_{fu} =	60	ksi
span properties:		
L=	108	in
a=	36	in

Table 4.12 Initial parameters for Faza sample EVH1.

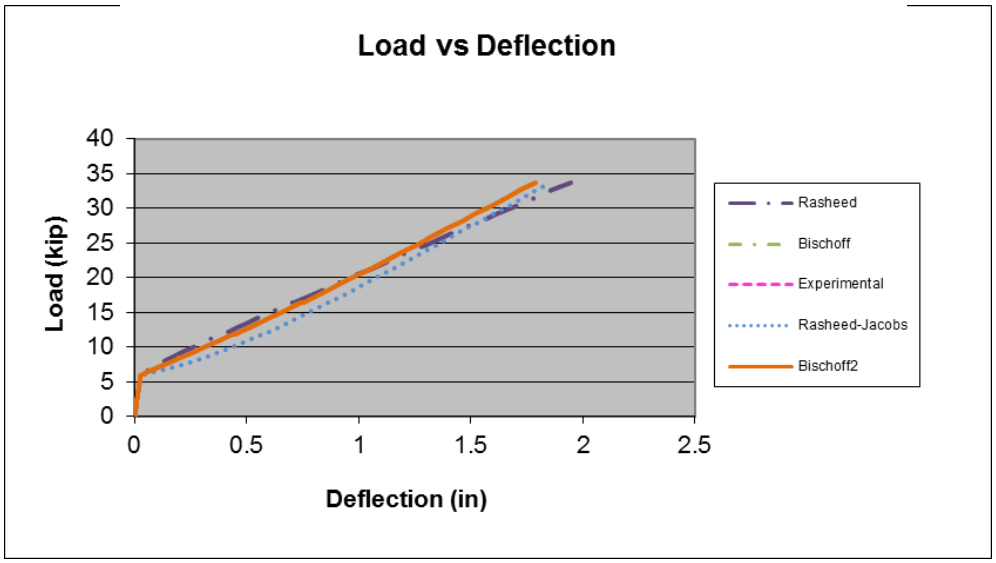

Figure 4.23 Load-deflection response for sample EVH1.

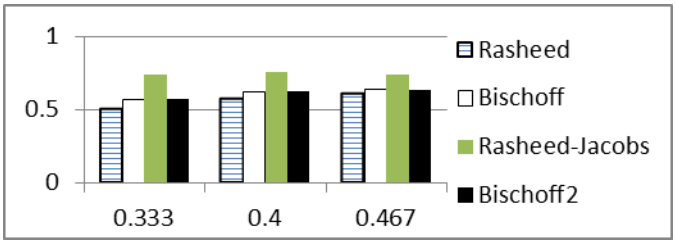

Table 4.13 Deflection comparison bar chart for sample EVH1.

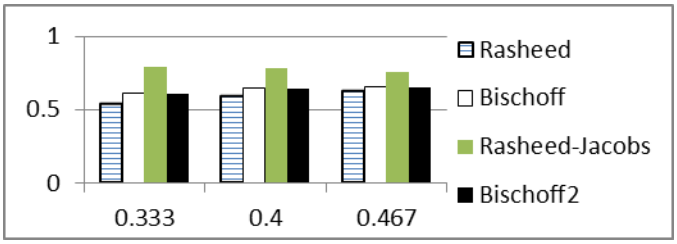

Table 4.14 Deflection comparison bar chart for dependent sample EVH2.

4.4.2 Kakizawa et al. (1993)

One Kakizawa et al. independent sample was used in this research, which is labeled as sample 2. No dependent samples were provided by the Kakizawa's research in the Gross database. Sample 2 was best represented by the Bischoff model for moment levels of $0.333M_n$ and $0.400M_n$. However, the moment level of $0.467M_n$ for the Kakizawa sample 2 was best represented by the Bischoff2 model. This sample was slightly over predicted by the Rasheed-Jacobs model.

section properties		
h=	150	mm
b=	100	mm
f'c	35.29874	MPA
E_c =	28060.64	MPA
E_s =	27299.02	MPA
A'f	0	mm^2
Af	78.59984	mm^2
d=	112.5	mm
d'=	0	mm
d''=	37.5	mm
f_{fu} =	1577.552	MPA
E_f =	129995.3	MPA
f'_{fu} =	0	MPA
span properties:		
L=	1700	mm
a=	700	mm

section properties		
h=	5.905512	in
b=	3.937008	in
f'c	5.119652	ksi
E_c =	4078.449	ksi
E_s =	3959.391	ksi
A'f	0	in^2
Af	0.12183	in^2
d=	4.429134	in
d'=	0	in
d''=	1.476378	in
f_{fu} =	228.8047	ksi
E_f =	18854.24	ksi
f'_{fu} =	0	ksi
span properties:		
L=	66.92914	in
a=	27.55906	in

Table 4.15 Initial parameters for Kakizawa et al. sample 2.

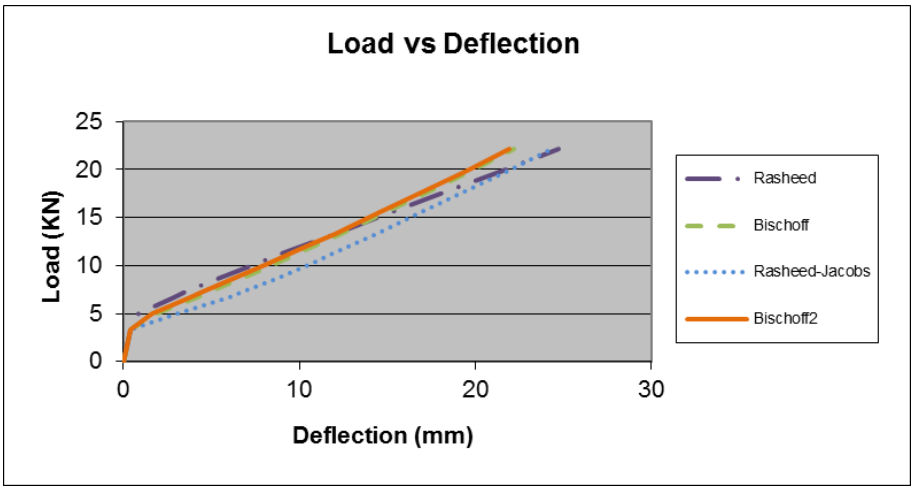

Figure 4.24 Load-deflection response for sample 2.

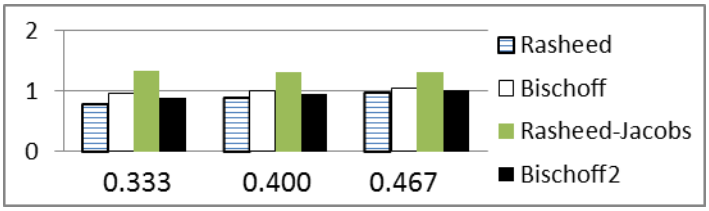

Table 4.16 Deflection comparison bar chart for sample 2.

4.4.3 Nakano et al. (1993)

One independent sample was used from the Nakano et al. paper which was RC-C1, and no dependent samples were used from Nakano's research in the Gross database. The Bischoff model best represented the RC-C1 sample in all three moment levels. The Rasheed-Jacobs model slightly over predicted the deflection for this sample, and therefore is on the conservative side for calculations compared to the other three deflection models.

section properties		
h=	299.9999	mm
b=	200	mm
f'c	29.42888	MPA
E_c =	25621.51	MPA
E_s =	20894.55	MPA
A'f	399.9992	mm^2
Af	399.9992	mm^2
d=	245	mm
d'=	54.99999	mm
d''=	54.99992	mm
f_{fu} =	1461.619	MPA
E_f =	119622.7	MPA
f'_{fu} =	1461.619	MPA
span properties:		
L=	2400	mm
a=	900	mm

section properties		
h=	11.81102	in
b=	7.874016	in
f'c	4.2683	ksi
E_c =	3723.937	ksi
E_s =	3030.5	ksi
A'f	0.62	in^2
Af	0.62	in^2
d=	9.645669	in
d'=	2.165354	in
d''=	2.165351	in
f_{fu} =	211.99	ksi
E_f =	17349.82	ksi
f'_{fu} =	211.99	ksi
span properties:		
L=	94.48819	in
a=	35.43307	in

Table 4.17 Initial parameters for Nakano et al. sample RC-C1.

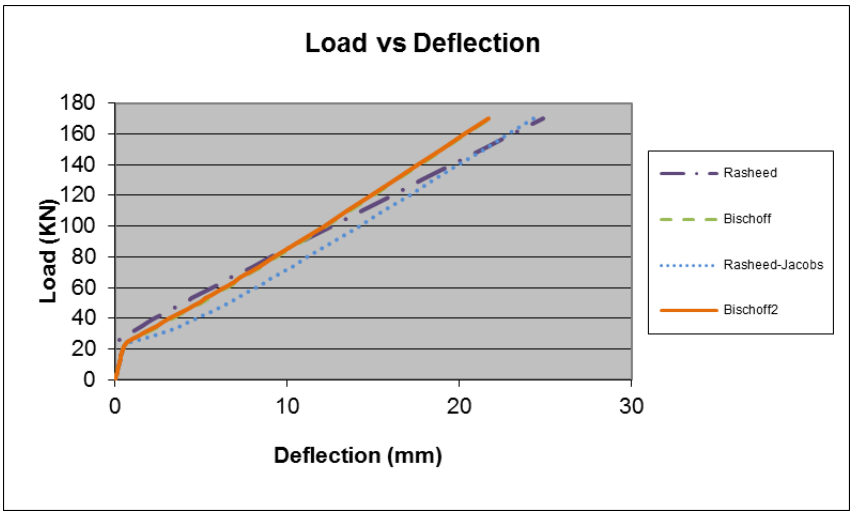

Figure 4.25 Load-deflection response for sample RC-C1.

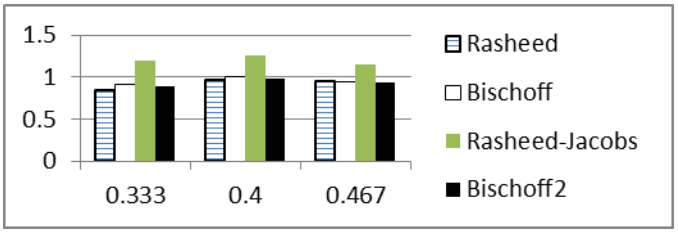

Table 4.18 Deflection comparison bar chart for sample RC-C1.

4.4.4 Benmokrane et al. (1996)

Two independent samples were used from Benmokrane et al. which are referred to as ISO1 and ISO3 as well as one dependent sample, ISO2, which is dependent on ISO1. ISO3 is the only sample from the Gross database that failed in rupture mode, and was best represented by Rasheed-Jacobs model in all three moment levels. ISO1 and ISO2 were both best represented by the Rasheed model in all three moment levels investigated. The ISO2 sample produces the same

load-deflection response at ISO1, with only the experimental deflection changing as shown in the bar chart in Tables 4.20 and 4.21.

4.4.4.1 – Sample ISO1

section properties		
h=	11.81102	in
b=	7.874016	in
f'c	6.236403	ksi
E_c =	4501.341	ksi
E_s =	4786.077	ksi
A'f	0.175	in^2
Af	0.8882	in^2
d=	10.23622	in
d'=	1.299213	in
d''=	1.5748	in
f_{fu} =	100.0725	ksi
E_f=	6091.371	ksi
f'_{fu} =	43.50979	ksi
span properties:		
L=	118.1102	in
a=	39.37008	in

section properties		
h=	299.9999	mm
b=	200	mm
f'c	42.99846	MPA
E_c =	30970.23	MPA
E_s =	32998.82	MPA
A'f	112.903	mm^2
Af	573.0311	mm^2
d=	260	mm
d'=	33.00001	mm
d''=	39.99992	mm
f_{fu} =	689.9752	MPA
E_f=	41998.5	MPA
f'_{fu} =	299.9893	MPA
span properties:		
L=	3000	mm
a=	1000	mm

Table 4.19 Initial parameters for Benmokrane et al. sample ISO1.

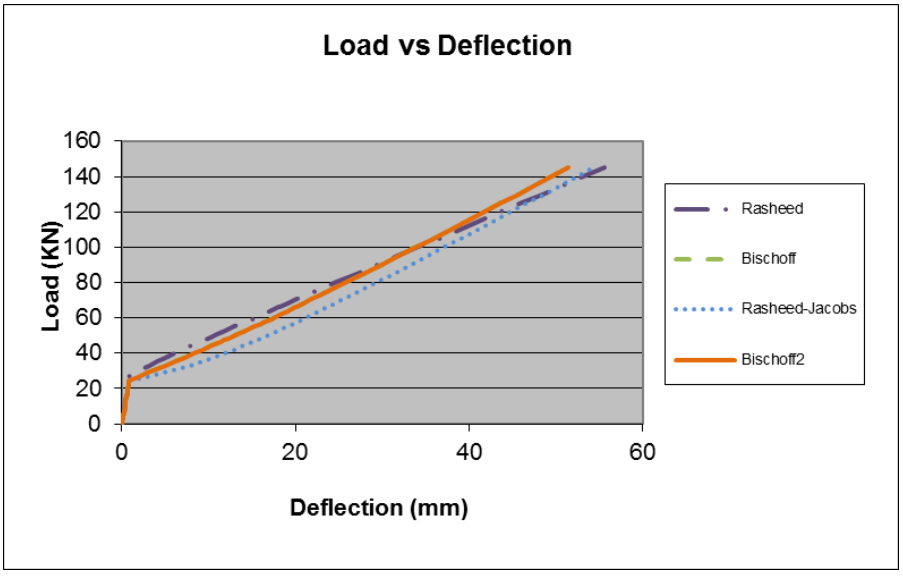

Figure 4.26 Load-deflection response for sample ISO1.

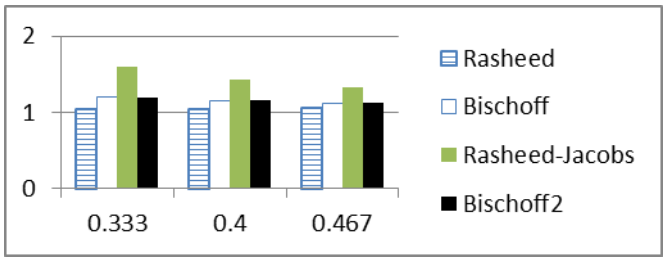

Table 4.20 Deflection comparison bar chart for sample ISO1.

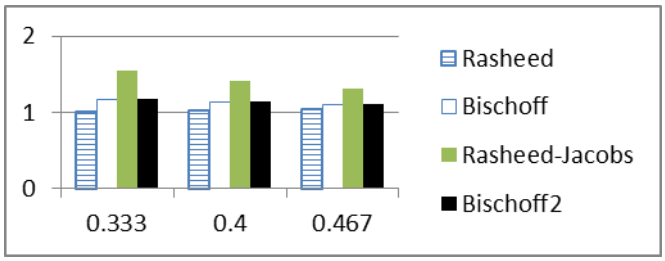

Table 4.21 Deflection comparison bar chart for dependent sample ISO2.

4.4.4.2 – Sample ISO3

section properties		
h=	549.9999	mm
b=	200	mm
f'c	42.99846	MPA
E_c =	30970.23	MPA
E_s =	32998.82	MPA
A'f	112.903	mm^2
Af	573.0311	mm^2
d=	510	mm
d'=	33.00001	mm
d''=	39.99992	mm
f_{fu} =	689.9752	MPA
E_f =	41998.5	MPA
f'_{fu} =	299.9893	MPA
span properties:		
L=	3000	mm
a=	1000	mm

section properties		
h=	21.65354	in
b=	7.874016	in
f'c	6.236403	ksi
E_c =	4501.341	ksi
E_s =	4786.077	ksi
A'f	0.175	in^2
Af	0.8882	in^2
d=	20.07874	in
d'=	1.299213	in
d''=	1.5748	in
f_{fu} =	100.0725	ksi
E_f =	6091.371	ksi
f'_{fu} =	43.50979	ksi
span properties:		
L=	118.1102	in
a=	39.37008	in

Table 4.22 Initial parameters of Benmokrane et al. Sample ISO3.

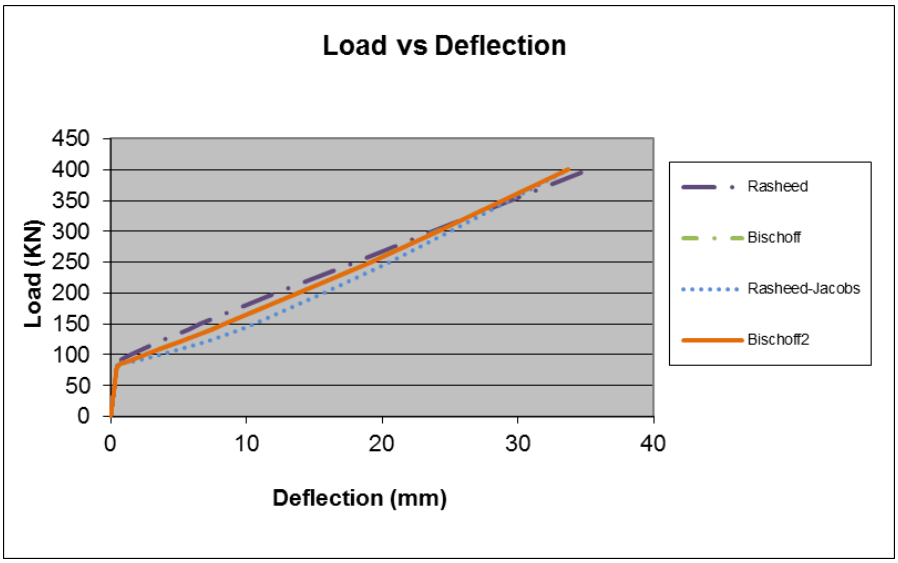

Figure 4.27 Load-deflection response for sample ISO3.

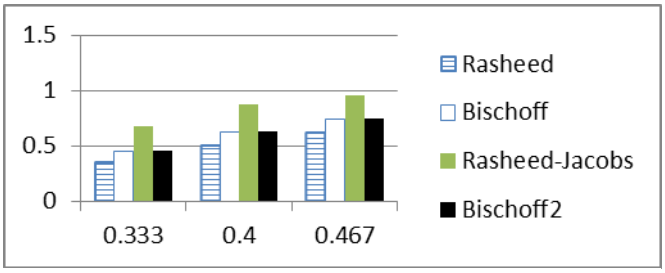

Table 4.23 Deflection comparison bar chart for sample ISO3.

4.4.5 Masmoudi et al. (1998)

Four independent samples were used from Masmoudi et al. including CB2B-1, CB3B-2, CB4B-1, and CB6B-1. Three dependent samples were used for deflection comparison including CB2B-2, dependent on CB2B-1, CB4B-2, dependent on CB4B-1, and CB6B-2, dependent on

CB6B-1. Once again with the Masmoudi et al. samples, the Rasheed-Jacobs model slightly over predicts the deflection and is on the conservative side. The independent sample deflections are predicted most accurately by the Bischoff2 model for 0.333Mn and 0.400 Mn, and by the Bischoff model for 0.467Mn. However, when the dependent sample deflections were compared, the Rasheed model best represented the samples. Overall, with both the dependent and independent samples, both the Rasheed and Bischoff2 models could be used to best represent the experimental deflections accurately.

4.4.5.1 – Sample CB2B-1

section properties		
h=	299.9999	mm
b=	200	mm
f'c	51.99814	MPA
E_c =	34057.43	MPA
E_s =	32998.82	MPA
A'f	157.0965	mm^2
Af	348.709	mm^2
d=	262.5499	mm
d'=	35.00001	mm
d''=	37.45001	mm
f_{fu} =	772.9722	MPA
E_f =	37598.65	MPA
f'_{fu} =	479.9828	MPA
span properties:		
L=	3000	mm
a=	1250	mm

section properties		
h=	11.81102	in
b=	7.874016	in
f'c	7.541697	ksi
E_c =	4950.048	ksi
E_s =	4786.077	ksi
A'f	0.2435	in^2
Af	0.5405	in^2
d=	10.33661	in
d'=	1.377953	in
d''=	1.47441	in
f_{fu} =	112.1102	ksi
E_f =	5453.227	ksi
f'_{fu} =	69.61566	ksi
span properties:		
L=	118.1102	in
a=	49.2126	in

Table 4.24 Initial parameters for Masmoudi et al. sample CB2B-1.

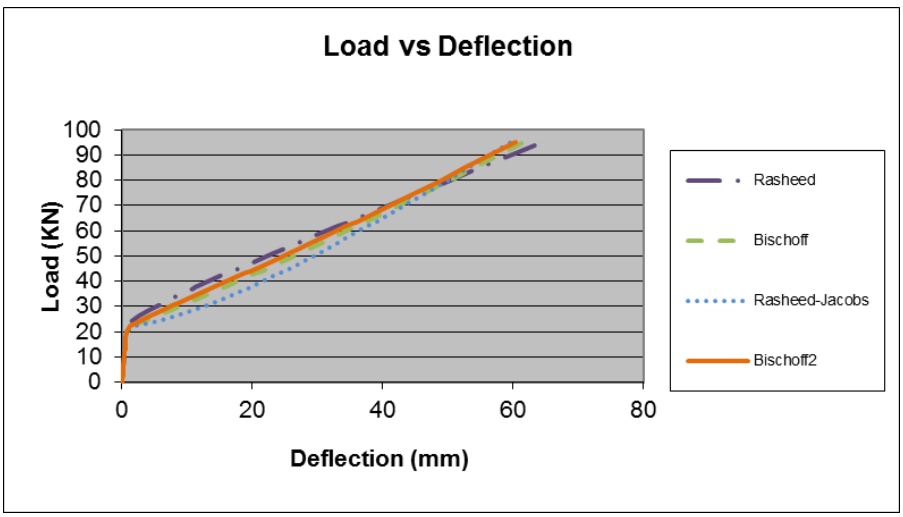

Figure 4.28 Load-deflection response for sample CB2B-1.

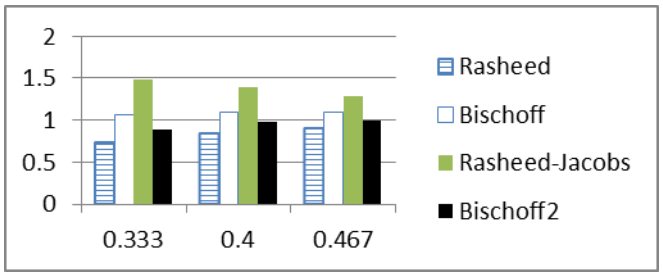

Table 4.25 Deflection comparison bar chart for sample CB2B-1.

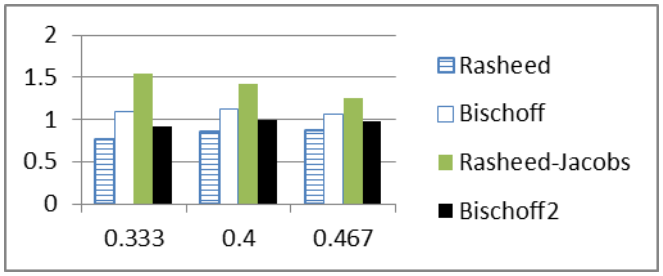

Table 4.26 Deflection comparison bar chart for dependent sample CB2B-2.

4.4.5.2 – Sample CB3B-2

section properties		
h=	299.9999	mm
b=	200	mm
f'c	51.99814	MPA
E_c =	34057.43	MPA
E_s =	32998.82	MPA
A'f	157.0965	mm^2
Af	523.0635	mm^2
d=	262.5499	mm
d'=	35.00001	mm
d''=	37.45001	mm
f_{fu} =	772.9722	MPA
E_f =	37598.65	MPA
f'_{fu} =	479.9828	MPA
span properties:		
L=	3000	mm
a=	1250	mm

section properties		
h=	11.81102	in
b=	7.874016	in
f'c	7.541697	ksi
E_c =	4950.048	ksi
E_s =	4786.077	ksi
A'f	0.2435	in^2
Af	0.81075	in^2
d=	10.33661	in
d'=	1.377953	in
d''=	1.47441	in
f_{fu} =	112.1102	ksi
E_f =	5453.227	ksi
f'_{fu} =	69.61566	ksi
span properties:		
L=	118.1102	in
a=	49.2126	in

Table 4.27 Initial parameters for Masmoudi et al. sample CB3B-

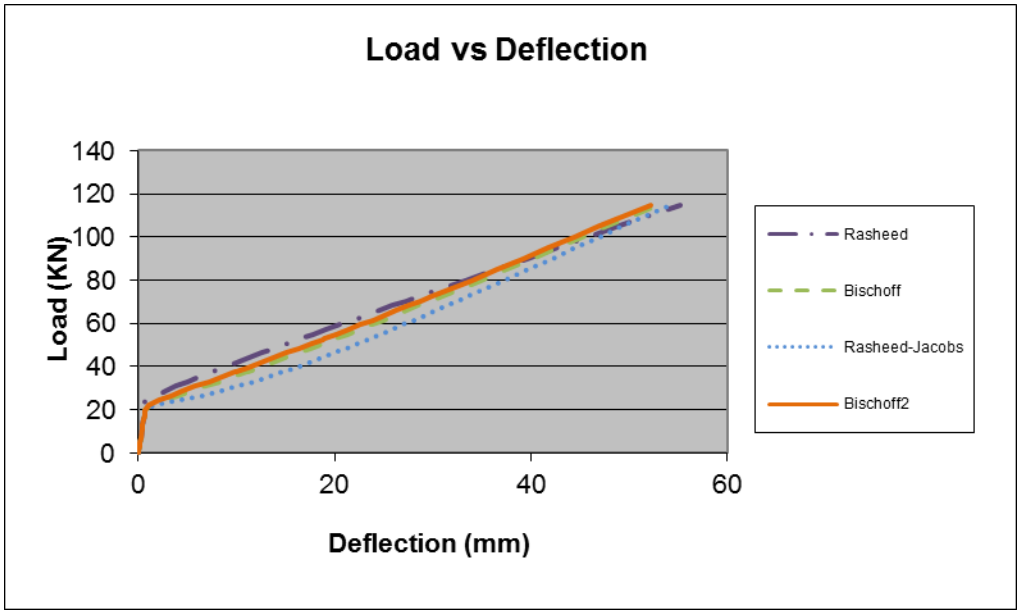

Figure 4.29 Load-deflection response for sample CB3B-2.

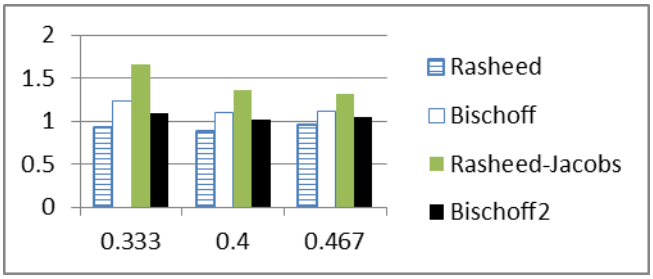

Table 4.28 Deflection comparison bar chart for sample CB3B-2.

4.4.5.3 – Sample CB4B-1

section properties		
h=	299.9999	mm
b=	200	mm
f'c	44.99839	MPA
E_c =	31682.28	MPA
E_s =	29998.93	MPA
A'f	157.0965	mm^2
Af	697.418	mm^2
d=	240.1	mm
d'=	35.00001	mm
d''=	59.89991	mm
f_{fu} =	772.9722	MPA
E_f =	37598.65	MPA
f'_{fu} =	479.9828	MPA
span properties:		
L=	3000	mm
a=	1250	mm

section properties		
h=	11.81102	in
b=	7.874016	in
f'c	6.526468	ksi
E_c =	4604.834	ksi
E_s =	4350.979	ksi
A'f	0.2435	in^2
Af	1.081	in^2
d=	9.452756	in
d'=	1.377953	in
d''=	2.358264	in
f_{fu} =	112.1102	ksi
E_f =	5453.227	ksi
f'_{fu} =	69.61566	ksi
span properties:		
L=	118.1102	in
a=	49.2126	in

Table 4.29 Initial parameters for Masmoudi et al. sample CB4B-1.

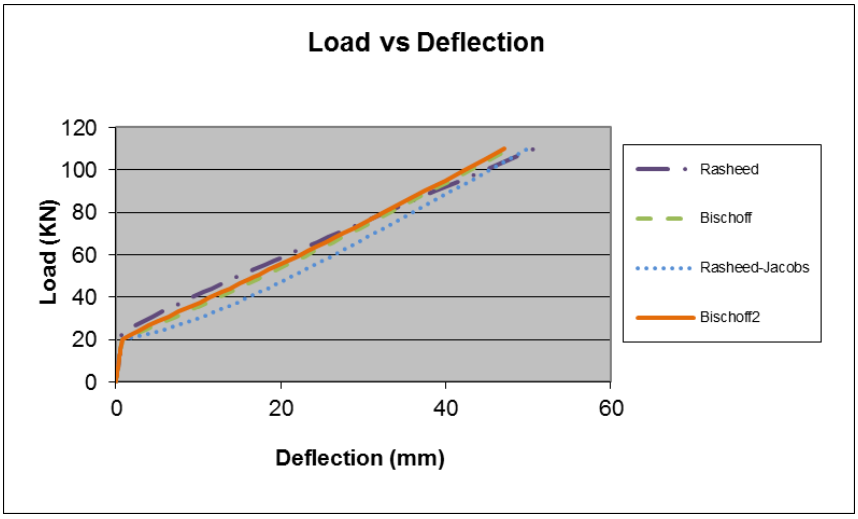

Figure 4.30 Load-deflection response for sample CB4B-1.

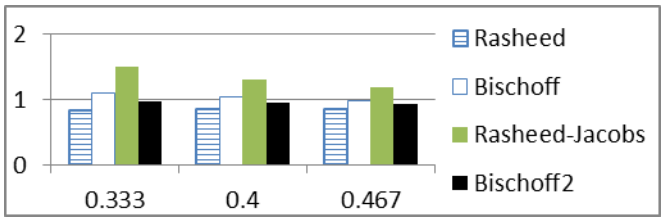

Table 4.30 Deflection comparison bar chart for sample CB4B-1.

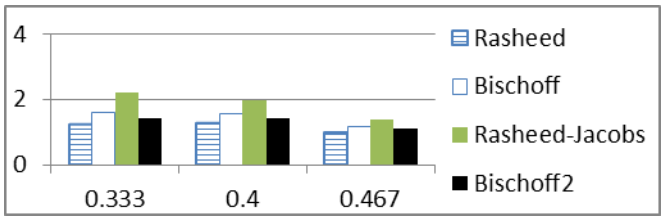

Table 4.31 Deflection comparison bar chart for dependent sample CB4B-1.

4.4.5.4 – Sample CB6B-1

section properties		
h=	299.9999	mm
b=	200	mm
f'c	44.99839	MPA
E_c =	31682.28	MPA
E_s =	29998.93	MPA
A'f	157.0965	mm^2
Af	1046.127	mm^2
d=	240.1	mm
d'=	35.00001	mm
d''=	59.89991	mm
f_{fu} =	772.9722	MPA
E_f =	37598.65	MPA
f'_{fu} =	479.9828	MPA
span properties:		
L=	3000	mm
a=	1250	mm

section properties		
h=	11.81102	in
b=	7.874016	in
f'c	6.526468	ksi
E_c =	4604.834	ksi
E_s =	4350.979	ksi
A'f	0.2435	in^2
Af	1.6215	in^2
d=	9.452756	in
d'=	1.377953	in
d''=	2.358264	in
f_{fu} =	112.1102	ksi
E_f =	5453.227	ksi
f'_{fu} =	69.61566	ksi
span properties:		
L=	118.1102	in
a=	49.2126	in

Table 4.32 Initial parameters for Masmoudi et al. sample

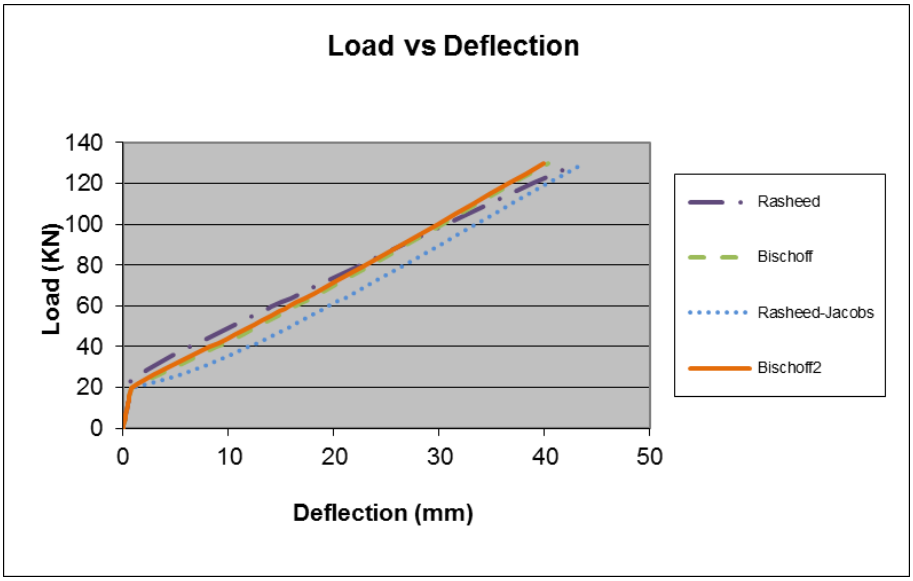

Figure 4.31 Load-deflection response for sample CB6B-1.

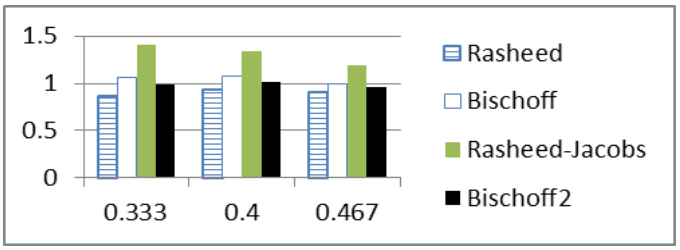

Table 4.33 Deflection comparison bar chart for sample CB6B-1.

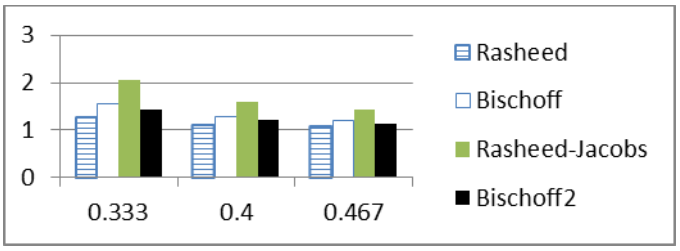

Table 4.34 Deflection comparison bar chart for dependent sample CB6B-2.

4.4.6 Theriault et al. (1998)

Six independent samples were used from Theriault et al. including BC2NA, BC2HA, BC2VA, BC4NA, BC4HA, and BC4VA. Two dependent samples BC2NB, dependent on BC2NA, and BC4VB, dependent on BC4VA, were also used to compare the experimental deflections from the Gross database. According to the samples excluding BC2VA, the Rasheed model is the best prediction for the experimental deflections. However, according to sample BC2VA, the Bischoff2 model is best for the $0.333M_n$ moment level, and the Rasheed-Jacobss model is the best fit for the $0.400M_n$ and $0.467M_n$ moment levels for predicting the experimental deflection. Other than for the sample BC2VA, the Rasheed-Jacobs model over predicts the deflection for each sample.

4.4.6.1 – Sample BC2NA

section properties		
h=	180	mm
b=	130	mm
f'c	53.0981	MPA
E_c =	34415.77	MPA
E_s =	32998.82	MPA
A'f	56.58053	mm^2
Af	237.6769	mm^2
d=	153.85	mm
d'=	23	mm
d''=	26.14999	mm
f_{fu} =	772.9722	MPA
E_f =	37998.64	MPA
f'_{fu} =	413.6852	MPA
span properties:		
L=	1500	mm
a=	500	mm

section properties		
h=	7.086614	in
b=	5.11811	in
f'c	7.701233	ksi
E_c =	5002.13	ksi
E_s =	4786.077	ksi
A'f	0.0877	in^2
Af	0.3684	in^2
d=	6.057087	in
d'=	0.905512	in
d''=	1.029527	in
f_{fu} =	112.1102	ksi
E_f =	5511.24	ksi
f'_{fu} =	60	ksi
span properties:		
L=	59.05512	in
a=	19.68504	in

Table 4.35 Initial parameters for Theriault et al. sample BC2NA.

Figure 4.32 Load-deflection response for sample BC2NA.

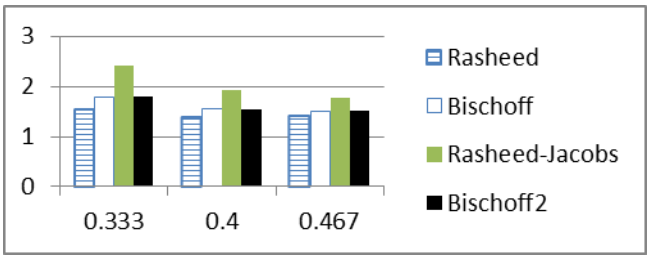

Table 4.36 Deflection comparison bar chart for sample BC2NA.

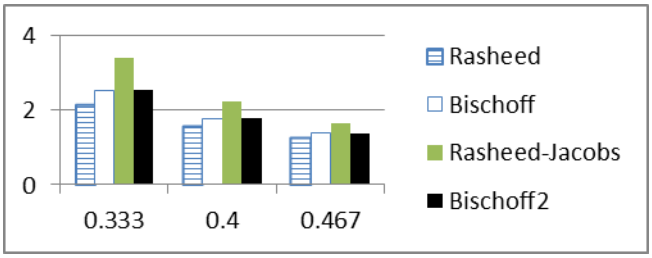

Table 4.37 Deflection comparison bar chart for dependent sample BC2NB.

4.4.6.2 – Sample BC2HA

section properties		
h=	180	mm
b=	130	mm
f'c	57.19796	MPA
E_c =	35719.73	MPA
E_s =	33998.78	MPA
A'f	56.58053	mm^2
Af	237.6769	mm^2
d=	153.85	mm
d'=	23	mm
d''=	26.14999	mm
f_{fu} =	772.9722	MPA
E_f =	37998.64	MPA
f'_{fu} =	413.6852	MPA

span properties:		
L=	1500	mm
a=	500	mm

section properties		
h=	7.086614	in
b=	5.11811	in
f'c	8.295867	ksi
E_c =	5191.654	ksi
E_s =	4931.109	ksi
A'f	0.0877	in^2
Af	0.3684	in^2
d=	6.057087	in
d'=	0.905512	in
d''=	1.029527	in
f_{fu} =	112.1102	ksi
E_f =	5511.24	ksi
f'_{fu} =	60	ksi

span properties:		
L=	59.05512	in
a=	19.68504	in

Table 4.38 Initial parameters for Theriault et al. sample BC2HA.

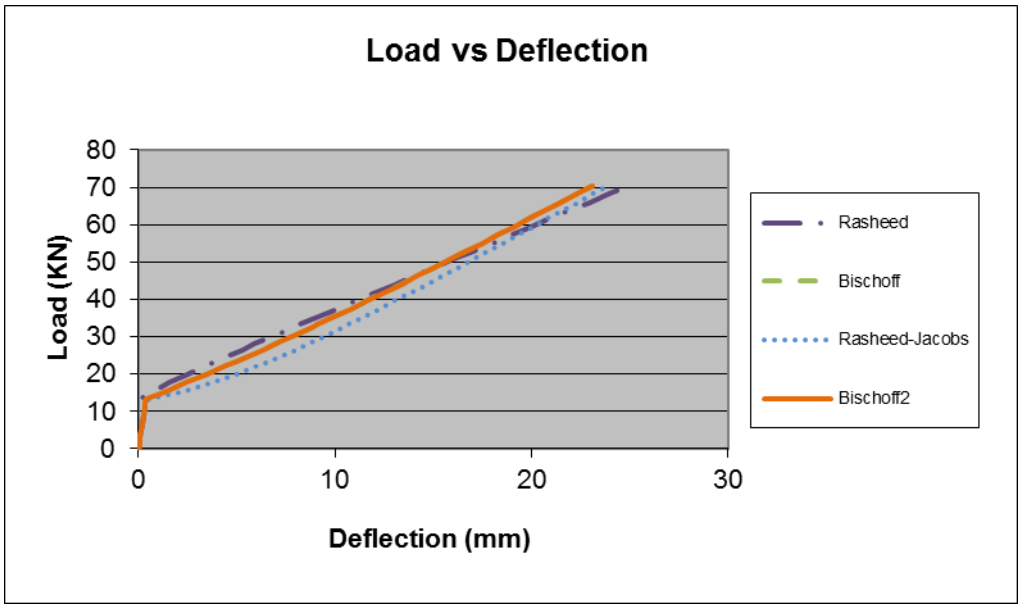

Figure 4.33 Load-deflection response for sample BC2HA.

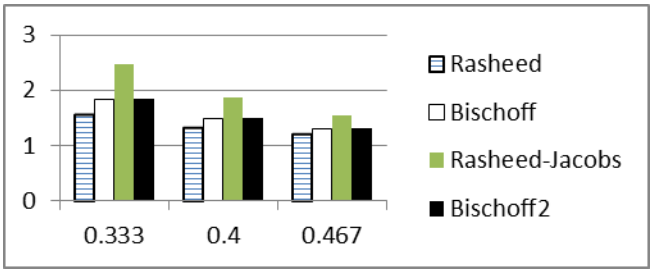

Table 4.39 Deflection comparison bar chart for sample BC2HA.

4.4.6.3 – Sample BC2VA

section properties		
h=	180	mm
b=	130	mm
f'c	97.39652	MPA
E_c =	46611.13	MPA
E_s =	42098.49	MPA
A'f	56.58053	mm^2
Af	237.6769	mm^2
d=	153.85	mm
d'=	23	mm

section properties		
h=	7.086614	in
b=	5.11811	in
f'c	14.12618	ksi
E_c =	6774.656	ksi
E_s =	6105.874	ksi
A'f	0.0877	in^2
Af	0.3684	in^2
d=	6.057087	in
d'=	0.905512	in

Table 4.40 Initial parameters for Theriault et al. sample BC2VA.

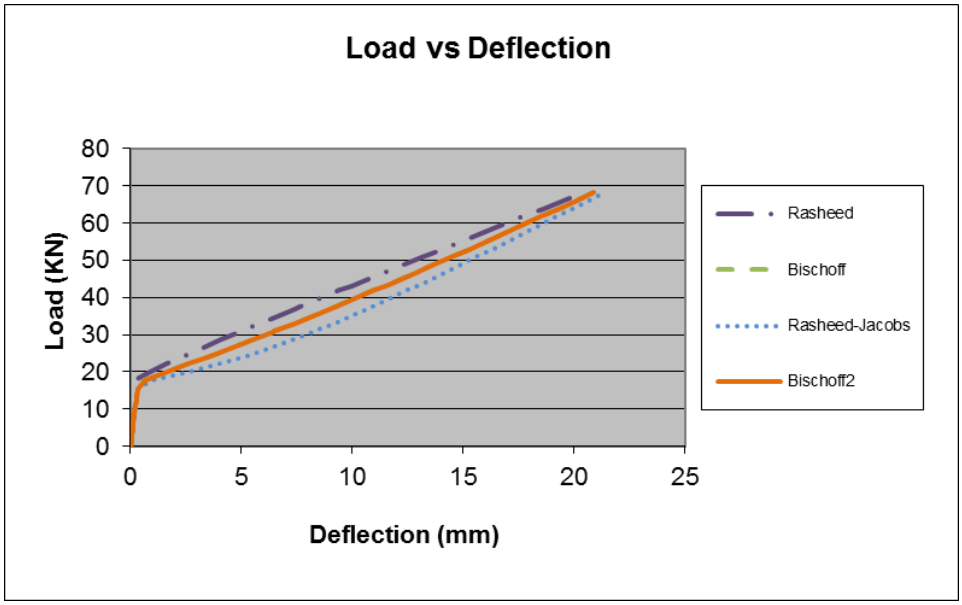

Figure 4.34 Load-deflection response for sample BC2VA.

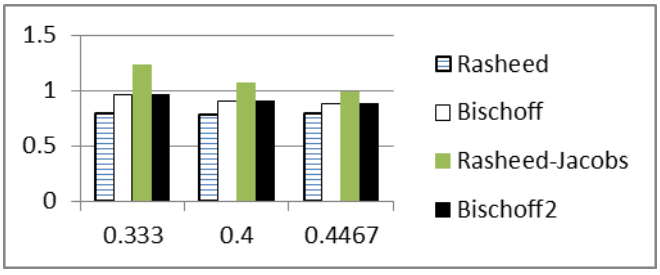

Table 4.41 Deflection comparison bar chart for sample BC2VA.

4.4.6.4 – Sample BC4NA

section properties		
h=	180	mm
b=	130	mm
f'c	46.19835	MPA
E_c =	32101.93	MPA
E_s =	31598.87	MPA
A'f	56.58053	mm^2
Af	475.3539	mm^2
d=	135.2	mm
d'=	23	mm
d''=	44.79999	mm

section properties		
h=	7.086614	in
b=	5.11811	in
f'c	6.700508	ksi
E_c =	4665.828	ksi
E_s =	4583.031	ksi
A'f	0.0877	in^2
Af	0.7368	in^2
d=	5.322835	in
d'=	0.905512	in
d''=	1.763779	in

Table 4.42 Initial parameters for Theriault et al. sample BC4NA.

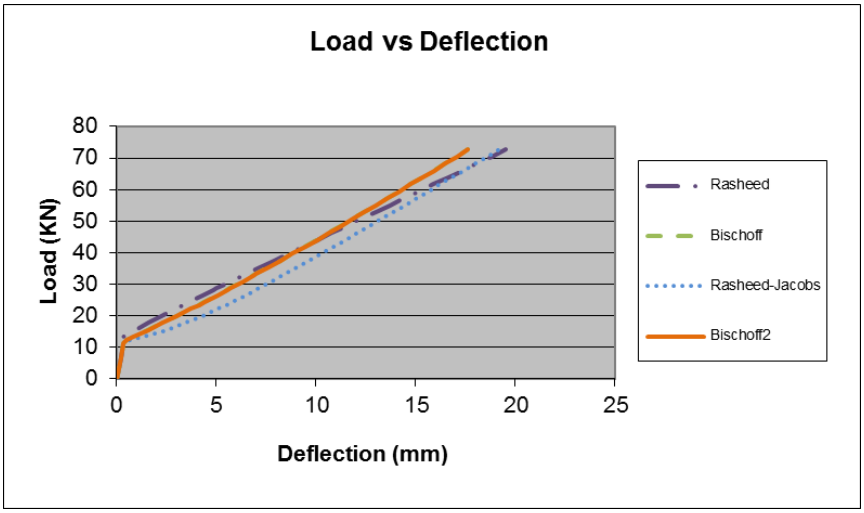

Figure 4.35 Load-deflection response for sample BC4NA.

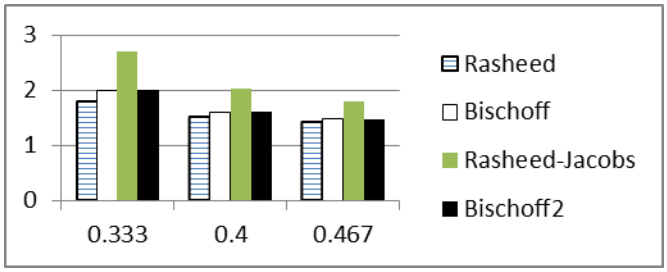

Table 4.43 Deflection comparison bar chart for sample BC4NA.

4.4.6.5 – Sample BC4HA

section properties		
h=	180	mm
b=	130	mm
f'c	53.89807	MPA
E_c =	34674.05	MPA
E_s =	33198.81	MPA
A'f	56.58053	mm^2
Af	475.3539	mm^2
d=	135.2	mm
d'=	23	mm
d''=	44.79999	mm
f_{fu} =	772.9722	MPA
E_f =	37998.64	MPA
f'_{fu} =	413.6852	MPA

section properties		
h=	7.086614	in
b=	5.11811	in
f'c	7.817259	ksi
E_c =	5039.67	ksi
E_s =	4815.083	ksi
A'f	0.0877	in^2
Af	0.7368	in^2
d=	5.322835	in
d'=	0.905512	in
d''=	1.763779	in
f_{fu} =	112.1102	ksi
E_f =	5511.24	ksi
f'_{fu} =	60	ksi

Table 4.44 Initial parameters for Theriault et al. sample BC4HA.

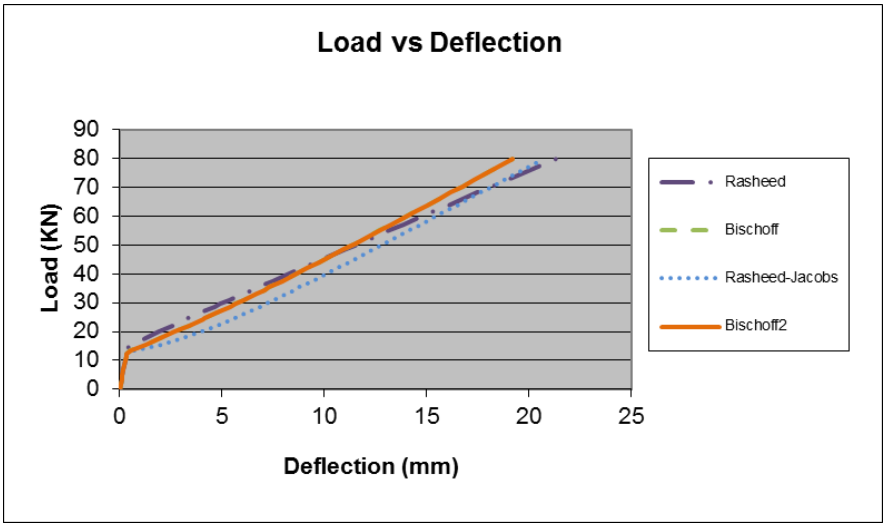

Figure 4.36 Load-deflection response for sample BC4HA.

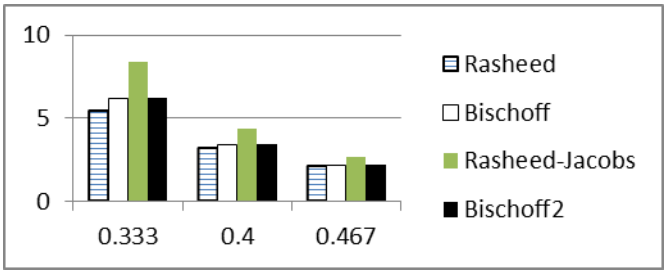

Table 4.45 Deflection comparison bar chart for sample BC4HA.

4.4.6.6 – Sample BC4VA

section properties		
h=	180	mm
b=	130	mm
f'c	93.49665	MPA
E_c =	45668.42	MPA
E_s =	41398.52	MPA
A'f	56.58053	mm^2
Af	475.3539	mm^2
d=	135.2	mm
d'=	23	mm
d''=	44.79999	mm

section properties		
h=	7.086614	in
b=	5.11811	in
f'c	13.56055	ksi
E_c =	6637.637	ksi
E_s =	6004.351	ksi
A'f	0.0877	in^2
Af	0.7368	in^2
d=	5.322835	in
d'=	0.905512	in
d''=	1.763779	in

Table 4.46 Initial parameters for Theriault et al. sample BC4VA.

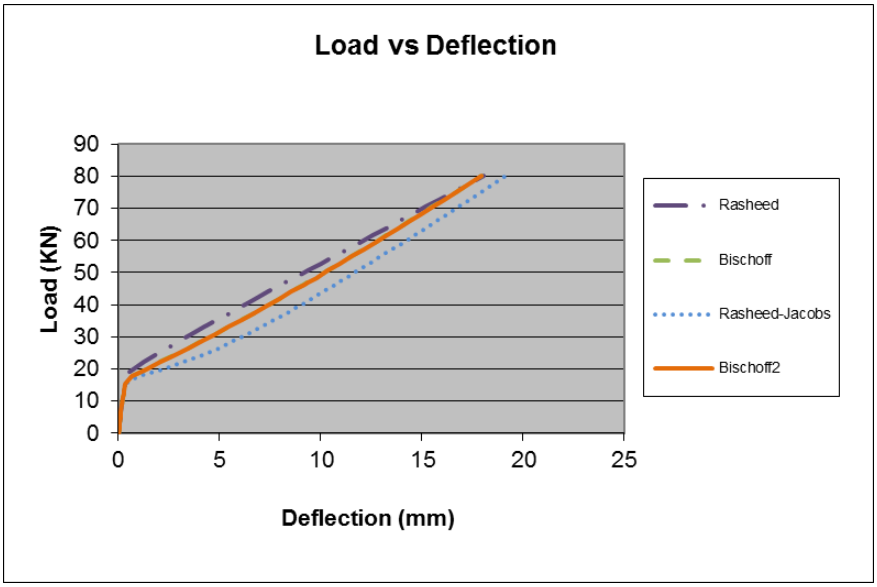

Figure 4.37 Load-deflection response for sample BC4VA.

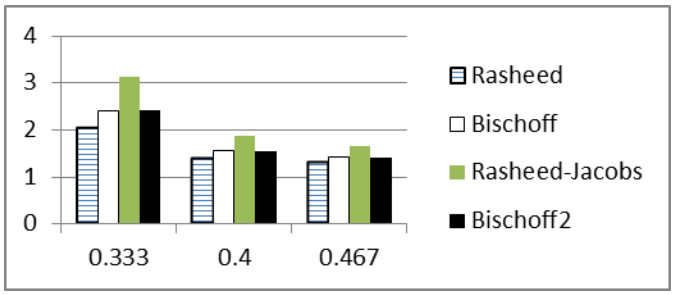

Table 4.48 Deflection comparison bar chart for sample BC4VA.

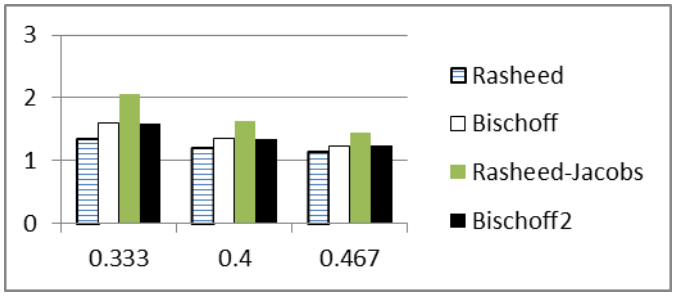

Table 4.47 Deflection comparison bar chart for dependent sample BC4VB.

4.4.7 Toutanji et al. (2000)

Two independent samples from Toutanji et al. were used for this research. These two samples were GB2 and GB3 with no dependent samples. The Rasheed model best represents the Toutanji et al. samples from the Gross database, with the Rasheed-Jacobs model predicting deflections on the conservative side.

4.4.7.1 –Sample GB2

section properties		
h=	299.9999	mm
b=	180	mm
f'c	34.99875	MPA
E_c =	27941.14	MPA
E_s =	34998.75	MPA
A'f	141.9352	mm^2
Af	379.9992	mm^2
d=	268	mm
d'=	29.99999	mm
d''=	31.99994	mm
f_{fu} =	694.9753	MPA
E_f =	39998.57	MPA
f'_{fu} =	413.6852	MPA
span properties:		
L=	2800	mm
a=	1200	mm

section properties		
h=	11.81102	in
b=	7.086614	in
f'c	5.076142	ksi
E_c =	4061.082	ksi
E_s =	5076.142	ksi
A'f	0.22	in^2
Af	0.589	in^2
d=	10.55118	in
d'=	1.181102	in
d''=	1.25984	in
f_{fu} =	100.7977	ksi
E_f =	5801.305	ksi
f'_{fu} =	60	ksi
span properties:		
L=	110.2362	in
a=	47.2441	in

Table 4.49 Initial parameters for Toutanji et al. sample GB2.

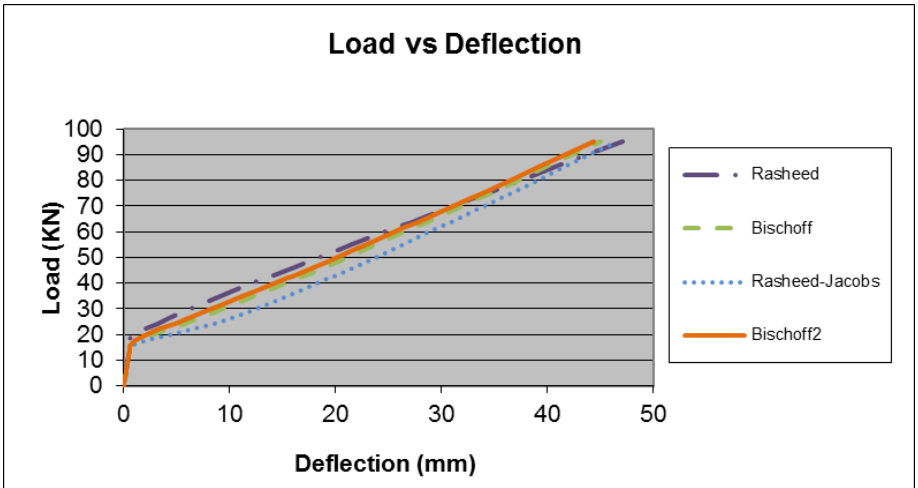

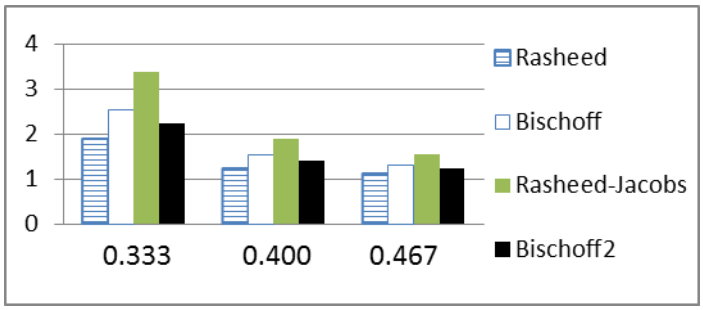

Table 4.50 Deflection comparison bar chart for sample GB2.

4.4.7.2 – Sample GB3

section properties		
h=	299.9999	mm
b=	180	mm
f'c	34.99875	MPA
E_c =	27941.14	MPA
E_s =	34998.75	MPA
A'f	141.9352	mm^2
Af	506.7087	mm^2
d=	255	mm
d'=	29.99999	mm
d''=	44.99991	mm
f_{fu} =	694.9753	MPA
E_f =	39998.57	MPA
f'_{fu} =	413.6852	MPA
span properties:		
L=	2800	mm
a=	1200	mm

section properties		
h=	11.81102	in
b=	7.086614	in
f'c	5.076142	ksi
E_c =	4061.082	ksi
E_s =	5076.142	ksi
A'f	0.22	in^2
Af	0.7854	in^2
d=	10.03937	in
d'=	1.181102	in
d''=	1.77165	in
f_{fu} =	100.7977	ksi
E_f =	5801.305	ksi
f'_{fu} =	60	ksi
span properties:		
L=	110.2362	in
a=	47.2441	in

Table 4.51 Initial parameters for Toutanji et al. sample GB3.

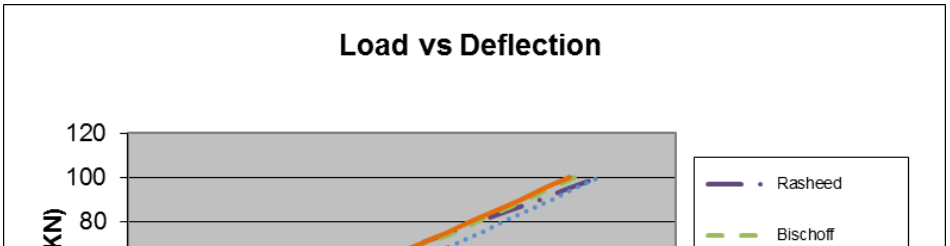

Figure 4.39 Load-deflection response for sample GB3.

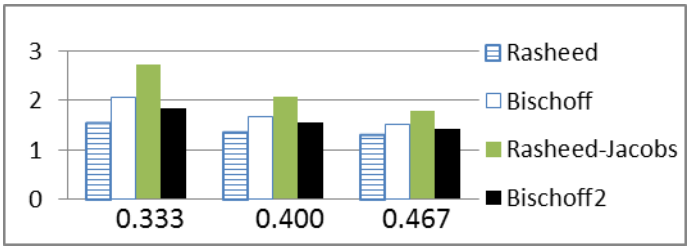

Table 4.52 Deflection comparison bar chart for sample GB3.

4.4.8 Kassem et al. (2003)

Six independent samples are from Kassem et al. with no dependent samples. These samples from the Gross database are IS4, IS6, IS8, CB4, CB6, and CB8. All of the Kassem et al. samples are best represented by the Rasheed-Jacobs model. The Rasheed, Bischoff, and Bischoff2 models all under predict the deflections in comparison to the experimental deflections provided, therefore the Rasheed-Jacobs best predicts the experimental deflections.

4.4.8.1 – Sample CB4

section properties		
h=	299.9999	mm
b=	200	mm
f'c	39.89857	MPA
E_c =	29832.98	MPA
E_s =	29498.95	MPA
A'f	200.0002	mm^2
Af	256.0001	mm^2
d=	246	mm
d'=	35.64999	mm
d''=	53.99992	mm
f_{fu} =	1987.929	MPA
E_f =	121995.6	MPA
f'_{fu} =	419.985	MPA

section properties		
h=	11.81102	in
b=	7.874016	in
f'c	5.786802	ksi
E_c =	4336.049	ksi
E_s =	4278.463	ksi
A'f	0.310001	in^2
Af	0.396801	in^2
d=	9.685039	in
d'=	1.403543	in
d''=	2.125981	in
f_{fu} =	288.3249	ksi
E_f =	17693.98	ksi
f'_{fu} =	60.91371	ksi

Table 4.53 Initial parameters for Kassem et al. sample CB4.

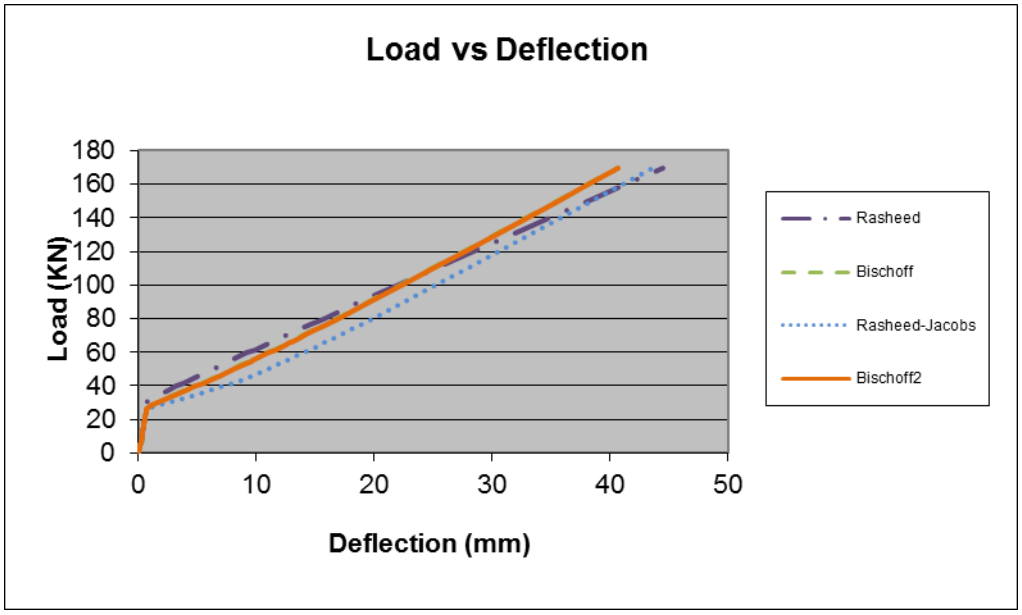

Figure 4.40 Load-deflection response for sample CB4.

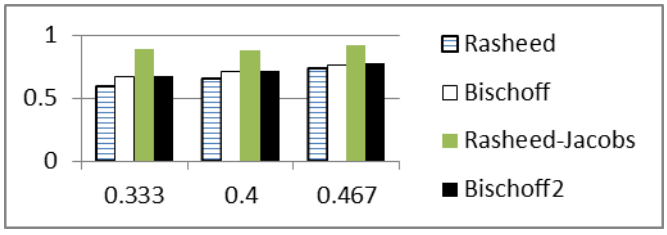

Table 4.54 Deflection comparison bar chart for sample CB4.

4.4.8.2 – Sample CB6

section properties		
h=	299.9999	mm
b=	200	mm
f'c	39.89857	MPA
E_c =	29832.98	MPA
E_s =	29498.95	MPA
A'f	200.0002	mm^2
Af	383.9999	mm^2
d=	246	mm
d'=	35.64999	mm

section properties		
h=	11.81102	in
b=	7.874016	in
f'c	5.786802	ksi
E_c =	4336.049	ksi
E_s =	4278.463	ksi
A'f	0.310001	in^2
Af	0.595201	in^2
d=	9.685039	in
d'=	1.403543	in

Table 4.55 Initial parameters for Kassem et al. sample CB6.

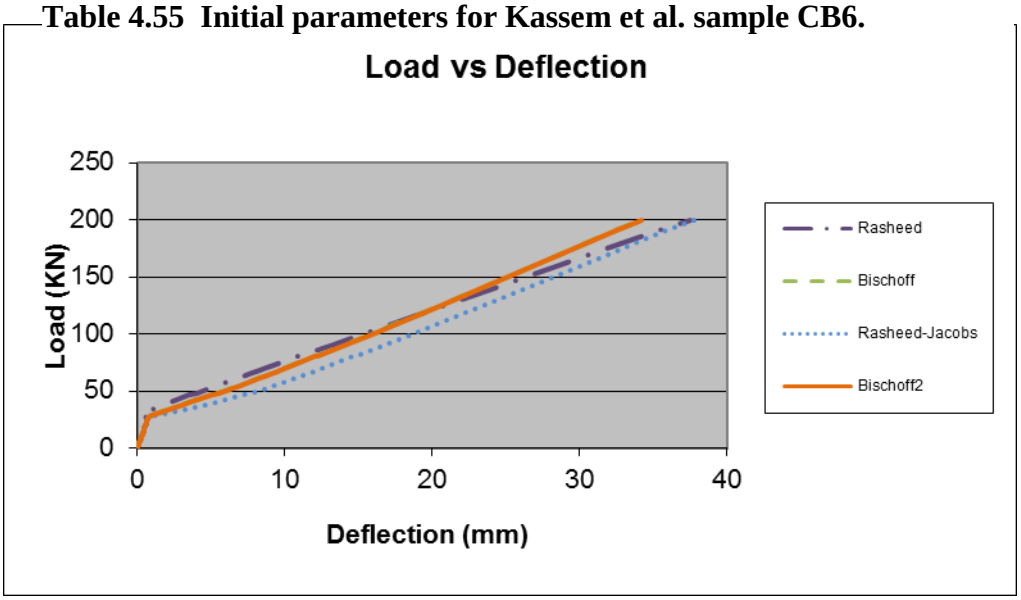

Figure 4.41 Load-deflection response for sample CB6.

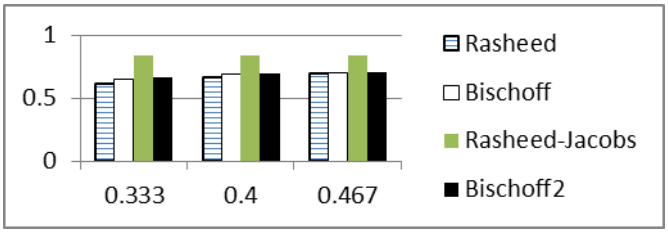

Table 4.56 Deflection comparison bar chart for sample CB6.

4.4.8.3 – Sample CB8

section properties		
h=	299.9999	mm
b=	200	mm
f'c	44.7984	MPA
E_c =	31611.8	MPA
E_s =	32898.83	MPA
A'f	200.0002	mm^2
Af	512.0003	mm^2
d=	246	mm
d'=	35.64999	mm

section properties		
h=	11.81102	in
b=	7.874016	in
f'c	6.497462	ksi
E_c =	4594.59	ksi
E_s =	4771.574	ksi
A'f	0.310001	in^2
Af	0.793602	in^2
d=	9.685039	in
d'=	1.403543	in

Table 4.57 Initial parameters for Kassem et al. sample CB8.

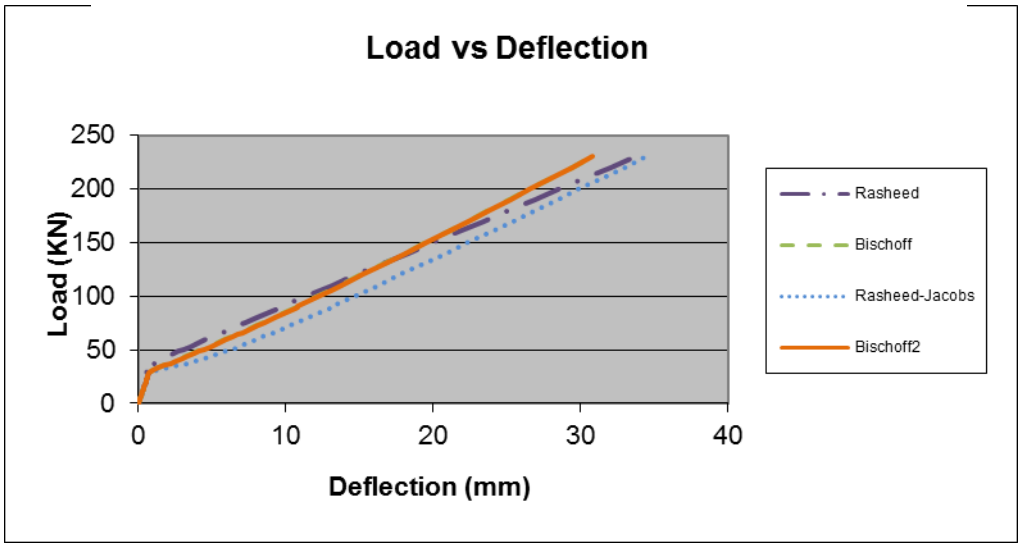

Figure 4.42 Load-deflection comparisons bar chart for sample CB8.

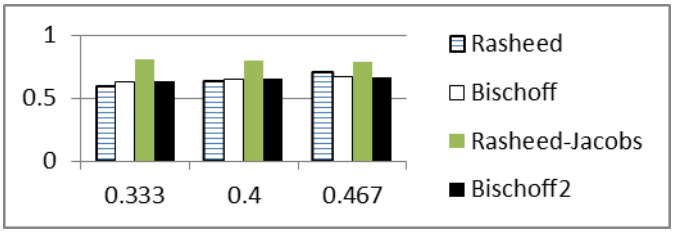

Table 4.58 Deflection comparison bar chart for samlple CB8.

4.4.8.4 – Sample IS4

section properties		
h=	299.9999	mm
b=	200	mm
f'c	40.39855	MPA
E_c =	30019.32	MPA
E_s =	31098.89	MPA
A'f	200.0002	mm^2
Af	284.0001	mm^2
d=	245.5	mm
d'=	35.64999	mm

section properties		
h=	11.81102	in
b=	7.874016	in
f'c	5.859318	ksi
E_c =	4363.132	ksi
E_s =	4510.515	ksi
A'f	0.310001	in^2
Af	0.440201	in^2
d=	9.665354	in
d'=	1.403543	in

Table 4.59 Initial parameters for Kassem et al. sample IS4.

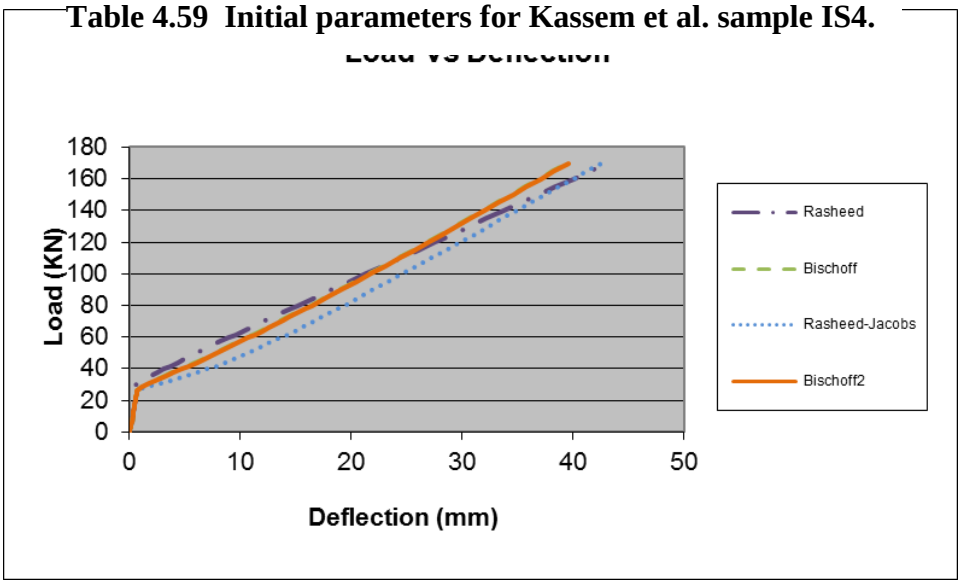

Figure 4.43 Load-deflection response for sample IS4.

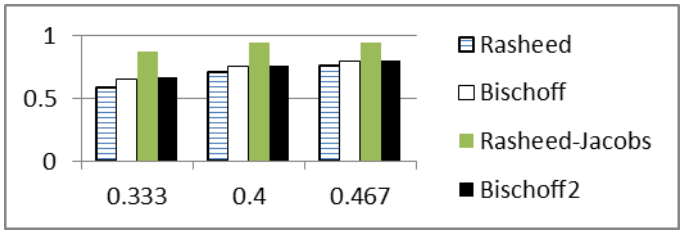

Table 4.60 Deflection comparison bar chart for sample IS4.

4.4.8.5 – Sample IS6

section properties		
h=	299.9999	mm
b=	200	mm
f'c	39.29859	MPA
E_c =	29607.82	MPA
E_s =	30198.92	MPA
A'f	200.0002	mm^2
Af	425.9998	mm^2

section properties		
h=	11.81102	in
b=	7.874016	in
f'c	5.699782	ksi
E_c =	4303.323	ksi
E_s =	4379.985	ksi
A'f	0.310001	in^2
Af	0.660291	in^2

Table 4.61 Initial parameters for Kassem et al. sample IS6.

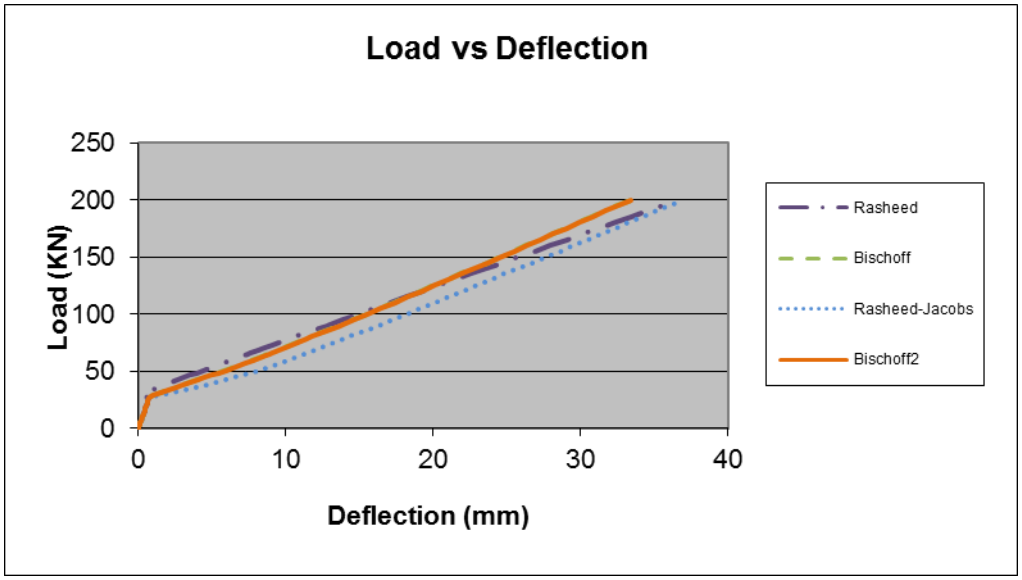

Figure 4.44 Load-deflection response for sample IS6.

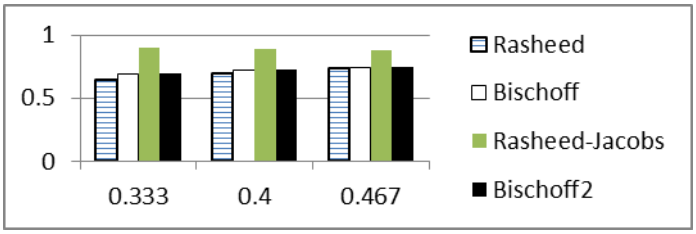

Table 4.62 Deflection comparison bar chart for sample IS6.

4.4.8.6 – Sample IS8

section properties		
h=	299.9999	mm
b=	200	mm
f'c	39.29859	MPA
E_c =	29607.82	MPA
E_s =	30198.92	MPA
A'f	200.0002	mm^2
Af	568.0002	mm^2
d=	245.5	mm
d'=	35.64999	mm

section properties		
h=	11.81102	in
b=	7.874016	in
f'c	5.699782	ksi
E_c =	4303.323	ksi
E_s =	4379.985	ksi
A'f	0.310001	in^2
Af	0.880402	in^2
d=	9.665354	in
d'=	1.403543	in

Table 4.63 Initial parameters for Kassem et al. sample IS8.

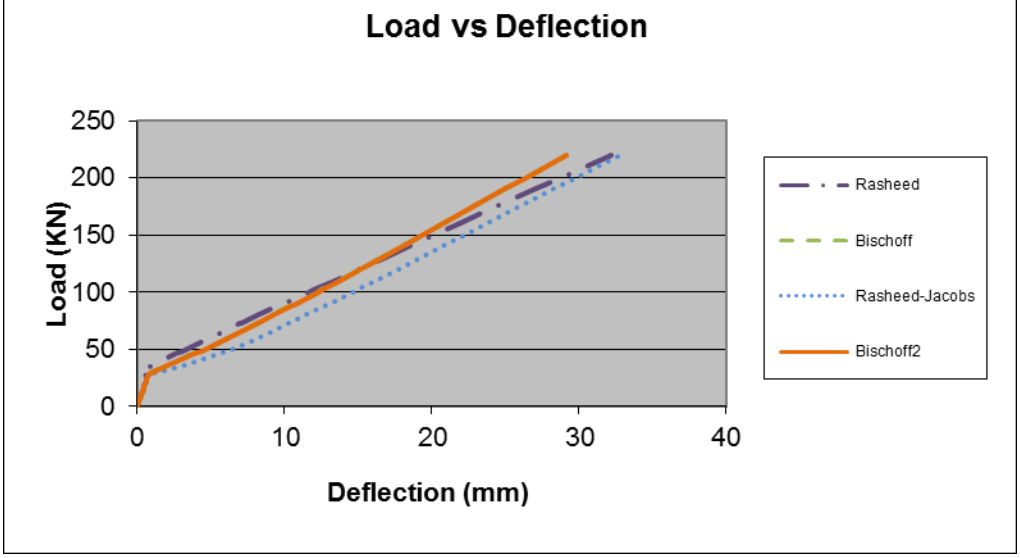

Figure 4.45 Load-deflection response for sample IS8.

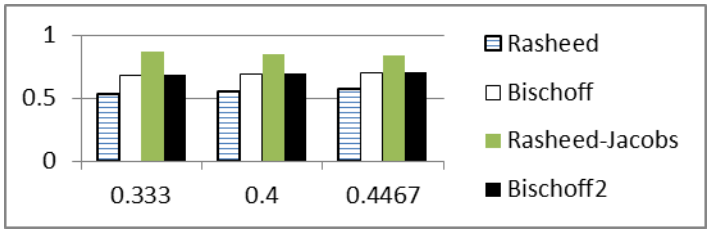

Table 4.64 Deflection comparison bar chart for sample IS8.

4.4.9 Yost et al. (2003)

Sixteen independent samples from Yost et al. are used from the Gross database, as well as 27 dependent samples. The sixteen independent samples are 1-NL, 2-NL, 3-NL, 4-NL, 1-NS, 2-NS, 3-NS, 4-NS, 1-HL, 2-HL, 3-HL, 4-HL, 1-HS, 2-HS, 3-HS, and 4-HS. All of the sixteen independent samples are labeled sample 'a' for the group. Then the 27 dependent samples are dependent on their same sample name, which are 1-NL (b and c), 2-NL (b and c), 3-NL (b and c), 4-NL (b and c), 1-NS (b and c), 2-NS (b and c), 3-NS (b and c), 4-NS (b and c), 1c-HS, 2-HS (b and c), 1-HL (b and c), 2-HL (b and c), 3-HL (b and c), and 4-HL (b and c). The majority of these samples, whether dependent or independent, are best represented by the Rasheed-Jacobs model. Therefore the newly presented model will best estimate the deflection expected to be equivalent to the actual experimental deflection.

4.4.9.1 – 1-NL

section properties		
h=	184.15	mm
b=	254	mm
f'c	40.33431	MPA
E_c =	29995.44	MPA
E_s =	43230.1	MPA
A'f	0	mm^2
Af	253.5479	mm^2
d=	139.7	mm
d'=	0	mm
d''=	44.45	mm
f_{fu} =	689.4753	MPA
E_f =	40334.31	MPA
f'_{fu} =	0	MPA
span properties:		
L=	2895.6	mm
a=	1295.4	mm

section properties		
h=	7.25	in
b=	10	in
f'c	5.85	ksi
E_c =	4359.662	ksi
E_s =	6270	ksi
A'f	0	in^2
Af	0.393	in^2
d=	5.5	in
d'=	0	in
d''=	1.75	in
f_{fu} =	100	ksi
E_f =	5850	ksi
f'_{fu} =	0	ksi
span properties:		
L=	114	in
a=	51	in

Table 4.65 Initial parameters for Yost et al. sample 1a-NL.

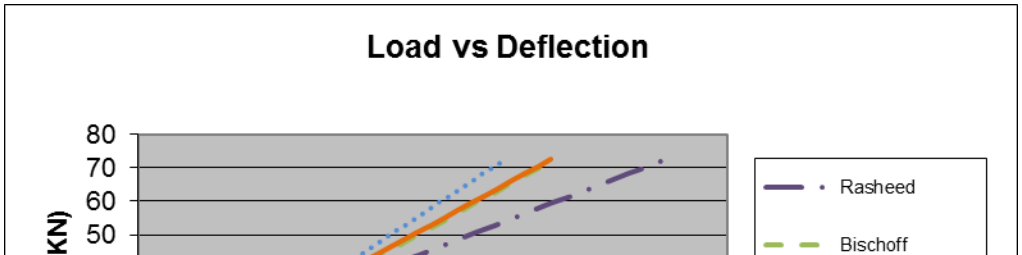

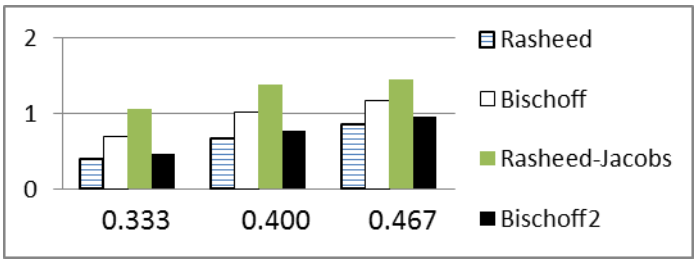

Table 4.66 Deflection comparison bar chart for sample 1a-NL.

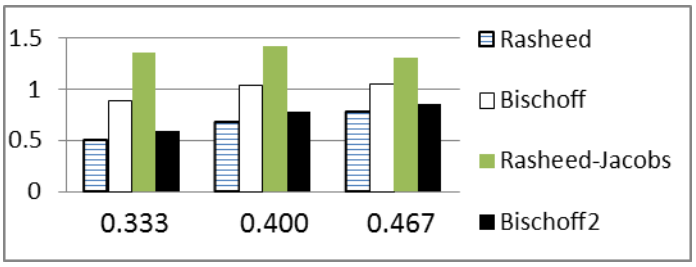

Table 4.67 Deflection comparison bar chart for dependent sample 1b-NL.

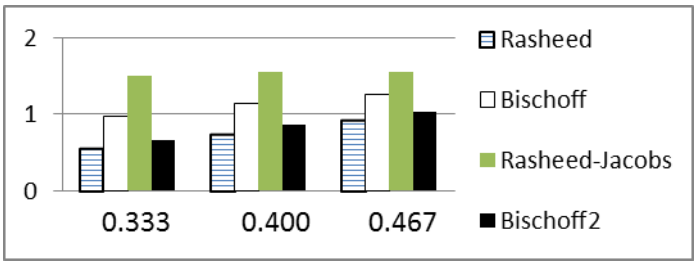

Table 4.68 Deflection comparison bar chart for dependent sample 1c-NL.

4.4.9.2 – 2-NL

section properties		
h=	184.15	mm
b=	304.8	mm
f'c	40.33431	MPA
E_c =	29995.44	MPA
E_s =	43230.1	MPA
A'f	0	mm^2
Af	396.1282	mm^2
d=	138.176	mm
d'=	0	mm
d''=	45.974	mm
f_{fu} =	689.4753	MPA
E_f =	40334.31	MPA
f'_{fu} =	0	MPA
span properties:		
L=	2895.6	mm
a=	1295.4	mm

section properties		
h=	7.25	in
b=	12	in
f'c	5.85	ksi
E_c =	4359.662	ksi
E_s =	6270	ksi
A'f	0	in^2
Af	0.614	in^2
d=	5.44	in
d'=	0	in
d''=	1.81	in
f_{fu} =	100	ksi
E_f =	5850	ksi
f'_{fu} =	0	ksi
span properties:		
L=	114	in
a=	51	in

Table 4.69 Initial parameters for Yost et al. sample 2a-NL.

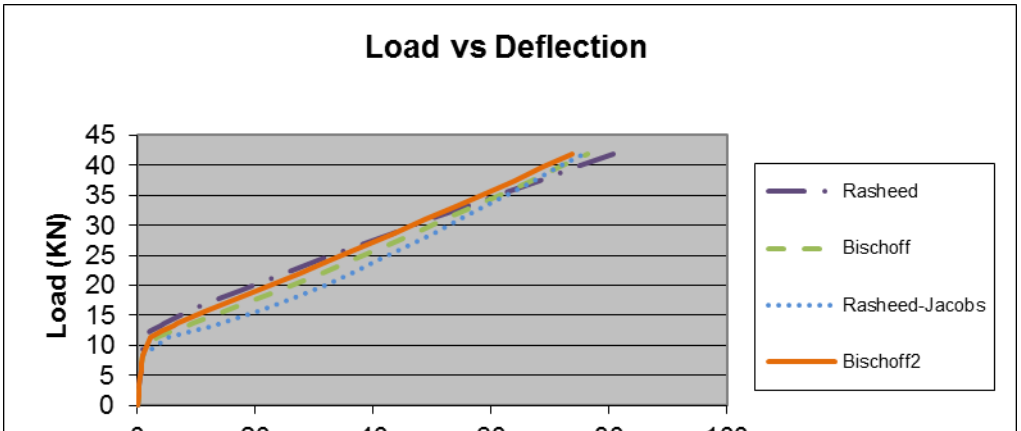

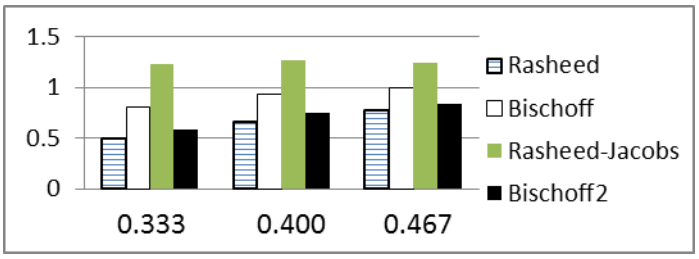

Table 4.70 Deflection comparison bar chart for sample 2a-NL.

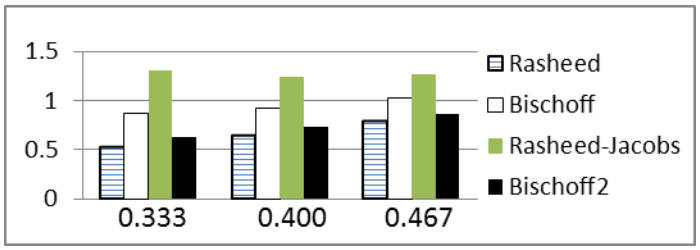

Table 4.71 Deflection comparison bar chart for dependent sample 2b-NL.

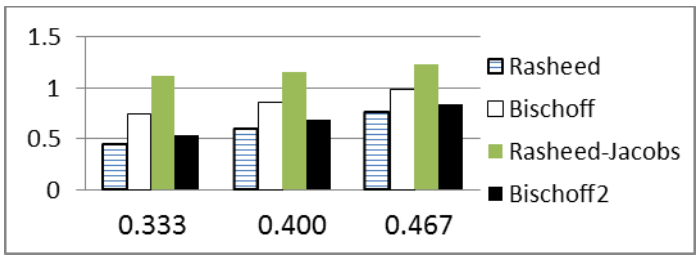

Table 4.72 Deflection comparison bar chart for dependent sample 2c-NL.

4.4.9.3 – 3-NL

section properties		
h=	184.15	mm
b=	241.3	mm
f'c	40.33431	MPA
E_c =	29995.44	MPA
E_s =	43230.1	MPA
A'f	0	mm^2
Af	396.1282	mm^2
d=	138.176	mm
d'=	0	mm
d''=	45.974	mm
f_{fu} =	689.4753	MPA

section properties		
h=	7.25	in
b=	9.5	in
f'c	5.85	ksi
E_c =	4359.662	ksi
E_s =	6270	ksi
A'f	0	in^2
Af	0.614	in^2
d=	5.44	in
d'=	0	in
d''=	1.81	in
f_{fu} =	100	ksi

Table 4.73 Initial parameters for Yost et al. sample 3a-NL

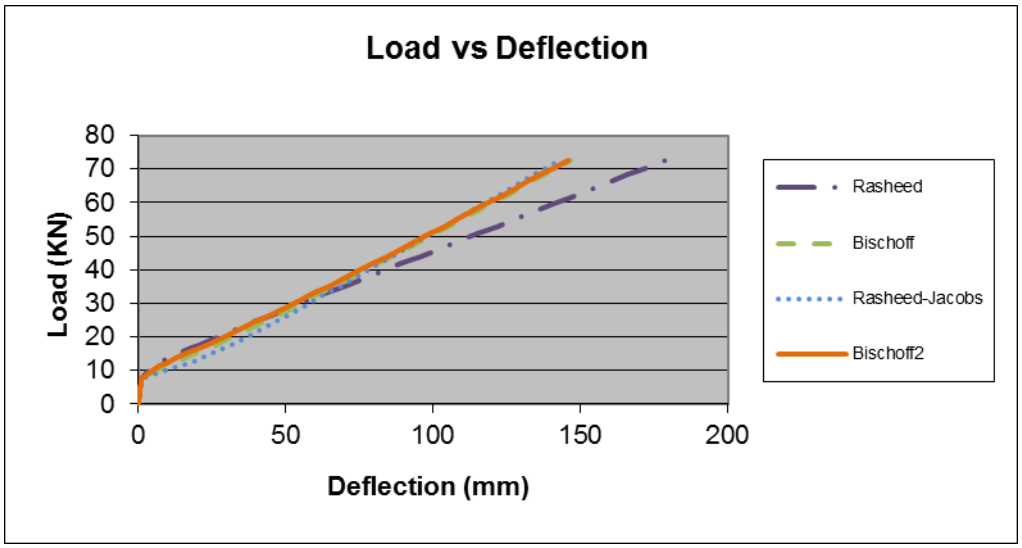

Figure 4.48 Load-deflection response for sample 3a-NL.

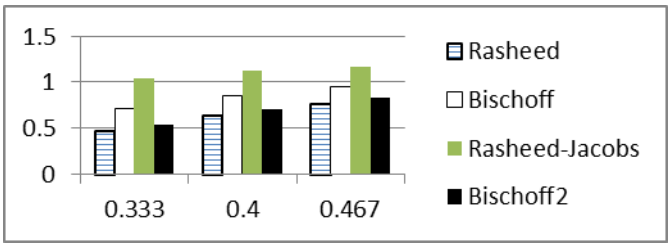

Table 4.74 Deflection comparison bar chart for sample 3a-NL.

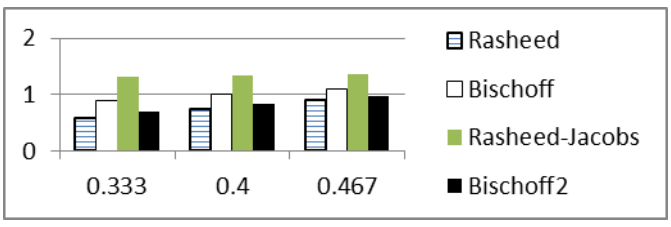

Table 4.75 Deflection comparison bar chart for dependent sample 3b-NL.

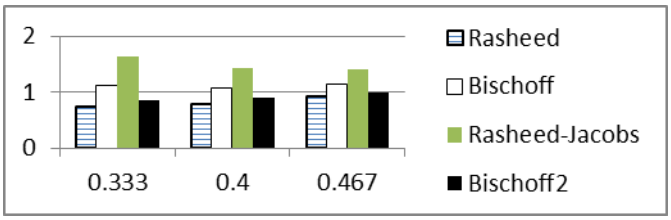

Table 4.76 Deflection comparison bar chart for dependent sample 3c-NL.

4.4.9.4 – 4-NL

section properties		
h=	184.15	mm
b=	203.2	mm
f'c	40.33431	MPA
E_c =	29995.44	MPA
E_s =	43230.1	MPA
A'f	0	mm^2
Af	396.1282	mm^2
d=	138.176	mm
d'=	0	mm
d''=	45.974	mm
f_{fu} =	689.4753	MPA
E_f =	40334.31	MPA
f'_{fu} =	0	MPA
span properties:		
L=	2895.6	mm
a=	1295.4	mm

section properties		
h=	7.25	in
b=	8	in
f'c	5.85	ksi
E_c =	4359.662	ksi
E_s =	6270	ksi
A'f	0	in^2
Af	0.614	in^2
d=	5.44	in
d'=	0	in
d''=	1.81	in
f_{fu} =	100	ksi
E_f =	5850	ksi
f'_{fu} =	0	ksi
span properties:		
L=	114	in
a=	51	in

Table 4.77 Initial parameters for Yost et al. 4a-NL.

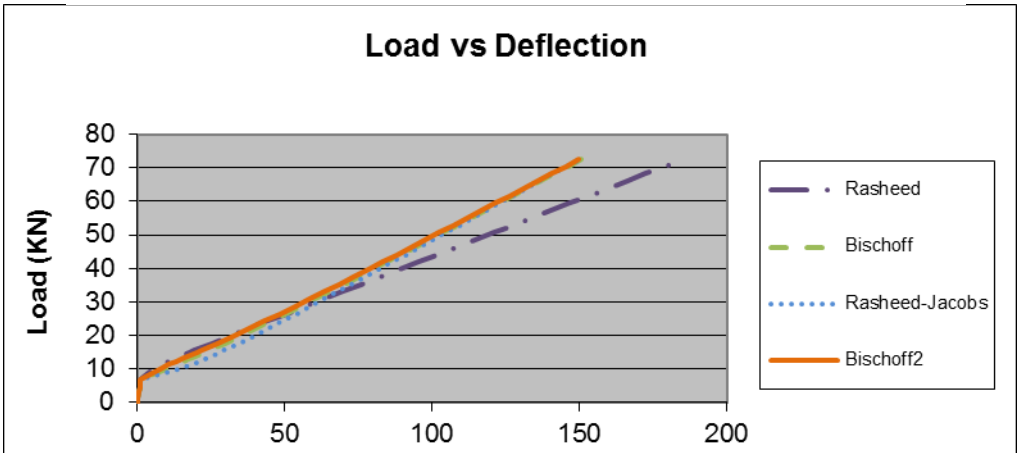

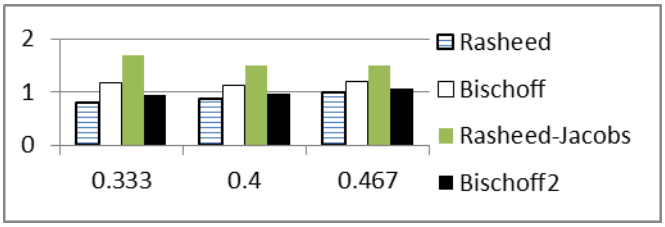

Table 4.78 Deflection comparison bar chart for sample 4a-NL.

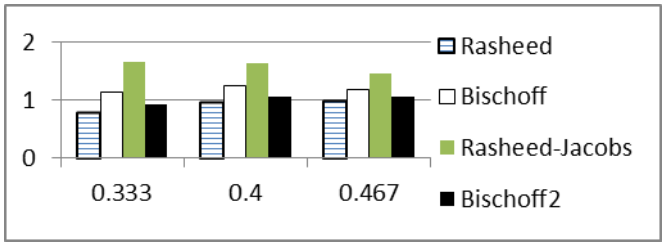

Table 4.79 Deflection comparison bar chart for dependent sample 4b-NL.

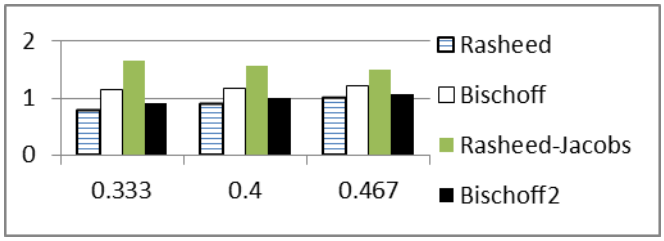

Table 4.80 Deflection comparison bar chart for dependent sample 4c-NL.

4.4.9.5 – 1-NS

section properties		
h=	285.75	mm
b=	228.6	mm
f'c	36.33535	MPA
E_c =	28469.68	MPA
E_s =	39851.67	MPA
A'f	0	mm^2
Af	570.3214	mm^2
d=	225.552	mm
d'=	0	mm

section properties		
h=	11.25	in
b=	9	in
f'c	5.27	ksi
E_c =	4137.902	ksi
E_s =	5780	ksi
A'f	0	in^2
Af	0.884	in^2
d=	8.88	in
d'=	0	in

Table 4.81 Initial parameters for Yost et al. sample 1a-NS.

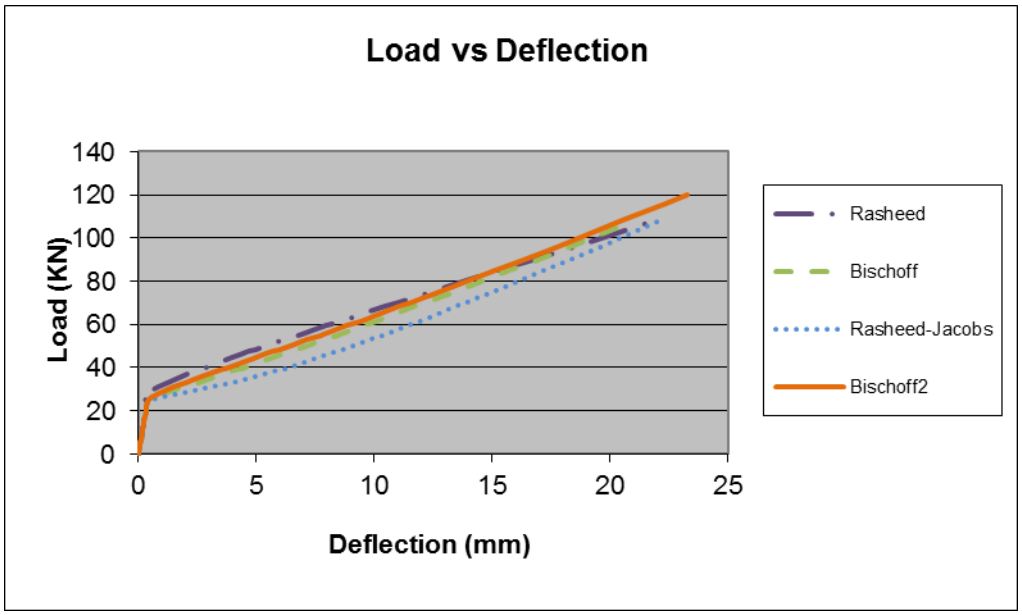

Figure 4.50 Load-deflection response for sample 1a-NS.

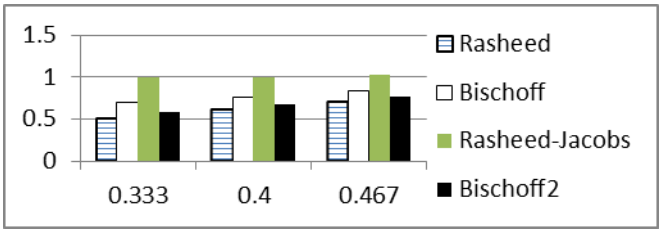

Table 4.82 Deflection comparison bar chart for sample 1a-NS.

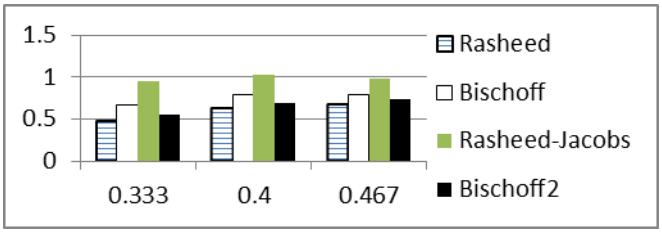

Table 4.83 Deflection comparison bar chart for dependent sample 1b-NS.

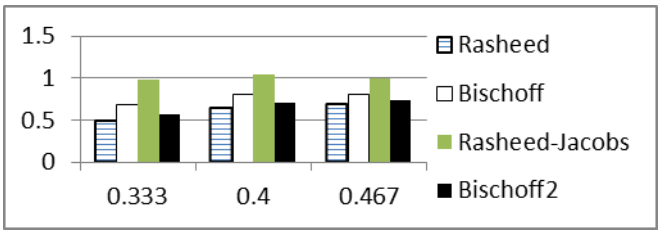

Table 4.84 Deflection comparison bar chart for dependent sample 1c-NS.

4.4.9.6 – 2-NS

section properties		
h=	285.75	mm
b=	228.6	mm
f'c	36.33535	MPA
E_c =	28469.68	MPA
E_s =	39851.67	MPA
A'f	0	mm^2
Af	854.837	mm^2
d=	225.552	mm
d'=	0	mm
d''=	60.198	mm
f_{fu} =	689.4753	MPA
E_f =	40334.31	MPA
f'_{fu} =	0	MPA
span properties:		
L=	2133.6	mm
a=	914.4	mm

section properties		
h=	11.25	in
b=	9	in
f'c	5.27	ksi
E_c =	4137.902	ksi
E_s =	5780	ksi
A'f	0	in^2
Af	1.325	in^2
d=	8.88	in
d'=	0	in
d''=	2.37	in
f_{fu} =	100	ksi
E_f =	5850	ksi
f'_{fu} =	0	ksi
span properties:		
L=	84	in
a=	36	in

Table 4.85 Initial parameters for Yost et al. sample 2a-NS.

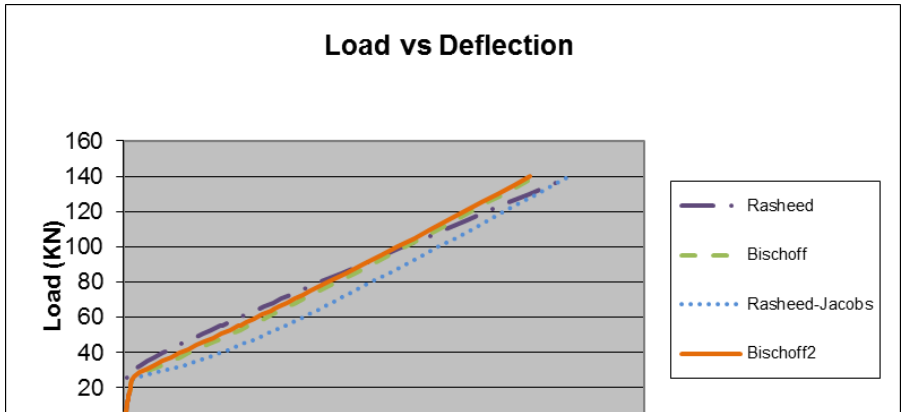

Figure 4.51 Load-deflection response for sample 2a-NS.

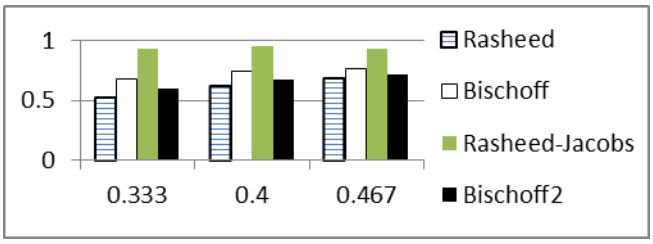

Table 4.86 Deflection comparison bar chart for sample 2a-NS.

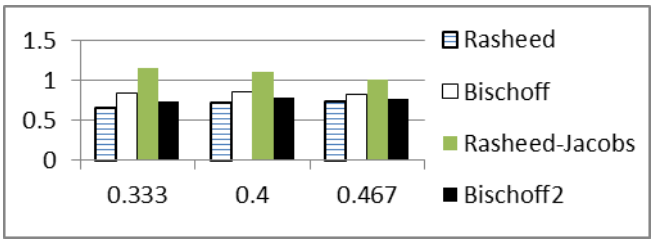

Table 4.87 Deflection comparison bar chart for dependent sample 2b-NS.

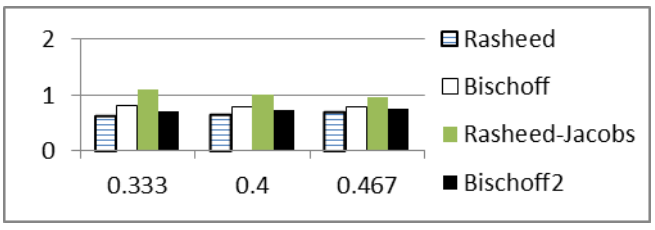

Table 4.88 Deflection comparison bar chart for dependent sample 2c-NS.

4.4.9.7 – 3-NS

section properties		
h=	285.75	mm
b=	254	mm
f'c	36.33535	MPA
E_c =	28469.68	MPA
E_s =	39851.67	MPA
A'f	0	mm^2
Af	1163.869	mm^2
d=	223.774	mm
d'=	0	mm
d''=	61.976	mm
f_{fu} =	689.4753	MPA
E_f =	40334.31	MPA
f'_{fu} =	0	MPA
span properties:		
L=	2133.6	mm
a=	914.4	mm

section properties		
h=	11.25	in
b=	10	in
f'c	5.27	ksi
E_c =	4137.902	ksi
E_s =	5780	ksi
A'f	0	in^2
Af	1.804	in^2
d=	8.81	in
d'=	0	in
d''=	2.44	in
f_{fu} =	100	ksi
E_f =	5850	ksi
f'_{fu} =	0	ksi
span properties:		
L=	84	in
a=	36	in

Table 4.89 Initial parameters for Yost et al. sample 3a-NS.

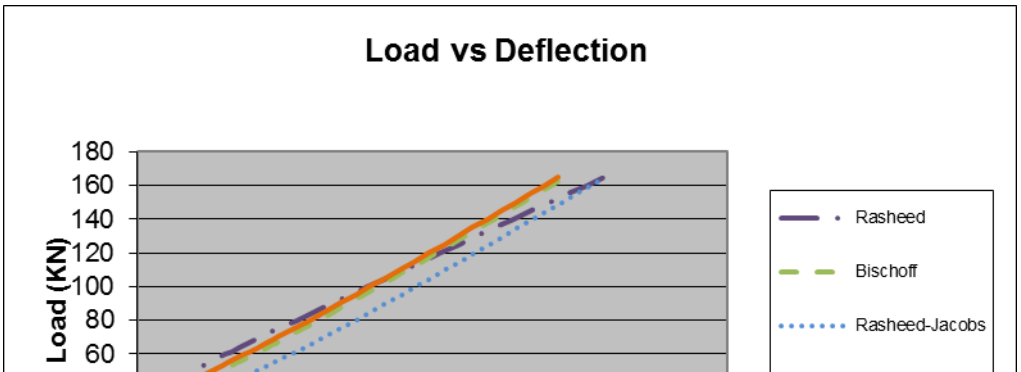

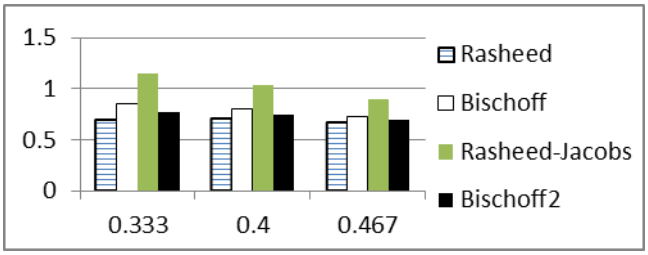

Table 4.90 Deflection comparison bar chart for sample 3a-NS.

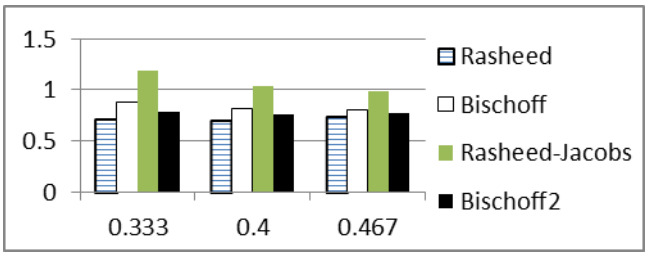

Table 4.91 Deflection comparison bar chart for dependent sample 3b-NS.

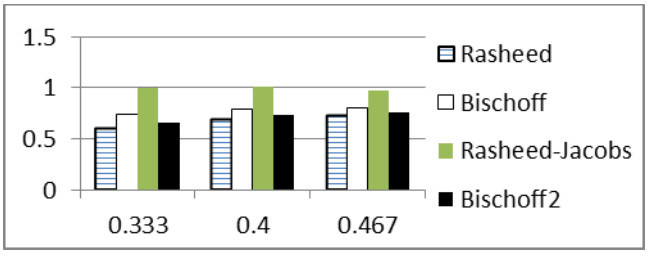

Table 4.92 Deflection comparison bar chart for dependent sample 3c-NS.

4.4.9.8 – 4-NS

section properties		
h=	285.75	mm
b=	228.6	mm
f'c	36.33535	MPA
E_c =	28469.68	MPA
E_s =	39851.67	MPA
A'f	0	mm^2

section properties		
h=	11.25	in
b=	9	in
f'c	5.27	ksi
E_c =	4137.902	ksi
E_s =	5780	ksi
A'f	0	in^2

Table 4.93 Initial parameters for Yost et al. sample 4a-NS.

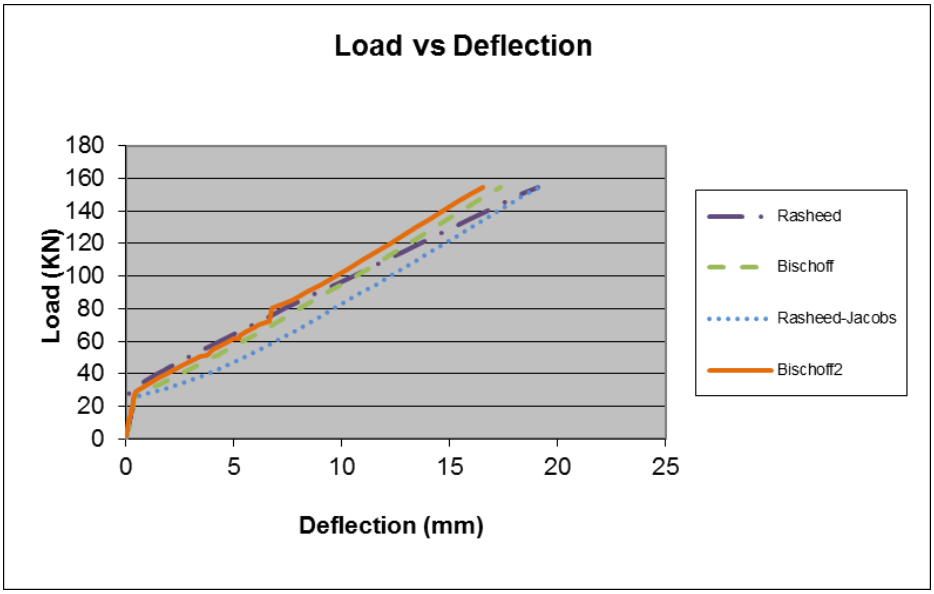

Figure 4.53 Load-deflection response for sample 4a-NS.

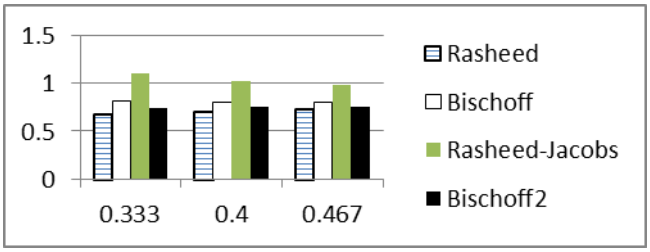

Table 4.94 Deflection comparison bar chart for sample 4a-NS.

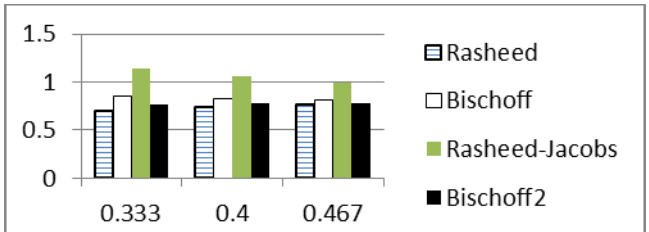

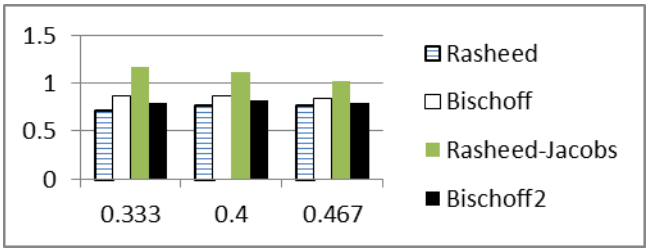

Table 4.96 Deflection comparison bar chart for dependent sample 4c-NS.

4.4.9.9 – 1-HS

section properties		
h=	285.75	mm
b=	203.2	mm
f'c	79.6344	MPA
E_c =	42147.16	MPA
E_s =	46056.95	MPA
A'f	0	mm^2
Af	570.3214	mm^2
d=	225.552	mm
d'=	0	mm
d''=	60.198	mm
f_{fu} =	689.4753	MPA
E_f =	40334.31	MPA
f'_{fu} =	0	MPA
span properties:		
L=	2133.6	mm
a=	914.4	mm

section properties		
h=	11.25	in
b=	8	in
f'c	11.55	ksi
E_c =	6125.843	ksi
E_s =	6680	ksi
A'f	0	in^2
Af	0.884	in^2
d=	8.88	in
d'=	0	in
d''=	2.37	in
f_{fu} =	100	ksi
E_f =	5850	ksi
f'_{fu} =	0	ksi
span properties:		
L=	84	in
a=	36	in

Table 4.97 Initial parameters for Yost et al. sample 1a-HS.

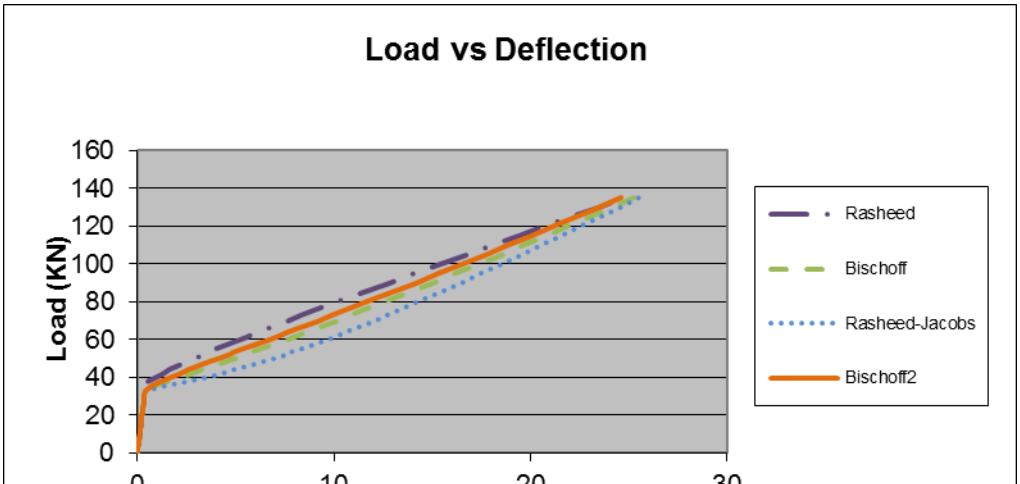

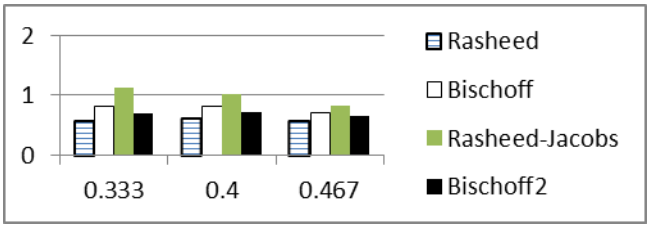

Table 4.98 Deflection comparison bar chart for sample 1a-HS.

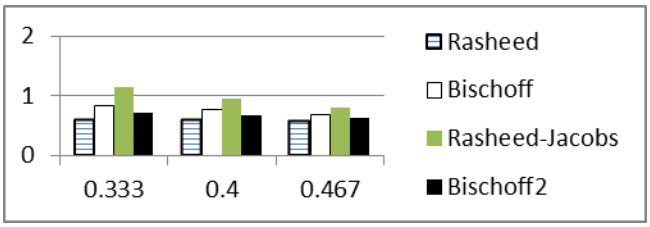

Table 4.99 Deflection comparison bar chart for dependent sample 1c-HS.

4.4.9.10 – 2-HS

section properties		
h=	285.75	mm
b=	152.4	mm
f'c	79.6344	MPA
E_c =	42147.16	MPA
E_s =	46056.95	MPA
A'f	0	mm^2
Af	570.3214	mm^2
d=	225.552	mm
d'=	0	mm
d''=	60.198	mm
f_{fu} =	689.4753	MPA
E_f =	40334.31	MPA

section properties		
h=	11.25	in
b=	6	in
f'c	11.55	ksi
E_c =	6125.843	ksi
E_s =	6680	ksi
A'f	0	in^2
Af	0.884	in^2
d=	8.88	in
d'=	0	in
d''=	2.37	in
f_{fu} =	100	ksi
E_f =	5850	ksi

Table 4.100 Initial parameters for Yost et al. sample 2a-HS.

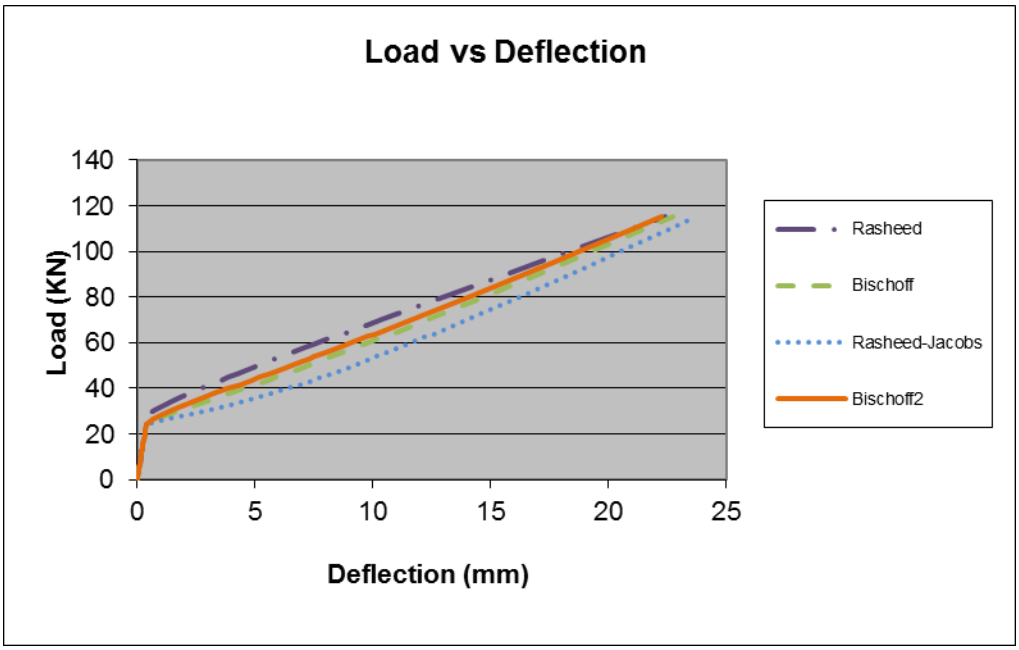

Figure 4.55 Load-deflection response for sample 2a-HS.

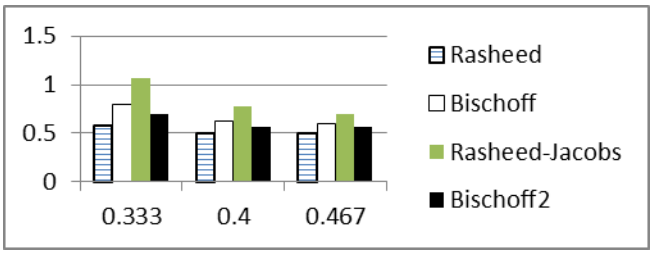

Table 4.101 Deflection comparison bar chart for sample 2a-HS.

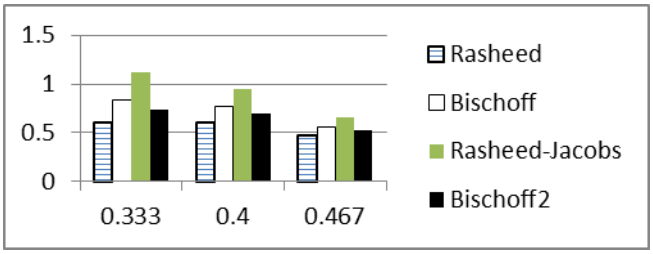

Table 4.102 Deflection comparison bar chart for dependent sample 2b-HS.

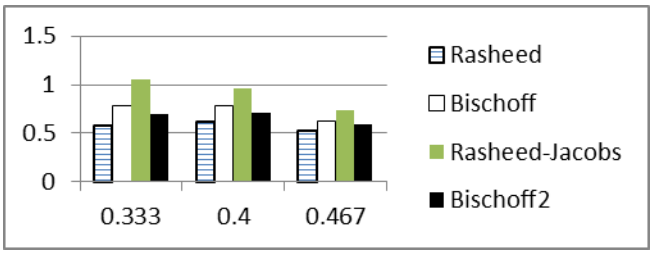

Table 4.103 Deflection comparison bar chart for dependent sample 2c-HS.

4.4.9.11 – 3-HS

section properties		
h=	285.75	mm
b=	165.1	mm
f'c	79.6344	MPA
E_c =	42147.16	MPA
E_s =	46056.95	MPA
A'f	0	mm^2
Af	776.1275	mm^2
d=	223.774	mm
d'=	0	mm
d''=	61.976	mm
f_{fu} =	689.4753	MPA
E_f =	40334.31	MPA
f'_{fu} =	0	MPA
span properties:		
L=	2133.6	mm
a=	914.4	mm

section properties		
h=	11.25	in
b=	6.5	in
f'c	11.55	ksi
E_c =	6125.843	ksi
E_s =	6680	ksi
A'f	0	in^2
Af	1.203	in^2
d=	8.81	in
d'=	0	in
d''=	2.44	in
f_{fu} =	100	ksi
E_f =	5850	ksi
f'_{fu} =	0	ksi
span properties:		
L=	84	in
a=	36	in

Table 4.104 Initial parameters for Yost et al. sample 3a-HS.

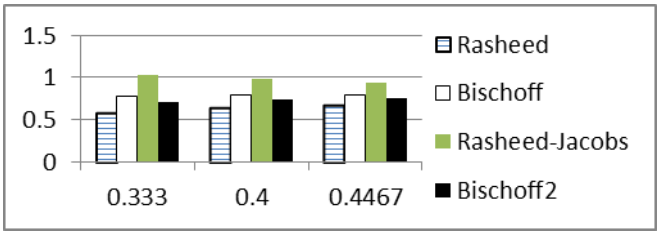

Table 4.105 Deflection comparison bar chart for sample 3a-HS.

4.4.9.12 – 4-HS

section properties		
h=	285.75	mm
b=	203.2	mm
f'c	79.6344	MPA
E_c =	42147.16	MPA
E_s =	46056.95	MPA
A'f	0	mm^2
Af	1163.869	mm^2
d=	223.774	mm
d'=	0	mm
d''=	61.976	mm
f_{fu} =	689.4753	MPA
E_f =	40334.31	MPA
f'_{fu} =	0	MPA
span properties:		
L=	2133.6	mm
a=	914.4	mm

section properties		
h=	11.25	in
b=	8	in
f'c	11.55	ksi
E_c =	6125.843	ksi
E_s =	6680	ksi
A'f	0	in^2
Af	1.804	in^2
d=	8.81	in
d'=	0	in
d''=	2.44	in
f_{fu} =	100	ksi
E_f =	5850	ksi
f'_{fu} =	0	ksi
span properties:		
L=	84	in
a=	36	in

Table 4.106 Initial parameters for Yost et al. sample 4a-HS.

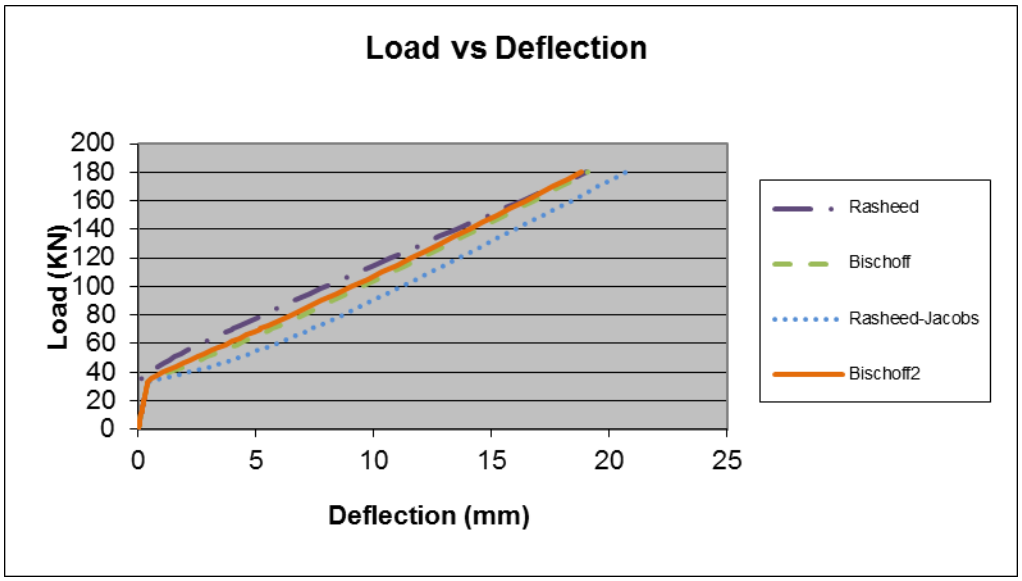

Figure 4.57 Load-deflection response for sample 4a-HS.

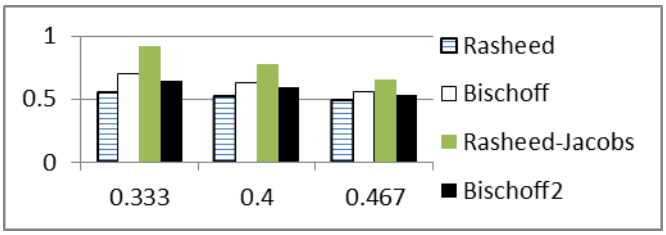

Table 4.107 Deflection comparison bar chart for sample 4a-HS.

4.4.9.13 – 1-HL

section properties		
h=	184.15	mm
b=	254	mm
f'c	79.4965	MPA
E_c =	42110.65	MPA
E_s =	45160.63	MPA
A'f	0	mm^2
Af	396.1282	mm^2
d=	138.176	mm
d'=	0	mm
d''=	45.974	mm
f_{fu} =	689.4753	MPA
E_f =	40334.31	MPA
f'_{fu} =	0	MPA
span properties:		
L=	2895.6	mm
a=	1295.4	mm

section properties		
h=	7.25	in
b=	10	in
f'c	11.53	ksi
E_c =	6120.537	ksi
E_s =	6550	ksi
A'f	0	in^2
Af	0.614	in^2
d=	5.44	in
d'=	0	in
d''=	1.81	in
f_{fu} =	100	ksi
E_f =	5850	ksi
f'_{fu} =	0	ksi
span properties:		
L=	114	in
a=	51	in

Table 4.108 Initial parameters for Yost et al. sample 1a-HL.

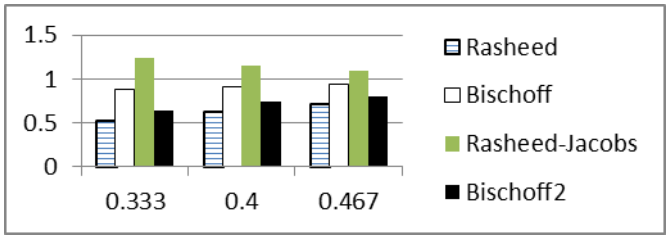

Table 4.109 Deflection comparison bar chart for sample 1a-HL.

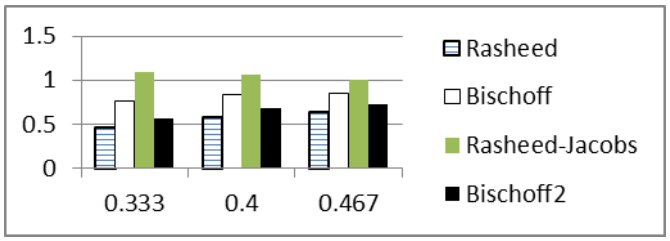

Table 4.110 Deflection comparison bar chart for dependent sample 1b-HL.

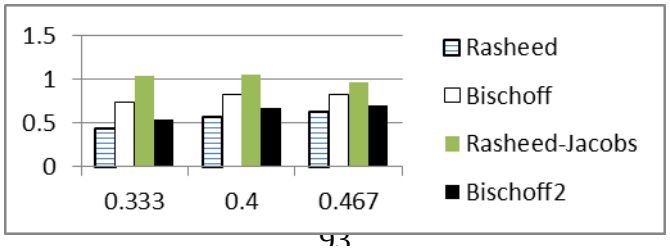

Table 4.111 Deflection comparison bar chart for dependent sample 1c-HL.

4.4.9.14 – 2-HL

section properties		
h=	184.15	mm
b=	190.5	mm
f'c	79.4965	MPA
E_c =	42110.65	MPA
E_s =	45160.63	MPA
A'f	0	mm^2
Af	396.1282	mm^2
d=	138.176	mm
d'=	0	mm
d''=	45.974	mm
f_{fu} =	689.4753	MPA
E_f =	40334.31	MPA
f'_{fu} =	0	MPA
span properties:		
L=	2895.6	mm
a=	1295.4	mm

section properties		
h=	7.25	in
b=	7.5	in
f'c	11.53	ksi
E_c =	6120.537	ksi
E_s =	6550	ksi
A'f	0	in^2
Af	0.614	in^2
d=	5.44	in
d'=	0	in
d''=	1.81	in
f_{fu} =	100	ksi
E_f =	5850	ksi
f'_{fu} =	0	ksi
span properties:		
L=	114	in
a=	51	in

Table 4.112 Initial parameters for Yost et al. sample 2a-HL.

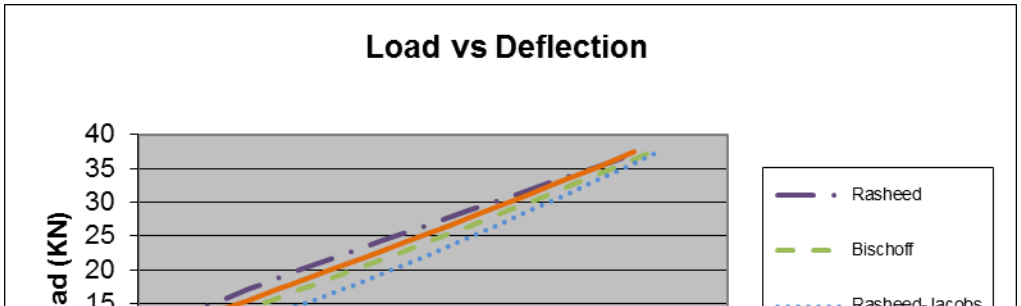

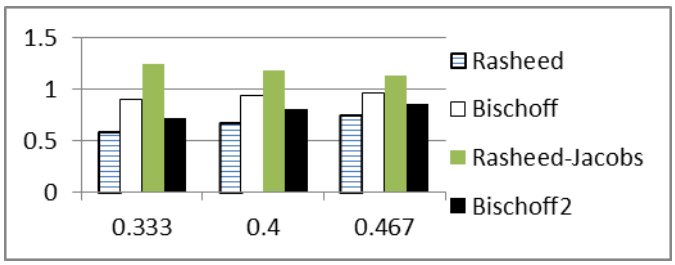

Table 4.113 Deflection comparison bar chart for sample 2a-HL.

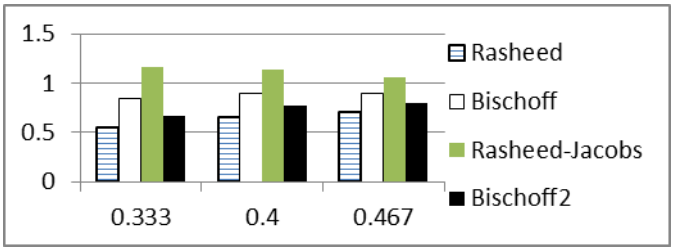

Table 4.114 Deflection comparison bar chart for dependent sample 2b-HL.

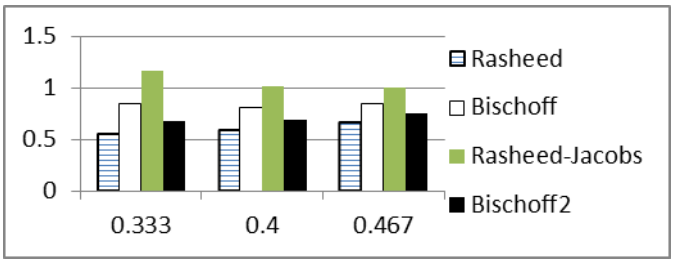

Table 4.115 Deflection comparison bar chart for dependent sample 2c-HL.

4.4.9.15 – 3-HL

section properties		
h=	184.15	mm
b=	152.4	mm
f'c	79.4965	MPA
E_c =	42110.65	MPA
E_s =	45160.63	MPA
A'f	0	mm^2
Af	396.1282	mm^2
d=	138.176	mm
d'=	0	mm
d''=	45.974	mm
f_{fu} =	689.4753	MPA
E_f =	40334.31	MPA
f'_{fu} =	0	MPA
span properties:		
L=	2895.6	mm
a=	1295.4	mm

section properties		
h=	7.25	in
b=	6	in
f'c	11.53	ksi
E_c =	6120.537	ksi
E_s =	6550	ksi
A'f	0	in^2
Af	0.614	in^2
d=	5.44	in
d'=	0	in
d''=	1.81	in
f_{fu} =	100	ksi
E_f =	5850	ksi
f'_{fu} =	0	ksi
span properties:		
L=	114	in
a=	51	in

Table 4.116 Initial parameters for Yost et al. sample 3a-HL.

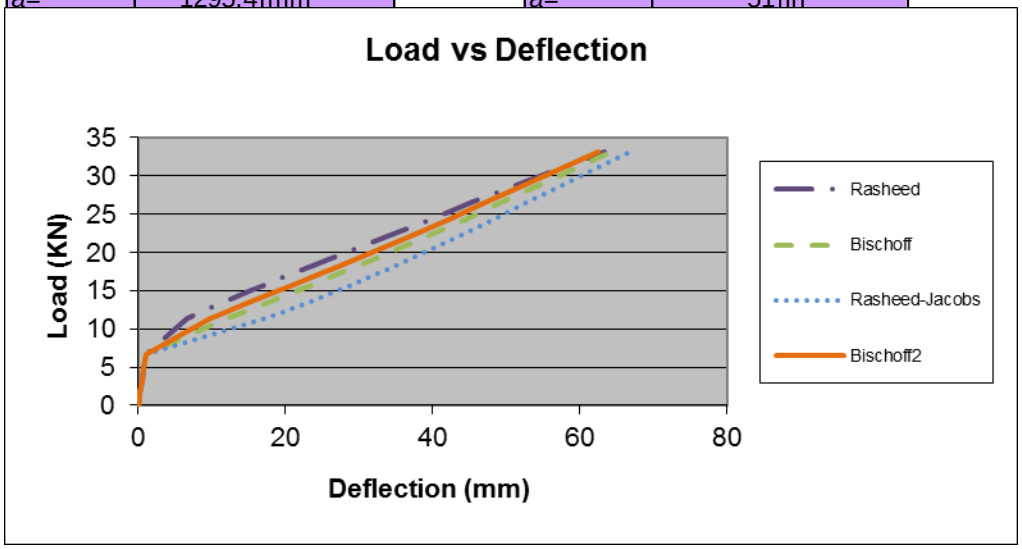

Figure 4.60 Load-deflection response for sample 3a-HL.

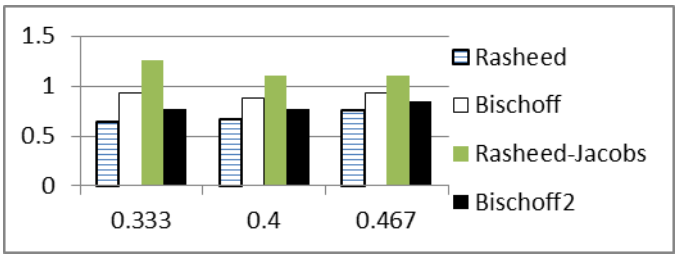

Table 4.117 Deflection comparison bar chart for sample 3a-HL.

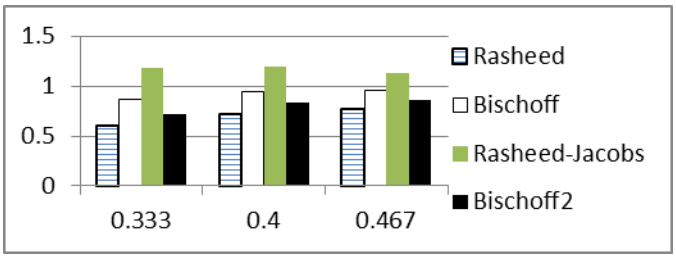

Table 4.118 Deflection comparison bar chart for dependent sample 3b-HL.

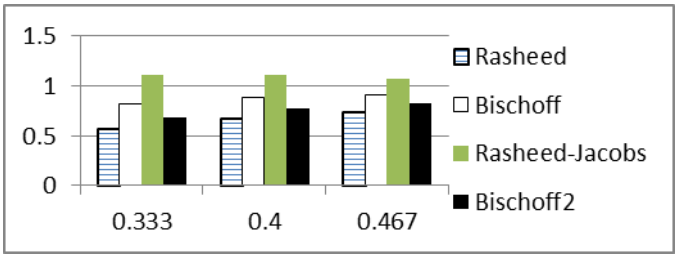

Table 4.119 Deflection comparison bar chart for dependent sample 3c-HL.

4.4.9.16 – 4-HL

section properties		
h=	184.15	mm
b=	177.8	mm
f'c	79.42756	MPA
E_c =	42092.39	MPA
E_s =	45160.63	MPA
A'f	0	mm^2
Af	570.3214	mm^2
d=	136.652	mm
d'=	0	mm
d''=	47.498	mm
f_{fu} =	689.4753	MPA
E_f =	40334.31	MPA
f'_{fu} =	0	MPA
span properties:		
L=	2895.6	mm
a=	1295.4	mm

section properties		
h=	7.25	in
b=	7	in
f'c	11.52	ksi
E_c =	6117.882	ksi
E_s =	6550	ksi
A'f	0	in^2
Af	0.884	in^2
d=	5.38	in
d'=	0	in
d''=	1.87	in
f_{fu} =	100	ksi
E_f =	5850	ksi
f'_{fu} =	0	ksi
span properties:		
L=	114	in
a=	51	in

Table 4.120 Initial parameters for Yost et al. sample 4a-HL.

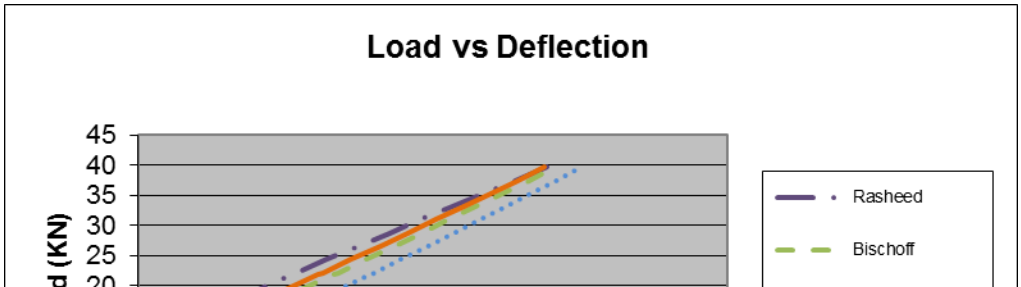

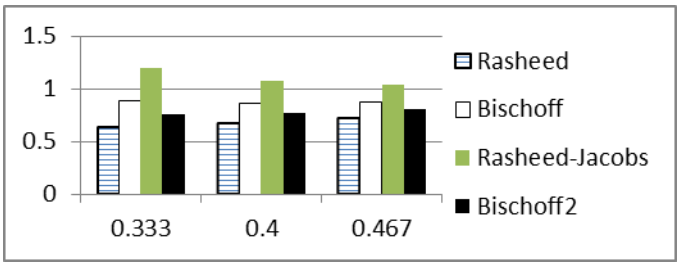

Table 4.121 Deflection comparison bar chart for sample 4a-HL.

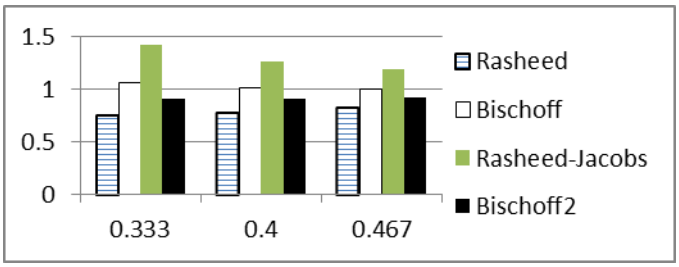

Table 4.122 Deflection comparison bar chart for dependent sample 4b-HL.

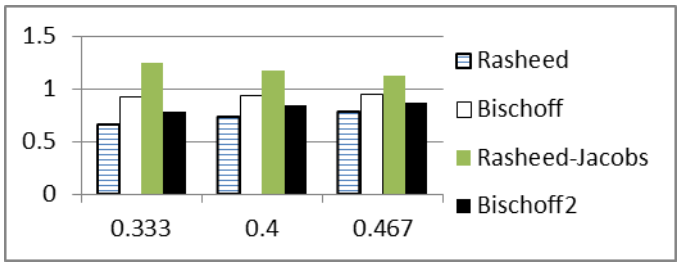

Table 4.123 Deflection comparison bar chart for

4.4.10 Theisz et al. (2004)

Four independent samples are from Theisz et al., with eight dependent samples. The four independent samples are 8-2-1, 8-3-1, 11-2-1, 11-3-1. With the dependent samples labeled as 8-2-2, 8-2-3, 8-3-2, 8-3-3, 11-2-2, 11-2-3, 11-3-2, and 11-3-3, and they depend on the independent sample respectively by name. One set of initial parameters and one load-deflection graph is shown for each of the independent samples. In this set of samples, the Bischoff2 model best predicted the obtained deflection closest to the experimental deflection for each of the three moment levels. In comparison, the Rasheed-Jacobs model slightly over predicted the deflection values and is considered conservative.

4.4.10.1 – 8-2

section properties		
h=	171.45	mm
b=	127	mm
f'c	60.32909	MPA
E_c=	36684.39	MPA
E_s=	51779.6	MPA
A'f	0	mm^2
Af	59.99988	mm^2
d=	142.875	mm
d'=	0	mm
d''=	28.575	mm
f_{fu}=	2635.864	MPA
E_f=	139274	MPA
f'_{fu}=	0	MPA
span properties:		
L=	1981.2	mm
a=	914.4	mm

section properties		
h=	6.75	in
b=	5	in
f'c	8.75	ksi
E_c=	5331.862	ksi
E_s=	7510	ksi
A'f	0	in^2
Af	0.093	in^2
d=	5.625	in
d'=	0	in
d''=	1.125	in
f_{fu}=	382.3	ksi
E_f=	20200	ksi
f'_{fu}=	0	ksi
span properties:		
L=	78	in
a=	36	in

Table 4.124 Initial parameters for Theisz et al. sample 8-2.

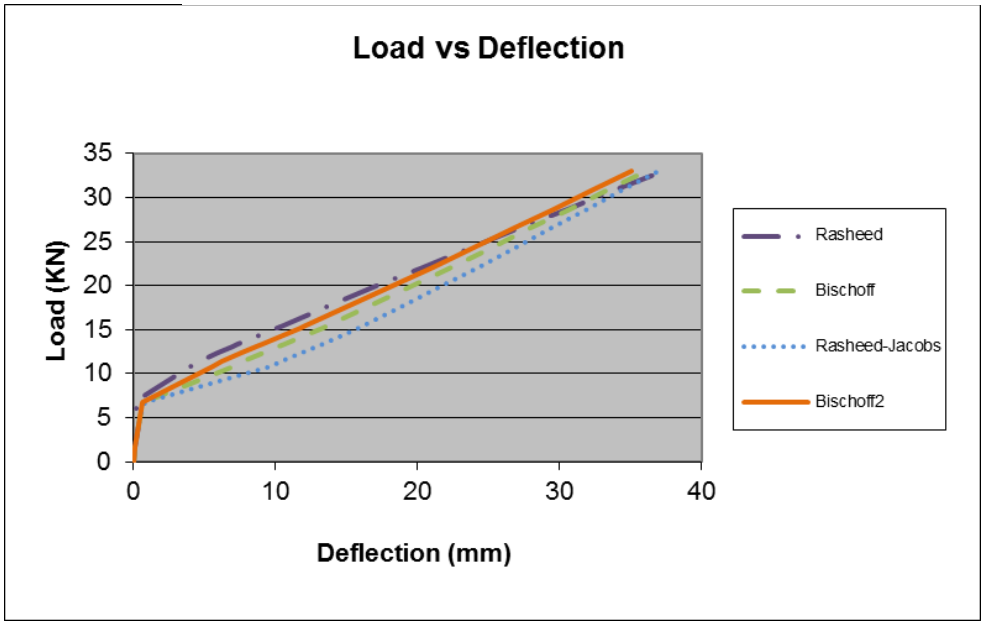

Figure 4.62 Load-deflection response for sample 8-2.

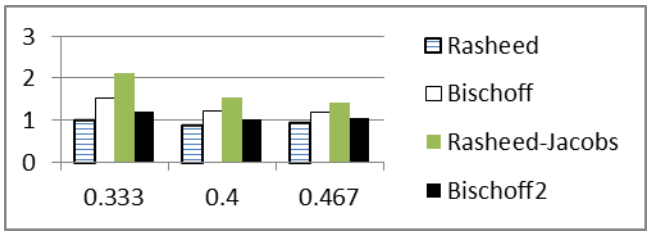

Table 4.125 Deflection comparison bar chart for sample 8-2-1.

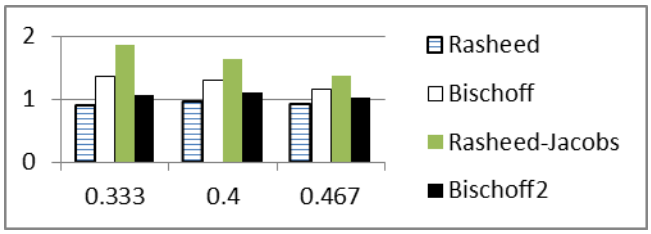

Table 4.126 Deflection comparison bar chart for sample 8-2-2.

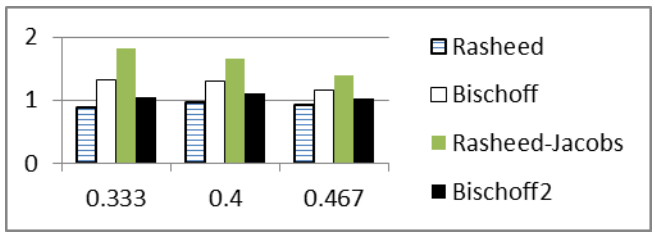

Table 4.127 Deflection comparison bar chart for sample 8-2-3.

4.4. 10.2 – 8-3

section properties		
h=	171.45	mm
b=	158.75	mm
f'c	61.84594	MPA
E_c=	37142.71	MPA
E_s=	53365.39	MPA
A'f	0	mm^2
Af	130.3223	mm^2
d=	141.2875	mm
d'=	0	mm
d''=	30.1625	mm
f_{fu}=	2457.29	MPA
E_f=	139274	MPA
f'_{fu}=	0	MPA
span properties:		
L=	1981.2	mm
a=	914.4	mm

section properties		
h=	6.75	in
b=	6.25	in
f'c	8.97	ksi
E_c=	5398.475	ksi
E_s=	7740	ksi
A'f	0	in^2
Af	0.202	in^2
d=	5.5625	in
d'=	0	in
d''=	1.1875	in
f_{fu}=	356.4	ksi
E_f=	20200	ksi
f'_{fu}=	0	ksi
span properties:		
L=	78	in
a=	36	in

Table 4.128 Initial parameters for Theisz et al. sample 8-3.

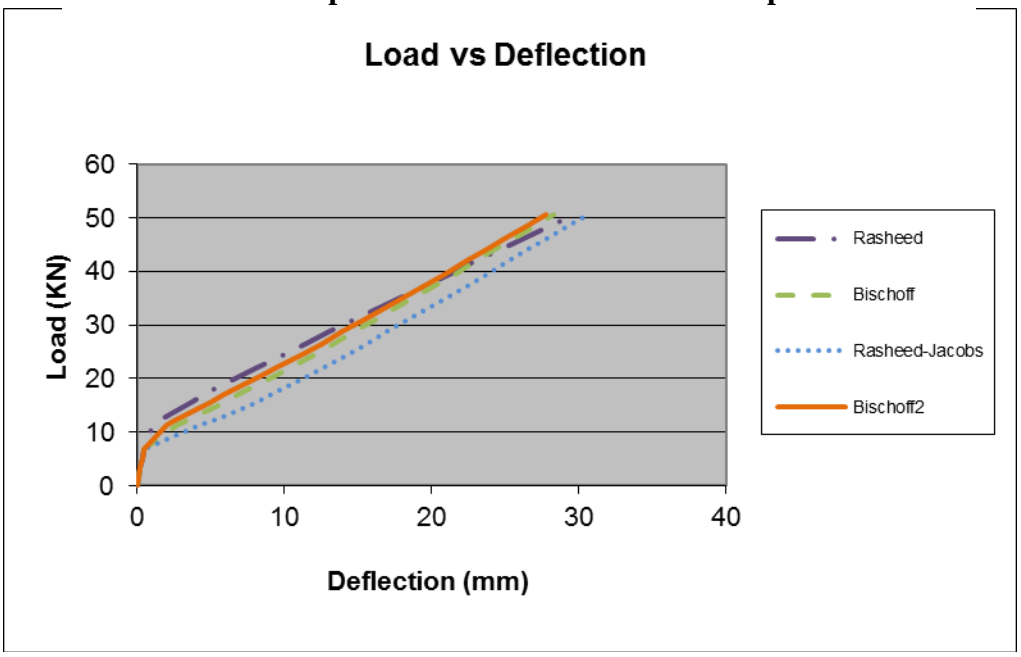

Figure 4.63 Load-deflection response for sample 8-3.

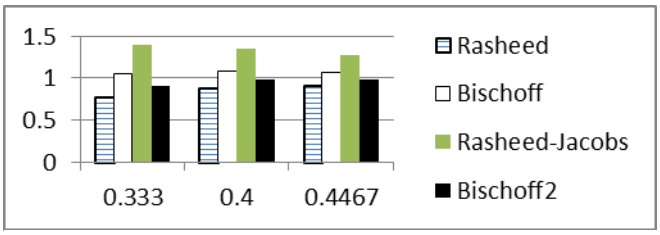

Table 4.129 Deflection comparison bar chart for sample 8-3-1.

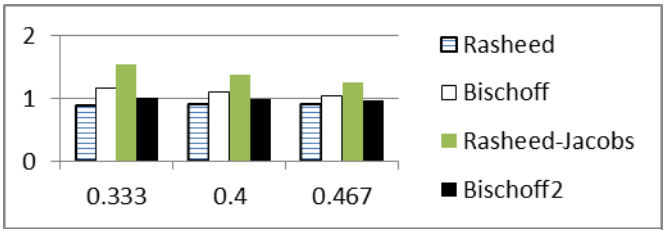

Table 4.130 Deflection comparison bar chart for sample 8-3-2.

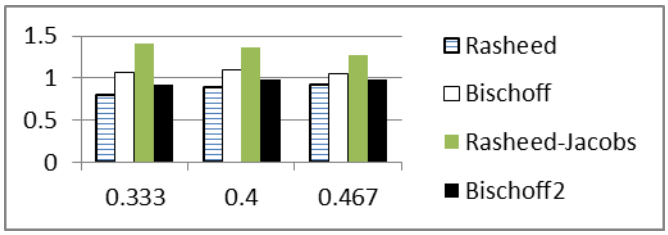

Table 4.131 Deflection comparison bar chart for sample 8-3-3.

4.4.10.3 – 11-2

section properties		
h=	171.45	mm
b=	88.9	mm
f'c	81.35809	MPA
E_c=	42600.85	MPA
E_s=	54606.45	MPA
A'f	0	mm^2
Af	59.99988	mm^2
d=	142.875	mm
d'=	0	mm
d''=	28.575	mm
f_{fu}=	2635.864	MPA
E_f=	139274	MPA
f'_{fu}=	0	MPA
span properties:		
L=	1981.2	mm
a=	914.4	mm

section properties		
h=	6.75	in
b=	3.5	in
f'c	11.8	ksi
E_c=	6191.785	ksi
E_s=	7920	ksi
A'f	0	in^2
Af	0.093	in^2
d=	5.625	in
d'=	0	in
d''=	1.125	in
f_{fu}=	382.3	ksi
E_f=	20200	ksi
f'_{fu}=	0	ksi
span properties:		
L=	78	in
a=	36	in

Table 4.132 Initial parameters for Theisz et al. sample 11-2.

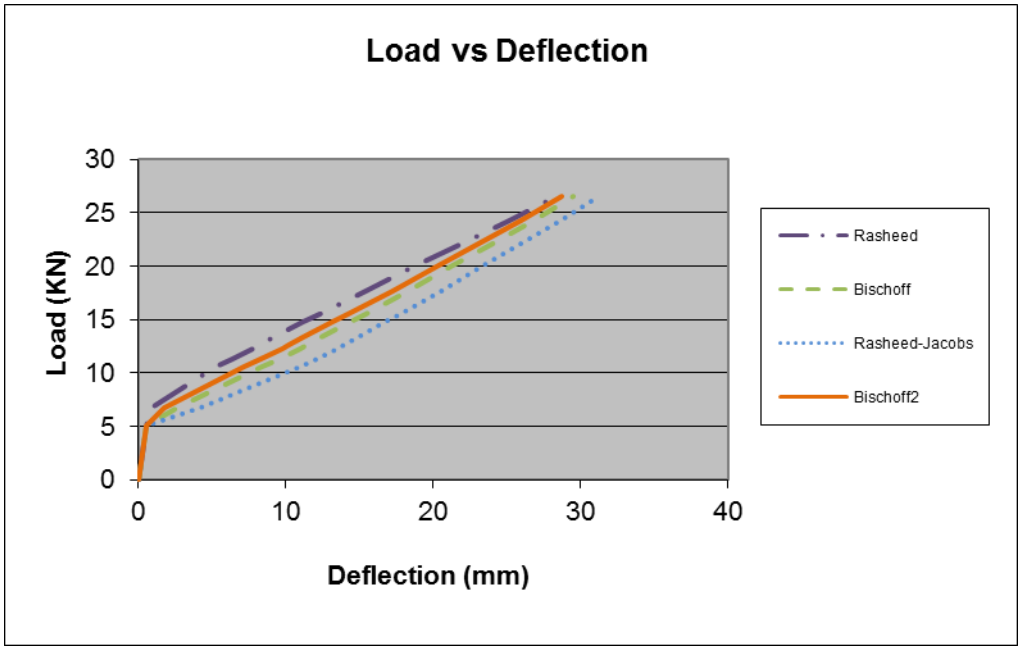

Figure 4.64 Load-deflection response for sample 11-2.

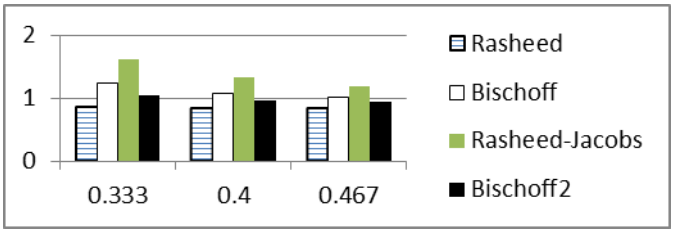

Table 4.133 Deflection comparison bar chart for sample 11-2-1.

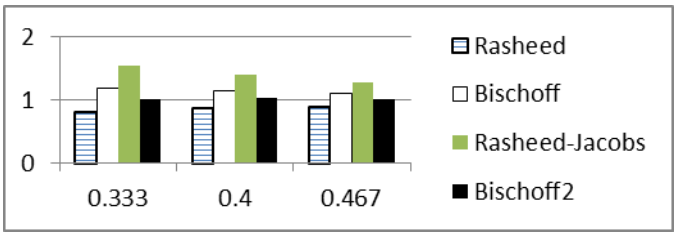

Table 4.134 Deflection comparison bar chart for sample 11-2-2.

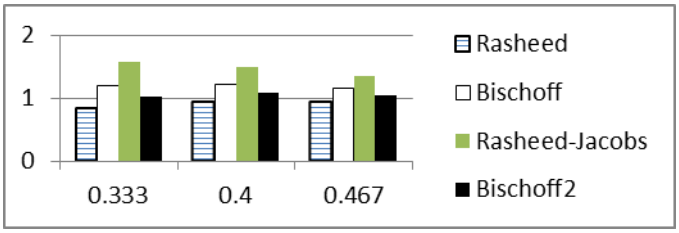

Table 4.135 Deflection comparison bar chart for sample 11-2-3.

4.4.10.4 – 11-3

section properties		
h=	171.45	mm
b=	120.65	mm
f'c	81.35809	MPA
E_c=	42600.85	MPA
E_s=	54606.45	MPA
A'f	0	mm^2
Af	130.3223	mm^2
d=	141.2875	mm
d'=	0	mm
d''=	30.1625	mm
f_{fu}=	2457.29	MPA
E_f=	139274	MPA
f'_{fu}=	0	MPA
span properties:		
L=	1981.2	mm
a=	914.4	mm

section properties		
h=	6.75	in
b=	4.75	in
f'c	11.8	ksi
E_c=	6191.785	ksi
E_s=	7920	ksi
A'f	0	in^2
Af	0.202	in^2
d=	5.5625	in
d'=	0	in
d''=	1.1875	in
f_{fu}=	356.4	ksi
E_f=	20200	ksi
f'_{fu}=	0	ksi
span properties:		
L=	78	in
a=	36	in

Table 4.136 Initial parameters for Theisz et al. sample 11-3.

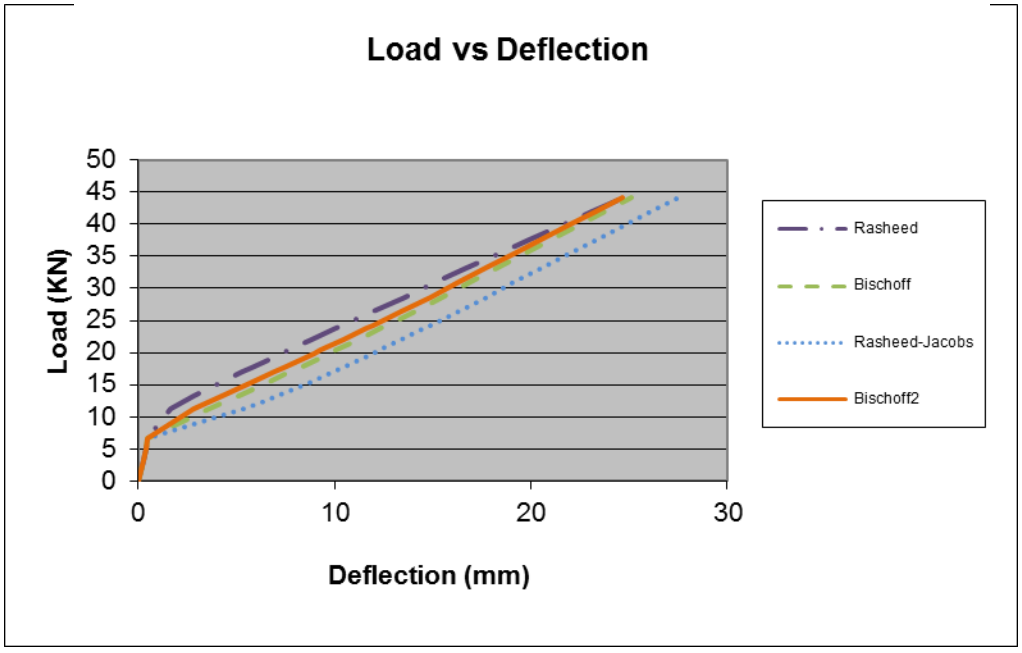

Figure 4.65 Load-deflection response for sample 11-3.

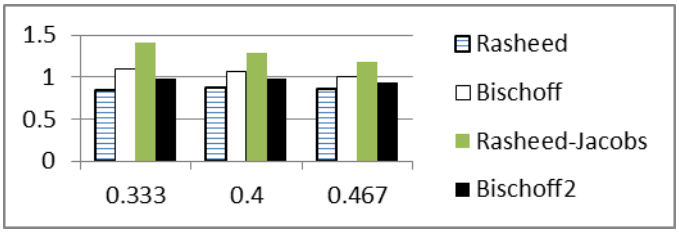

Table 4.137 Deflection comparison bar chart for sample 11-3-1.

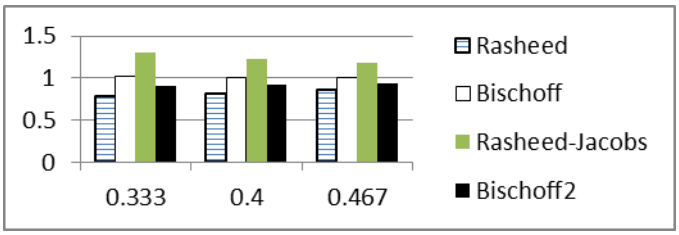

Table 4.138 Deflection comparison bar chart for sample 11-3-2.

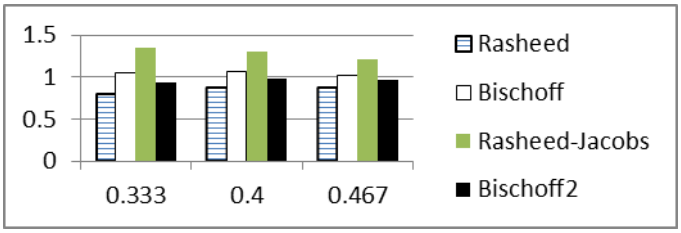

Table 4.139 Deflection comparison bar chart for sample 11-3-3.

4.4.11 Al-Sunna (2006)

Eleven independent Al-Sunna samples were used in this research from the Gross database, with seven more dependent samples included for the deflection value comparison. The eleven independent samples are BC1a, BC2a, BC3a, BG2a, BG3a, SC2a, SC2b, SC3a, SC3b, SG2a, and SG3a. The dependent samples are BC1b, BC2b, BC3b, BG2b, BG3b, SG2b, and SG3b, where these samples are dependent on their counter-part sample a. The Rasheed-Jacobs model best represents the majority of the Al-Sunna samples in all three moment levels for both independent and dependent samples. The main outliers are BG3b, SG3a, and SG3b.

4.4.11.1 – BC1a

section properties		
h=	250	mm
b=	150	mm
f'c	55.39802	MPA
E_c =	35153.22	MPA
E_s =	31498.87	MPA
A'f	0	mm^2
Af	95.00755	mm^2

section properties		
h=	9.84252	in
b=	5.905512	in
f'c	8.034808	ksi
E_c =	5109.314	ksi
E_s =	4568.528	ksi
A'f	0	in^2
Af	0.147262	in^2

Table 4.140 Initial parameters for Al-Sunna sample BC1a.

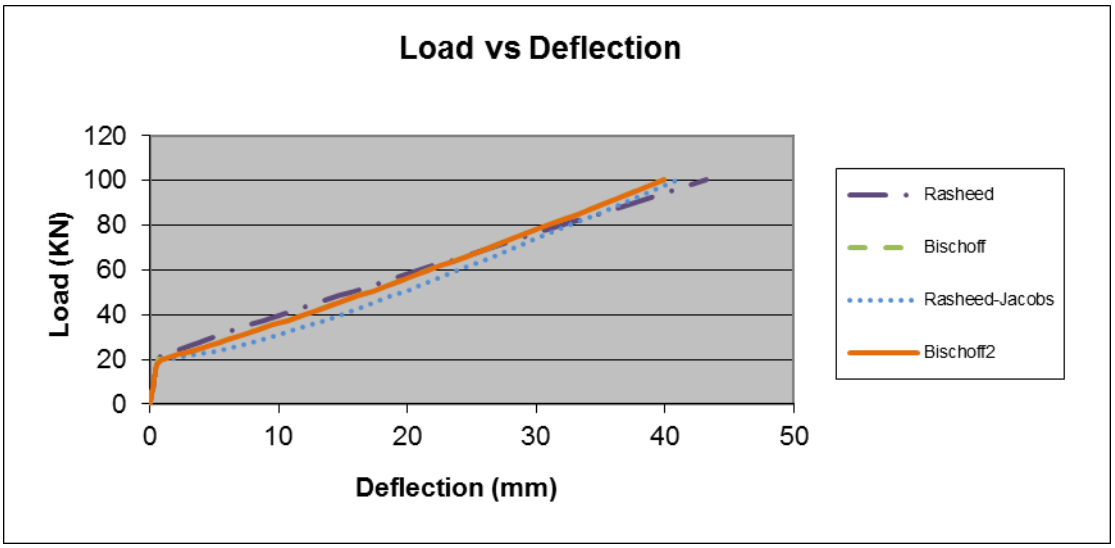

Figure 4.66 Load-deflection response for sample BC1a.

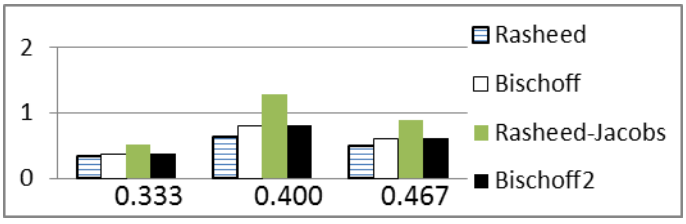

Table 4.141 Deflection comparison bar chart for

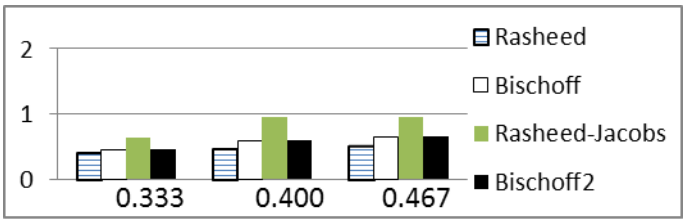

Table 4.142 Deflection comparison bar chart for dependent sample BC1b.

4.4.11.2 – BC2a

section properties		
h=	250	mm
b=	150	mm
f'c	52.59811	MPA
E_c =	34253.35	MPA
E_s =	31498.87	MPA
A'f	0	mm^2
Af	213.9918	mm^2
d=	220.235	mm
d'=	0	mm
d''=	29.76502	mm
f_{fu} =	1324.952	MPA
E_f =	131745.3	MPA
f'_{fu} =	413.6852	MPA
span properties:		
L=	2300	mm
a=	766.9999	mm

section properties		
h=	9.84252	in
b=	5.905512	in
f'c	7.628716	ksi
E_c =	4978.524	ksi
E_s =	4568.528	ksi
A'f	0	in^2
Af	0.331688	in^2
d=	8.670669	in
d'=	0	in
d''=	1.171851	in
f_{fu} =	192.1682	ksi
E_f =	19108.05	ksi
f'_{fu} =	60	ksi
span properties:		
L=	90.55118	in
a=	30.19685	in

Table 4.143 Initial parameters for Al-Sunna sample BC2a.

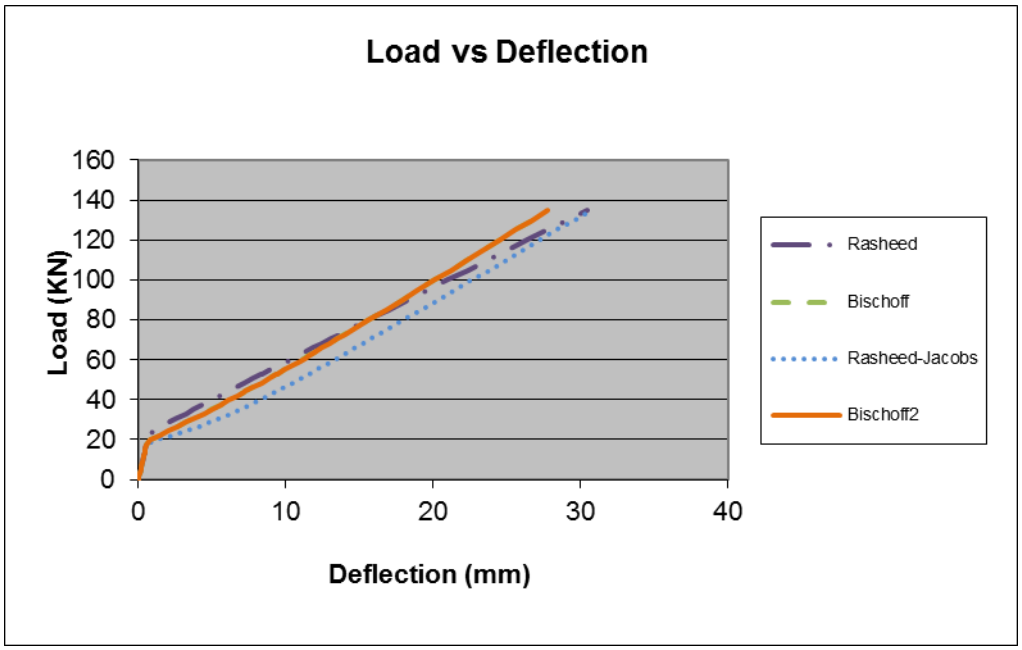

Figure 4.67 Load-deflection response for sample BC2a.

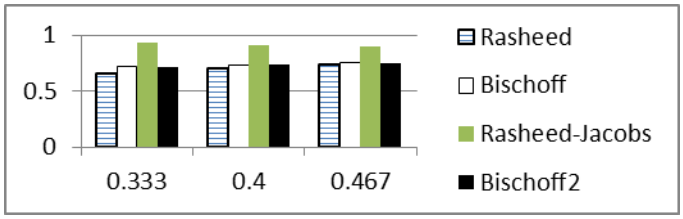

Table 4.144 Deflection comparison bar chart for sample BC2a.

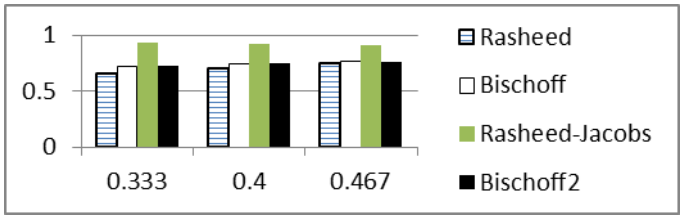

Table 4.145 Deflection comparison bar chart for dependent sample BC2b.

4.4.11.3 – BC3a

section properties		
h=	250	mm
b=	150	mm
f'c	51.79814	MPA
E_c =	33991.87	MPA
E_s =	31498.87	MPA
A'f	0	mm^2
Af	380.0309	mm^2
d=	218.65	mm
d'=	0	mm
d''=	31.35	mm
f_{fu} =	1474.947	MPA
E_f =	118595.8	MPA
f'_{fu} =	413.6852	MPA
span properties:		
L=	2300	mm
a=	766.9999	mm

section properties		
h=	9.84252	in
b=	5.905512	in
f'c	7.51269	ksi
E_c =	4940.519	ksi
E_s =	4568.528	ksi
A'f	0	in^2
Af	0.589049	in^2
d=	8.608268	in
d'=	0	in
d''=	1.234252	in
f_{fu} =	213.9231	ksi
E_f =	17200.87	ksi
f'_{fu} =	60	ksi
span properties:		
L=	90.55118	in
a=	30.19685	in

Table 4.146 Initial parameters for Al-Sunna sample BC3a.

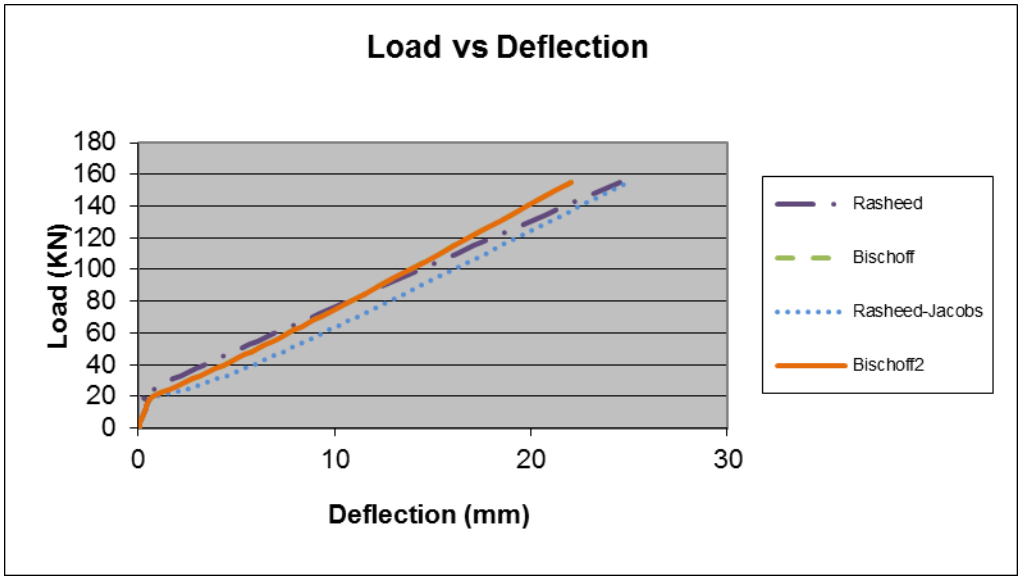

Figure 4.68 Load-deflection response for sample BC3a.

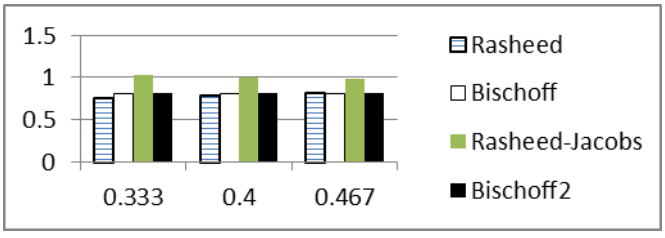

Table 4.147 Deflection comparison bar chart

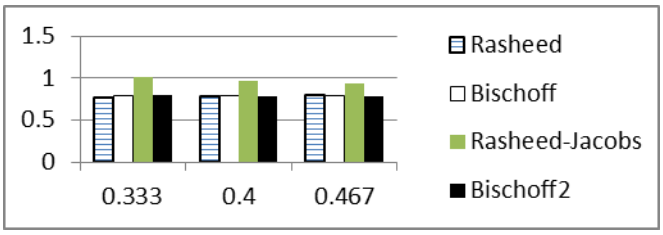

Table 4.148 Deflection comparison bar chart for dependent sample BC3b.

4.4.11.4 – BG2a

section properties		
h=	250	mm
b=	150	mm
f'c	47.6983	MPA
E_c =	32618.9	MPA
E_s =	31498.87	MPA
A'f	0	mm^2
Af	253.3537	mm^2
d=	218.65	mm
d'=	0	mm
d''=	31.35	mm
f_{fu} =	619.9778	MPA
E_f =	41598.51	MPA
f'_{fu} =	413.6852	MPA
span properties:		
L=	2300	mm
a=	766.9999	mm

section properties		
h=	9.84252	in
b=	5.905512	in
f'c	6.918057	ksi
E_c =	4740.967	ksi
E_s =	4568.528	ksi
A'f	0	in^2
Af	0.392699	in^2
d=	8.608268	in
d'=	0	in
d''=	1.234252	in
f_{fu} =	89.92023	ksi
E_f =	6033.358	ksi
f'_{fu} =	60	ksi
span properties:		
L=	90.55118	in
a=	30.19685	in

Table 4.149 Initial parameters for Al-Sunna sample BG2a.

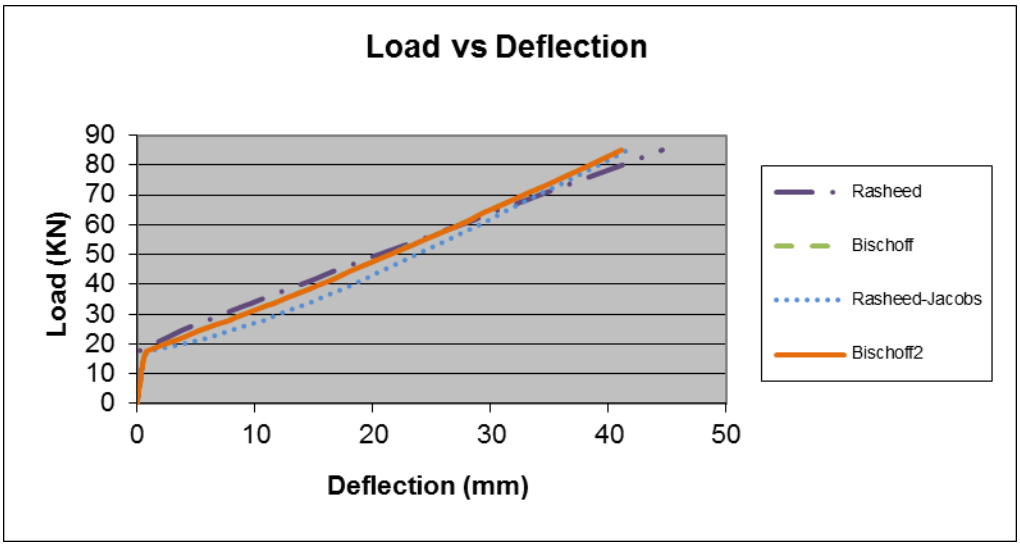

Figure 4.69 Load-deflection response for sample BG2a.

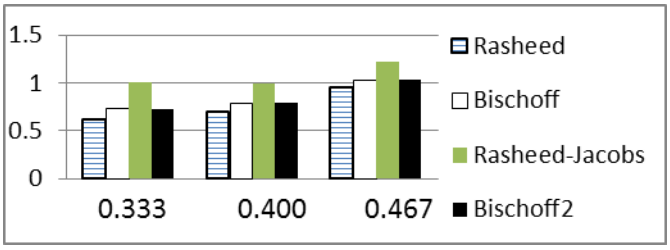

Table 4.150 Deflection comparison bar chart for sample BG2a.

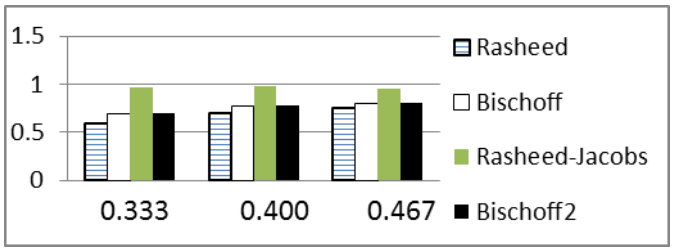

Table 4.151 Deflection comparison bar chart for dependent sample BG2b.

4.4.11.5 – BG3a

section properties		
h=	250	mm
b=	150	mm
f'c	46.49833	MPA
E_c =	32205.99	MPA
E_s =	31498.87	MPA
A'f	0	mm^2
Af	1140.092	mm^2
d=	193.45	mm
d'=	0	mm
d''=	56.55	mm
f_{fu} =	669.976	MPA
E_f =	41948.5	MPA
f'_{fu} =	413.6852	MPA
span properties:		
L=	2300	mm
a=	766.9999	mm

section properties		
h=	9.84252	in
b=	5.905512	in
f'c	6.744017	ksi
E_c =	4680.952	ksi
E_s =	4568.528	ksi
A'f	0	in^2
Af	1.767146	in^2
d=	7.616142	in
d'=	0	in
d''=	2.226378	in
f_{fu} =	97.17186	ksi
E_f =	6084.119	ksi
f'_{fu} =	60	ksi
span properties:		
L=	90.55118	in
a=	30.19685	in

Table 4.152 Initial parameters for Al-Sunna sample BG3a.

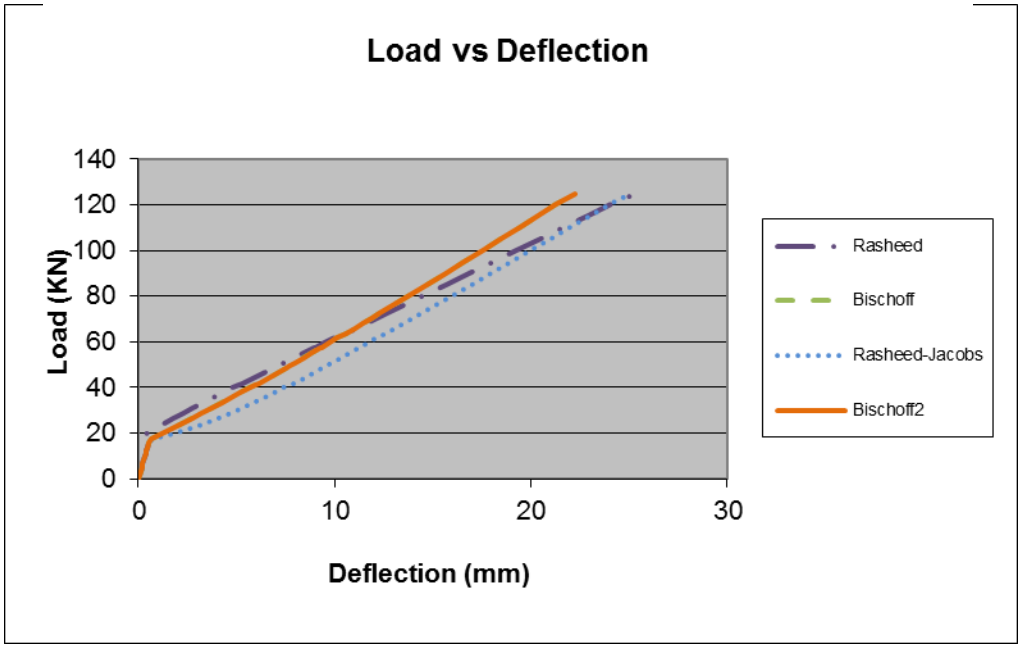

Figure 4.70 Load-deflection response for sample BG3a.

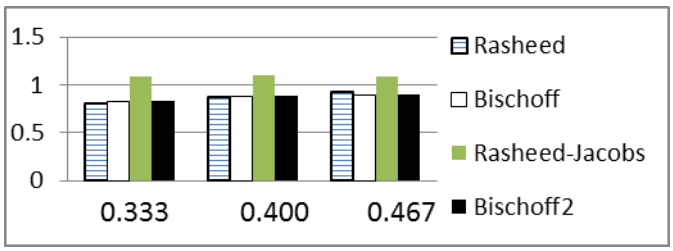

Table 4.153 Deflection comparison bar chart for sample BG3a.

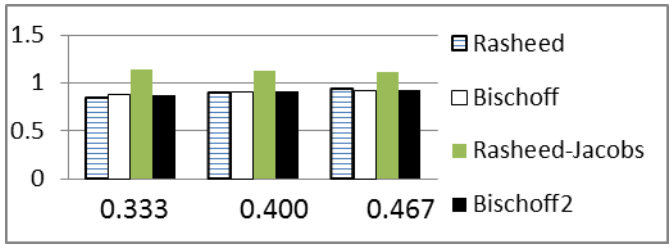

Table 4.154 Deflection comparison bar chart for dependent sample BG3b.

4.4.11.6 – SC2a

section properties		
h=	120	mm
b=	500	mm
f'c	50.99817	MPA
E_c =	33728.36	MPA
E_s =	31498.87	MPA
A'f	0	mm^2
Af	285.322	mm^2
d=	77.235	mm
d'=	0	mm
d''=	42.76499	mm
f_{fu} =	1324.952	MPA
E_f =	131745.3	MPA
f'_{fu} =	413.6852	MPA
span properties:		
L=	2100	mm
a=	750	mm

section properties		
h=	4.724409	in
b=	19.68504	in
f'c	7.396664	ksi
E_c =	4902.22	ksi
E_s =	4568.528	ksi
A'f	0	in^2
Af	0.44225	in^2
d=	3.040748	in
d'=	0	in
d''=	1.683661	in
f_{fu} =	192.1682	ksi
E_f =	19108.05	ksi
f'_{fu} =	60	ksi
span properties:		
L=	82.67717	in
a=	29.52756	in

Table 4.155 Initial parameters for Al-Sunna sample SC2a.

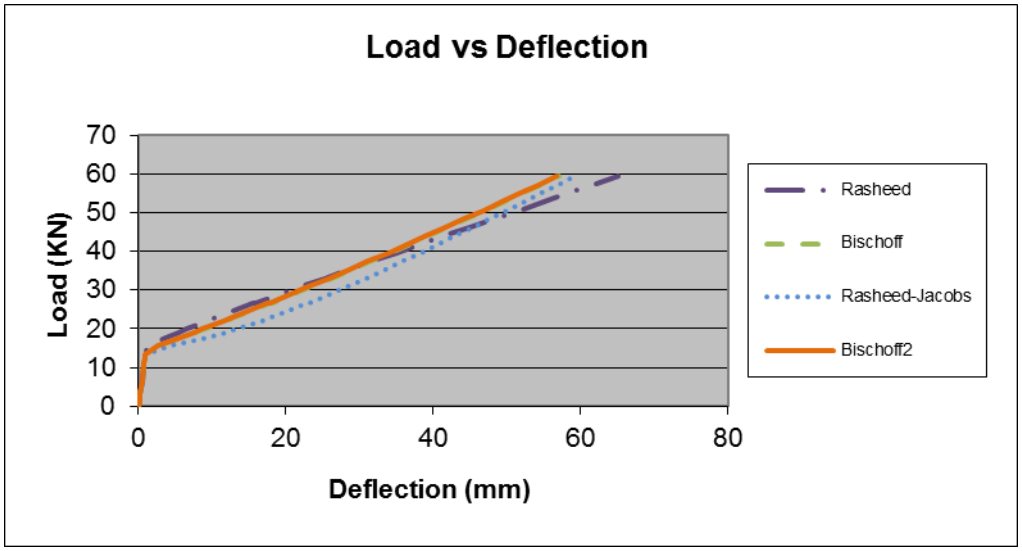

Figure 4.71 Load-deflection response for sample SC2a.

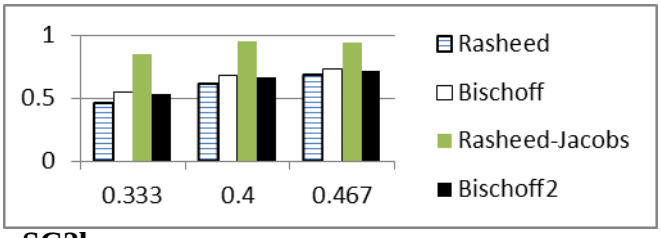

Table 4.156 Deflection comparison bar chart for sample SC2a.

4.4.11.7 – SC2b

section properties		
h=	120	mm
b=	500	mm
f'c	50.99817	MPA
E_c =	33728.36	MPA
E_s =	31498.87	MPA
A'f	0	mm^2
Af	285.322	mm^2
d=	80.23499	mm
d'=	0	mm
d''=	39.765	mm
f_{fu} =	1324.952	MPA
E_f =	131745.3	MPA
f'_{fu} =	413.6852	MPA
span properties:		
L=	2100	mm
a=	750	mm

section properties		
h=	4.724409	in
b=	19.68504	in
f'c	7.396664	ksi
E_c =	4902.22	ksi
E_s =	4568.528	ksi
A'f	0	in^2
Af	0.44225	in^2
d=	3.158858	in
d'=	0	in
d''=	1.565551	in
f_{fu} =	192.1682	ksi
E_f =	19108.05	ksi
f'_{fu} =	60	ksi
span properties:		
L=	82.67717	in
a=	29.52756	in

Table 4.157 Initial parameters for Al-Sunna sampel SC2b.

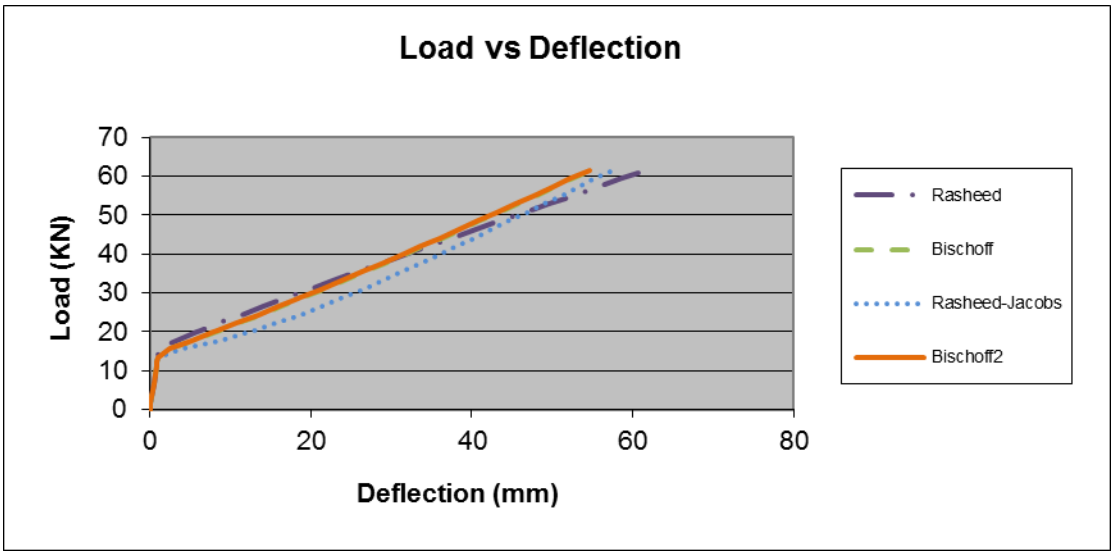

Figure 4.72 Load-deflection response for sample SC2b.

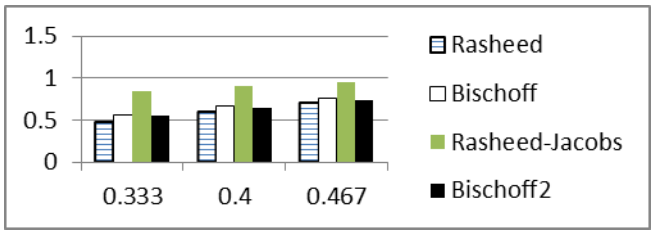

Table 4.158 Deflection comparison bar chart for sample SC2b.

4.4.11.8 – SC3a

section properties		
h=	120	mm
b=	500	mm
f'c	49.79822	MPA
E_c =	33329.2	MPA
E_s =	31498.87	MPA
A'f	0	mm^2
Af	506.7074	mm^2
d=	71.15	mm
d'=	0	mm
d''=	48.84999	mm
f_{fu} =	1474.947	MPA
E_f =	118595.8	MPA
f'_{fu} =	413.6852	MPA
span properties:		
L=	2100	mm
a=	750	mm

section properties		
h=	4.724409	in
b=	19.68504	in
f'c	7.222625	ksi
E_c =	4844.204	ksi
E_s =	4568.528	ksi
A'f	0	in^2
Af	0.785398	in^2
d=	2.801181	in
d'=	0	in
d''=	1.923228	in
f_{fu} =	213.9231	ksi
E_f =	17200.87	ksi
f'_{fu} =	60	ksi
span properties:		
L=	82.67717	in
a=	29.52756	in

Table 4.159 Initial parameters for Al-Sunna sample SC3a.

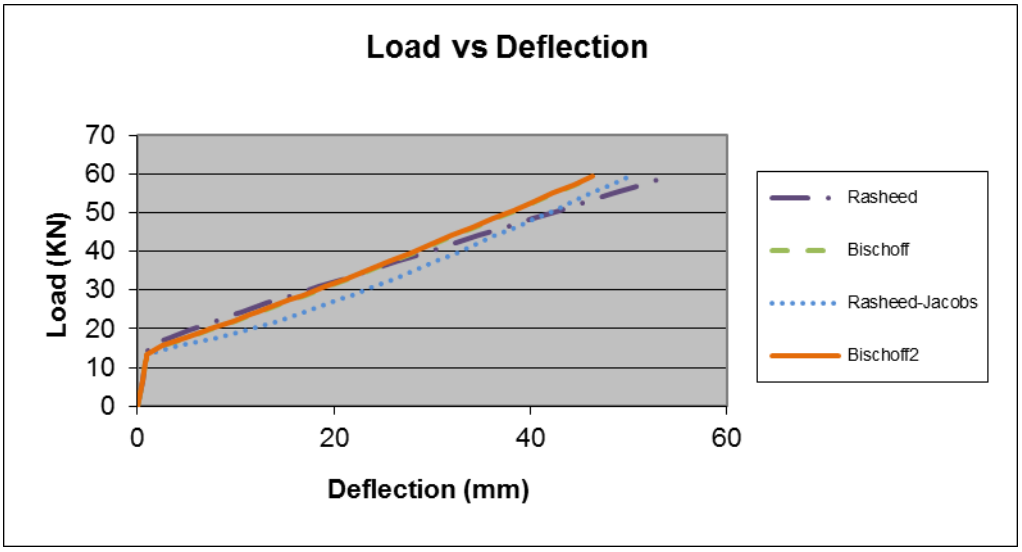

Figure 4.73 Load-deflection response for sample SC3a.

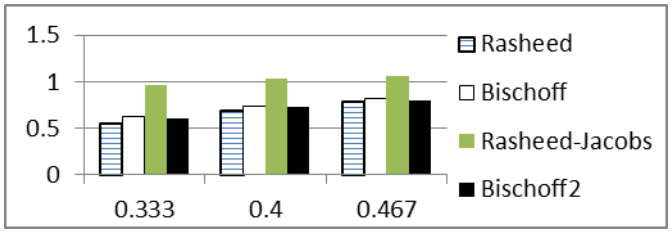

Table 4.160 Deflection comparison bar chart for sample SC3a.

4.4.11.9 – SC3b

section properties		
h=	120	mm
b=	500	mm
f'c	49.79822	MPA
E_c =	33329.2	MPA
E_s =	31498.87	MPA
A'f	0	mm^2
Af	506.7074	mm^2
d=	77.65001	mm
d'=	0	mm
d''=	42.34998	mm
f_{fu} =	1474.947	MPA
E_f =	118595.8	MPA
f'_{fu} =	413.6852	MPA
span properties:		
L=	2100	mm
a=	750	mm

section properties		
h=	4.724409	in
b=	19.68504	in
f'c	7.222625	ksi
E_c =	4844.204	ksi
E_s =	4568.528	ksi
A'f	0	in^2
Af	0.785398	in^2
d=	3.057087	in
d'=	0	in
d''=	1.667322	in
f_{fu} =	213.9231	ksi
E_f =	17200.87	ksi
f'_{fu} =	60	ksi
span properties:		
L=	82.67717	in
a=	29.52756	in

Table 4.161 Initial parameters for Al-Sunna sample SC3b.

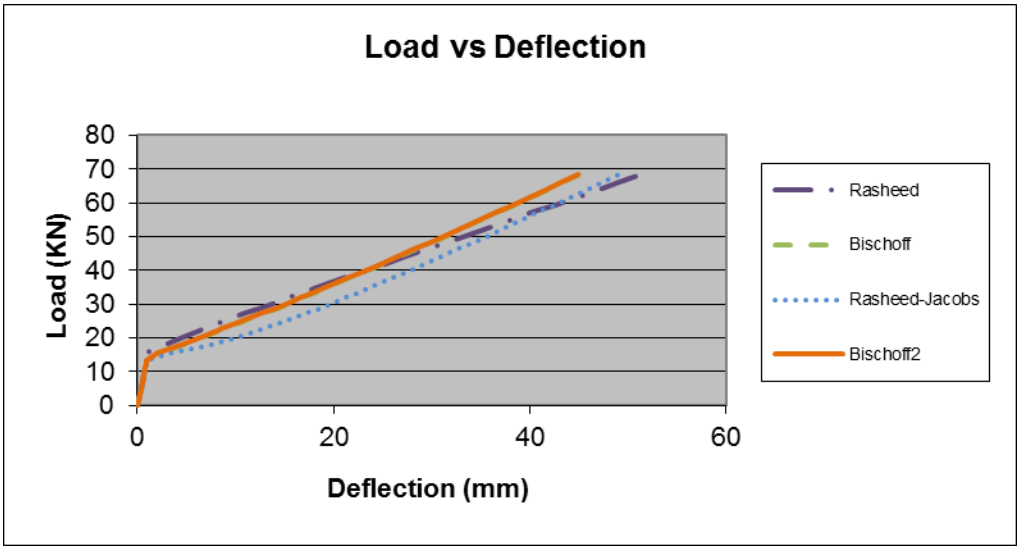

Figure 4.74 Load-deflection response for sample SC3b.

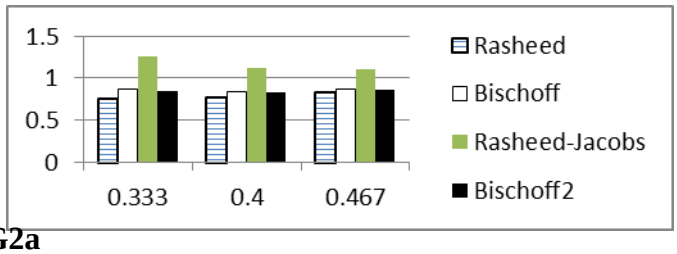

Table 4.162 Deflection comparison bar chart for samples SC3b.

4.4.11.10 – SG2a

section properties		
h=	120	mm
b=	500	mm
f'c	46.19835	MPA
E_c =	32101.93	MPA
E_s =	31498.87	MPA
A'f	0	mm^2
Af	356.6528	mm^2
d=	84.23501	mm
d'=	0	mm
d''=	35.76498	mm
f_{fu} =	664.9762	MPA
E_f =	42748.47	MPA
f'_{fu} =	413.6852	MPA

span properties:		
L=	2100	mm
a=	750	mm

section properties		
h=	4.724409	in
b=	19.68504	in
f'c	6.700508	ksi
E_c =	4665.828	ksi
E_s =	4568.528	ksi
A'f	0	in^2
Af	0.552813	in^2
d=	3.316339	in
d'=	0	in
d''=	1.40807	in
f_{fu} =	96.4467	ksi
E_f =	6200.145	ksi
f'_{fu} =	60	ksi

span properties:		
L=	82.67717	in
a=	29.52756	in

Table 4.163 Initial parameters for Al-Sunna sample SG2a.

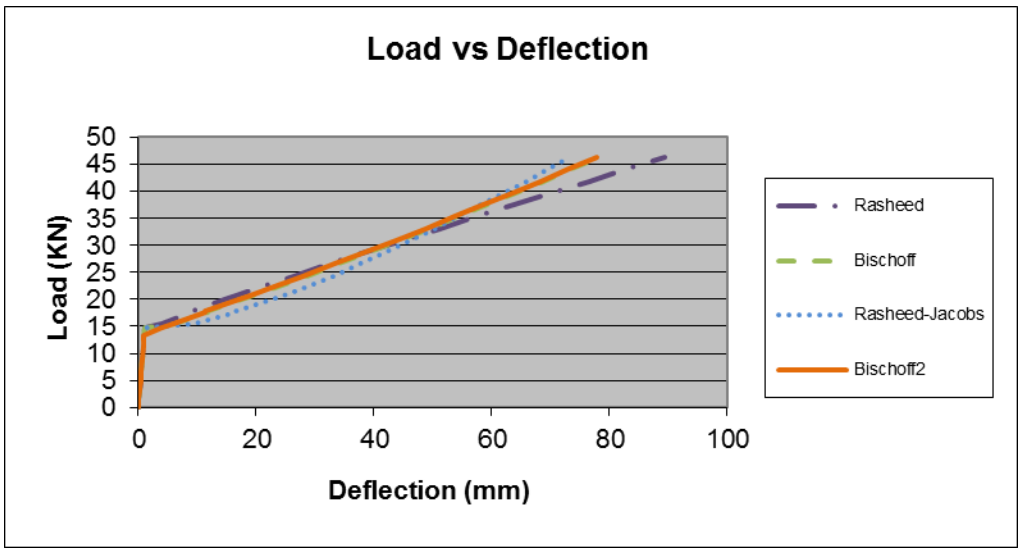

Figure 4.75 Load-deflection response for sample SG2a.

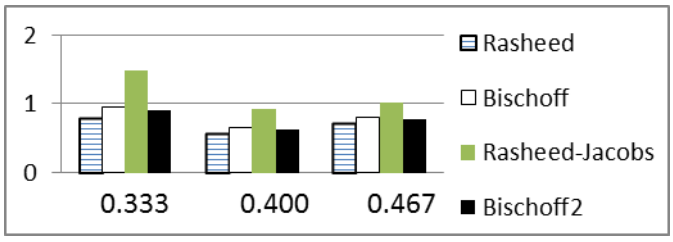

Table 4.164 Deflection comparison bar chart for sample SG2a.

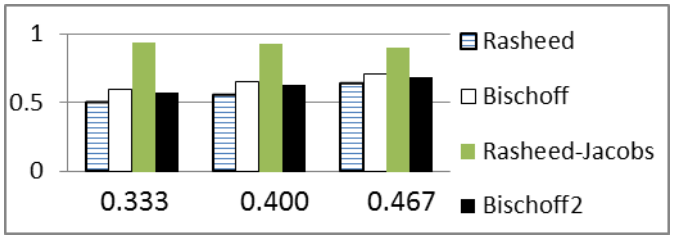

Table 4.165 Deflection comparison bar chart for dependent sample SG2b.

4.4.11.11 – SG3a

section properties		
h=	120	mm
b=	500	mm
f'c	45.89836	MPA
E_c =	31997.53	MPA
E_s =	31498.87	MPA
A'f	0	mm^2
Af	1425.115	mm^2
d=	70.47499	mm
d'=	0	mm
d''=	49.525	mm
f_{fu} =	669.976	MPA
E_f =	41948.5	MPA
f'_{fu} =	413.6852	MPA
span properties:		
L=	2100	mm
a=	750	mm

section properties		
h=	4.724409	in
b=	19.68504	in
f'c	6.656998	ksi
E_c =	4650.654	ksi
E_s =	4568.528	ksi
A'f	0	in^2
Af	2.208932	in^2
d=	2.774606	in
d'=	0	in
d''=	1.949803	in
f_{fu} =	97.17186	ksi
E_f =	6084.119	ksi
f'_{fu} =	60	ksi
span properties:		
L=	82.67717	in
a=	29.52756	in

Table 4.166 Initial parameters for Al-Sunna sample SG3a.

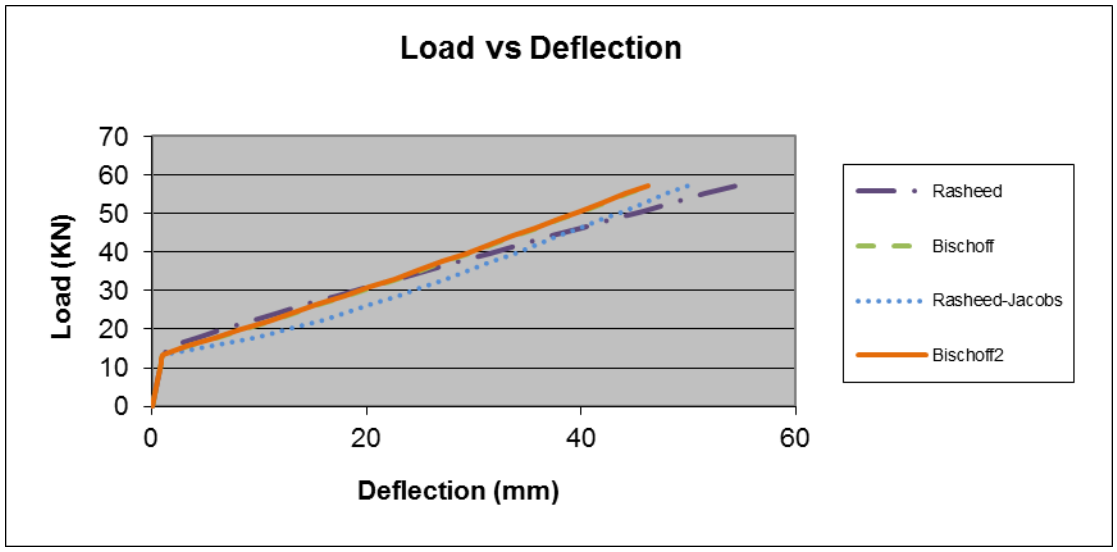

Figure 4.76 Load-deflection response for sample SG3a.

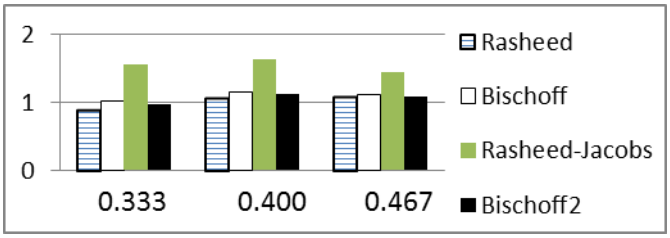

Table 4.167 Deflection comparison bar chart

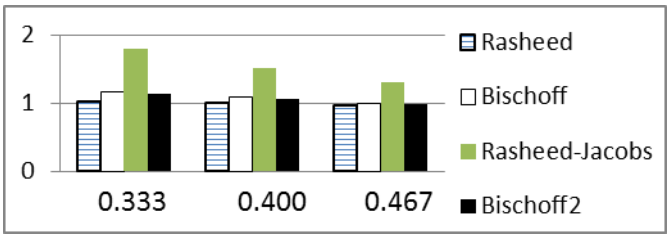

Table 4.168 Deflection comparison bar chart for dependent sample SG3b.

4.5 Statistical Analysis

Using statistical analysis, we processed two groups of samples. The first group of samples from the Gross database is the 56 independent samples. The second group of samples analyzed statistically is the 106 samples from the Gross database consisting of both the 56 independent samples and the 50 dependent samples combined. The predicted deflection compared to the experimental deflection was first evaluated. These calculated deflection ratios are used to determine the overall average for each group of samples, the standard deviation for each group of samples, and the coefficient of variation for each group of samples for all three moment levels of $0.333M_n$, $0.400M_n$, and $0.467M_n$. The average of the results is calculated by

$$Average = \frac{\sum \frac{Predicted\ Deflection}{Experimental\ Deflection}}{\#\ of\ samples} \tag{51}$$

The greater the average compared to unity, the more conservative the model is expected to be. The estimated standard deviation is based on the sample, and is calculated by

$$STD = \sqrt{\frac{\sum (x-\bar{x})^2}{(n-1)}} \tag{52}$$

Where x takes on each value in the sample, $\bar{x}$ is the sample mean average, and n is the sample size. The coefficient of variation is the ratio between the standard deviation and the average respectively.

$$Coefficient\ of\ Variation = \frac{Standard\ Deviation}{Average} \quad (53)$$

The closer the coefficient of variation value is to zero, the better fit the model will be overall for each group of samples. Alongside these statistical values, we graphed the predicted deflection vs. the experimental deflection for each of the three moment levels. This allows for a 20% spread to be seen visually in comparison to a less or more according to the line that would be considered an exact match between the predicted and experimental deflection values. Also, a comparison between the predicted and experimental deflection ratio vs. the tension FRP reinforcement ration, ρ. The ρ-values were pulled from the Gross database for this comparison.

4.5.1 Independent Sample Results

0.333Mn	56 Samples			Rasheed	Bischoff	Rasheed-Jacobs	Bischoff2
Average				0.873422	1.229014	1.4541798	0.9936522
Standard Deviation				0.735417	0.935539	1.1154156	0.8319932
Coefficient of variation				84%	76%	77%	84%

Table 4.169 Statistical analysis for 0.333Mn results for independent group of 56 samples.

From table 4.169, 4.170, and 4.171, it can be seen that the Rasheed and the Bischoff2 models are under conservative when predicting the deflection, with Bischoff2 model being the better of the two, meaning the Rasheed model under predicts by too much. Also, the Bischoff and the Rasheed-Jacobs models are over conservative, with the Rasheed-Jacobs model being too conservative. In using the coefficient of variation, the Bischoff equation seems to be the best model with the value closest to zero, however, the Rasheed-Jacobs model comes in a very close second behind the Bischoff model, providing the same coefficient of variation for both the 0.400Mn and 0.467M_n moment levels. The results were very similar with all three moment levels, however as the moment level increases from 0.333 to 0.467M_n, the coefficient of variation decreases from an 80% average to a 30% average, resulting in a value closer to what was

expected. The $0.467M_n$ statistical calculations provided an average closest to 1 and the coefficient of variation closest to zero. Therefore the $0.467M_n$ moment level is the best level to use for predictions. This is expected as we move away from the cracking moment.

0.400Mn	56 Samples	Rasheed	Bischoff	Rasheed-Jacobs	Bischoff2
Average		0.8490645	1.0941122	1.2498192	0.9280896
Standard Deviation		0.3986596	0.4672900	0.5369367	0.4296761
Coefficient of variation		47%	43%	43%	46%

Table 4.170 Statistical analysis for 0.400Mn results for independent group of 56 samples.

0.467Mn	56 Samples	Rasheed	Bischoff	Rasheed-Jacobs	Bischoff2
Average		0.870630	1.043017	1.158192	0.915213
Standard Deviation		0.269163	0.307268	0.338122	0.281331
Coefficient of variation		31%	29%	29%	31%

Table 4.171 Statistical analysis for 0.467Mn results for independent group of 56 samples.

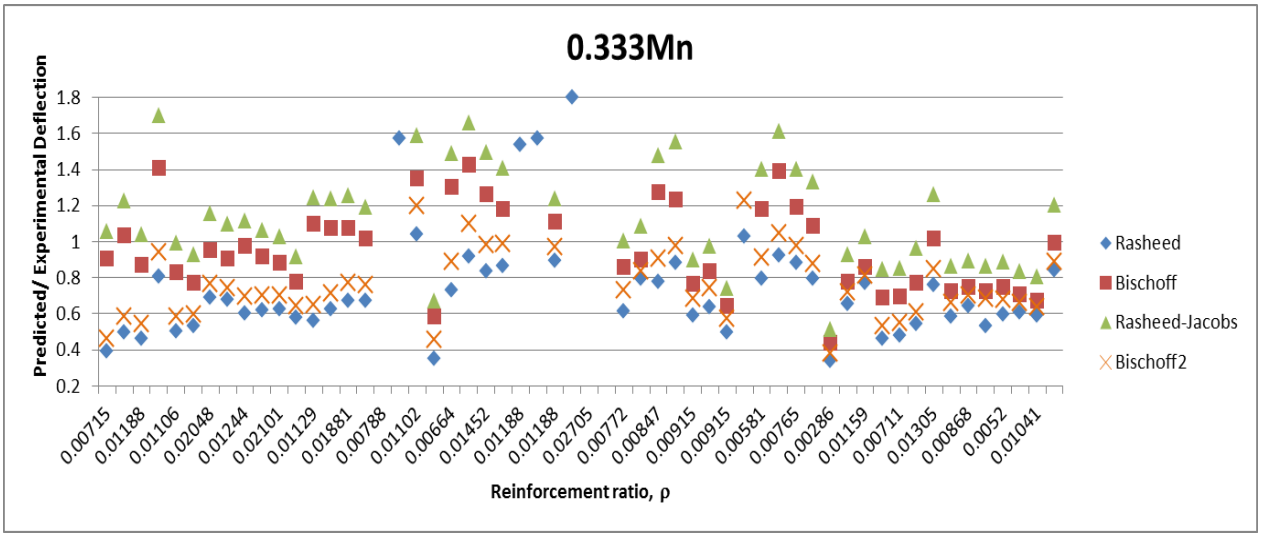

Figure 4.77 Deflection ratio vs. reinforcement ratio for independent samples at 0.333Mn.

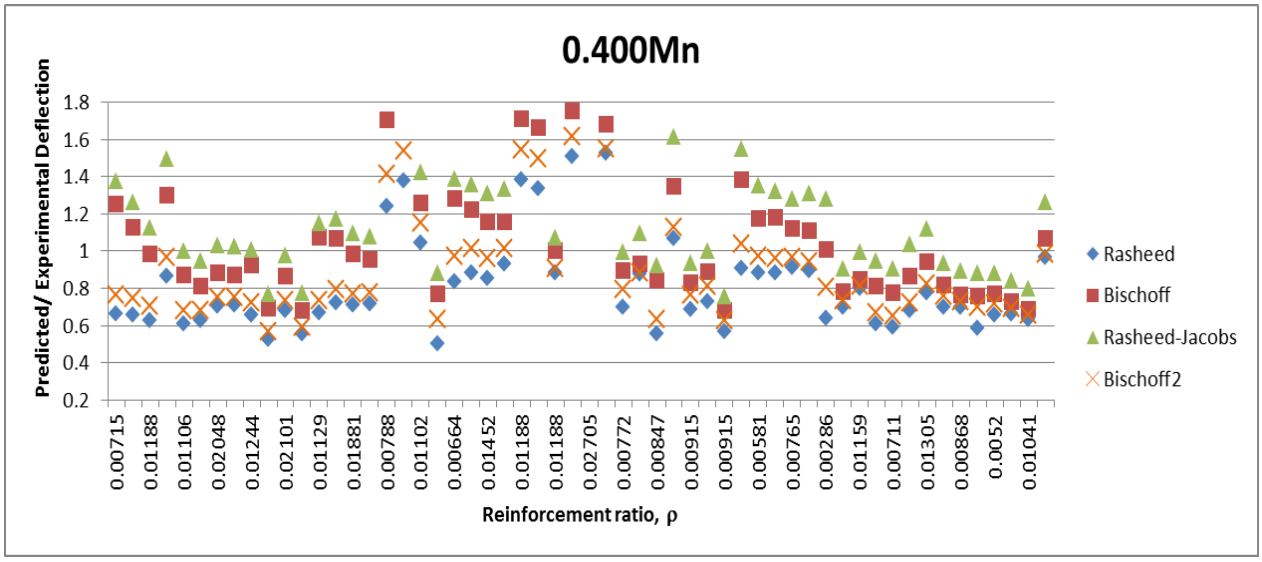

Figure 4.78 Deflection ratio vs. reinforcement ratio for independent samples at 0.400Mn.

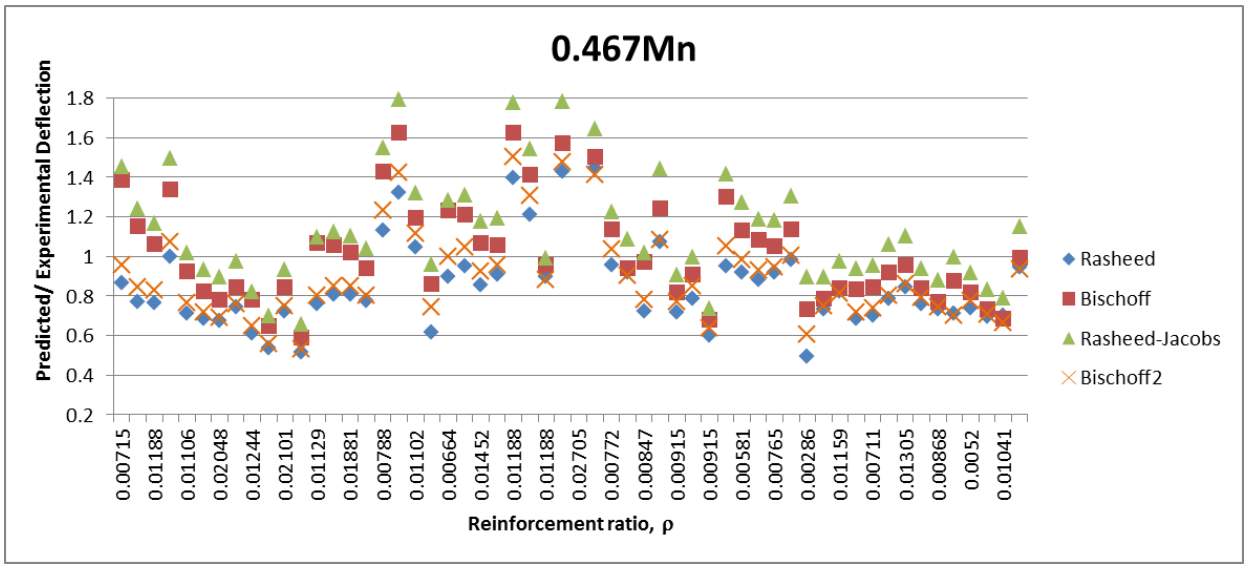

Figure 4.79 Deflection ratio vs. reinforcement ratio for independent samples at 0.467Mn.

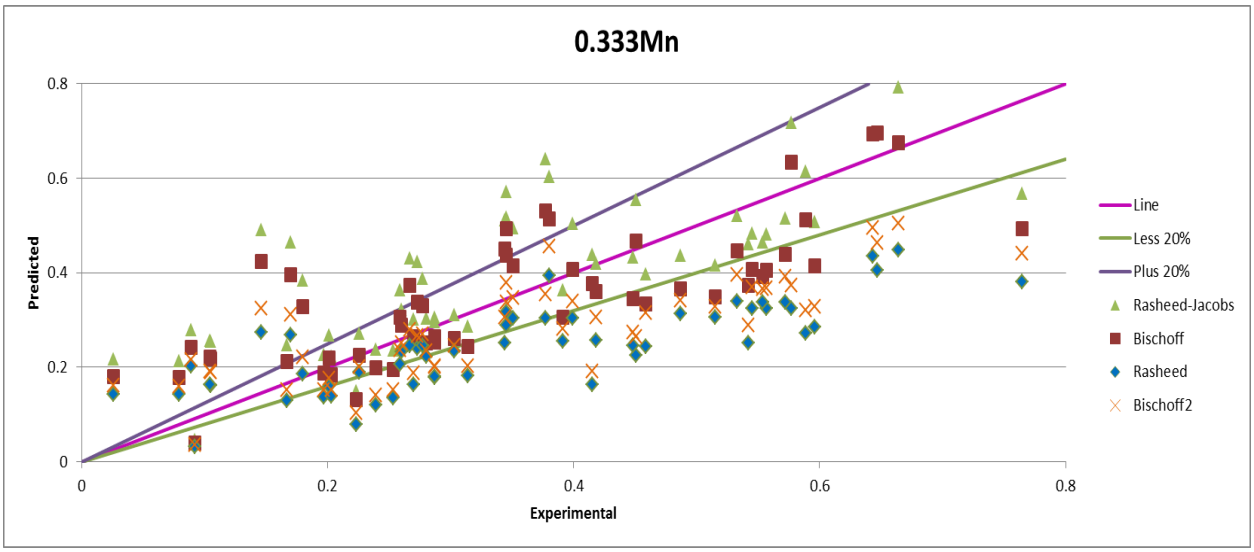

Figure 4.80 Predicted vs. experimental deflection values for independent samples at 0.333Mn.

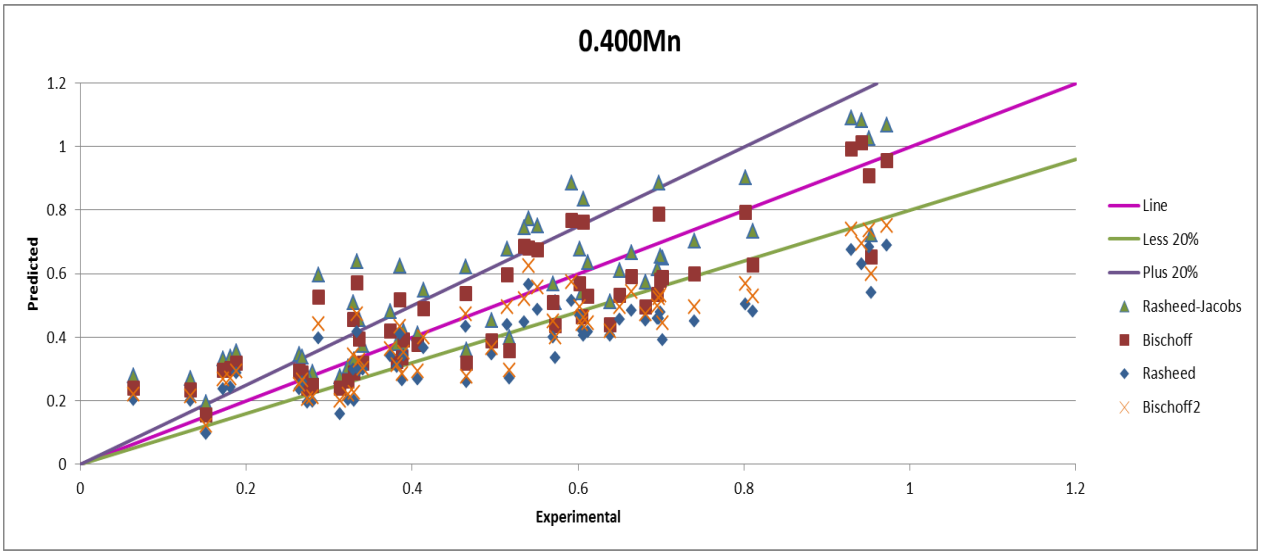

Figure 4.81 Predicted vs. experimental deflection values for independent samples at 0.400Mn.

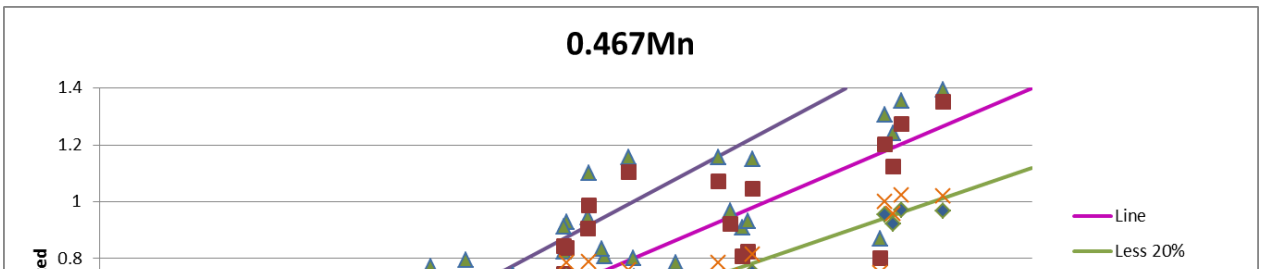

Figure 4.82 Predicted vs. experimental deflection values for independent samples at 0.467Mn.

4.5.2 Combined Dependent and Independent Samples Results

0.333Mn	All samples	Rasheed	Bischoff	Rasheed-Jacobs	Bischoff2
Average		0.809893	1.162551	1.401486	0.925646
Standard Deviation		0.573035	0.724810	0.866596	0.649498
Coefficient of variation		71%	62%	62%	70%

Table 4.172 Statistical analysis for 0.333Mn results for combined group of 106 samples.

0.400Mn	All samples	Rasheed	Bischoff	Rasheed-Jacobs	Bischoff2
Average		0.823690	1.083441	1.247508	0.905500
Standard Deviation		0.322500	0.379511	0.438610	0.348591
Coefficient of variation		39%	35%	35%	38%

Table 4.173 Statistical analysis for 0.400Mn results for combined group of 106 samples.

0.467Mn	All samples	Rasheed	Bischoff	Rasheed-Jacobs	Bischoff2
Average		0.846110	1.031156	1.150418	0.895745
Standard Deviation		0.226288	0.263511	0.291633	0.236813
Coefficient of variation		27%	26%	25%	26%

Table 4.174 Statistical analysis for 0.467Mn results for combined group of 106 samples.

Similar results as the group of 56 samples were found with the group of 106 samples. The Rasheed and Bischoff2 models both under predict the deflection for all three moment levels. Also, the Bischoff and Rasheed-Jacobs models over predict the deflections with the Rasheed-Jacobs model being more conservative than the Bischoff model, and with the $0.467M_n$ moment level being the best prediction for deflection. According to the coefficient of variation, the Rasheed-Jacobs and the Bischoff model are pretty well the same throughout being considered as the best models. However, with the $0.467M_n$ moment level, which contains the coefficient of variation closest to zero, the Rasheed-Jacobs model surpasses the Bischoff and provides the best model for predicting deflection. Along with the statistical analysis provided, the deflection ratio vs. the reinforcement ratio and the predicted deflection vs. the experimental deflection are provided as additional supporting graphs.

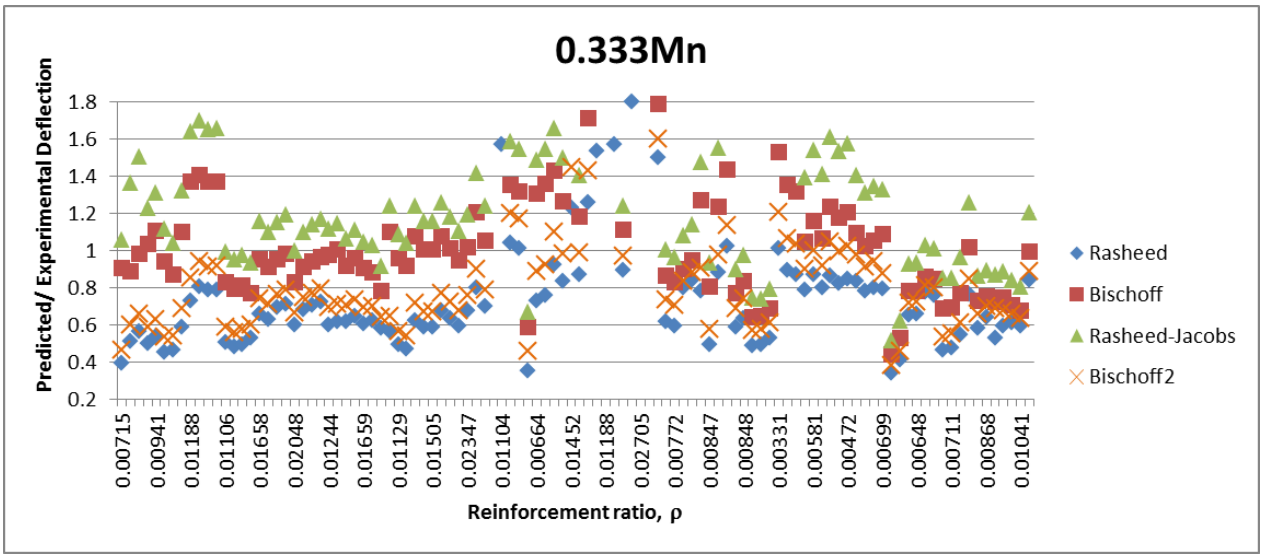

Figure 4.83 Deflection ratio vs. reinforcement ratio for all samples at 0.333Mn.

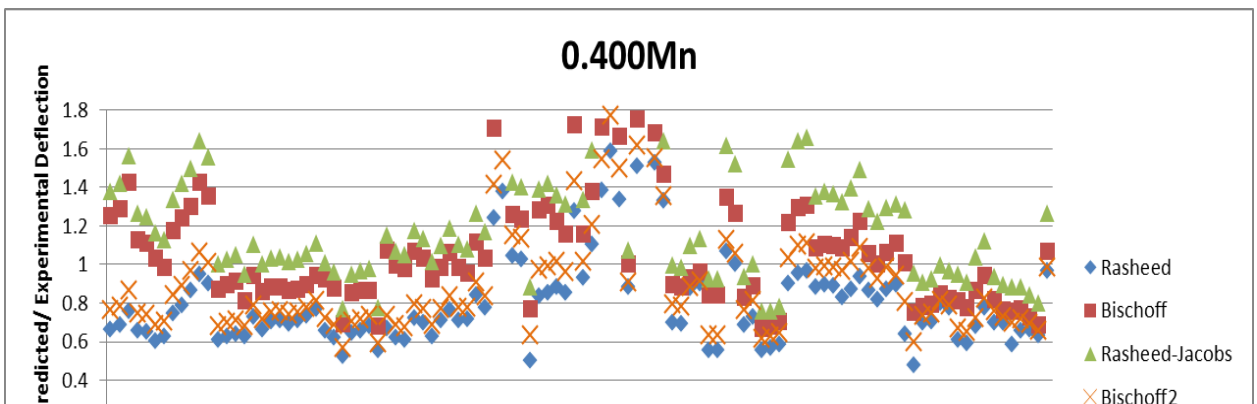

Figure 4.84 Deflection ratio vs. reinforcement ratio for all samples at 0.400Mn.

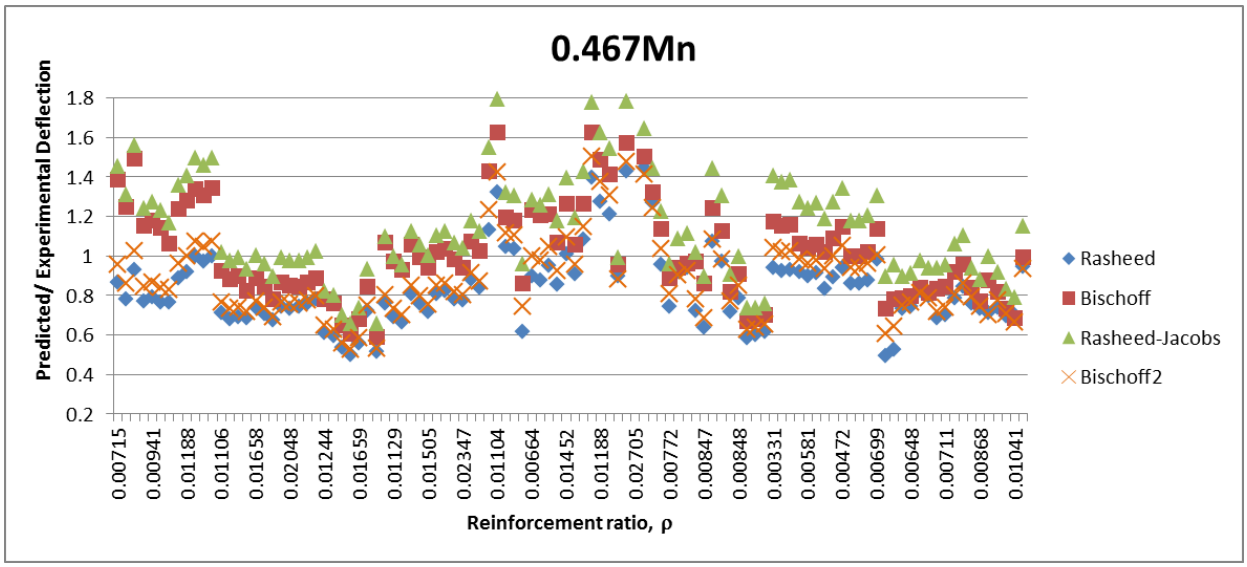

Figure 4.85 Deflection ratio vs. reinforcement ratio for all samples at 0.467Mn.

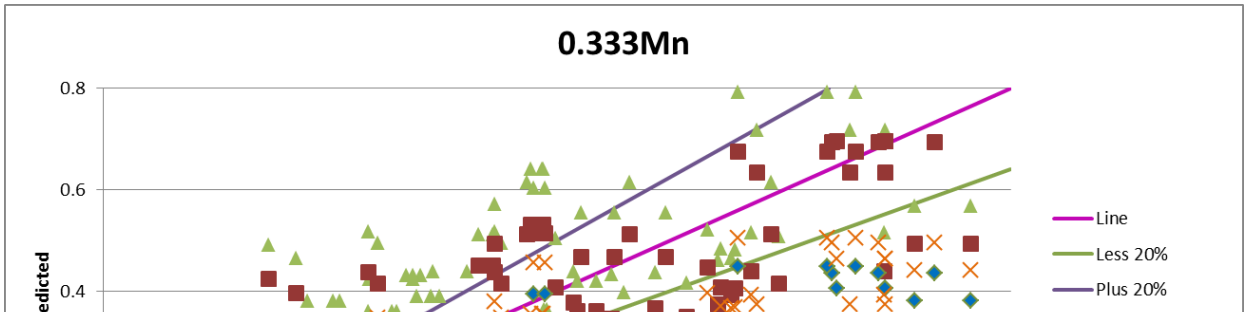

Figure 4.86 Predicted vs. experimental deflection values for all samples at 0.333Mn.

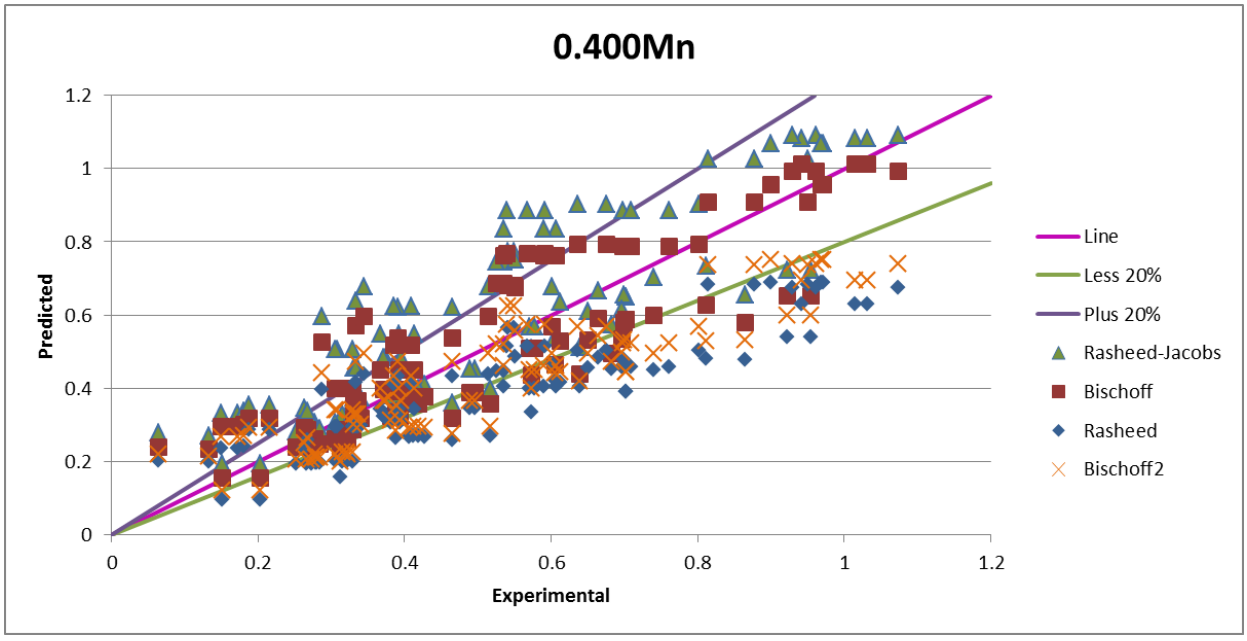

Figure 4.87 Predicted vs. experimental deflection values for all samples at 0.400Mn.

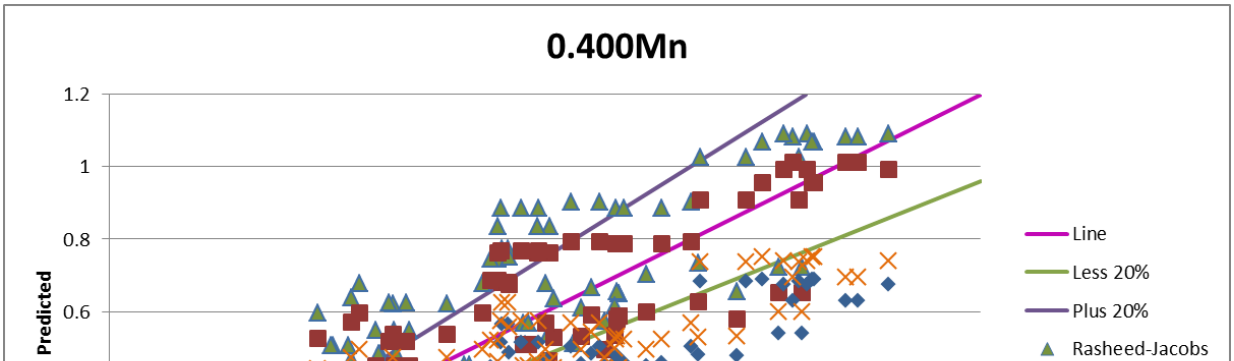

Figure 4.88 Predicted vs. experimental deflection values for all samples at 0.467Mn.

4.6 Deflection Correspondence

We also did individual deflection correspondence between the predicted deflection for each model and experimental deflection provided by the Gross database. For this comparison we found the ratio between each individual predicted deflection and experimental deflection respectively. Therefore,

$$Deflection\ ratio = \frac{Predicted\ Deflection}{Experimental\ Deflection} \tag{54}$$

This deflection ratio was then subtracted from the value of 1 to determine the difference that each predicted model deflection was from the given experimental value. The model that provided the smallest difference was therefore considered the best deflection correlation model for that sample. This was done for each individual sample and shown in table form for both the group of 56 independent samples and the 106 dependent and independent combined samples. Table 4.175 shows an example sample of these deflection correlations being evaluated and analyzed.

$\gamma_{predict}/\gamma_{exp}$ Rasheed	$\gamma_{predict}/\gamma_{exp}$ Bischoff	$\gamma_{predict}/\gamma_{exp}$ Rasheed-Jacobs	$\gamma_{predict}/\gamma_{exp}$ Bischoff2	1-ANS Rasheed	1-ANS Bischoff	1-ANS Rasheed-Jacobs	1-ANS Bischoff2	Value closest to 0	Best Method Correlation
0.5898252	0.6832028	0.90015559	0.68608217	0.4101748	0.3167972	0.09984441	0.313918	0.09984441	Rasheed-Jacobs
0.6848627	0.7592976	0.93670815	0.76160801	0.3151373	0.2407024	0.06329185	0.238392	0.06329185	Rasheed-Jacobs
0.7182575	0.7685393	0.90735912	0.77031062	0.2817425	0.2314607	0.09264088	0.229689	0.09264088	Rasheed-Jacobs

Table 4.175 Example deflection correspondence for determining best model for each individual sample.

56 Independent Samples	Moment Levels	Rasheed	Bischoff	Rasheed-Jacobs	Bischoff2	Percentage			
						Rasheed	Bischoff	Rasheed-Jacobs	Bischoff2
	0.333	10	13	27	6	18%	23%	48%	11%
	0.4	9	7	31	9	16%	13%	55%	16%
	0.467	12	11	28	5	21%	20%	50%	9%

Table 4.176 Combined individual results for 56 independent samples.

Total All 106 Samples	Moment Levels	Rasheed	Bischoff	Rasheed-Jacobs	Bischoff2	Percentage			
						Rasheed	Bischoff	Rasheed-Jacobs	Bischoff2
	0.333	16	28	47	15	15%	26%	44%	14%
	0.4	19	17	53	17	18%	16%	50%	16%
	0.467	20	21	51	14	19%	20%	48%	13%

Table 4.177 Combined individual results for all 106 samples.

According to both Table 1.176 and 1.177, the Rasheed-Jacobs model had the best deflection correspondence for individual samples for all three moment levels. This was consistent with both the group of 56 and the combined 106. The Bischoff model was determined to be the second best model correlation with this analysis for the $0.333M_n$ moment level. The rest of the results were a toss-up between the Rasheed, Bischoff, and Bischoff2 models for deflection correspondence. For the combined 106 samples, the $0.333M_n$ moment level produced 44.34% of samples best represented by the Rasheed-Jacobs model. The $0.400M_n$ moment level produced 50% of the 106 samples best represented by the Rasheed-Jacobs model, with the second highest percentage going to the Rasheed model at 17.93%. For the 106 combined samples, the $0.467M_n$ moment level was best represented by the Rasheed-Jacobs model with 48.11% percent of the samples, and the next highest percentage of 20.76% being best represented by the Rasheed model, with the Bischoff model being the second best model at 19.81%. This direct deflection correspondence was the best analysis for determining the best model, because each individual sample of the 106 combined were analyzed individually according to their predicted and experimental deflection values.

Chapter 5 - Conclusion and Recommendations

5.1 Conclusion

An extensive analysis study is conducted to process samples from the Gross database through four deflection calculation equations, three from the literature and one proposed by this study. It is evident from the statistical results that the Bischoff2 equation has the closest mean value to 1.0 on the unconservative side while the Bischoff equation has the closest mean value to 1.0 on the conservative side. On the other hand, the Rasheed equation shows a consistent mean value for all three moment levels examined. On the other hand, the Rasheed-Jacobs equation was shown to yield the highest number of times its prediction is the closest to the experimental values for the two database types processed. Multiple deflection analyses were done on 56 independent samples as well as 50 dependent samples. From these results, it can be shown that the Rasheed-Jacobs model was consistently on the conservative side throughout analyzing the 106 samples, although in the deflection correlation analysis, the Rasheed-Jacobs model provided the best correlated deflection between the predicted and experimental deflections for the most individual samples. The direct deflection correspondence was the best analysis for this research, because it provided one-on-one analysis for each individual predicted and experimental deflection. The Bischoff, Rasheed, and Bischoff2 models also provided good representations of multiple samples analyzed, but not as many as the Rasheed-Jacobs model. The Rasheed and Bischoff2 models consistently under predicted the deflection. Therefore, the Rasheed and Bischoff2 models are slightly on the un-conservative side which isn't necessarily as good as being on the conservative side, but can be used to provide reliable model predictions for deflection. The Bischoff model was the most comparable to the newly suggested Rasheed-Jacobs model, with the Bischoff model being less conservative than the Rasheed-Jacobs model. With the Rasheed-Jacobs model of the four to predict the experimental deflection the closest with the most accuracy.

5.2 Recommendations

Further research and calculations can be done to better predict the response of FRP reinforced beam deflection values. All four of the models compared in this research are good representations of the deflections, but more analysis should be continued for better calibration of a more consistent model that yields closer results for experiments.

References

Almusallan, T. H. (1997). "Analytical Prediction of Flexural Behavior of Concrete Beams Reinforced by FRP Bars." *J. Compos. Materials*., 31(7), 640-657.

Al-Sunna, R. A. S. (2006). "Deflection Behavior of FRP Reinforced Concrete Flexural Members." Ph.D. Dissertation, University of Sheffield, Sheffield, England, 318pp.

Benmokrane, B., Chaallal, O., and Masmoudi, R. (1996). "Flexural Response of Concrete Beams Reinforced with FRP Reinforcing Bars." *ACI Struct. J*., 91(2), 46-55.

Bischoff, P. H. and Gross, S. P. (2011a). "Equivalent Moment of Inertia Base on Integration of Curvature." *J. Compos. Constr*., 15(3), 263-273.

Bischoff, P. H. and Gross, S. P. (2011b). "Design Approach for Calculating Deflection of FRP-Reinforced Concrete." *J. Compos. Constr*., 15(4), 490-499.

Faza, S. S. (1991). "Bending and Bond Behavior and Design of Concrete Beams Reinforced with Fiber Reinforced Plastic Rebars." Ph.D. Dissertation, West Virginia University, Morgantown, WV, 200pp.

Kakazawa, T., Ohno, S., and Yonezawa, T. (1993). "Flexural Behavior and Energy Absorption

of Carbon FRP Reinforced Concrete Beams." *Fiber Reinforced Plastic Reinforcement for Concrete Structures*, ACI SP-138, ACI, Farmington Hills, MI, 585-598.

Kassem, C., El-Salakawy, E., and Benmokrane, B. (2003). "Deflection Behavior of Concrete Beams Reinforced with Carbon FRP Composite Bars." *Deflection Control for the Future*, ACI SP-210, editor N.J. Gardner, ACI, Farmingtion Hills, MI, 173-190.

Masmoudi, R., Theriault, M., and Benmokrane, B. (1998). "Flexural Behavior of Concrete Beams Reinforced with Deformed Fiber Reinforced Plastic Reinforcing Rods." *ACI Struct. J.*, 95(6), 665-675.

Nakano, K., Matsuzaki, Y., Fukuyama, H., and Teshigawara, M. (1993). "Flexural Performance of Concrete Beams Reinforced with Continuous Fiber Bars." *Fiber Reinforced Plastic Reinforcement for Concrete Structures*, ACI SP-138, ACI, Farmington Hills, MI, 743-766.

Pecce, M., Manfredi, G., Consenza, E., (2000). "Experimental Response and Code Models of GFRP RC Beams in Bending." *J. Compos. Constr*., 4(4), 182-190.

Rasheed, H. A., Nayal, R. and Melhem H. G. (2004). "Response Prediction of Concrete Beams Reinforced with FRP Bars," *Compos. Struct*., 65(2), 193-204.

Theisz, P., Gross, S. P., Dinehart, D. W., and Yost, J. R. (2004). "Experimental Tests of High-Strength Concrete Beams Reinforced with CFRP Bars." *Proceedings of the Fourth International Conference on Advance Composite Materials in Bridges and Structures* – Calgary, Canada, Paper No. 153, 1-8.

Theriault, M., and Benmokrane, B. (1998). "Effects of FRP Reinforcement Ratio and Concrete Strength on Flexural Behavior of Concrete Beams." *J. Compos. Constr*., ASCE, 2(1), 7-16.

Toutanji, H., and Saafi, M. (2000). "Flexural Behavior of Concrete Beams Reinforced with Glass

Fiber-Reinforced Polymer Bars." *ACI Struct. J.*, 97(5), 712-719.

Yost, J. R., Gross, S. P., and Dinehart, D. W. (2003). "Effective Moment of Inertia for Glass Fiber-Reinforced Polymer Reinforced Concrete Beams." *ACI Struct. J.*, 100(6), 732-739.

Appendix A - Moment-Curvature graphs

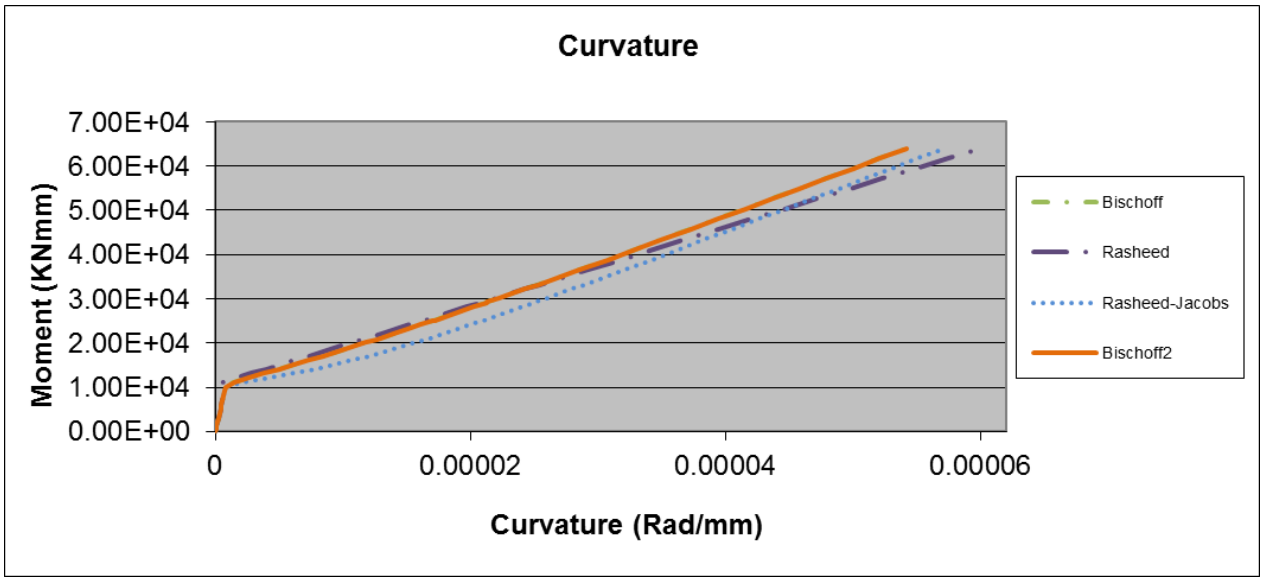

Author: Faza Sample: ED Dependent Sample: EF

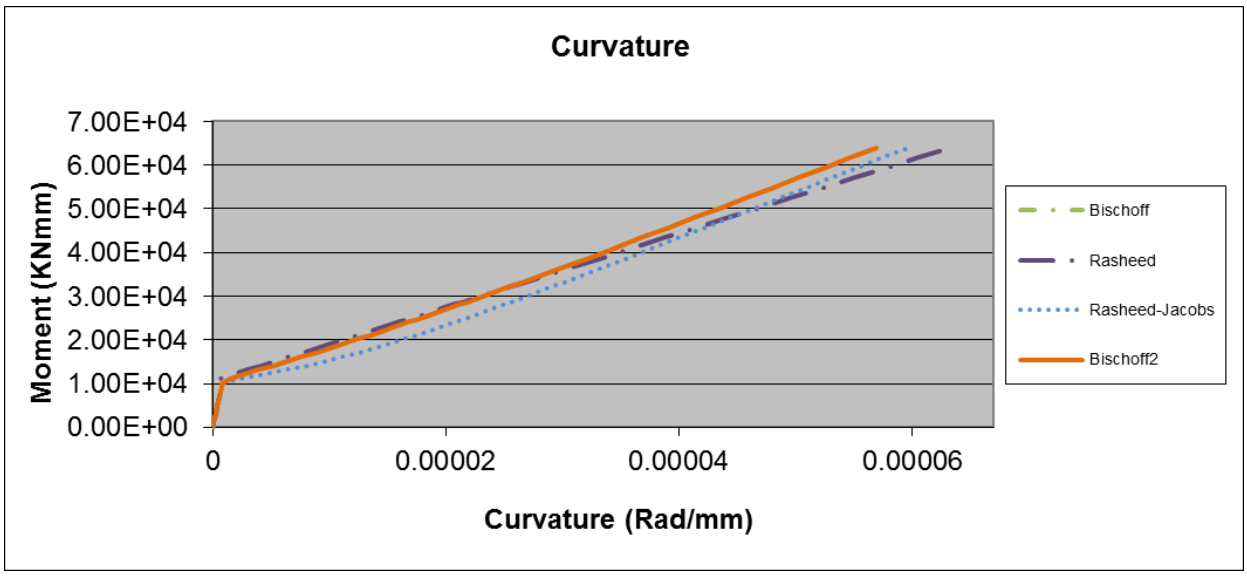

Author: Faza Sample: EE Dependent: None

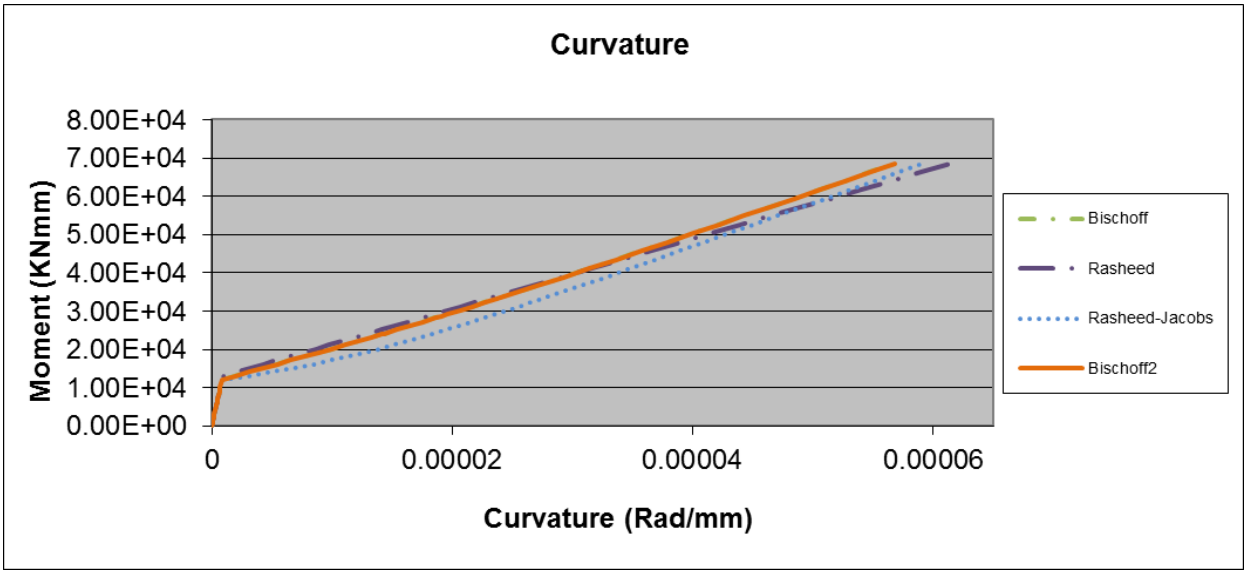

Author: Faza Sample: EVH1 Dependent: EVH2

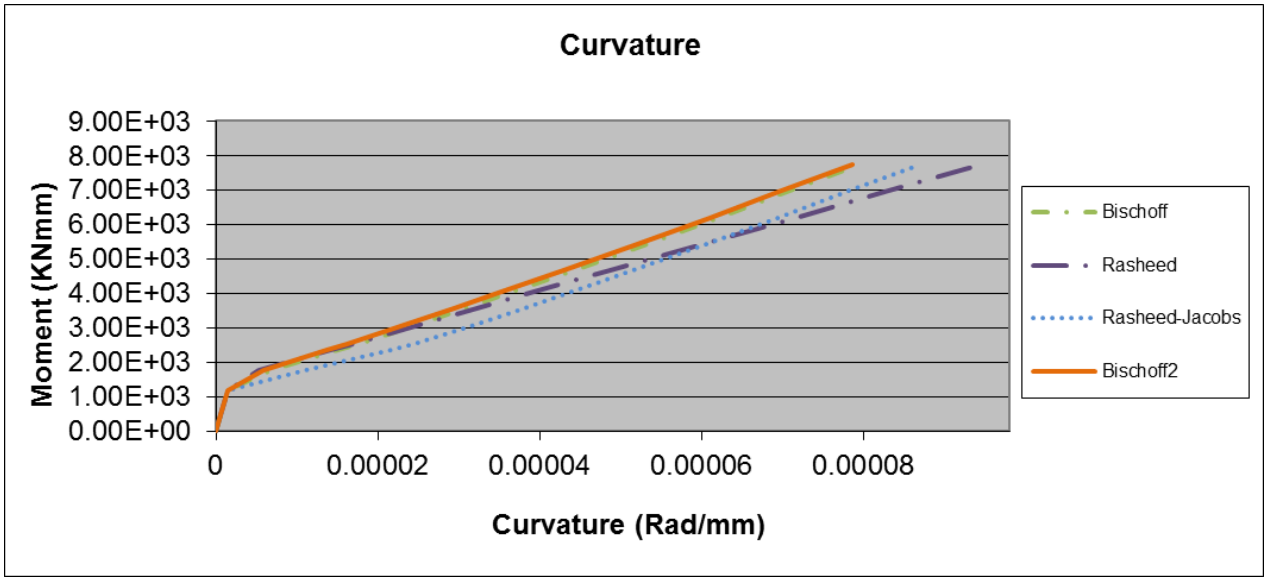

Author: Kakizawa et al. Sample: 2 Dependent: None

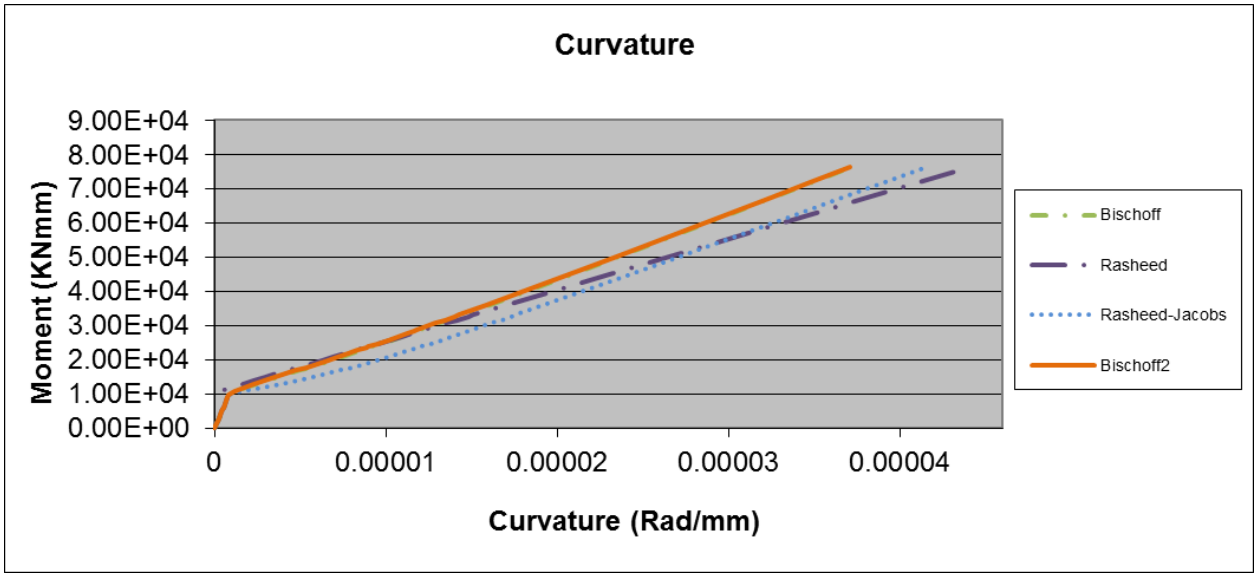

Author: Nakano et al. Sample: RC-C1 Dependent: None

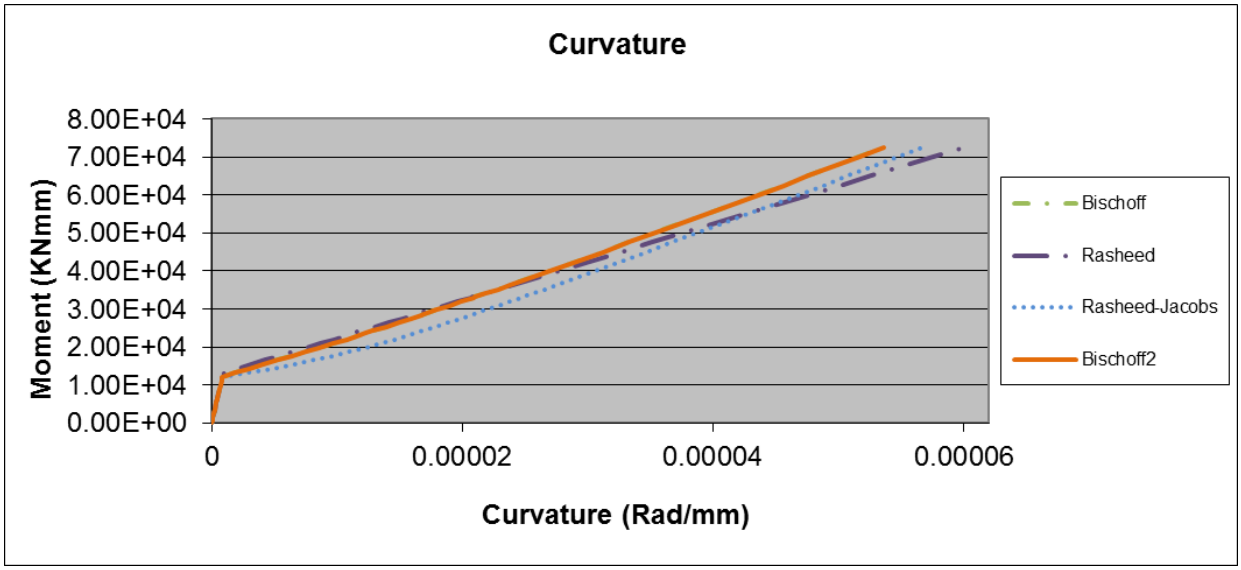

Author: Benmokrane et al. Sample: ISO1 Dependent: ISO2

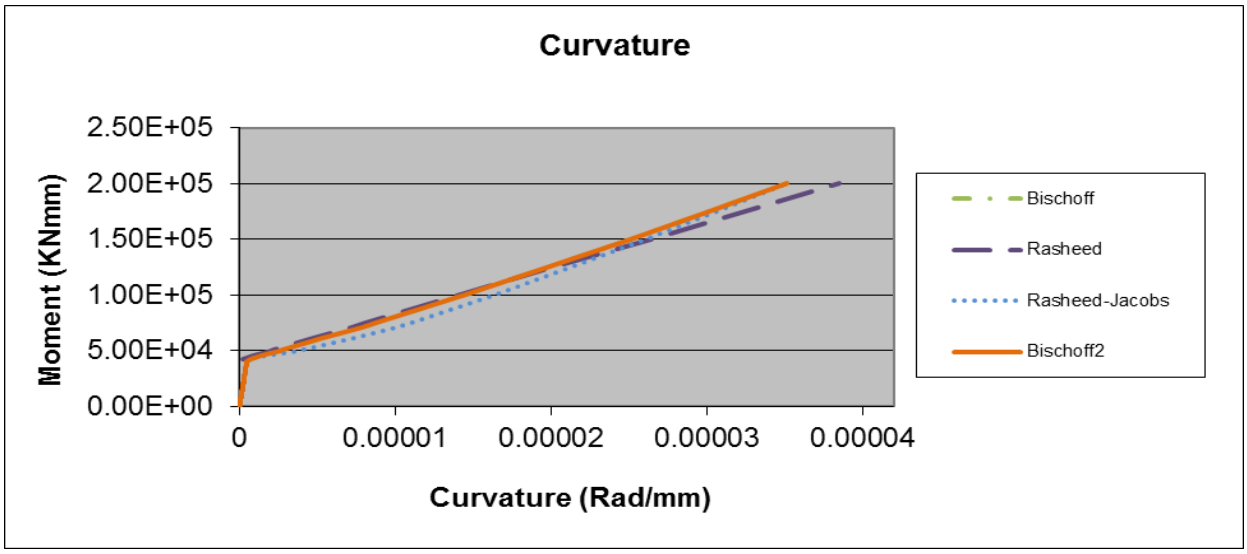

Author: Benmokrane et al. Sample: ISO3 Dependent: None

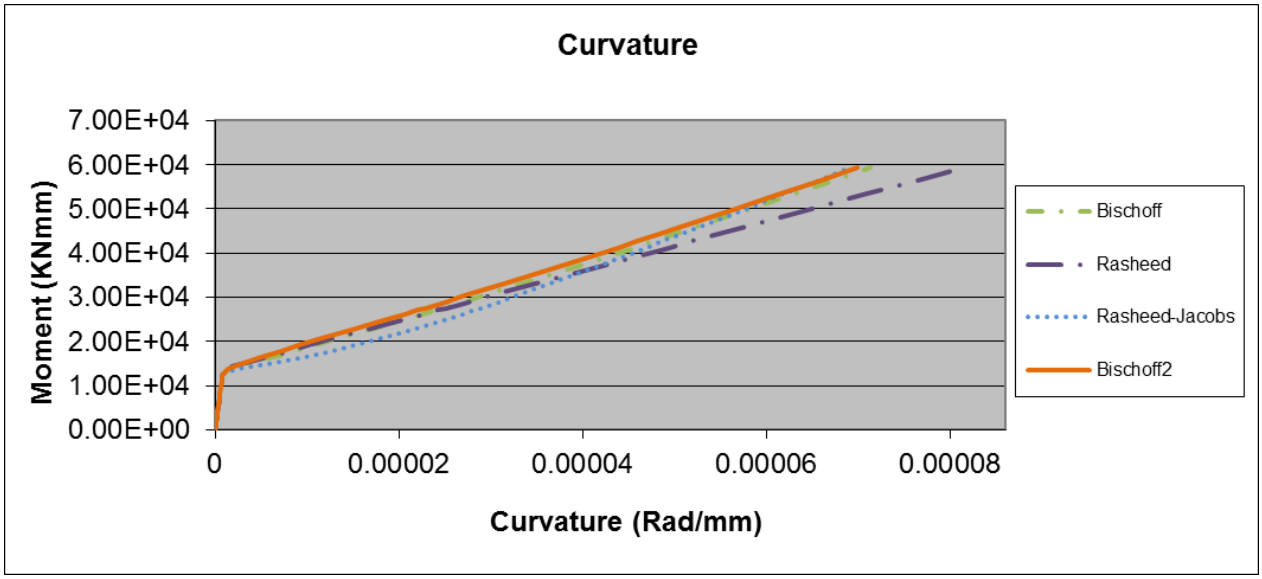

Author: Masmoudi et al. Sample: CB2B-1 Dependent: CB2B-2

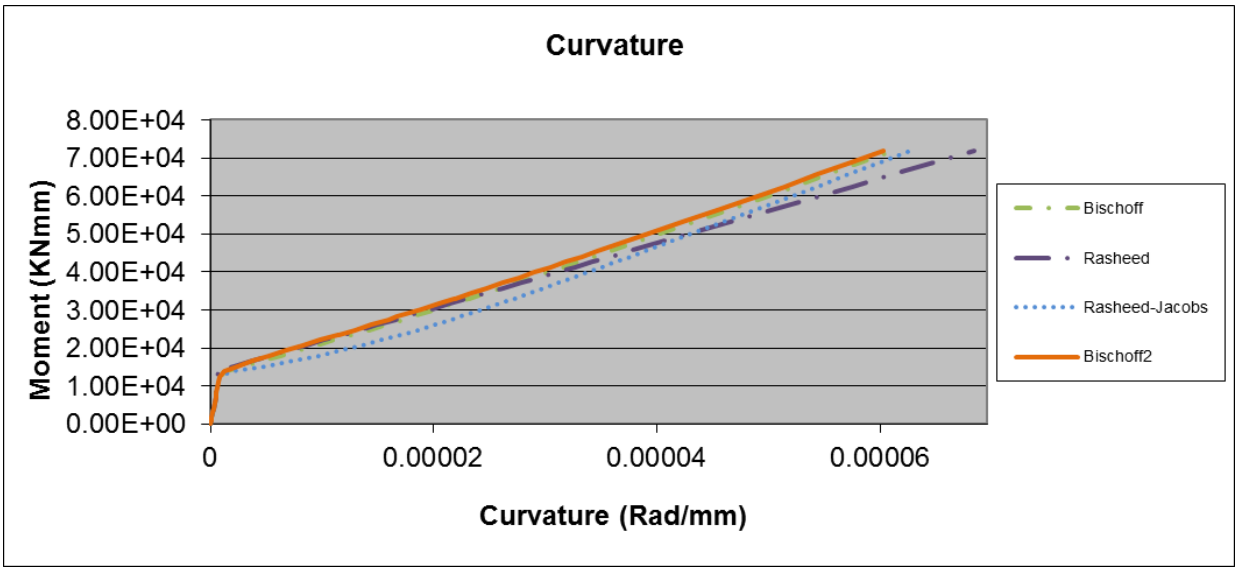

Author: Masmoudi et al. Sample: CB3B-2 Dependent: None

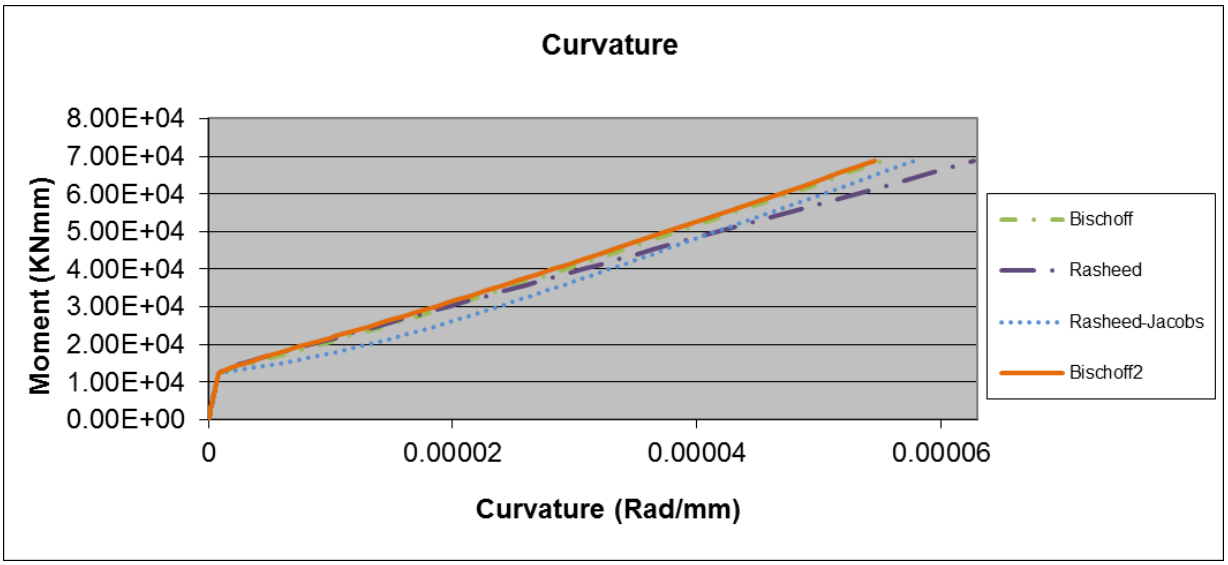

Author: Masmoudi et al. Sample: CB4B-1 Dependent: CB4B-2

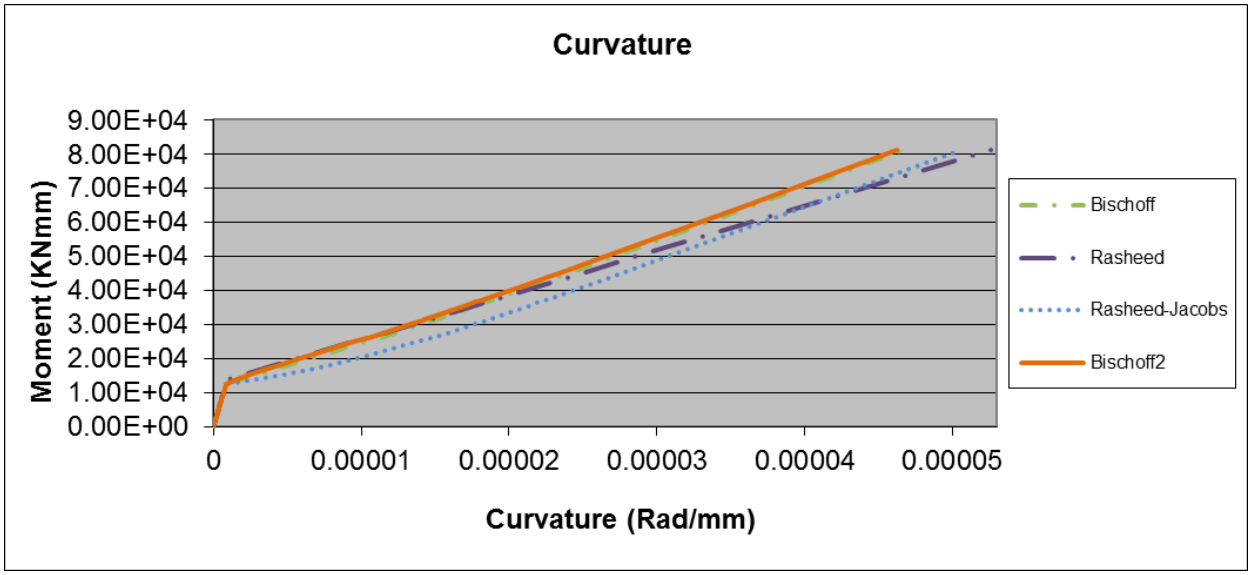

Author: Masmoudi et al. Sample: CB6B-1 Dependent: CB6B-2

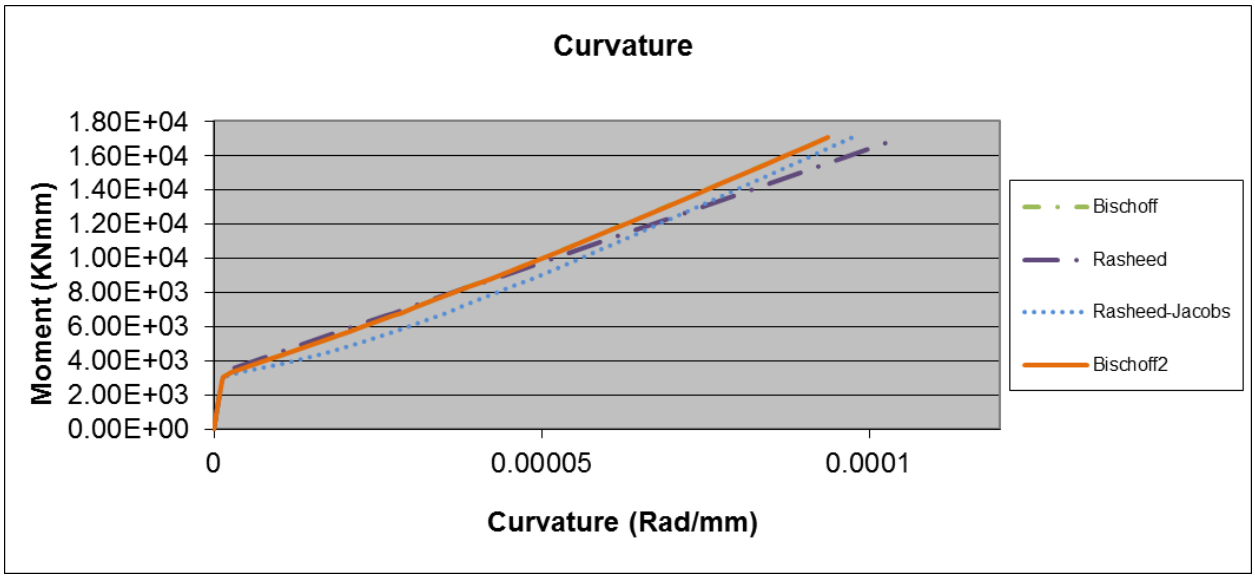

Author: Theriault et al. Sample: BC2NA Dependent: BC2NB

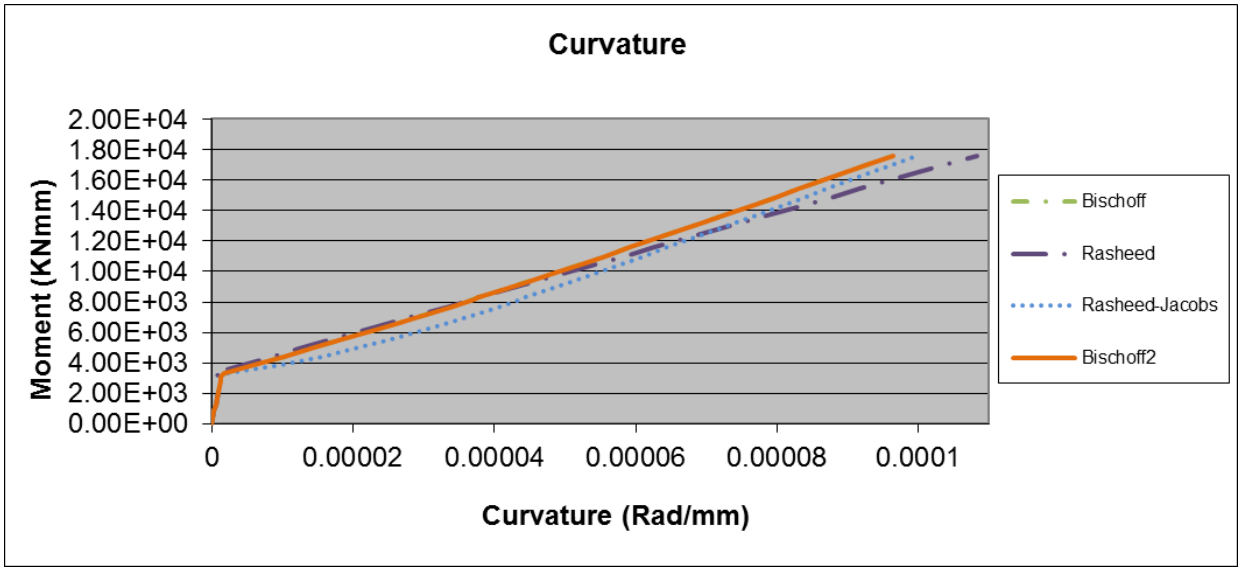

Author: Theriault et al. Sample: BC2HA Dependent: None

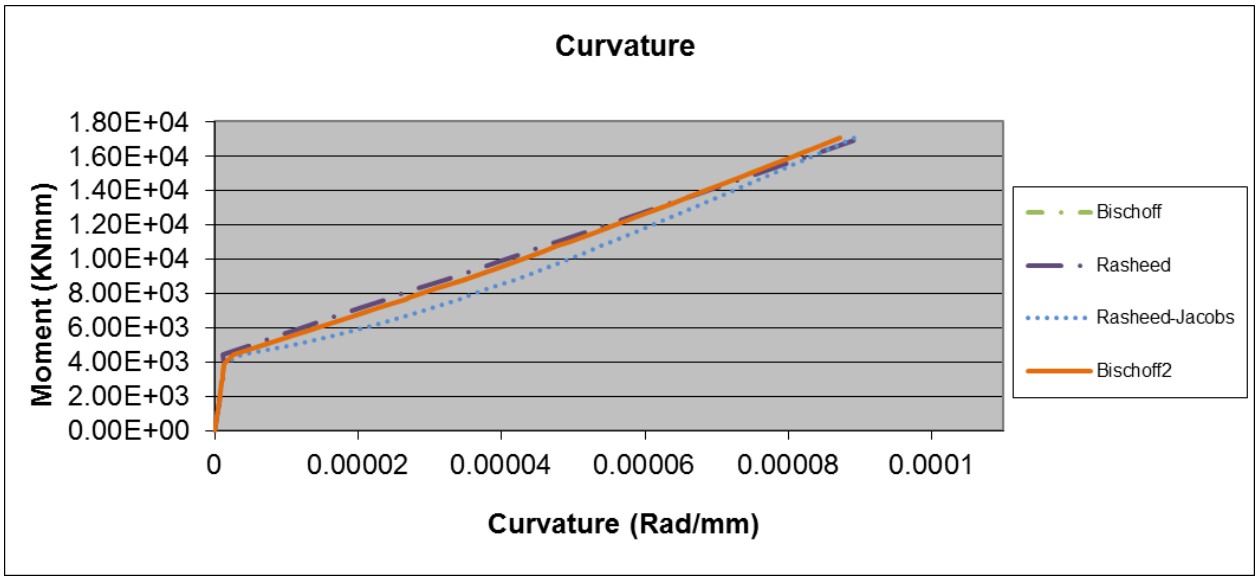

Author: Theriault et al. Sample: BC2VA Dependent: None

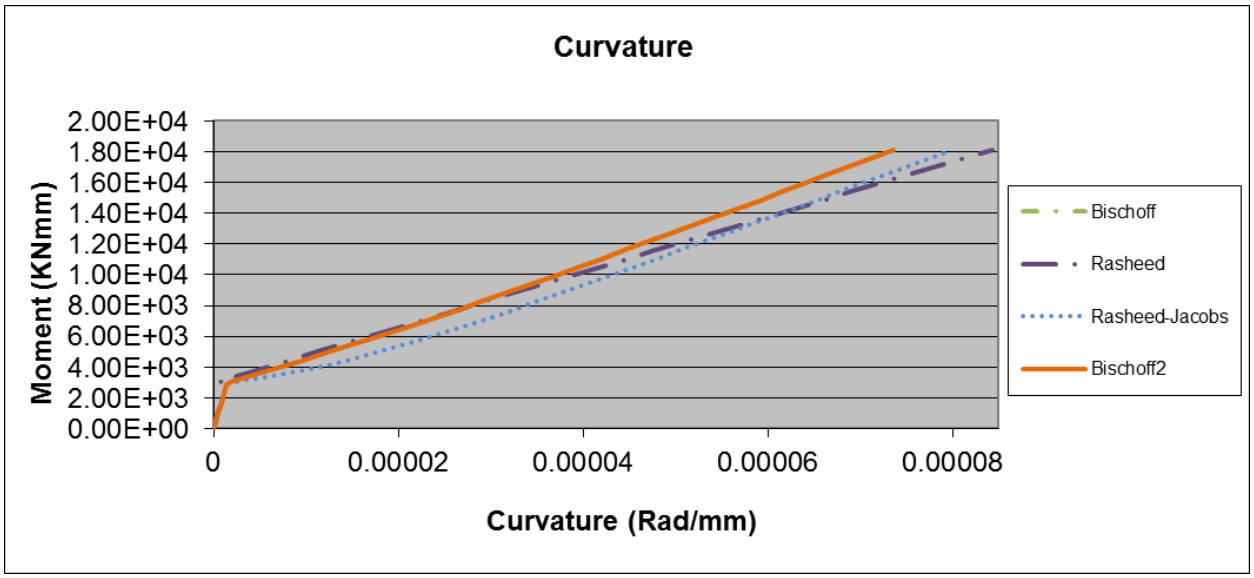

Author: Theriault et al. Sample: BC4NA Dependent: None

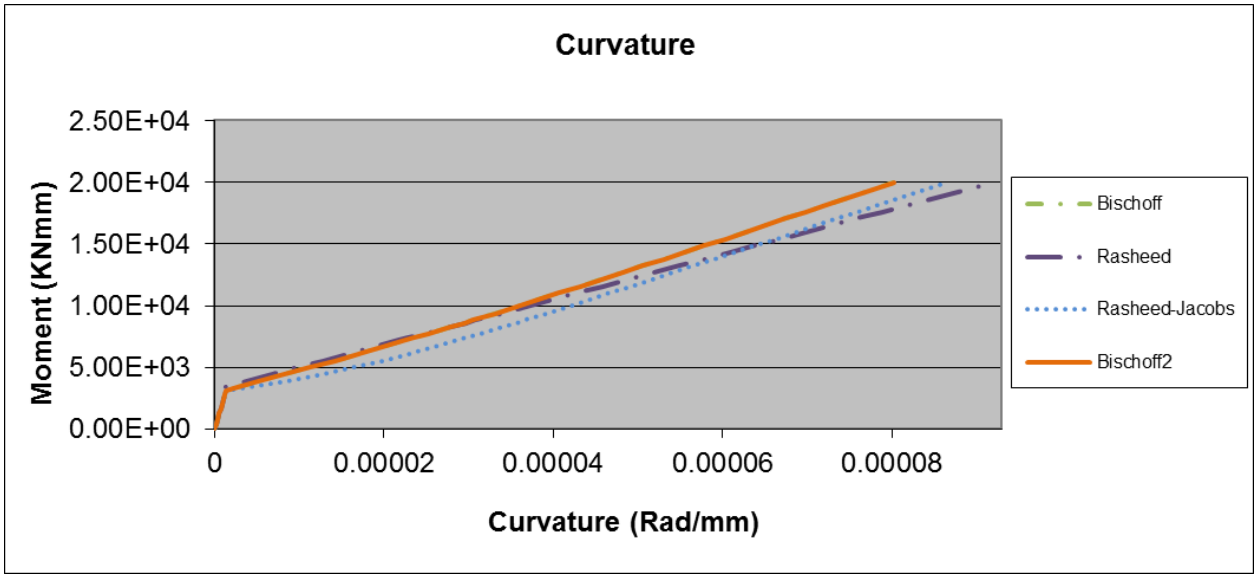

Author: Theriault et al. Sample: BC4HA Dependent: None

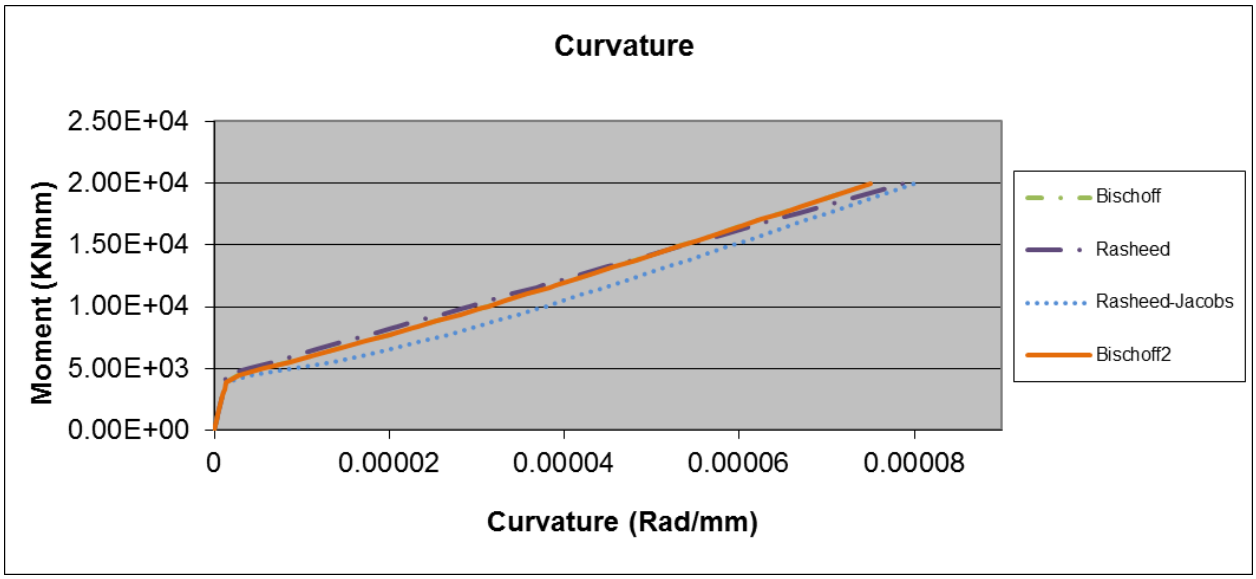

Author: Theriault et al. Sample: BC4VA Dependent: BC4VB

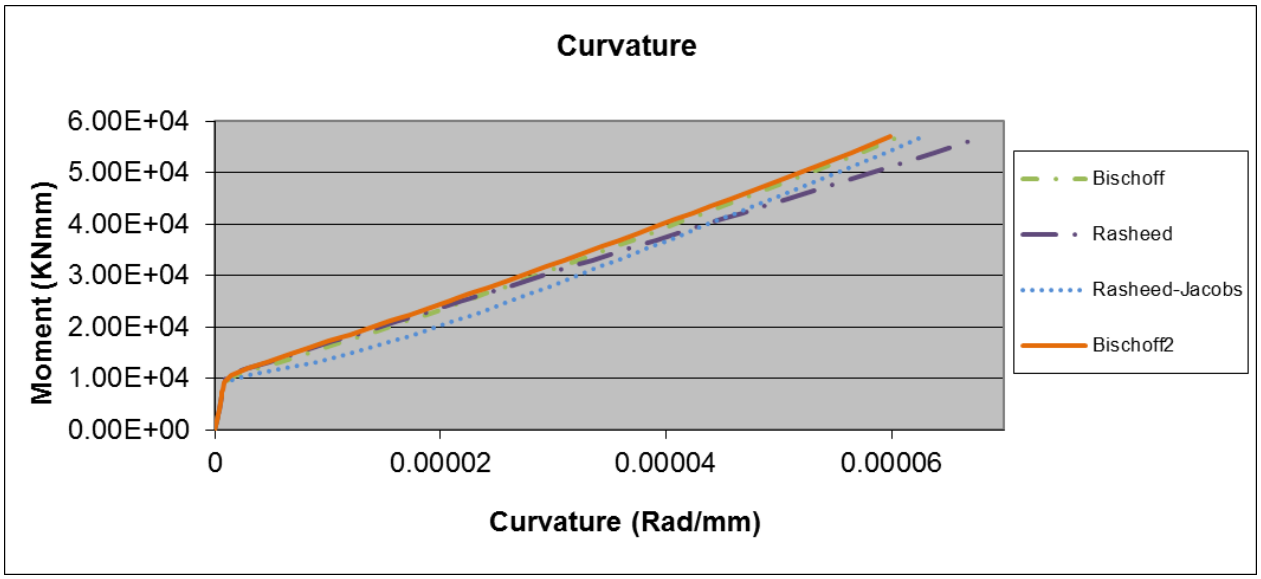

Author: Toutanji et al. Sample: GB2 Dependent: None

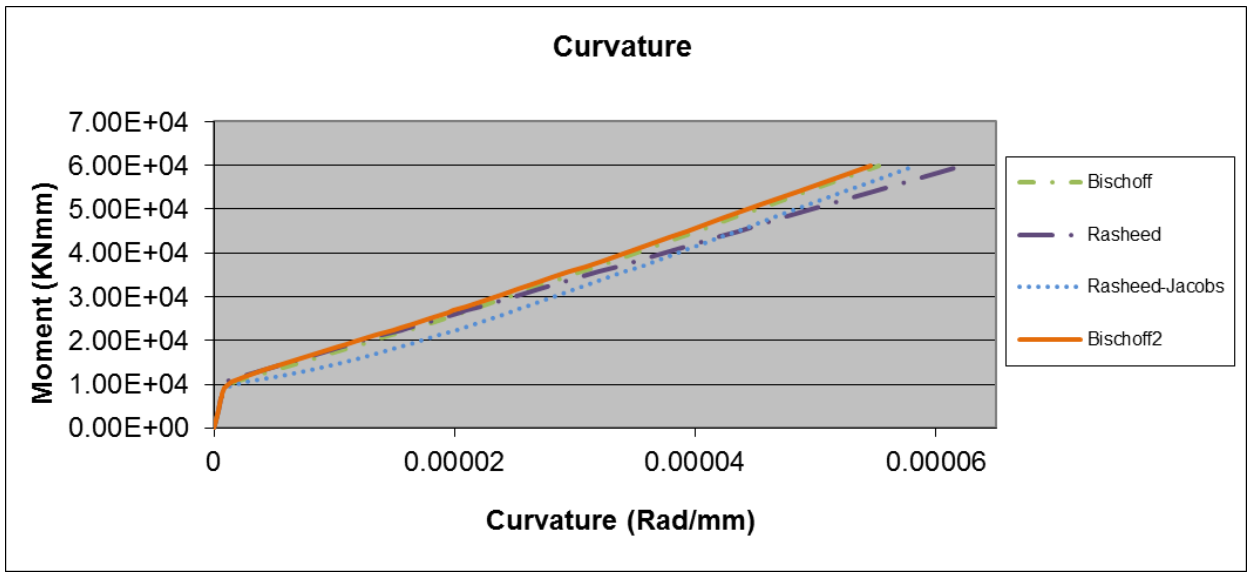

Author: Toutanji et al. Sample: GB3 Dependent: None

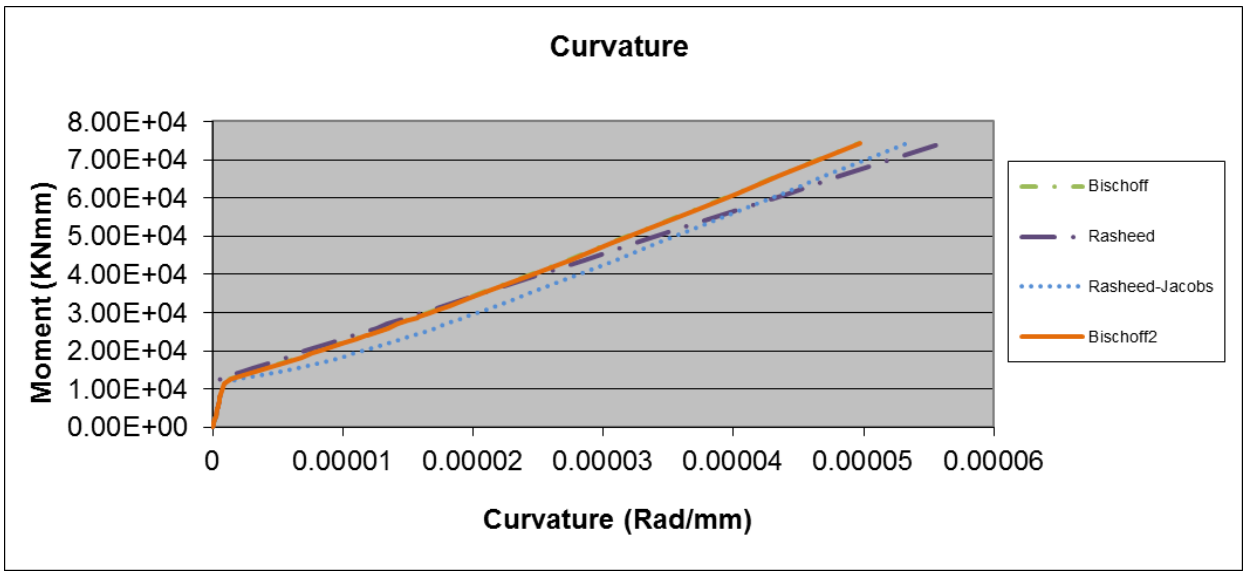

Author: Kassem et al. Sample: CB4 Dependent: None

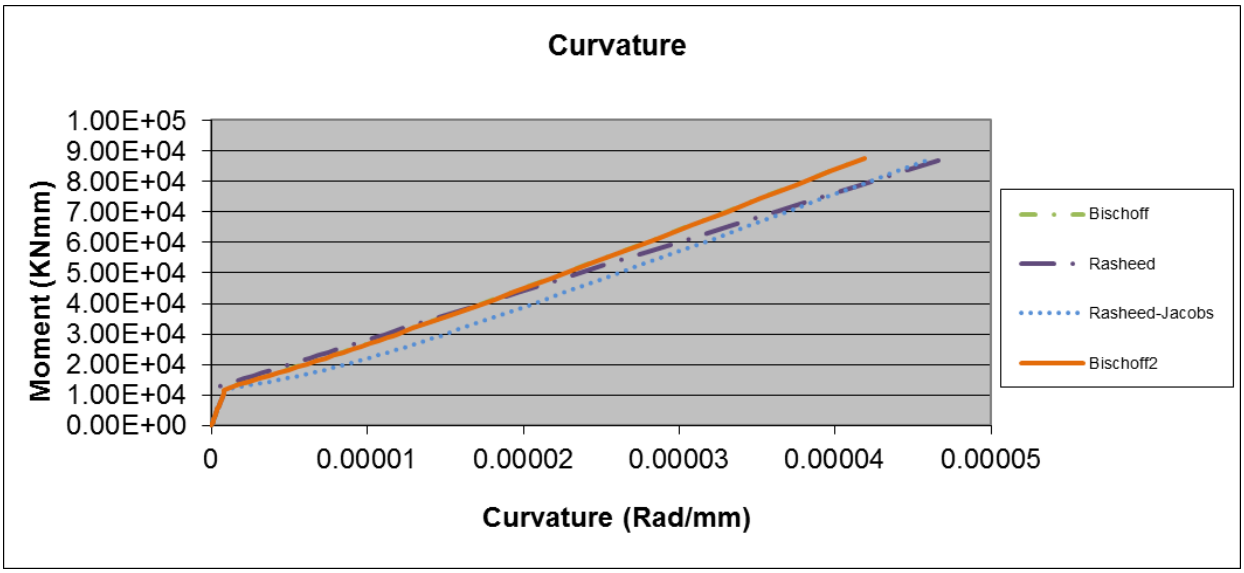

Author: Kassem et al. Sample: CB6 Dependent: None

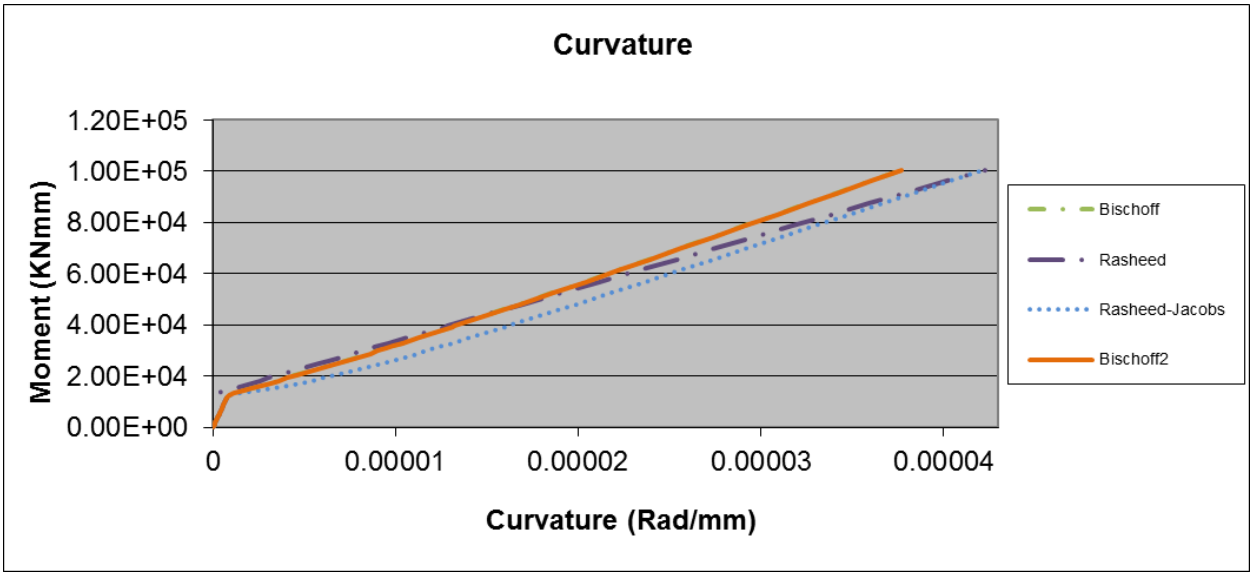

Author: Kassem et al. Sample: CB8 Dependent: None

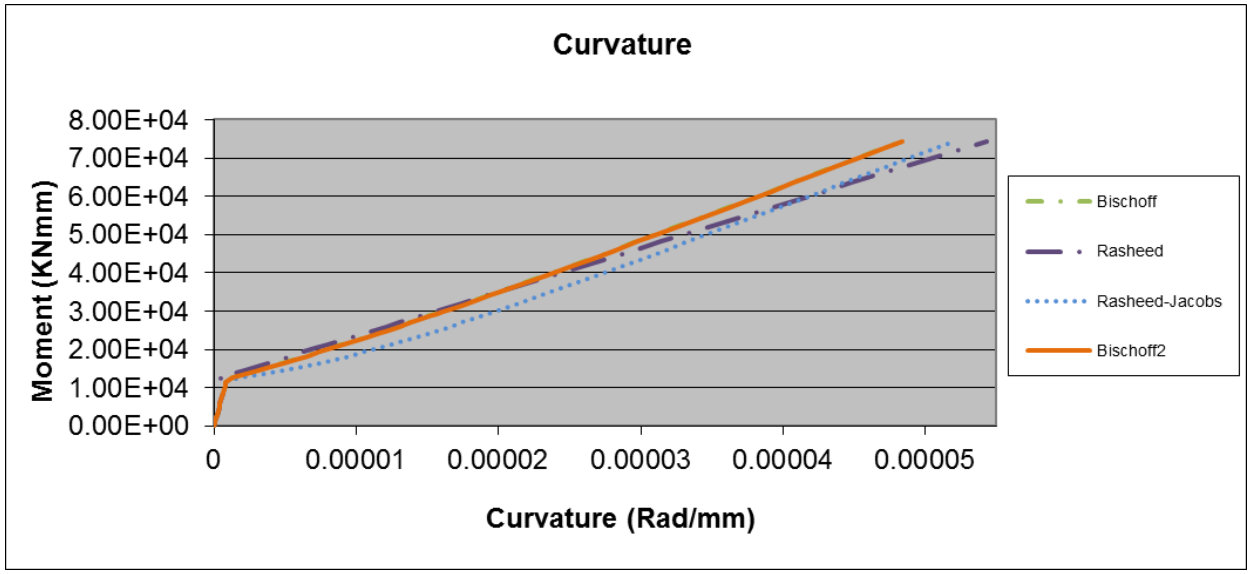

Author: Kassem et al. Sample: IS4 Dependent: None

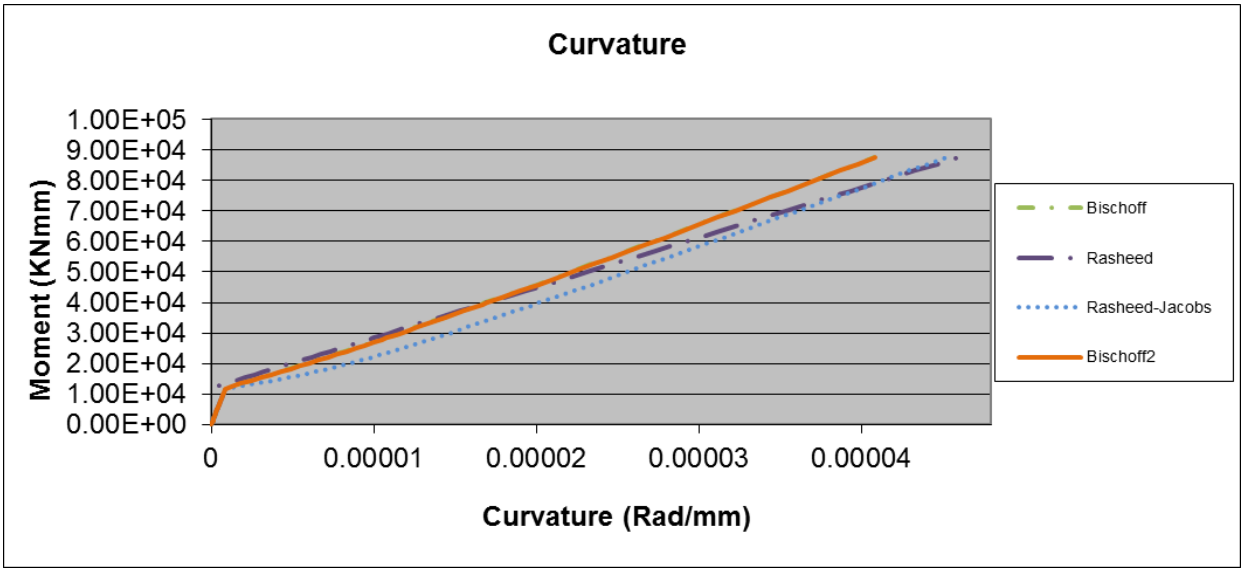

Author: Kassem et al. Sample: IS6 Dependent: None

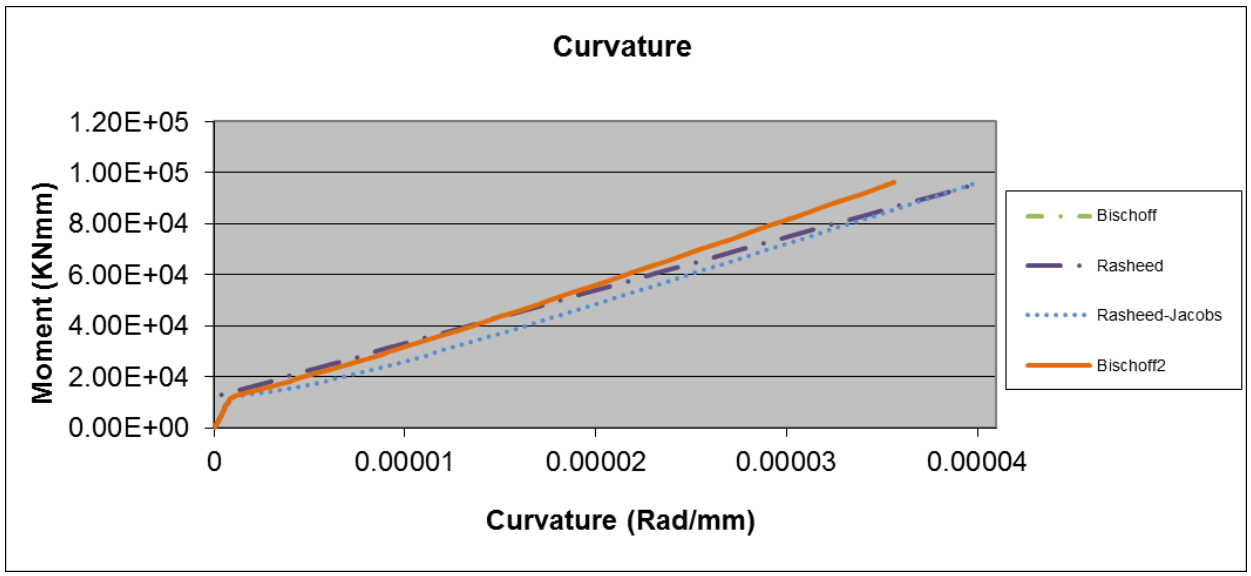

Author: Kassem et al. Sample: IS8 Dependent: None

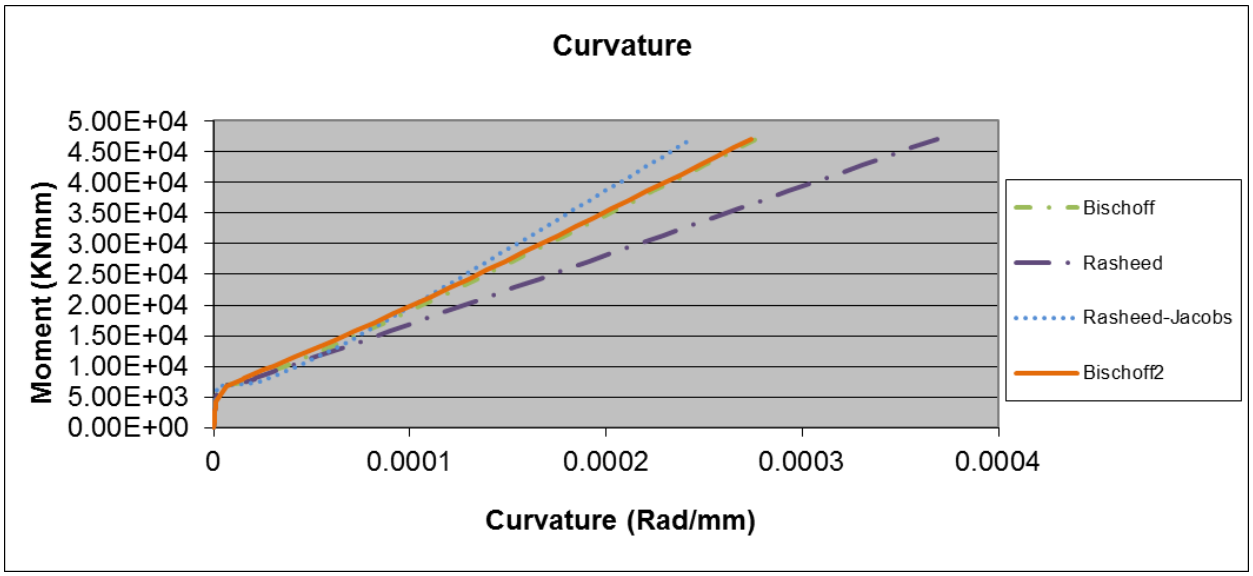

Author: Yost et al. Sample: 1a– NL Dependent: 1b-NL, 1c-NL

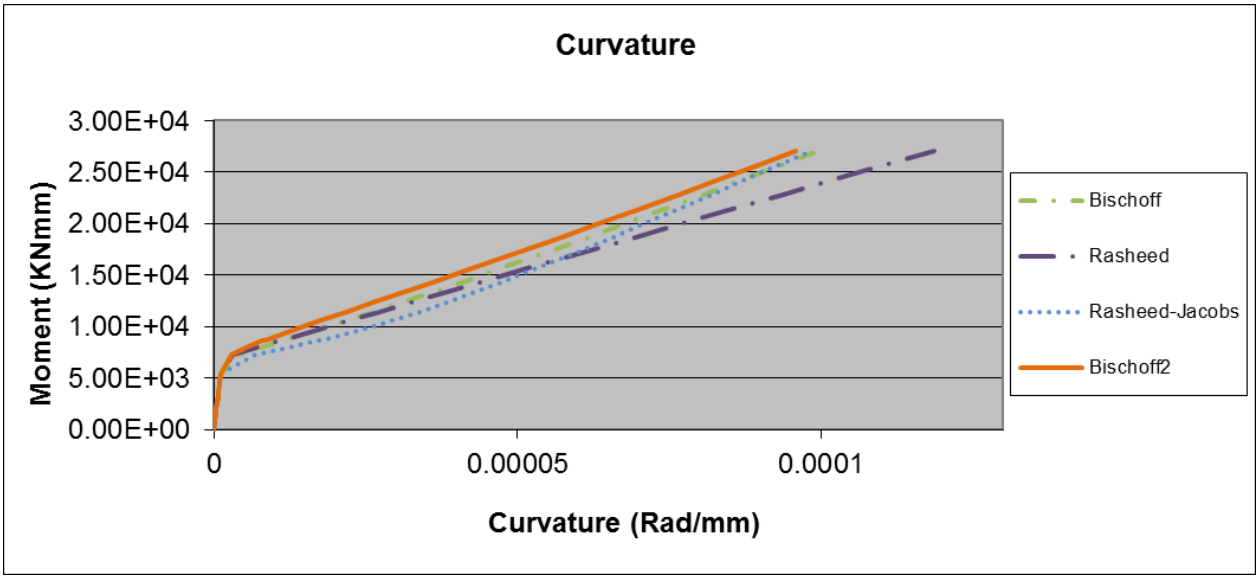

Author: Yost et al. Sample: 2a– NL Dependent: 2b-NL, 2c-NL

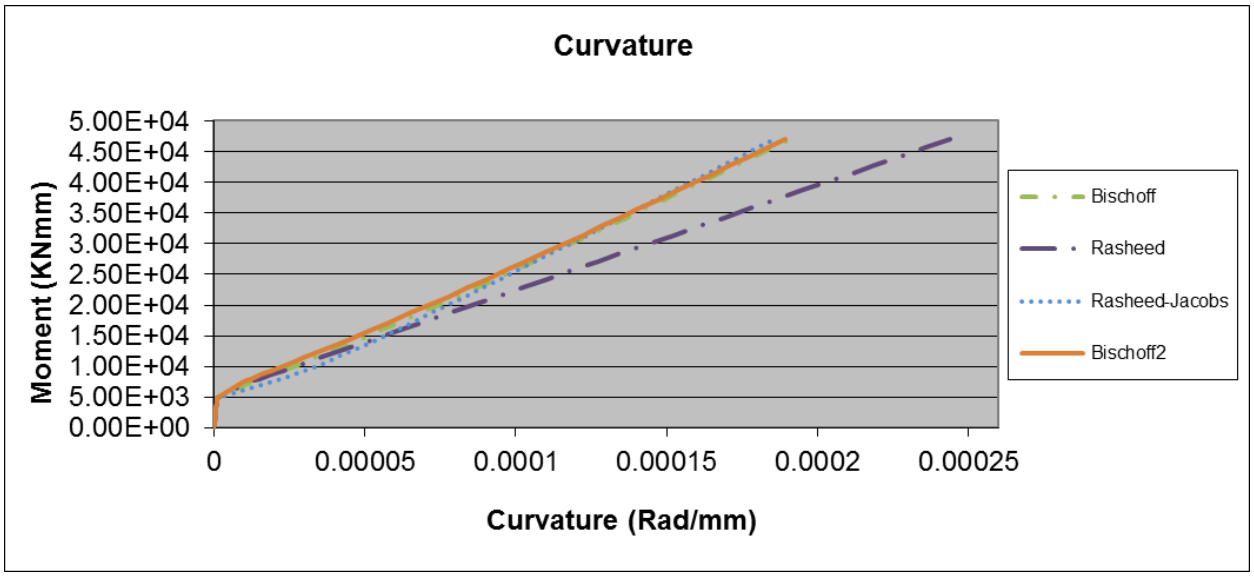

Author: Yost et al. Sample: 3a– NL Dependent: 3b-NL, 3c-NL

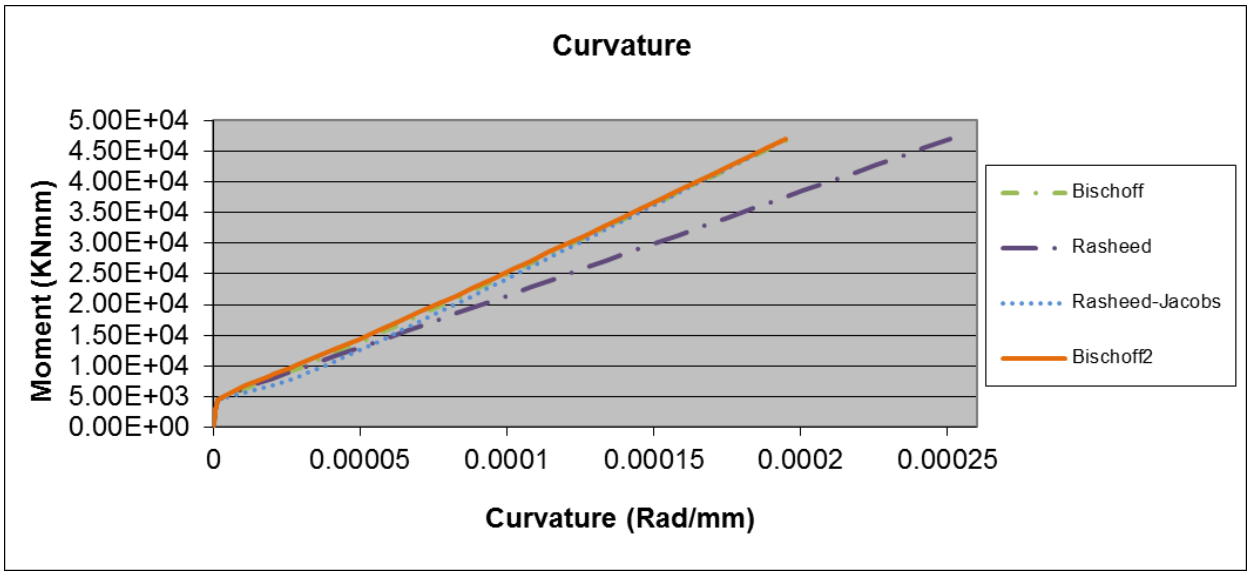

Author: Yost et al. Sample: 4a– NL Dependent: 4b-NL, 4c-NL

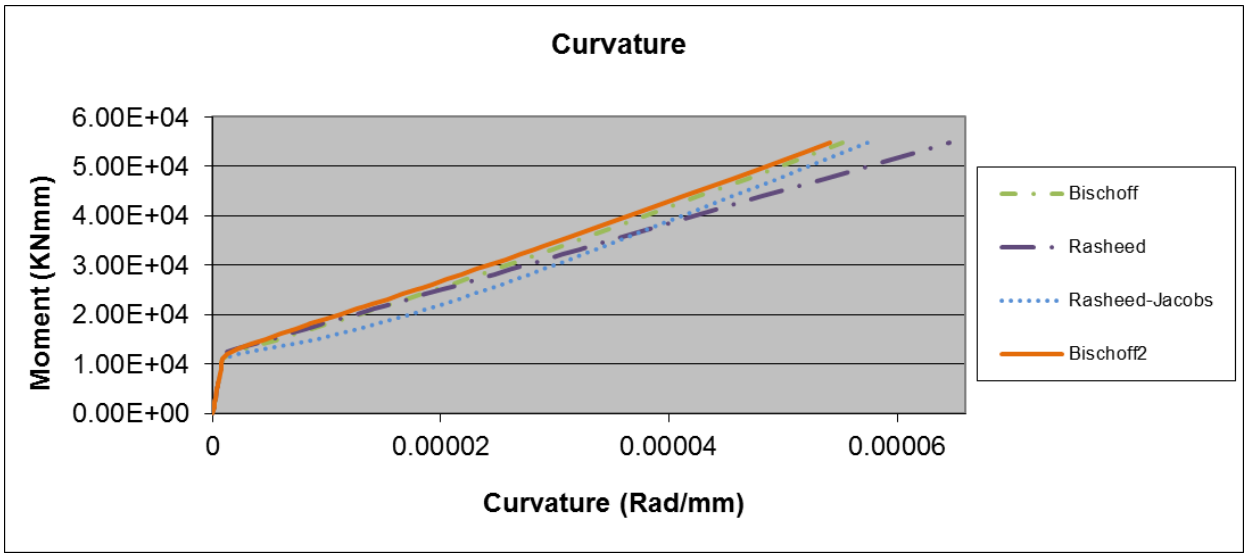

Author: Yost et al. Sample: 1a– NS Dependent: 1b-NS, 1c-NS

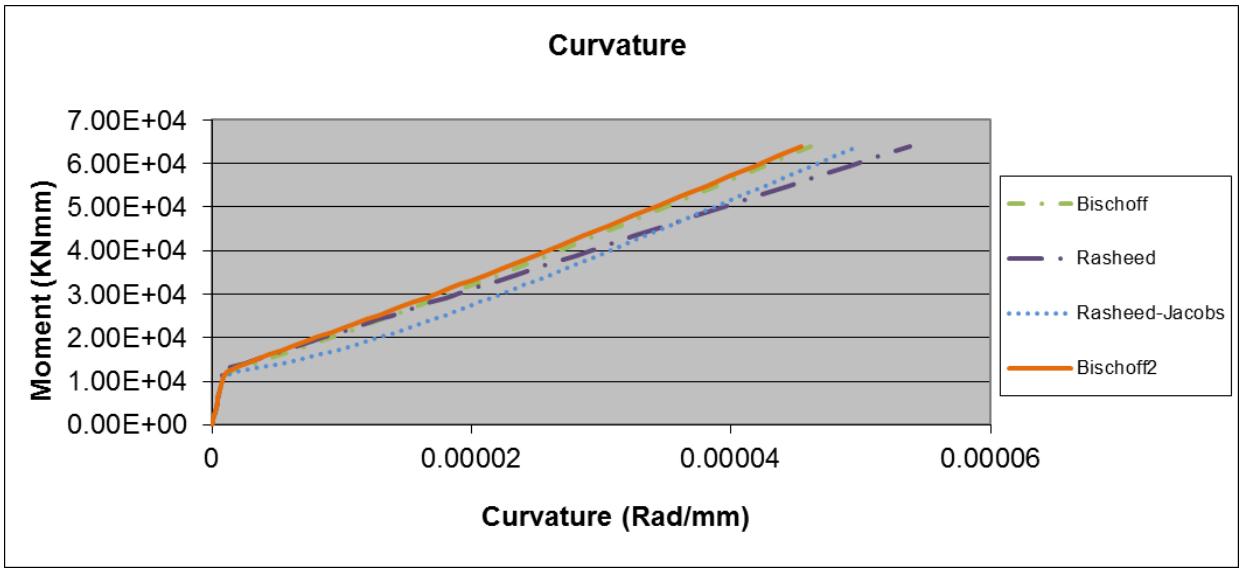

Author: Yost et al. Sample: 2a– NS Dependent: 2b-NS, 2c-NS

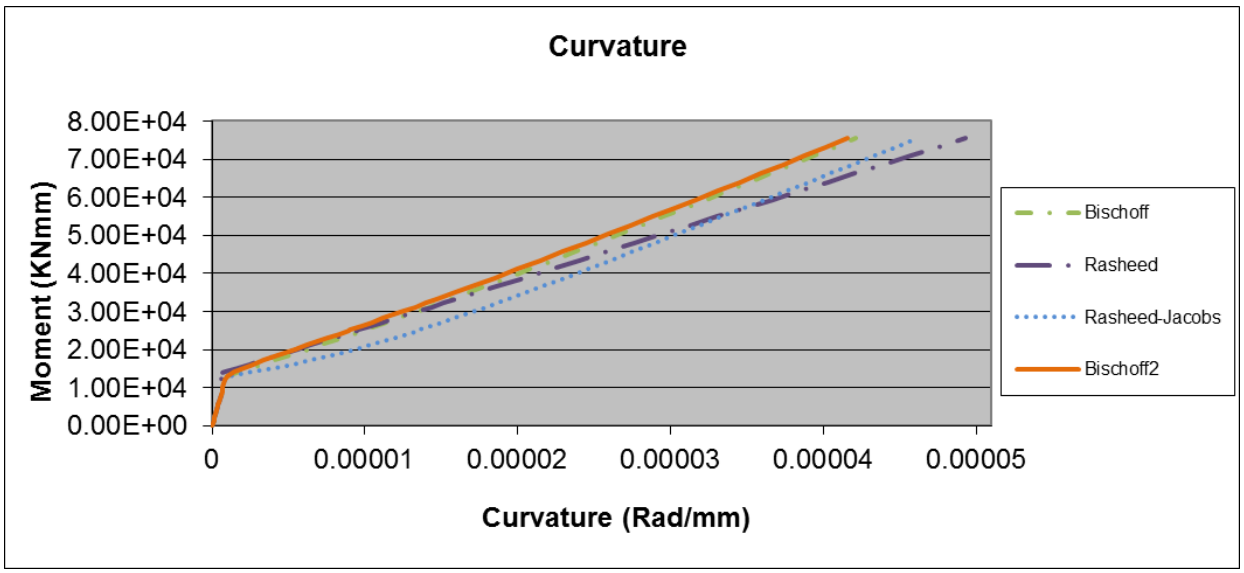

Author: Yost et al. Sample: 3a– NS Dependent: 3b-NS, 3c-NS

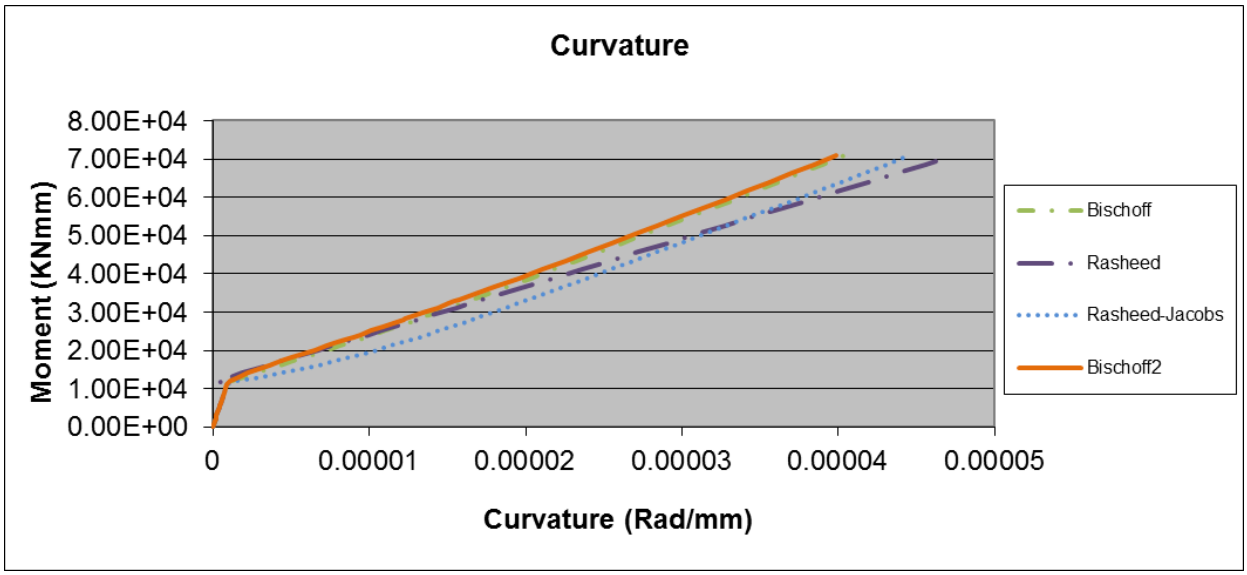

Author: Yost et al. Sample: 4a– NS Dependent: 4b-NS, 4c-NS

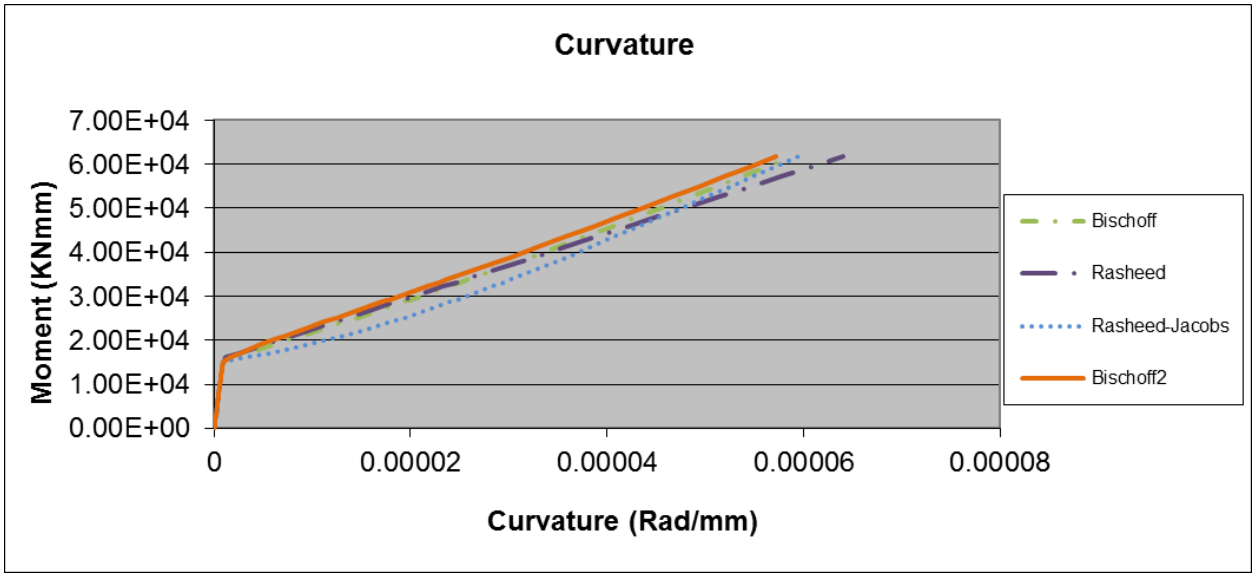

Author: Yost et al. Sample: 1a– HS Dependent: 1c-HS

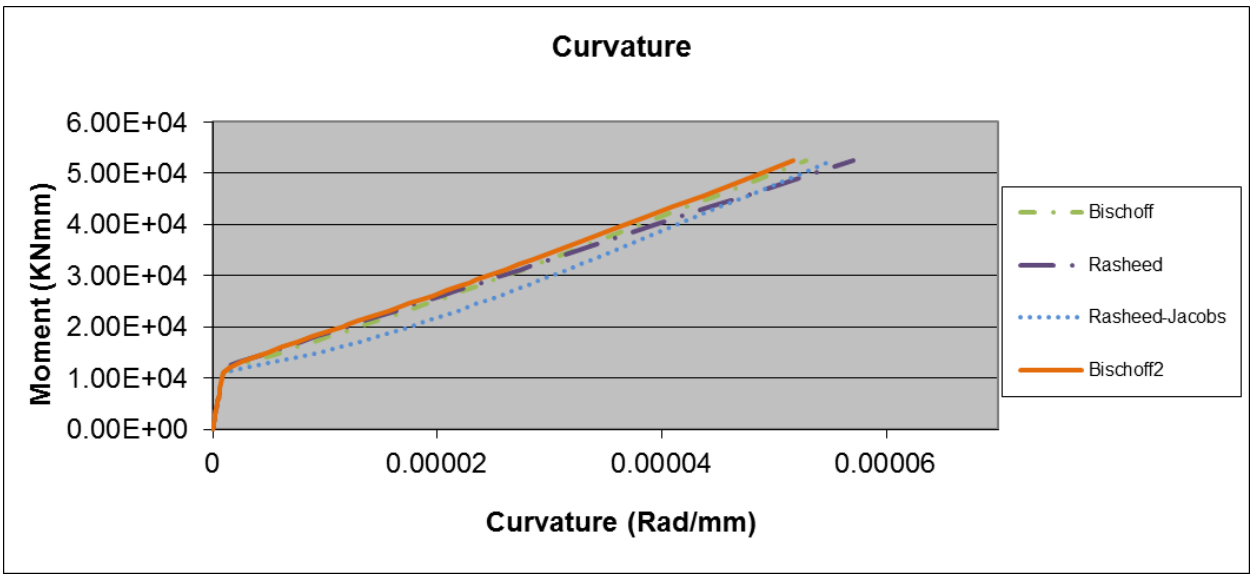

Author: Yost et al. Sample: 2a– HS Dependent: 2b-HS, 2c-HS

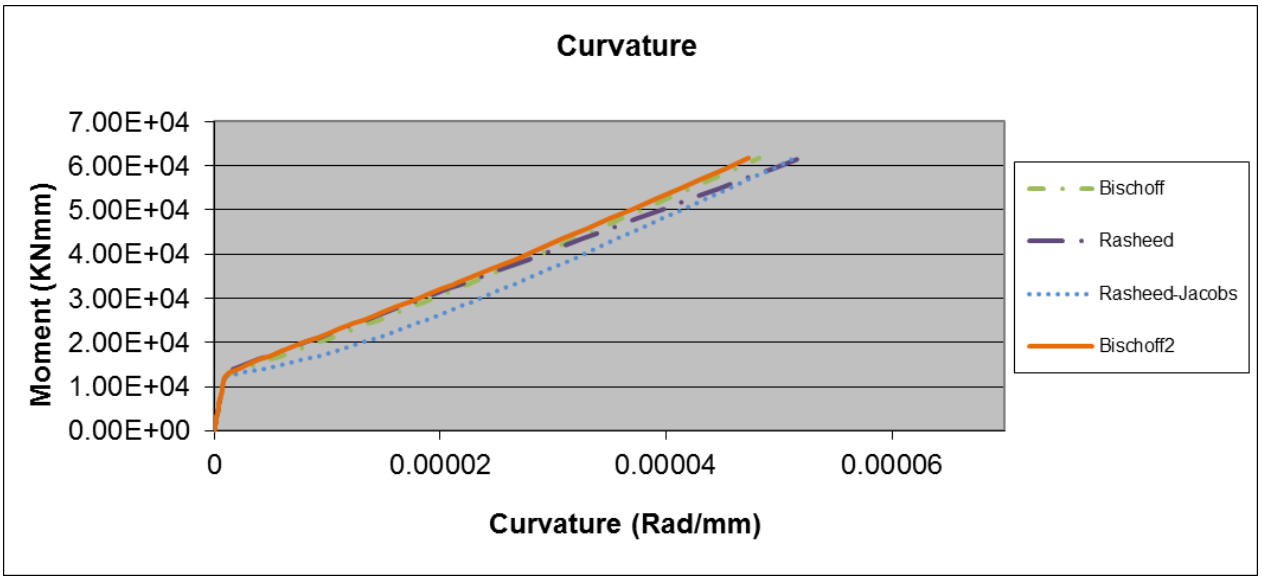

Author: Yost et al. Sample: 3a– HS Dependent: None

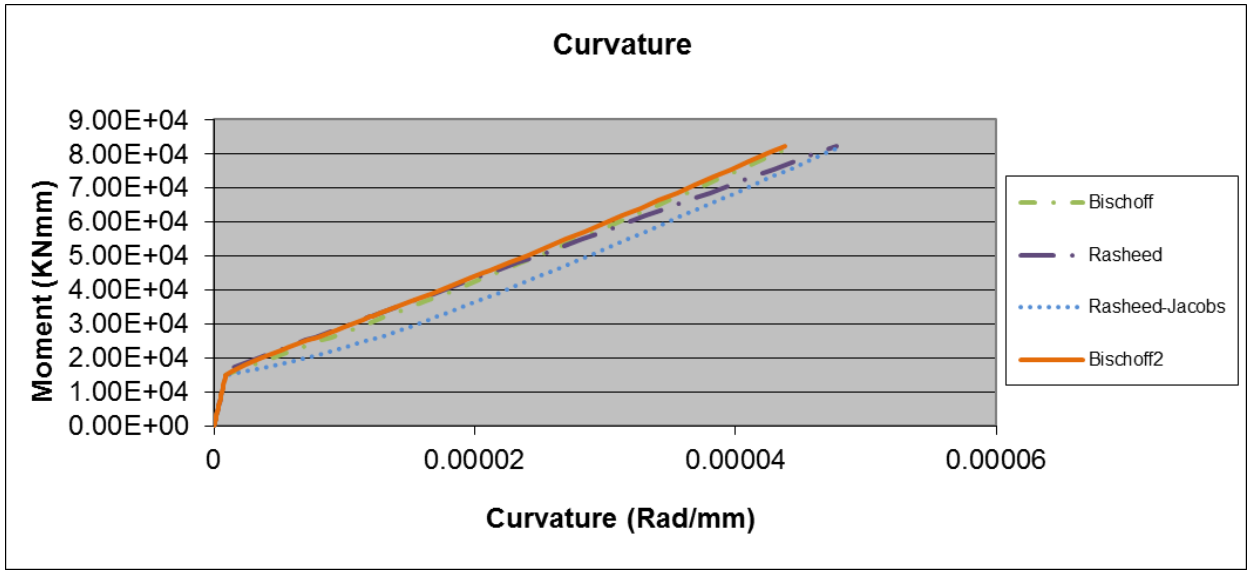

Author: Yost et al. Sample: 4a– HS Dependent: None

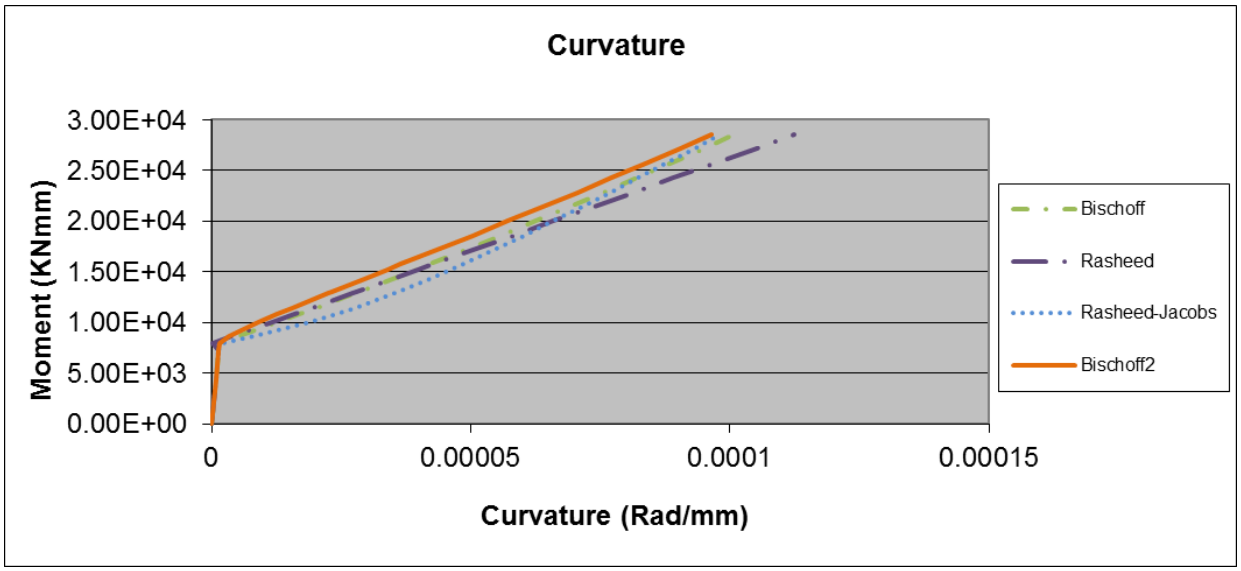

Author: Yost et al. Sample: 1a– HL Dependent: 1b-HL, 1c-HL

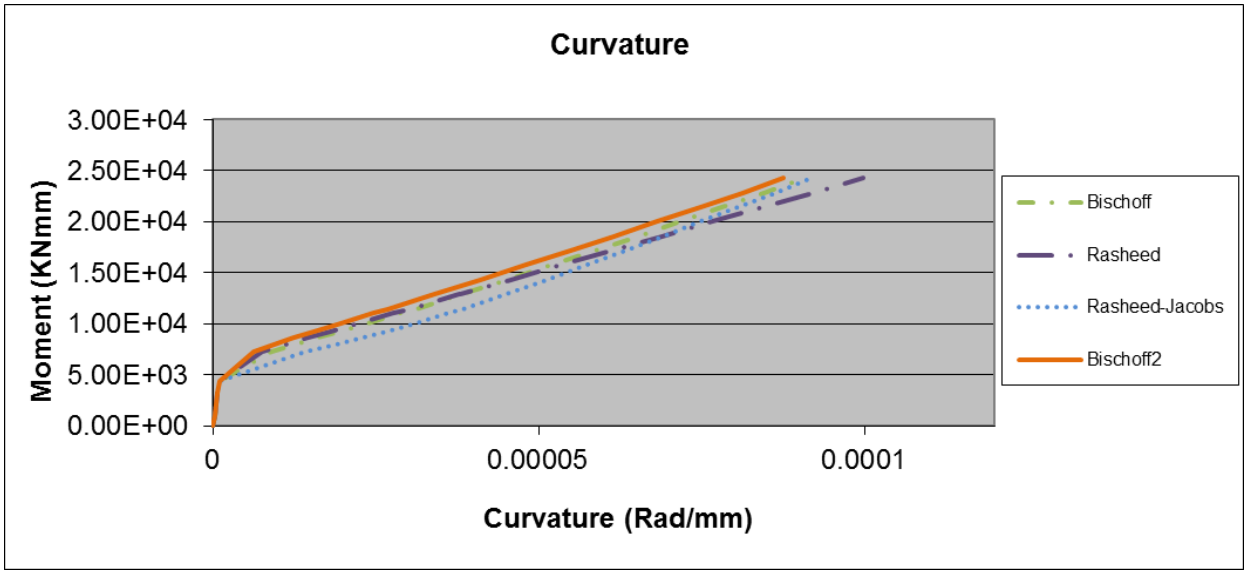

Author: Yost et al. Sample: 2a– HL Dependent: 2b-HL, 2c-HL

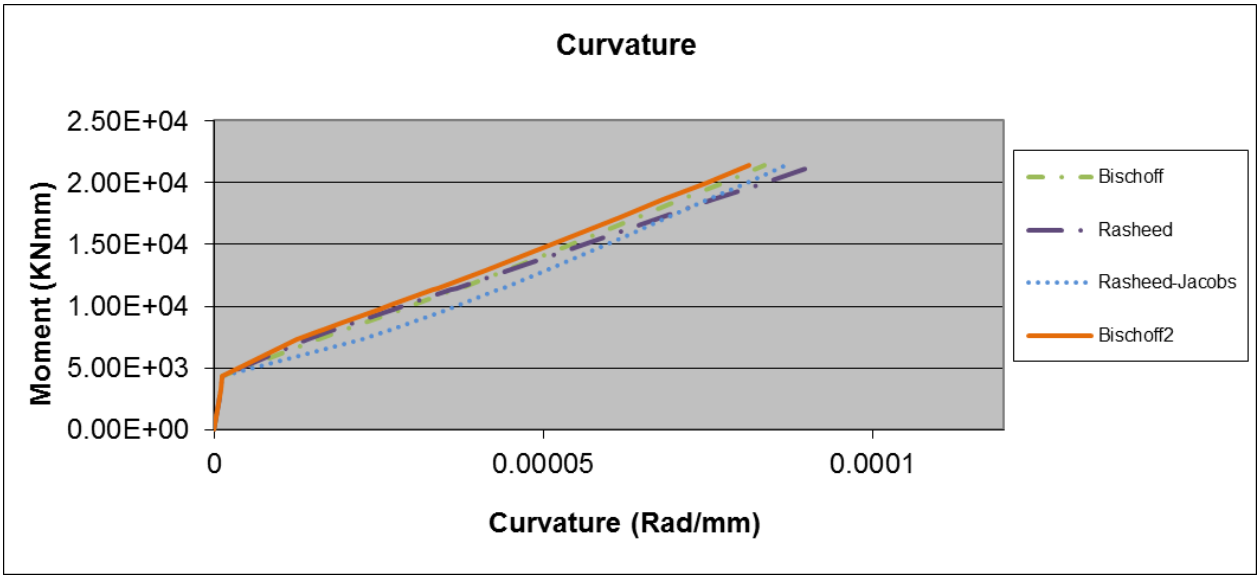

Author: Yost et al. Sample: 3a– HL Dependent: 3b-HL, 3c-HL

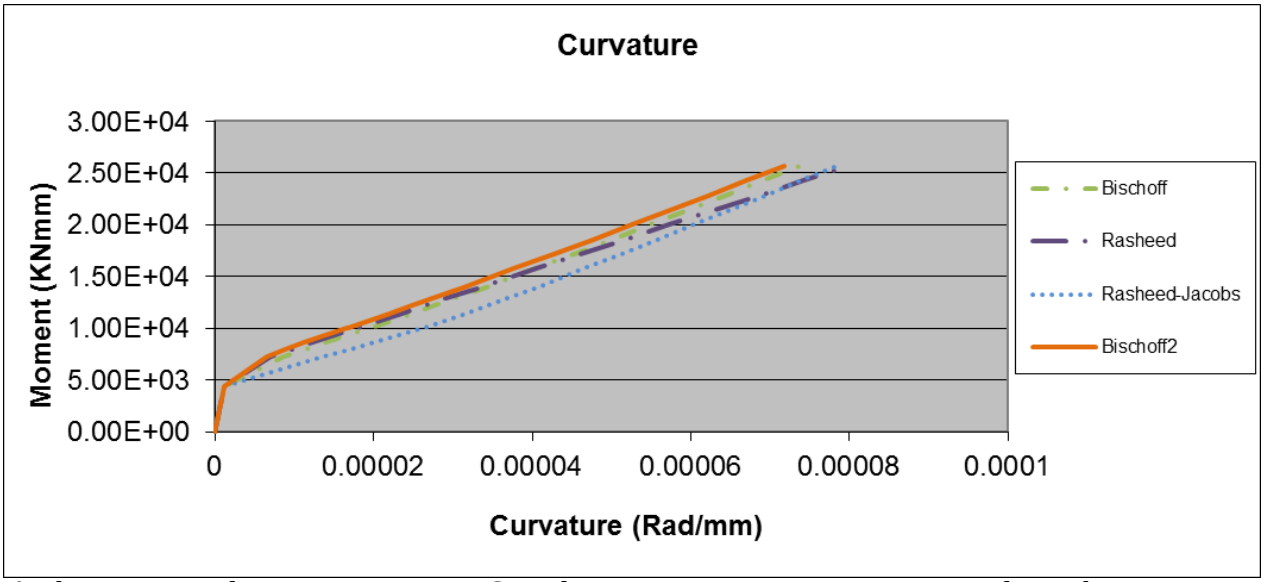

Author: Yost et al. Sample: 4a– HL Dependent: 4b-HL, 4c-HL

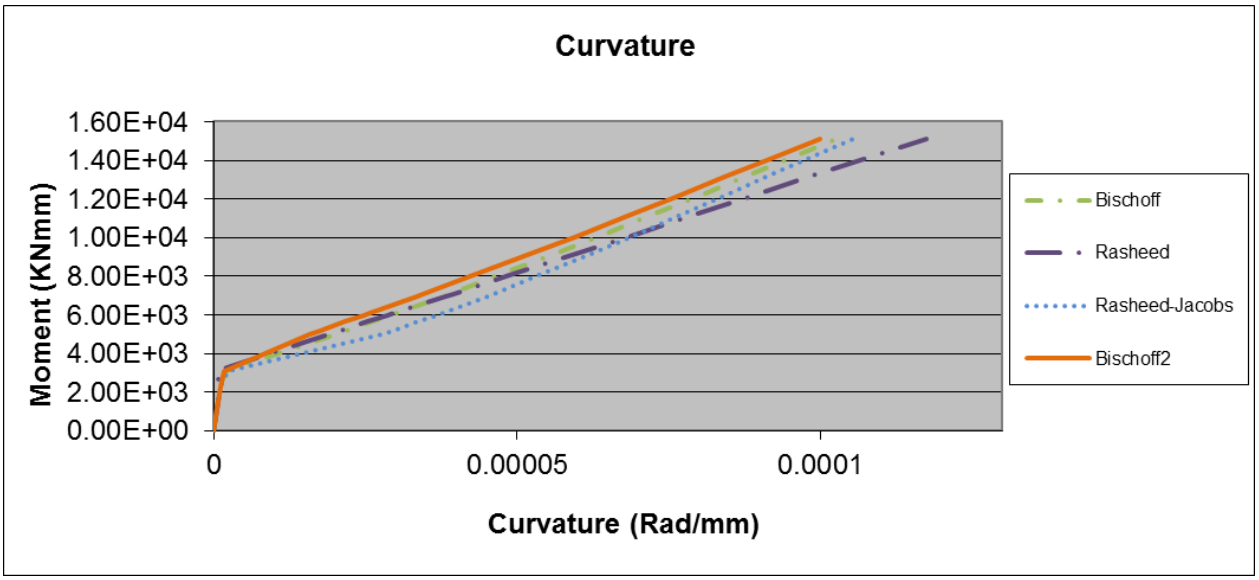

Author: Theisz et al. Sample: 8-2-1 Dependent: 8-2-2, 8-2-3

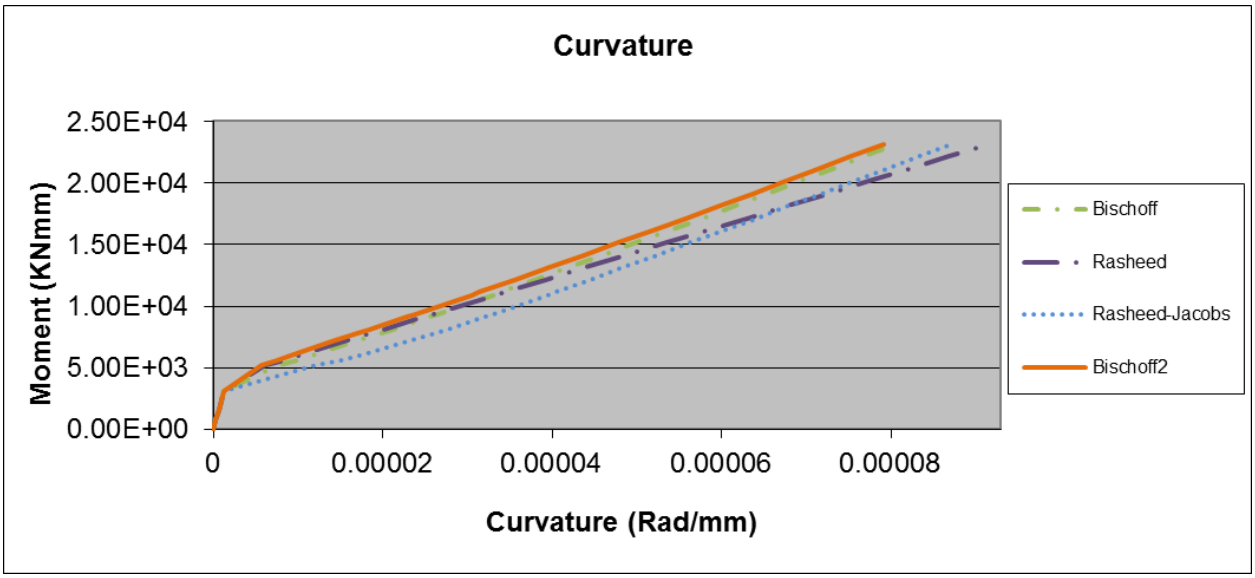

Author: Theisz et al. Sample: 8-3-1 Dependent: 8-3-2, 8-3-3

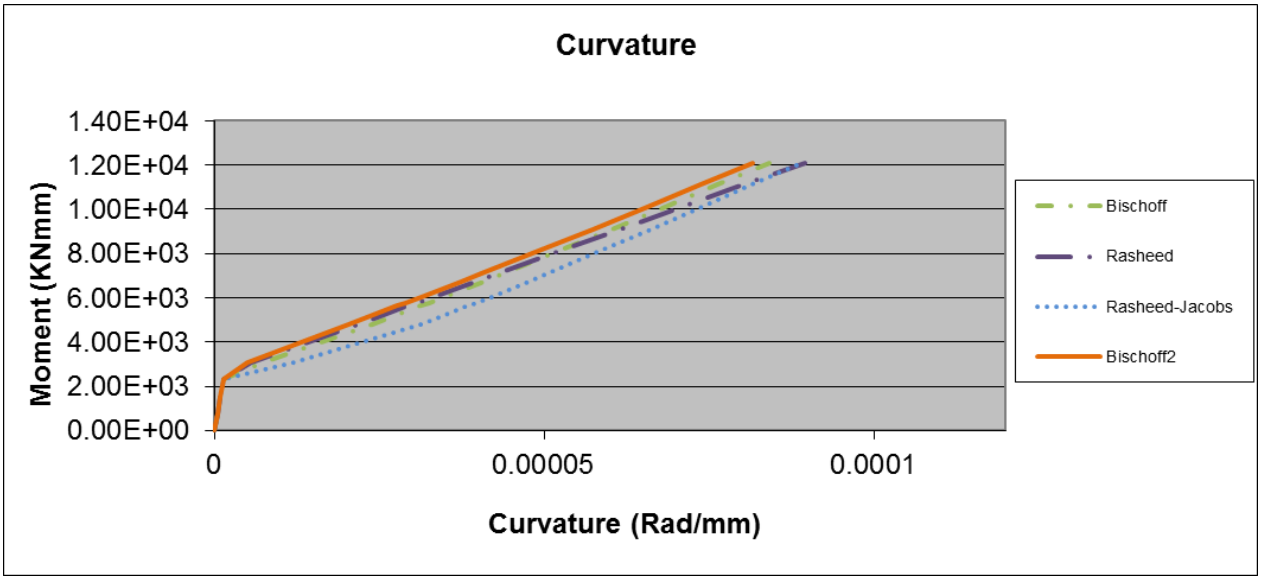

Author: Theisz et al. Sample: 11-2-1 Dependent: 11-2-2, 11-2-3

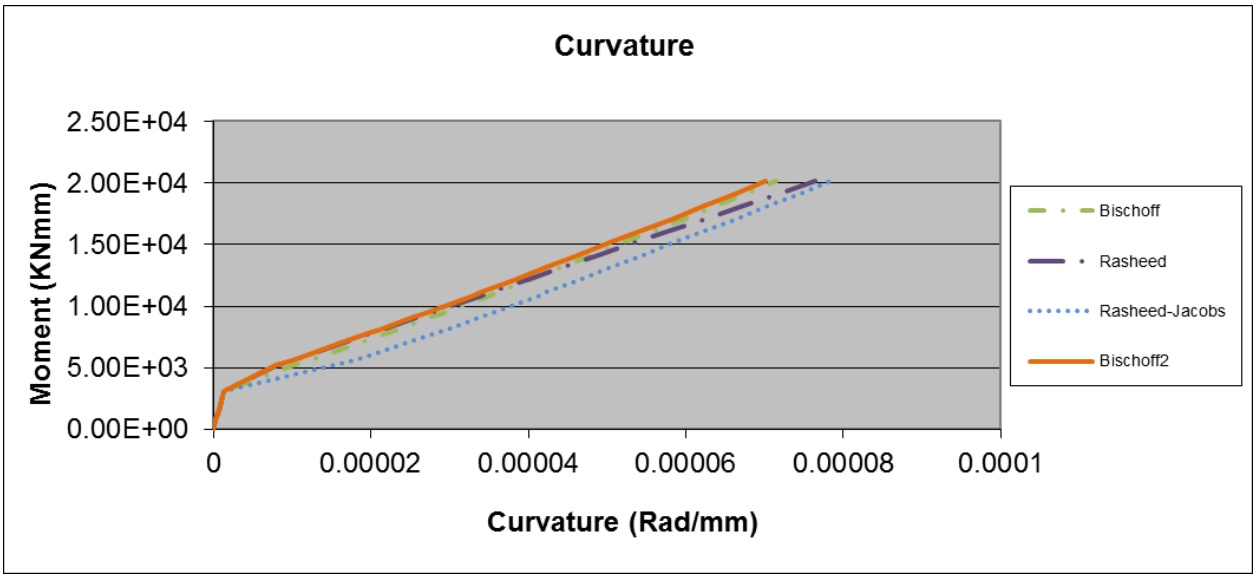

Author: Theisz et al. Sample: 11-3-1 Dependent: 11-3-2, 11-3-3

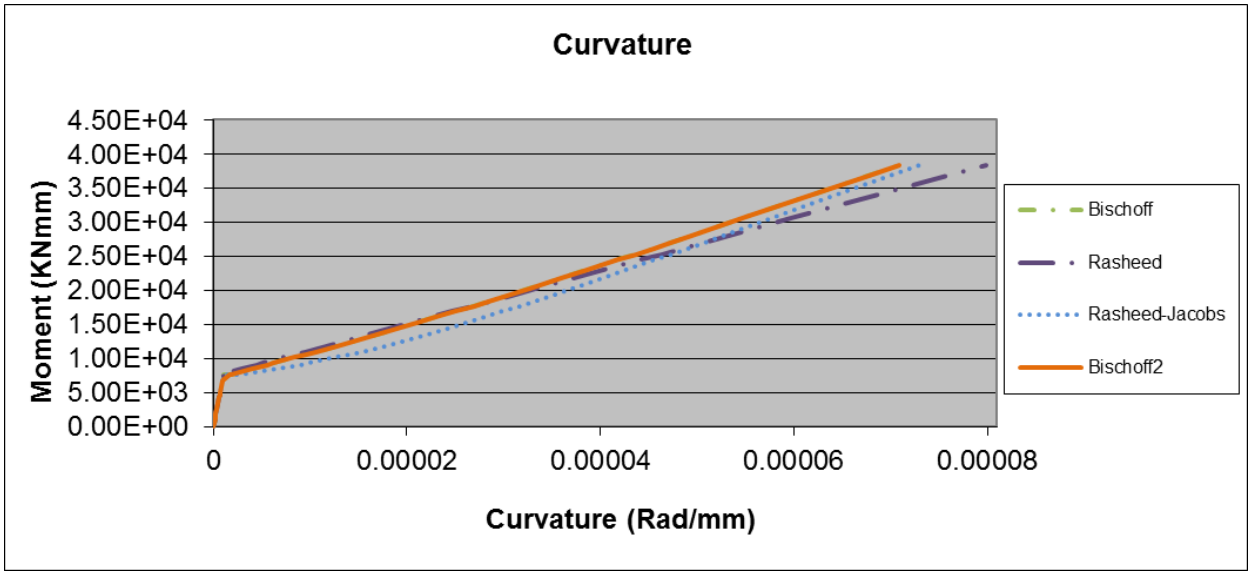

Author: Al-Sunna Sample: BC1a Dependent: BC1b

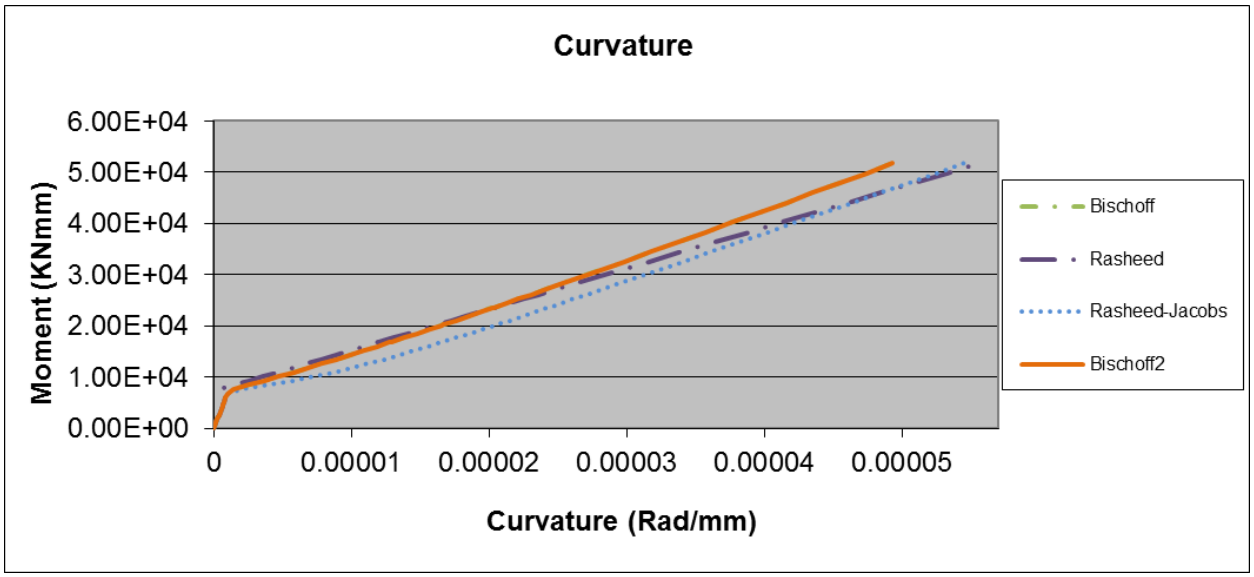

Author: Al-Sunna Sample: BC2a Dependent: BC2b

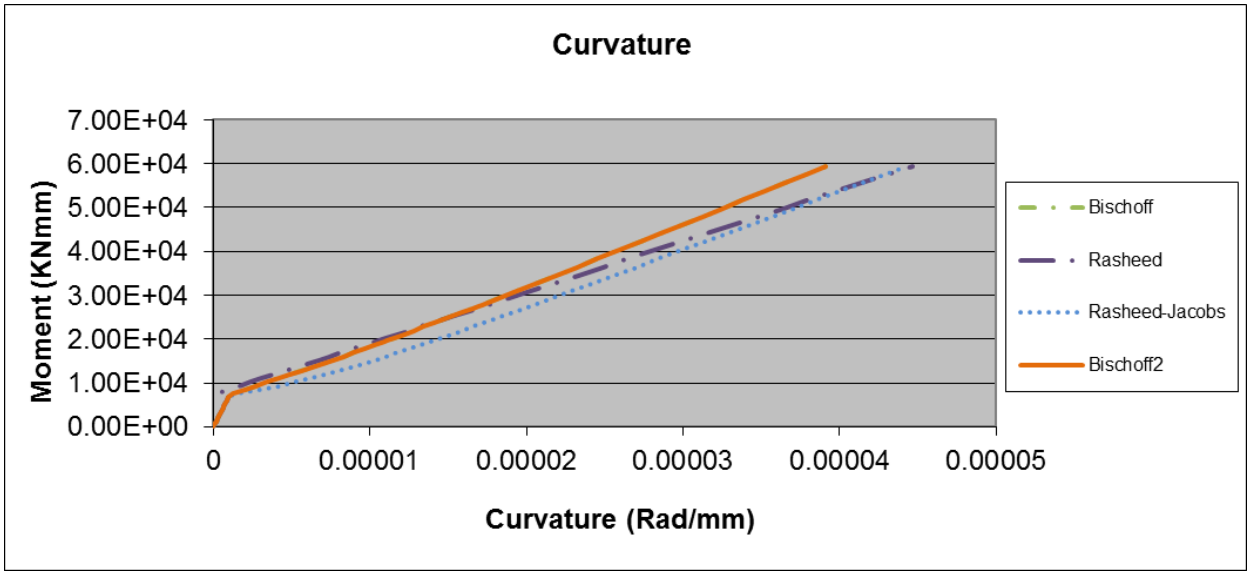

Author: Al-Sunna Sample: BC3a Dependent: BC3b

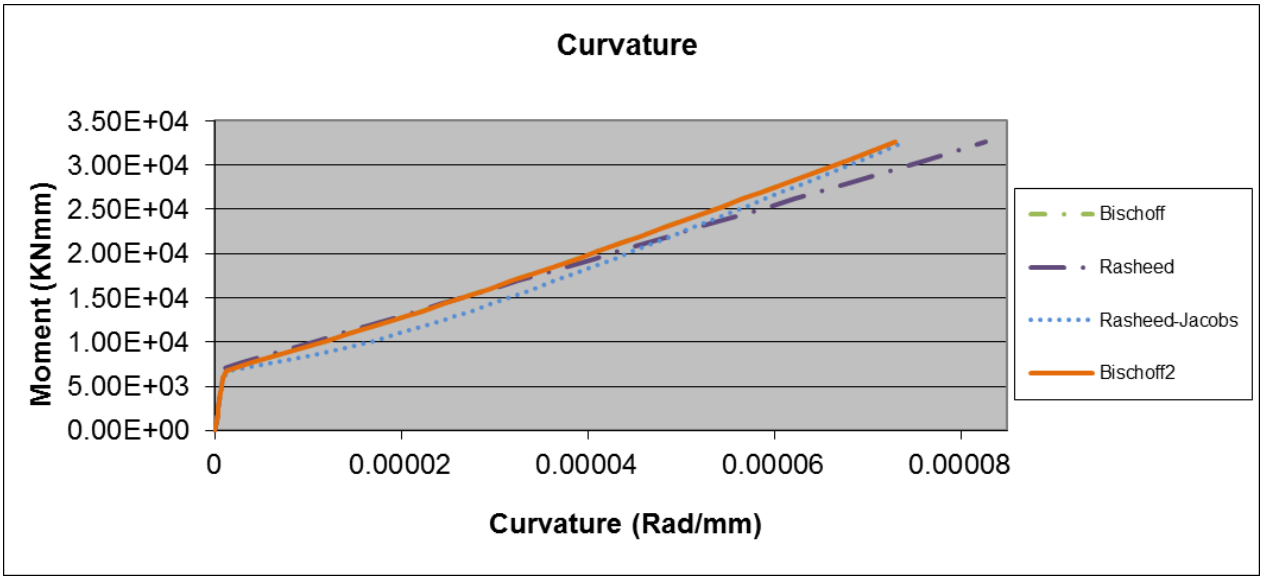

Author: Al-Sunna Sample: BG2a Dependent: BG2b

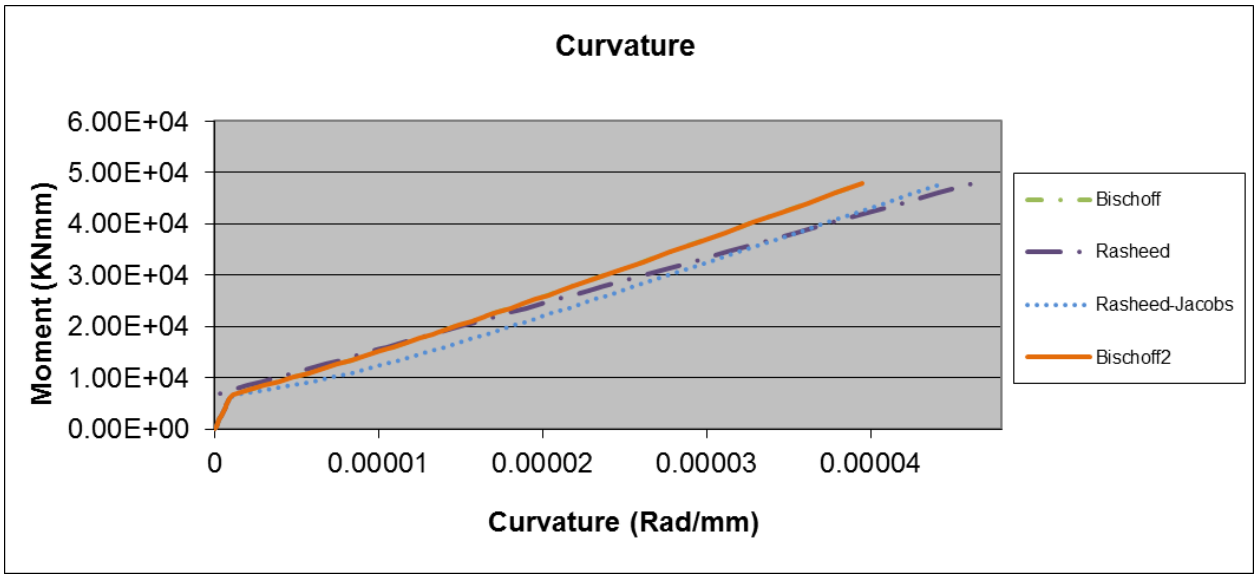

Author: Al-Sunna Sample: BG3a Dependent: BG3b

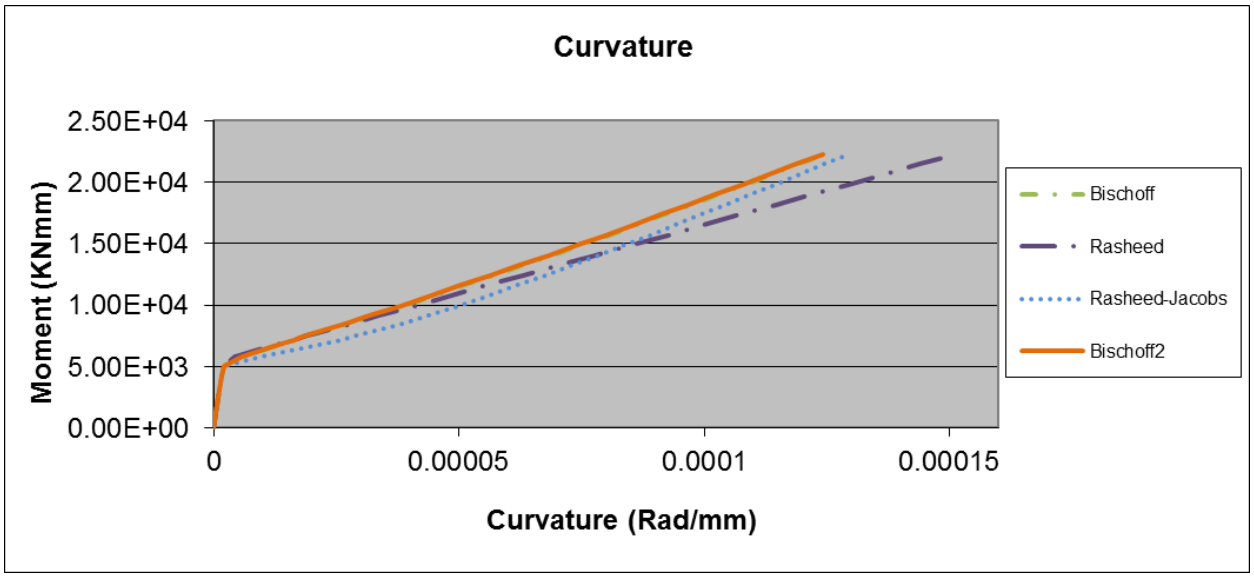

Author: Al-Sunna Sample: SC2a Dependent: None

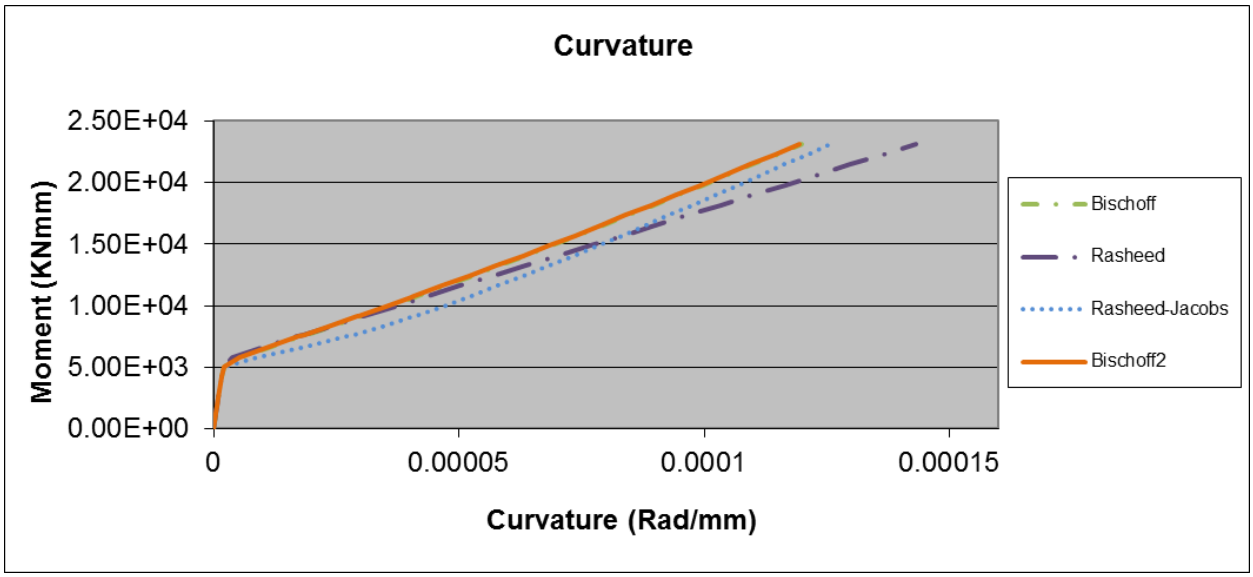

Author: Al-Sunna Sample: SC2b Dependent: None

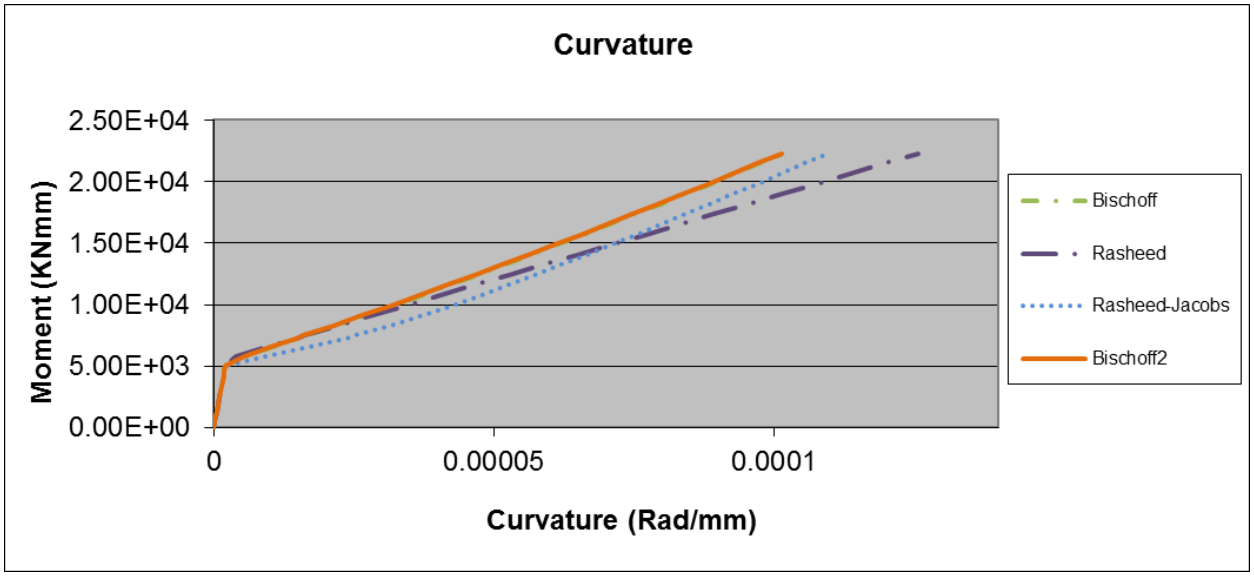

Author: Al-Sunna Sample: SC3a Dependent: None

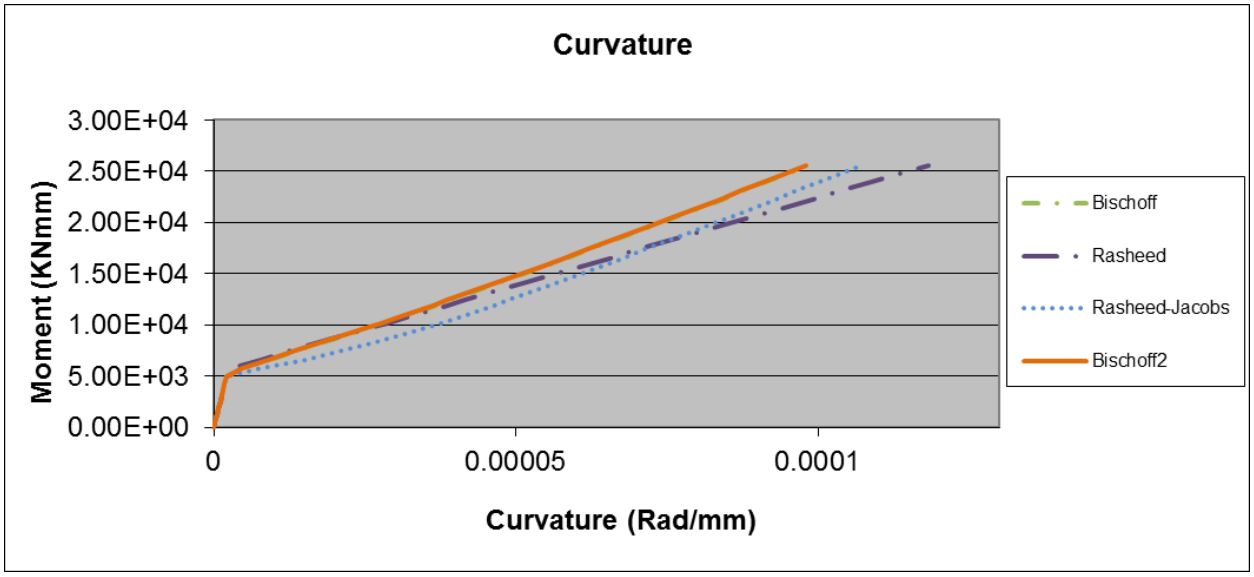

Author: Al-Sunna Sample: SC3b Dependent: None

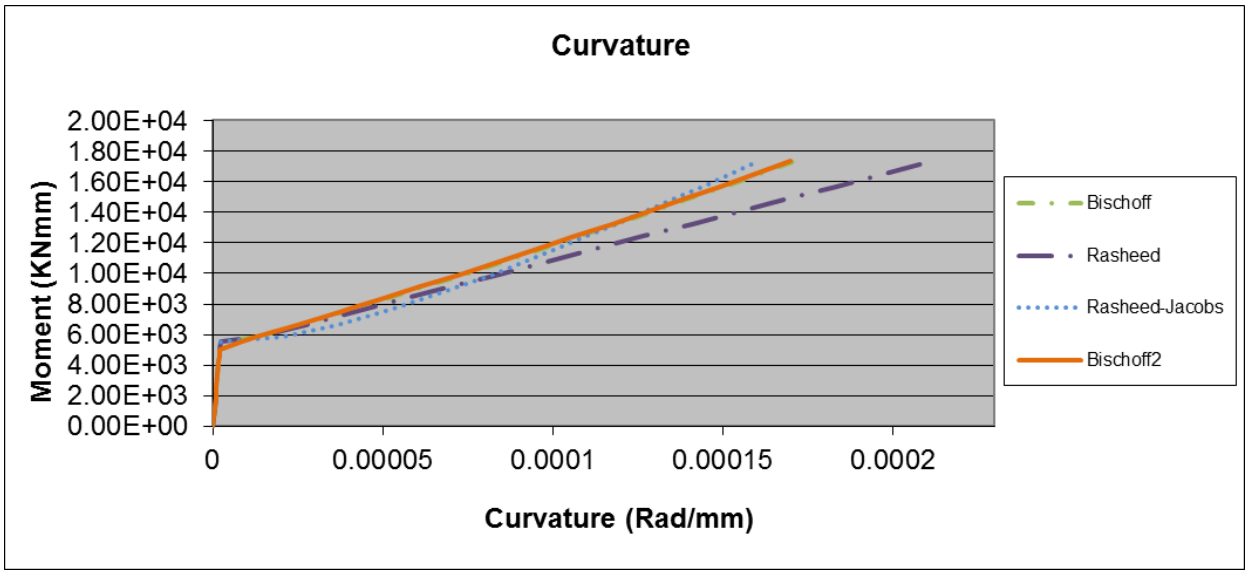

Author: Al-Sunna Sample: SG2a Dependent: SG2b

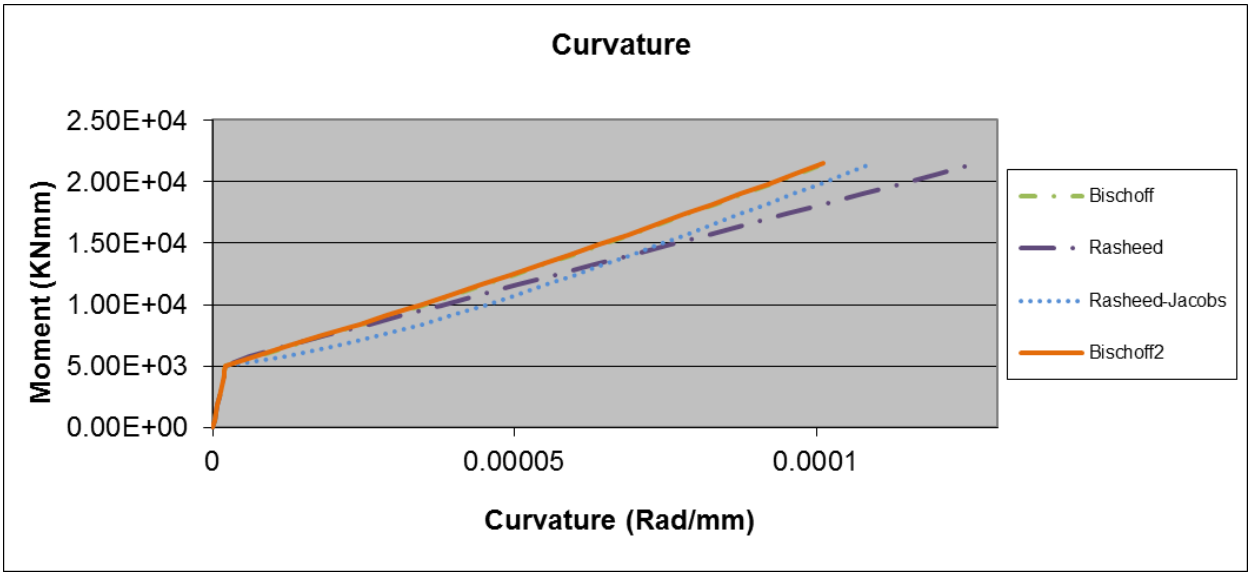

Author: Al-Sunna Sample: SG3a Dependent: SG3b

Appendix B - Notations

a	beam shear span
A_f	area of tension FRP
A'_f	area of compression FRP
b	width of section
d	effective depth of section
d’	depth of the centroid of compression reinforcement
d”	depth of the centroid of tension reinforcement to extreme tension fiber
E_c	Secant modulus of concrete at $4{,}723\sqrt{f'c}$ (Metric)
E_f	Young’s modulus of FRP reinforcement in tension
E'_f	Young’s modulus of FRP reinforcement in compression
f_f	stress in FRP bars in tension
f'_f	stress in FRP bars in compression
f_r	rupture modulus of concrete
f_{fu}	ultimate strength of the FRP bars in tension
f'_{fu}	ultimate strength of the FRP bars in compression
f'_c	compression strength of concrete
h	height of section
I_{cr}	cracking moment of inertia
I_{en}	beam effective moment of inertia at ultimate load
I_g	uncracked moment of inertia
L	beam span
L_g	length of bean at specific deflection
M	moment of beam at specific deflection
M_{cr}	cracking moment of the section
M_n	nominal moment at ultimate capacity
P	load of beam at specific deflection
P_{cr}	cracking load of the section
P_n	nominal load at ultimate capacity

y_{top}	distance from centroid to the top of the section
y_{bot}	distance from the centroid to the bottom of the section
α	conversion between nonlinear stress-strain relationship and equivalent rectangular distribution
β_1	neutral axis depth multiplier to give the depth of equivalent rectangular stress block
ε_{cu}	strain of the extreme concrete fiber in compression = 0.003
ε'_c	strain corresponding to f'_c
ε_{fu}	ultimate strain of FRP in tension
ε'_{fu}	ultimate strain of FRP in compression
ρ_f	tension FRP reinforcement ratio
ρ'_f	compression FRP reinforcement ratio
γ	centroid location of concrete force in compression from top extreme fiber
ϕ_{cr}	cracking moment curvature
ϕ_n	ultimate moment curvature

Appendix C - Calculated and Experimental Deflections (in.)

Collected at 0.333Mn

Where I = independent samples and D = dependent sample

		Load @ deflection (kip)	Rasheed	Bischoff	Rasheed-Jacobs	Bischoff 2	Experimental
Yost1a-NL	I	2.324	0.163493	0.376421	0.438257	0.191585	0.415
Yost1b-NL	D	2.324	0.163493	0.285013	0.438257	0.191585	0.321
Yost1c-NL	D	2.324	0.163493	0.285013	0.438257	0.191585	0.291
Yost2a-NL	I	3.062	0.224988	0.466864	0.554102	0.264976	0.451
Yost2b-NL	D	3.062	0.224988	0.466864	0.554102	0.264976	0.422
Yost2c-NL	D	3.062	0.224988	0.466864	0.554102	0.264976	0.496
Yost3a-NL	I	2.668	0.272782	0.511731	0.614755	0.319904	0.589
Yost3b-NL	D	2.668	0.272782	0.511731	0.614755	0.319904	0.464
Yost3c-NL	D	2.668	0.272782	0.511731	0.614755	0.319904	0.374
Yost4a-NL	I	2.404	0.304598	0.531221	0.641144	0.354169	0.377
Yost4b-NL	D	2.404	0.304598	0.531221	0.641144	0.354169	0.388
Yost4c-NL	D	2.404	0.304598	0.531221	0.641144	0.354169	0.387
Yost1a-NS	I	8.874	0.120124	0.198282	0.238184	0.139927	0.239
Yost1b-NS	D	8.874	0.120124	0.198282	0.238184	0.139927	0.25
Yost1c-NS	D	8.874	0.120124	0.198282	0.238184	0.139927	0.244
Yost2a-NS	I	10.402	0.134355	0.194936	0.23591	0.151695	0.253
Yost2b-NS	D	10.402	0.134355	0.194936	0.23591	0.151695	0.204
Yost2c-NS	D	10.402	0.134355	0.194936	0.23591	0.151695	0.214
Yost3a-NS	I	12.314	0.136273	0.187725	0.22762	0.151003	0.197
Yost3b-NS	D	12.314	0.136273	0.187725	0.22762	0.151003	0.191
Yost3c-NS	D	12.314	0.136273	0.187725	0.22762	0.151003	0.227
Yost4a-NS	I	11.524	0.138053	0.184521	0.223642	0.151241	0.203
Yost4b-NS	D	11.524	0.138053	0.184521	0.223642	0.151241	0.196
Yost4c-NS	D	11.524	0.138053	0.184521	0.223642	0.151241	0.191
Yost1a-HS	I	11.886	0.162588	0.26433	0.302199	0.187367	0.27
Yost1c-HS	D	11.886	0.162588	0.26433	0.302199	0.187367	0.263
Yost2a-HS	I	10.066	0.177462	0.264085	0.306255	0.201939	0.287
Yost2b-HS	D	10.066	0.177462	0.264085	0.306255	0.201939	0.275
Yost2c-HS	D	10.066	0.177462	0.264085	0.306255	0.201939	0.292
Yost3a-HS	I	11.826	0.179283	0.253092	0.296259	0.201487	0.287
Yost4a-HS	I	15.764	0.182384	0.244642	0.287629	0.20195	0.314
Yost1a-HL	I	3.772	0.324136	0.633296	0.717265	0.373277	0.577
Yost1b-HL	D	3.772	0.324136	0.633296	0.717265	0.373277	0.659

Yost1c-HL	D	3.772	0.324136	0.633296	0.717265	0.373277	0.69
Yost2a-HL	I	3.196	0.404284	0.695633	0.801689	0.463543	0.647
Yost2b-HL	D	3.196	0.404284	0.695633	0.801689	0.463543	0.69
Yost2c-HL	D	3.196	0.404284	0.695633	0.801689	0.463543	0.69
Yost3a-HL	I	2.806	0.43461	0.693318	0.808591	0.494764	0.643
Yost3b-HL	D	2.806	0.43461	0.693318	0.808591	0.494764	0.684
Yost3c-HL	D	2.806	0.43461	0.693318	0.808591	0.494764	0.733
Yost4a-HL	I	3.504	0.447511	0.674698	0.793203	0.503892	0.664
Yost4b-HL	D	3.504	0.447511	0.674698	0.793203	0.503892	0.56
Yost4c-HL	D	3.504	0.447511	0.674698	0.793203	0.503892	0.639
Toutanji-GB2	I	6.85	0.27438	0.422845	0.491743	0.32495	0.146
Toutanji-GB3	I	7.176	0.267284	0.395025	0.464801	0.311438	0.17
Benmokrane ISO1	I	10.63	0.394563	0.513164	0.603997	0.45599	0.38
Benmokrane ISO2	D	10.63	0.394563	0.513164	0.603997	0.45599	0.39
Benmokrane ISO3	I	22.798	0.078993	0.130546	0.150012	0.102451	0.223
Masmoudi CB2B-1	I	6.958	0.251482	0.449083	0.512328	0.305721	0.344
Masmoudi CB2B-2	D	6.958	0.251482	0.449083	0.512328	0.305721	0.331
Masmoudi CB3B-2	I	8.464	0.317569	0.49292	0.572055	0.379265	0.345
Masmoudi CB4B-1	I	7.916	0.288026	0.436824	0.516911	0.338084	0.345
Masmoudi CB4B-2	D	7.916	0.288026	0.436824	0.516911	0.338084	0.234
Masmoudi CB6B-1	I	9.394	0.304611	0.414723	0.494014	0.346198	0.351
Masmoudi CB6B-2	D	9.394	0.304611	0.414723	0.494014	0.346198	0.242
Theriault BC2NA	I	5.096	0.161218	0.217006	0.254213	0.1893	0.105
Theriault BC2NB	D	5.096	0.161218	0.217006	0.254213	0.1893	0.075
Theriault BC2HA	I	5.244	0.163312	0.220654	0.257696	0.192045	0.104
Theriault BC2VA	I	6.916	0.233108	0.288414	0.322181	0.251762	0.26
Theriault BC4NA	I	5.266	0.142177	0.177463	0.213437	0.159051	0.079
Theriault BC4HA	I	5.526	0.142204	0.180733	0.217096	0.161032	0.026
Theriault BC4VA	I	7.524	0.202338	0.241279	0.279351	0.215877	0.089
Theriault BC4VB	D	7.524	0.202338	0.241279	0.279351	0.215877	0.135
Al-Sunna BG2a	I	6.31	0.257291	0.36035	0.420667	0.305971	0.418
Al-Sunna BG2b	D	6.31	0.257291	0.36035	0.420667	0.305971	0.435
Al-Sunna BG3a	I	9.242	0.223478	0.251578	0.303882	0.234123	0.28
Al-Sunna BG3b	D	9.242	0.223478	0.251578	0.303882	0.234123	0.266
Al-Sunna SG2a	I	3.322	0.130104	0.212579	0.246673	0.151501	0.167

Al-Sunna SG2b	D	3.322	0.130104	0.212579	0.246673	0.151501	0.264
Al-Sunna SG3a	I	4.2	0.240726	0.337011	0.424138	0.266685	0.273
Al-Sunna SG3b	D	4.2	0.240726	0.337011	0.424138	0.266685	0.235
Faza-ED	I	10.272	0.33738	0.439513	0.514889	0.392439	0.572
Faza-EE	I	10.056	0.338928	0.445906	0.521145	0.396238	0.533
Faza-EF	D	10.272	0.33738	0.439513	0.514889	0.392439	0.689
Faza-EVH1	I	11.764	0.379621	0.493556	0.568533	0.439636	0.765
Faza-EVH2	D	11.764	0.379621	0.493556	0.568533	0.439636	0.716
Theisz-8-2-1	I	2.45	0.181816	0.274977	0.379642	0.216651	0.18
Theisz 8-2-2	D	2.45	0.181816	0.274977	0.379642	0.216651	0.203
Theisz 8-2-3	D	2.45	0.181816	0.274977	0.379642	0.216651	0.209
Theisz 8-3-1	I	3.828	0.203405	0.271562	0.3607	0.23378	0.259
Theisz 8-3-2	D	3.828	0.203405	0.271562	0.3607	0.23378	0.234
Theisz 8-3-3	D	3.828	0.203405	0.271562	0.3607	0.23378	0.255
Theisz 11-2-1	I	2.368	0.230797	0.329394	0.430486	0.278997	0.267
Theisz 11-2-2	D	2.368	0.230797	0.329394	0.430486	0.278997	0.28
Theisz 11-2-3	D	2.368	0.230797	0.329394	0.430486	0.278997	0.273
Theisz 11-3-1	I	3.828	0.231825	0.303813	0.389135	0.2712	0.277
Theisz 11-3-2	D	3.828	0.231825	0.303813	0.389135	0.2712	0.297
Theisz 11-3-3	D	3.828	0.231825	0.303813	0.389135	0.2712	0.289
Kakizawa - 2	I	1.636	0.159667	0.218904	0.267857	0.176009	0.201
Al- Sunna BC1a	I	4.442	0.031348	0.040265	0.047501	0.034869	0.092
Al-Sunna BC1b	D	4.442	0.031348	0.040265	0.047501	0.034869	0.076
Al -Sunna BC2a	I	9.838	0.255694	0.304814	0.364226	0.28156	0.391
Al-Sunna BC2b	D	9.838	0.255694	0.304814	0.364226	0.28156	0.389
Al -Sunna BC3a	I	5.768	0.234306	0.260091	0.31149	0.245891	0.303
Al-Sunna BC3b	D	5.768	0.234306	0.260091	0.31149	0.245891	0.308
Al -Sunna SC2a	I	4.294	0.251081	0.373961	0.460621	0.289333	0.542
Al -Sunna SC2b	I	4.568	0.284629	0.413889	0.507771	0.328047	0.596
Al- Sunna SC3a	I	4.414	0.244696	0.344833	0.433065	0.273139	0.448
Al -Sunna SC3b	I	5.104	0.304487	0.406225	0.50345	0.338385	0.399
Kassem IS4	I	12.518	0.324527	0.405376	0.481687	0.367939	0.557
Kassem IS6	I	14.62	0.312857	0.365348	0.436276	0.340639	0.487
Kassem IS8	I	16.28	0.243349	0.332976	0.398271	0.314729	0.459
Kassem CB4	I	12.316	0.324713	0.407222	0.483685	0.368878	0.545
Kassem CB6	I	15.138	0.337601	0.391508	0.464368	0.366036	0.554
Kassem CB8	I	16.916	0.305127	0.347905	0.415479	0.3277685	0.515
Nakano RC-C1	I	11.822	0.190169	0.224839	0.272075	0.201298	0.226

Appendix D - Calculated and Experimental Deflections (in.)

Collected at 0.400Mn

Where I = independent samples and D = dependent sample

		Load @ deflection (kip)	Rasheed	Bischoff	Rasheed-Jacobs	Bischoff 2	Experimental
Yost1a-NL	I	2.79	0.404105	0.761269	0.836227	0.462412	0.607
Yost1b-NL	D	2.79	0.404105	0.761269	0.836227	0.462412	0.59
Yost1c-NL	D	2.79	0.404105	0.761269	0.836227	0.462412	0.535
Yost2a-NL	I	3.674	0.459701	0.787215	0.884422	0.522859	0.698
Yost2b-NL	D	3.674	0.459701	0.787215	0.884422	0.522859	0.709
Yost2c-NL	D	3.674	0.459701	0.787215	0.884422	0.522859	0.761
Yost3a-NL	I	3.202	0.503689	0.79205	0.903412	0.567241	0.802
Yost3b-NL	D	3.202	0.503689	0.79205	0.903412	0.567241	0.675
Yost3c-NL	D	3.202	0.503689	0.79205	0.903412	0.567241	0.637
Yost4a-NL	I	2.886	0.513207	0.768309	0.885801	0.573394	0.592
Yost4b-NL	D	2.886	0.513207	0.768309	0.885801	0.573394	0.54
Yost4c-NL	D	2.886	0.513207	0.768309	0.885801	0.573394	0.568
Yost1a-NS	I	10.648	0.20109	0.28817	0.330314	0.224224	0.33
Yost1b-NS	D	10.648	0.20109	0.28817	0.330314	0.224224	0.321
Yost1c-NS	D	10.648	0.20109	0.28817	0.330314	0.224224	0.315
Yost2a-NS	I	12.482	0.202376	0.262712	0.306335	0.219122	0.323
Yost2b-NS	D	12.482	0.202376	0.262712	0.306335	0.219122	0.278
Yost2c-NS	D	12.482	0.202376	0.262712	0.306335	0.219122	0.306
Yost3a-NS	I	14.778	0.198054	0.247002	0.289776	0.210817	0.28
Yost3b-NS	D	14.778	0.198054	0.247002	0.289776	0.210817	0.279
Yost3c-NS	D	14.778	0.198054	0.247002	0.289776	0.210817	0.285
Yost4a-NS	I	13.828	0.195473	0.238518	0.280541	0.206091	0.274
Yost4b-NS	D	13.828	0.195473	0.238518	0.280541	0.206091	0.266
Yost4c-NS	D	13.828	0.195473	0.238518	0.280541	0.206091	0.253
Yost1a-HS	I	14.264	0.267012	0.376528	0.41089	0.293709	0.407
Yost1c-HS	D	14.264	0.267012	0.376528	0.41089	0.293709	0.428
Yost2a-HS	I	12.078	0.270935	0.357597	0.398555	0.294708	0.517
Yost2b-HS	D	12.078	0.270935	0.357597	0.398555	0.294708	0.419
Yost2c-HS	D	12.078	0.270935	0.357597	0.398555	0.294708	0.412
Yost3a-HS	I	14.192	0.264915	0.335673	0.379156	0.284923	0.388
Yost4a-HS	I	18.916	0.259643	0.316847	0.361198	0.275822	0.466
Yost1a-HL	I	4.526	0.630793	1.0115	1.083618	0.694577	0.942
Yost1b-HL	D	4.526	0.630793	1.0115	1.083618	0.694577	1.015

Yost1c-HL	D	4.526	0.630793	1.0115	1.083618	0.694577	1.031
Yost2a-HL	I	3.836	0.673928	0.991697	1.09136	0.739667	0.93
Yost2b-HL	D	3.836	0.673928	0.991697	1.09136	0.739667	0.962
Yost2c-HL	D	3.836	0.673928	0.991697	1.09136	0.739667	1.073
Yost3a-HL	I	3.366	0.689039	0.955845	1.068774	0.750449	0.972
Yost3b-HL	D	3.366	0.689039	0.955845	1.068774	0.750449	0.9
Yost3c-HL	D	3.366	0.689039	0.955845	1.068774	0.750449	0.968
Yost4a-HL	I	4.204	0.682726	0.907703	1.027118	0.736101	0.951
Yost4b-HL	D	4.204	0.682726	0.907703	1.027118	0.736101	0.814
Yost4c-HL	D	4.204	0.682726	0.907703	1.027118	0.736101	0.878
Toutanji-GB2	I	8.22	0.415384	0.570022	0.637568	0.471274	0.334
Toutanji-GB3	I	8.61	0.395178	0.524527	0.595334	0.441612	0.287
Benmokrane ISO1	I	6.378	0.564281	0.679611	0.771986	0.623091	0.541
Benmokrane ISO2	D	6.378	0.564281	0.679611	0.771986	0.623091	0.55
Benmokrane ISO3	I	27.358	0.157801	0.240346	0.275556	0.198783	0.313
Masmoudi CB2B-1	I	8.348	0.447202	0.687087	0.74376	0.519796	0.535
Masmoudi CB2B-2	D	8.348	0.447202	0.687087	0.74376	0.519796	0.525
Masmoudi CB3B-2	I	10.156	0.487688	0.673949	0.750609	0.557358	0.551
Masmoudi CB4B-1	I	9.498	0.439685	0.595491	0.676989	0.494327	0.515
Masmoudi CB4B-2	D	9.498	0.439685	0.595491	0.676989	0.494327	0.345
Masmoudi CB6B-1	I	11.272	0.432437	0.538425	0.621778	0.472213	0.465
Masmoudi CB6B-2	D	11.272	0.432437	0.538425	0.621778	0.472213	0.391
Theriault BC2NA	I	6.116	0.237585	0.294179	0.331232	0.266008	0.172
Theriault BC2NB	D	6.116	0.237585	0.294179	0.331232	0.266008	0.15
Theriault BC2HA	I	6.292	0.241687	0.30077	0.336648	0.270894	0.181
Theriault BC2VA	I	8.3	0.344058	0.389852	0.418275	0.352885	0.39
Theriault BC4NA	I	6.32	0.200763	0.23303	0.27117	0.214965	0.133
Theriault BC4HA	I	6.632	0.202481	0.238834	0.277203	0.219345	0.064
Theriault BC4VA	I	9.03	0.286946	0.316736	0.35436	0.291945	0.188
Theriault BC4VB	D	9.03	0.286946	0.316736	0.35436	0.291945	0.216
Al-Sunna BG2a	I	7.572	0.398837	0.509209	0.568256	0.451191	0.57
Al-Sunna BG2b	D	7.572	0.398837	0.509209	0.568256	0.451191	0.577
Al-Sunna BG3a	I	11.09	0.298835	0.317919	0.37524	0.30157	0.341
Al-Sunna BG3b	D	11.09	0.298835	0.317919	0.37524	0.30157	0.331
Al-Sunna SG2a	I	3.986	0.39099	0.589052	0.648795	0.442916	0.702
Al-Sunna SG2b	D	3.986	0.39099	0.589052	0.648795	0.442916	0.702
Al-Sunna SG3a	I	5.04	0.411056	0.518195	0.622909	0.434008	0.385
Al-Sunna SG3b	D	5.04	0.411056	0.518195	0.622909	0.434008	0.41
Faza-ED	I	12.326	0.478719	0.578531	0.654759	0.532364	0.699
Faza-EE	I	12.068	0.484633	0.590332	0.665758	0.541298	0.665
Faza-EF	D	12.326	0.478719	0.578531	0.654759	0.532364	0.865
Faza-EVH1	I	14.116	0.540875	0.650966	0.723805	0.59804	0.954
Faza-EVH2	D	14.116	0.540875	0.650966	0.723805	0.59804	0.923

Theisz-8-2-1	I	2.938	0.295954	0.400365	0.507349	0.338915	0.329
Theisz 8-2-2	D	2.938	0.295954	0.400365	0.507349	0.338915	0.309
Theisz 8-2-3	D	2.938	0.295954	0.400365	0.507349	0.338915	0.306
Theisz 8-3-1	I	4.592	0.296654	0.364865	0.455848	0.328098	0.336
Theisz 8-3-2	D	4.592	0.296654	0.364865	0.455848	0.328098	0.331
Theisz 8-3-3	D	4.592	0.296654	0.364865	0.455848	0.328098	0.333
Theisz 11-2-1	I	2.842	0.343528	0.448638	0.548234	0.399149	0.414
Theisz 11-2-2	D	2.842	0.343528	0.448638	0.548234	0.399149	0.393
Theisz 11-2-3	D	2.842	0.343528	0.448638	0.548234	0.399149	0.367
Theisz 11-3-1	I	4.592	0.323776	0.395936	0.482554	0.365224	0.374
Theisz 11-3-2	D	4.592	0.323776	0.395936	0.482554	0.365224	0.395
Theisz 11-3-3	D	4.592	0.323776	0.395936	0.482554	0.365224	0.372
Kakizawa - 2	I	1.962	0.236061	0.292845	0.345841	0.249589	0.264
Al- Sunna BC1a	I	5.33	0.097005	0.153717	0.195378	0.122164	0.152
Al-Sunna BC1b	D	5.33	0.097005	0.153717	0.195378	0.122164	0.204
Al -Sunna BC2a	I	11.806	0.345246	0.38756	0.45142	0.36567	0.496
Al-Sunna BC2b	D	11.806	0.345246	0.38756	0.45142	0.36567	0.489
Al -Sunna BC3a	I	13.842	0.306522	0.324088	0.380896	0.311058	0.382
Al-Sunna BC3b	D	13.842	0.306522	0.324088	0.380896	0.311058	0.394
Al -Sunna SC2a	I	5.154	0.449758	0.599979	0.703036	0.49418	0.74
Al -Sunna SC2b	I	5.48	0.480148	0.627758	0.7341	0.527468	0.811
Al- Sunna SC3a	I	5.296	0.41665	0.528835	0.634221	0.443395	0.612
Al -Sunna SC3b	I	6.124	0.467715	0.56864	0.676642	0.49629	0.602
Kassem IS4	I	15.022	0.456011	0.531098	0.610538	0.494524	0.65
Kassem IS6	I	17.544	0.421136	0.464095	0.540342	0.440865	0.605
Kassem IS8	I	19.534	0.335088	0.434997	0.507747	0.400377	0.573
Kassem CB4	I	14.78	0.457959	0.535008	0.614437	0.497433	0.696
Kassem CB6	I	18.166	0.452681	0.495745	0.573691	0.471928	0.682
Kassem CB8	I	20.3	0.404297	0.437345	0.510898	0.4186708	0.639
Nakano RC-C1	I	14.186	0.259843	0.286905	0.338304	0.264575	0.268

Appendix E - Calculated and Experimental Deflection (in.) Collected at 0.467Mn

Where I = independent samples and D = dependent sample

		Load @ deflection (kip)	Rasheed	Bischoff	Rasheed-Jacobs	Bischoff 2	Experimental
Yost1a-NL	I	3.254	0.689411	1.103052	1.15712	0.758536	0.795
Yost1b-NL	D	3.254	0.689411	1.103052	1.15712	0.758536	0.882
Yost1c-NL	D	3.254	0.689411	1.103052	1.15712	0.758536	0.74
Yost2a-NL	I	4.286	0.718134	1.070777	1.155284	0.785852	0.929
Yost2b-NL	D	4.286	0.718134	1.070777	1.155284	0.785852	0.907
Yost2c-NL	D	4.286	0.718134	1.070777	1.155284	0.785852	0.938
Yost3a-NL	I	3.734	0.751459	1.044786	1.148526	0.813508	0.981
Yost3b-NL	D	3.734	0.751459	1.044786	1.148526	0.813508	0.845
Yost3c-NL	D	3.734	0.751459	1.044786	1.148526	0.813508	0.815
Yost4a-NL	I	3.366	0.733614	0.985745	1.099956	0.78966	0.735
Yost4b-NL	D	3.366	0.733614	0.985745	1.099956	0.78966	0.754
Yost4c-NL	D	3.366	0.733614	0.985745	1.099956	0.78966	0.734
Yost1a-NS	I	12.422	0.287135	0.371752	0.412125	0.30774	0.403
Yost1b-NS	D	12.422	0.287135	0.371752	0.412125	0.30774	0.421
Yost1c-NS	D	12.422	0.287135	0.371752	0.412125	0.30774	0.415
Yost2a-NS	I	14.562	0.272606	0.326681	0.371212	0.284735	0.397
Yost2b-NS	D	14.562	0.272606	0.326681	0.371212	0.284735	0.369
Yost2c-NS	D	14.562	0.272606	0.326681	0.371212	0.284735	0.386
Yost3a-NS	I	17.24	0.260639	0.302692	0.347155	0.268229	0.387
Yost3b-NS	D	17.24	0.260639	0.302692	0.347155	0.268229	0.35
Yost3c-NS	D	17.24	0.260639	0.302692	0.347155	0.268229	0.355
Yost4a-NS	I	16.132	0.255711	0.291457	0.335546	0.260783	0.344
Yost4b-NS	D	16.132	0.255711	0.291457	0.335546	0.260783	0.337
Yost4c-NS	D	16.132	0.255711	0.291457	0.335546	0.260783	0.328
Yost1a-HS	I	16.64	0.378818	0.482475	0.509311	0.400049	0.618
Yost1c-HS	D	16.64	0.378818	0.482475	0.509311	0.400049	0.635
Yost2a-HS	I	14.092	0.367391	0.445488	0.483124	0.384799	0.687
Yost2b-HS	D	14.092	0.367391	0.445488	0.483124	0.384799	0.734
Yost2c-HS	D	14.092	0.367391	0.445488	0.483124	0.384799	0.655
Yost3a-HS	I	16.556	0.352125	0.413477	0.455905	0.365262	0.488
Yost4a-HS	I	22.07	0.338872	0.386338	0.431239	0.347853	0.654
Yost1a-HL	I	5.28	0.966064	1.352612	1.392676	1.020154	1.267
Yost1b-HL	D	5.28	0.966064	1.352612	1.392676	1.020154	1.393

Yost1c-HL	D	5.28	0.966064	1.352612	1.392676	1.020154	1.452
Yost2a-HL	I	4.474	0.96981	1.274971	1.356573	1.022607	1.204
Yost2b-HL	D	4.474	0.96981	1.274971	1.356573	1.022607	1.28
Yost2c-HL	D	4.474	0.96981	1.274971	1.356573	1.022607	1.354
Yost3a-HL	I	3.928	0.954917	1.201478	1.304663	1.001028	1.179
Yost3b-HL	D	3.928	0.954917	1.201478	1.304663	1.001028	1.16
Yost3c-HL	D	3.928	0.954917	1.201478	1.304663	1.001028	1.22
Yost4a-HL	I	4.904	0.922793	1.124386	1.239632	0.959327	1.192
Yost4b-HL	D	4.904	0.922793	1.124386	1.239632	0.959327	1.049
Yost4c-HL	D	4.904	0.922793	1.124386	1.239632	0.959327	1.099
Toutanji-GB2	I	9.59	0.561324	0.709068	0.772	0.613915	0.497
Toutanji-GB3	I	10.046	0.527072	0.647634	0.717002	0.568449	0.399
Benmokrane ISO1	I	14.882	0.736537	0.83777	0.928651	0.783892	0.702
Benmokrane ISO2	D	14.882	0.736537	0.83777	0.928651	0.783892	0.71
Benmokrane ISO3	I	31.918	0.241748	0.339277	0.378174	0.292538	0.393
Masmoudi CB2B-1	I	9.74	0.657606	0.906151	0.944512	0.73346	0.734
Masmoudi CB2B-2	D	9.74	0.657606	0.906151	0.944512	0.73346	0.751
Masmoudi CB3B-2	I	11.848	0.664101	0.844268	0.913763	0.730935	0.697
Masmoudi CB4B-1	I	11.082	0.597058	0.745078	0.823629	0.646807	0.698
Masmoudi CB4B-2	D	11.082	0.597058	0.745078	0.823629	0.646807	0.59
Masmoudi CB6B-1	I	13.152	0.563015	0.656956	0.742711	0.594629	0.621
Masmoudi CB6B-2	D	13.152	0.563015	0.656956	0.742711	0.594629	0.519
Theriault BC2NA	I	7.136	0.315569	0.367101	0.402091	0.339843	0.226
Theriault BC2NB	D	7.136	0.315569	0.367101	0.402091	0.339843	0.247
Theriault BC2HA	I	7.34	0.321604	0.374914	0.409015	0.346628	0.265
Theriault BC2VA	I	9.682	0.457045	0.48561	0.506778	0.449992	0.509
Theriault BC4NA	I	7.372	0.260148	0.285991	0.325299	0.268842	0.182
Theriault BC4HA	I	7.738	0.263762	0.294178	0.333393	0.275593	0.126
Theriault BC4VA	I	10.534	0.372567	0.38857	0.424693	0.365101	0.258
Theriault BC4VB	D	10.534	0.372567	0.38857	0.424693	0.365101	0.294
Al-Sunna BG2a	I	8.834	0.54412	0.648096	0.700618	0.590589	0.57
Al-Sunna BG2b	D	8.834	0.54412	0.648096	0.700618	0.590589	0.729
Al-Sunna BG3a	I	12.938	0.374813	0.382247	0.444133	0.367132	0.407
Al-Sunna BG3b	D	12.938	0.374813	0.382247	0.444133	0.367132	0.398
Al-Sunna SG2a	I	4.65	0.683914	0.922166	0.966282	0.738579	0.947
Al-Sunna SG2b	D	4.65	0.683914	0.922166	0.966282	0.738579	1.073
Al-Sunna SG3a	I	5.88	0.589905	0.684603	0.794335	0.596776	0.55
Al-Sunna SG3b	D	5.88	0.589905	0.684603	0.794335	0.596776	0.608
Faza-ED	I	14.38	0.622011	0.710909	0.785773	0.667089	0.866
Faza-EE	I	14.078	0.632347	0.727452	0.800558	0.680742	0.802
Faza-EF	D	14.38	0.622011	0.710909	0.785773	0.667089	1.064
Faza-EVH1	I	16.468	0.7044	0.800751	0.869095	0.750491	1.173
Faza-EVH2	D	16.468	0.7044	0.800751	0.869095	0.750491	1.145

Theisz-8-2-1	I	3.428	0.417504	0.521344	0.623042	0.460797	0.443
Theisz 8-2-2	D	3.428	0.417504	0.521344	0.623042	0.460797	0.452
Theisz 8-2-3	D	3.428	0.417504	0.521344	0.623042	0.460797	0.45
Theisz 8-3-1	I	5.358	0.392938	0.455081	0.545675	0.420334	0.428
Theisz 8-3-2	D	5.358	0.392938	0.455081	0.545675	0.420334	0.438
Theisz 8-3-3	D	5.358	0.392938	0.455081	0.545675	0.420334	0.43
Theisz 11-2-1	I	3.316	0.460053	0.563452	0.658401	0.516449	0.552
Theisz 11-2-2	D	3.316	0.460053	0.563452	0.658401	0.516449	0.516
Theisz 11-2-3	D	3.316	0.460053	0.563452	0.658401	0.516449	0.49
Theisz 11-3-1	I	5.358	0.417723	0.485378	0.572428	0.456892	0.485
Theisz 11-3-2	D	5.358	0.417723	0.485378	0.572428	0.456892	0.486
Theisz 11-3-3	D	5.358	0.417723	0.485378	0.572428	0.456892	0.475
Kakizawa - 2	I	2.29	0.31525	0.363278	0.418362	0.321605	0.32
Al- Sunna BC1a	I	6.218	0.170501	0.253485	0.310058	0.209869	0.345
Al-Sunna BC1b	D	6.218	0.170501	0.253485	0.310058	0.209869	0.325
Al -Sunna BC2a	I	13.774	0.435509	0.467479	0.535174	0.447178	0.595
Al-Sunna BC2b	D	13.774	0.435509	0.467479	0.535174	0.447178	0.585
Al -Sunna BC3a	I	16.15	0.379145	0.38658	0.448647	0.374679	0.46
Al-Sunna BC3b	D	16.15	0.379145	0.38658	0.448647	0.374679	0.476
Al -Sunna SC2a	I	6.012	0.660302	0.806825	0.909839	0.69452	0.966
Al -Sunna SC2b	I	6.394	0.684765	0.824603	0.930491	0.72104	0.974
Al- Sunna SC3a	I	6.178	0.596673	0.697526	0.807526	0.608574	0.758
Al -Sunna SC3b	I	7.144	0.636266	0.720801	0.832719	0.649102	0.754
Kassem IS4	I	17.526	0.589146	0.651111	0.731669	0.616471	0.776
Kassem IS6	I	20.468	0.53017	0.559508	0.640373	0.53798	0.725
Kassem IS8	I	22.79	0.492562	0.602678	0.687706	0.483786	0.689
Kassem CB4	I	17.244	0.592825	0.656778	0.737033	0.62113	0.803
Kassem CB6	I	21.194	0.568502	0.596615	0.679069	0.574614	0.815
Kassem CB8	I	23.682	0.533341	0.524156	0.603309	0.5069903	0.762
Nakano RC-C1	I	16.55	0.330336	0.34675	0.401697	0.325949	0.349